Universidade de Aveiro
2020

João Miguel
Peixoto Martins

Calibração de modelos constitutivos termomecânicos para chapas metálicas através de medições de campo total

Calibration of thermo-mechanical constitutive models for sheet metals from full-field measurements

Calibration de modèles thermo-mécaniques pour les tôles métalliques à partir de mesures de champs

Universidade de Aveiro
2020

João Miguel
Peixoto Martins

Calibração de modelos constitutivos termomecânicos para chapas metálicas através de medições de campo total

Calibration of thermo-mechanical constitutive models for sheet metals from full-field measurements

Calibration de modèles thermo-mécaniques pour les tôles métalliques à partir de mesures de champs

Dissertação apresentada à Universidade de Aveiro e Université Bretagne Sud para cumprimento dos requisitos necessários à obtenção do grau de Doutor em Engenharia Mecânica, realizada sob orientação científica de António Gil D'Orey de Andrade Campos, Professor Auxiliar com Agregação do Departamento de Engenharia Mecânica da Universidade de Aveiro, e de Sandrine Thuillier, Professeur des Université da Université Bretagne Sud.

The jury

President	**Pascale BALLAND** Professeur, Université Savoie-Mont Blanc
Members	**Fabrice PIERRON** Professeur, University of Southampton
	Fabrice RICHARD Maître de conférences HDR, Université de Franche-Comté
	José XAVIER Professor Auxiliar, Universidade Nova de Lisboa
	Sandrine THUILLIER Professeur, Université Bretagne Sud (supervisor)
	António ANDRADE-CAMPOS Professor Auxiliar com Agregação, Universidade de Aveiro (supervisor)

Acknowledgements

First and foremost, I would like to express my sincere gratitude to my supervisors Professor António Andrade Campos and Professeur Sandrine Thuillier. Thank you so much for providing me this rewarding experience. Your continuous support and valuable guidance were fundamental in making this PhD a productive and stimulating journey.

I would like to acknowledge my colleagues of the M9'calibre group. All the scientific and non-scientific discussions created a highly motivating environment.

I would also like to thank all the colleagues and staff of IRDL. I am grateful for the helpful and kind way in which you received me in Lorient.

Many thanks to my friends and family for the all the moments of good mood and incentive. In particular, thanks to my sister, Tozé and little Daniel for their presence and constant support. To my parents, Clara and Eduardo, whose unconditional support and encouragement all these years got me here, my deepest gratitude. Finally, special thanks to Sílvia for sharing the good and bad moments over these years, your endless patience and full support gave me the extra strength and motivation to make this possible.

This thesis is sponsored by a scientific research grant from the Portuguese Foundation for Science and Technology (FCT) with reference SFRH/BD/117432/2016 and by the Région Bretagne (France). It was also supported by the funding from the Research Fund for Coal and Steel under grant agreement No 888153. It is also acknowledge the financial support of the Portuguese Foundation for Science and Technology (FCT) under the projects PTDC/EME-APL/29713/2017 (CENTRO-01-0145-FEDER-029713), PTDC/EME-EME/31243/2017 (POCI-01-0145-FEDER-031243) and PTDC/EME-EME/30592/2017 (POCI-01-0145-FEDER-030592) by UE/FEDER through the programs CENTRO 2020 and COMPETE 2020, and UID/EMS/00481/2013-FCT under CENTRO-01-0145-FEDER-022083. It is also acknowledge publishers, copyright holders and scientific journals editors for providing the licences allowing the print and electronic reuse of the papers published under the scope of this research.

palavras-chave

Elasto-plasticidade; Termo-elasto-viscoplasticidade; Anisotropia; Calibração de modelos constitutivos; Testes mecânicos heterogêneos

resumo

Atualmente, as ferramentas de simulação numérica, como o método dos elementos finitos, são essenciais para projetar e otimizar processos de estampagem de chapas metálicas. Estas ferramentas de simulação utilizam modelos constitutivos para descrever o comportamento termomecânico do material, estando o seu sucesso dependente da qualidade destes modelos e consequentemente da sua calibração. Os processos mais recentes de calibração têm como base medições de campo total, testes heterogêneos e métodos de análise inversa. A combinação destes três elementos permite extrair mais informação de um ensaio mecânico quando comparado com os procedimentos clássicos de calibração que usam testes homogéneos. Deste modo, este novo conceito de calibração tem o potencial de reduzir o número de testes necessários e simplificar o processo.

Esta tese pretende assim contribuir para o processo de calibração de modelos termomecânicos propondo novas metodologias baseadas neste novo conceito. O ponto de partida para este trabalho é a revisão geral de quatro métodos inversos, designadamente o método Finite Element Model Updating (FEMU), o Constitutive Equation Gap Method, o Equilibrium Gap Method e o Virtual Fields Method (VFM). Os algoritmos e o processo de implementação de cada método são apresentados detalhadamente nesta revisão, assim como uma discussão dos pontos fortes e fracos de cada método. É também apresentado um estudo comparativo, considerando uma formulação para pequenas deformações, para modelos de elasticidade linear e plasticidade não linear, adotando as mesmas condições para cada método. Esta revisão mostra que o método FEMU é o método de análise inversa mais simples de implementar. O estudo comparativo mostra que os outros três métodos apresentam um desempenho superior em termos de eficiência computacional. Quando comparado com os outros métodos, o VFM apresenta uma resposta equilibrada em termos de precisão dos resultados de calibração e eficiência computacional. No seguimento desta revisão é apresentada uma análise á precisão do VFM e FEMU para modelos de plasticidade considerando uma formulação para grandes deformações. Os resultados obtidos indicam que o método FEMU é sensível à distribuição dos valores de deformação presentes na base de dados do teste heterogéneo, uma vez que os valores de deformação com maior representatividade na base de dados têm um impacto superior nos resultados da calibração. Para as mesmas condições, o VFM apresenta uma resposta mais robusta quando comparado com o FEMU.

Dois testes heterogéneos são avaliados como potenciais bases de dados a combinar com o VFM. O objetivo desta avaliação é propor uma metodologia de um só teste para calibração de modelos anisotrópicos de plasticidade. O primeiro teste a ser estudado é um teste de tração biaxial de um provete cruciforme. São analisadas três geometrias para o provete como possíveis candidatas a combinar com o VFM. Esta análise mostra que a inclusão de perturbações geométricas na geometria do provete leva a um aumento da heterogeneidade e informação criada pelo teste. Além disso, os resultados obtidos com o teste biaxial na calibração de dois modelos anisotrópicos de plasticidade são bastante precisos. O segundo teste avaliado consiste num teste de tração uniaxial num provete com geometria otimizada. Os resultados da calibração com este provete mostram uma boa descrição do comportamento do material para a direção de carregamento. No entanto, os resultados indicam que um teste com apenas uma direção de carregamento é insuficiente para uma calibração precisa de um modelo anisotrópico de plasticidade. Além desta análise, este estudo também revela que o VFM é sensível ao número de campos virtuais selecionados.

A última parte deste trabalho incide sobre a calibração de modelos de termo-elasto-viscoplasticidade. É proposto um teste heterogéneo termomecânico realizado num equipamento de testes Gleeble para criar uma base de dados experimental. A análise deste teste mostra que são atingidas gamas consideráveis de temperatura, deformação e velocidade de deformação. A primeira metodologia proposta combina este teste heterogéneo e o método FEMU, a sua avaliação é efetuada usando uma base de dados virtual. Esta avaliação incluí a análise detalhada da sensibilidade de cada parâmetro do modelo Johnson-Cook. Os resultados mostram que a calibração simultânea de todos os parâmetros pode ser alcançada com razoável sucesso através desta metodologia. Numa segunda metodologia proposta, o mesmo teste heterogéneo é usado juntamente com o VFM para calibrar uma versão modificada do modelo de Johnson-Cook. A base de dados experimental é gerada para um aço de alta resistência. Os resultados do processo de calibração mostram que é possível obter uma descrição razoável da tensão de escoamento do material. Globalmente, os resultados das duas metodologias mostram que estas são alternativas bastante promissoras aos métodos clássicos de calibração.

Intentionally blank page.

keywords Elasto-plasticity; Thermo-elasto-viscoplasticity; Anisotropy ; Calibration of constitutive models; Heterogeneous tests

abstract Nowadays, simulation tools, like the finite element method, are essential to design and optimise sheet metal forming processes. These tools use constitutive models to describe the thermo-mechanical behaviour of the material and their success is inherently dependent on the quality of the models and, consequently, on its calibration. Recent calibration procedures rely on full-field measurements, heterogeneous tests, and inverse analysis methods. The combination of these three elements leads to more information extracted from a single mechanical test when compared to classical procedures that use homogeneous tests. This new concept of calibration has the potential to reduce the number of tests required and simplify the process.

This thesis contributes to the calibration process of thermo-mechanical constitutive models by proposing new calibration methodologies based on this new concept. An overview of four inverse methods, namely the Finite Element Model Updating (FEMU), the Constitutive Equation Gap Method, the Equilibrium Gap Method and the Virtual Fields Method (VFM) is the starting point for this work. Details on the algorithms and implementation of each method are given, as well as a discussion on strengths and weaknesses. A comparative study in the framework of infinitesimal strains, on linear elasticity and non-linear plasticity, under the same conditions, is presented. This overview shows that FEMU is the most straightforward method to implement. The comparative study also shows that the other three methods outperform it in terms of computational efficiency. The VFM presents a balanced response in terms of accuracy and computational efficiency when compared to the other methods. An additional analysis of the accuracy of VFM and FEMU for plasticity models within finite strains framework is also presented. The results indicate that FEMU is sensitive to the distribution of the strain values present in the database of the test. The strain values with more representation in the database have more impact on the calibration results. In the same conditions, the VFM shows a more robust response when compared to FEMU.

Two heterogeneous tests are then evaluated as potential databases to combine with the VFM. The aim is to propose a single test calibration methodology for anisotropic plasticity models. The first test is a biaxial tension test of a cruciform specimen. Three cruciform geometries are analysed as potential candidates to combine with the VFM. The analysis of the geometries shows that the inclusion of geometric perturbations in the specimen creates additional heterogeneity and enhances the information of this test. Accurate results are reached for the calibration of two anisotropic plasticity models. The second heterogeneous test is a uniaxial standard test with an

optimized specimen shape. The calibration results show a good description of the material behaviour for the loading direction. However, a test in a single loading direction seems insufficient to accurately calibrate an anisotropic plasticity model. Moreover, the sensitivity of the VFM to the number of virtual fields is revealed in this study.

The last part of this work focuses on the calibration of thermo-elasto-viscoplasticity models. A heterogeneous thermo-mechanical test performed on a Gleeble machine is proposed to generate the experimental database. The analysis of the test shows a considerable range of temperatures, strain values and strain-rates. A first methodology that combines the FEMU with this heterogeneous test is evaluated using virtual data. A detailed sensitivity analysis of the Johnson-Cook material parameters is performed. The simultaneous calibration of all the parameters in the model is achieved with reasonable success. In a second methodology, the test is coupled with the VFM to calibrate a modified version of the Johnson-Cook model. The experimental database is then generated for a high strength steel. The calibration results show that a reasonable description of the flow stress evolution is attained. Overall, the two methodologies are promising alternatives to classical procedures.

Intentionally blank page.

mots clés

Élasto-plasticité; Thermo-élasto-viscoplasticité; Anisotropie; Calibration de modèles mécaniques; Essais mécaniques hétérogènes

résumé

De nos jours, les outils de simulation, comme la méthode des éléments finis, sont devenus essentiels pour concevoir et optimiser les procédés de mise en forme des tôles métalliques. Ces outils utilisent des modèles pour décrire le comportement thermo-mécanique du matériau et leur succès dépend de façon intrinsèque de la qualité du modèle et, par conséquent, de sa calibration. Les procédures récentes de calibration reposent sur des mesures de champ, des essais hétérogènes et des méthodes d'analyse inverse. La combinaison de ces trois éléments permet d'extraire davantage d'informations d'un essai mécanique par rapport aux procédures classiques, qui utilisent des essais homogènes. Ce nouveau concept de calibration a le potentiel de réduire le nombre d'essais requis et de simplifier l'identification des paramètres.

Cette thèse contribue au processus de calibration des modèles de comportement thermo-mécanique en proposant de nouvelles méthodologies de calibration fondées sur ce nouveau concept. Un aperçu de quatre méthodes inverses, à savoir Finite Element Model Updating (FEMU), Constitutive Equation Gap Method, Equilibrium Gap Method et Virtual Fields Method (VFM) est le point de départ de ce travail. Les algorithmes et la mise en œuvre de chaque méthode sont détaillés et une discussion sur les points forts et les points faibles est menée. Une étude comparative dans le cadre des déformations infinitésimales, pour l'élasticité linéaire et la plasticité non linéaire, est présentée. Cet aperçu montre que la méthode FEMU est la plus simple à mettre en œuvre. L'étude comparative montre également que les trois autres méthodes la surpassent quand l'efficacité du calcul est considérée. La méthode VFM présente une réponse équilibrée au regard de la précision et de l'efficacité du calcul par rapport aux autres méthodes. Une analyse supplémentaire sur la précision des méthodes VFM et FEMU pour les modèles de plasticité dans le cadre de transformations finies est également présentée. Les résultats indiquent que la méthode FEMU est sensible à la distribution des valeurs des déformations présentes dans la base de données expérimentale. En effet, les valeurs de déformations les plus représentées ont un impact plus important sur les résultats de la calibration. Dans les mêmes conditions, la méthode VFM montre une réponse plus robuste par rapport à FEMU.

Deux tests hétérogènes sont ensuite évalués en tant que bases de données potentielles à combiner avec la méthode VFM. L'objectif est de proposer une méthodologie de calibration à partir d'un test mécanique unique pour les modèles de plasticité anisotrope. Le premier essai est un test de traction biaxiale d'un échantillon cruciforme. Trois géométries sont analysées en tant que candidats potentiels à combiner avec la méthode VFM. L'analyse des géométries montre que l'intégration de perturbations géométriques dans l'échantillon crée une hétérogénéité supplémentaire et améliore les informations de ce test. Des résultats précis sont obtenus pour la calibration de deux modèles de plasticité anisotrope. Le second test hétérogène est un test standard de traction uniaxiale avec une forme d'échantillon optimisée. Les résultats de la calibration montrent une bonne description du comportement du matériau dans la direction de la force appliquée. Cependant, un test dans une seule direction de chargement semble insuffisant pour calibrer avec précision un modèle de plasticité anisotrope. De plus, cette étude révèle la sensibilité de la méthode VFM au nombre de champs virtuels.

La dernière partie de ce travail se concentre sur la calibration d'un modèle de thermo-élasto-viscoplasticité. Un essai hétérogène en déformations et en température réalisé avec une machine Gleeble est proposé pour générer la base de données expérimentale. L'analyse de l'essai montre une gamme importante de températures, de valeurs de déformation et de vitesse de déformation. Une première méthodologie qui combine la méthode FEMU avec cet essai hétérogène est évaluée à l'aide de données virtuelles. Une analyse de sensibilité détaillée des paramètres du modèle de Johnson-Cook est effectuée. La calibration simultanée de tous les paramètres du modèle est réalisée avec un succès raisonnable. Dans une seconde méthodologie, le test est couplé avec la méthode VFM pour calibrer une version modifiée du modèle de Johnson-Cook. La base de données expérimentale est alors obtenue pour un acier à haute résistance. Les résultats de la calibration montrent qu'une description raisonnable de l'évolution de la contrainte d'écoulement est obtenue. Dans l'ensemble, les deux méthodologies sont des alternatives prometteuses aux procédures classiques.

Intentionally blank page.

Contents

Intentionally blank page.

Chapter 1

Introduction

1.1 Motivation and background

Numerical simulation and its accuracy

Numerical simulation tools have assumed a preponderant role in the engineering development process of a new product. These tools are indispensable to virtually test new concepts, select the best materials, and optimise, with the advantage of avoiding the time and costs of physical prototyping. This reduction of time and costs is crucial in a variety of industries such as automotive, aerospace and electronics. For instance, in the automotive industry, a common application of numerical simulation tools, namely the finite element method, aims the feasibility evaluation of body car parts by sheet metal forming [1].
Currently, the technical and economic impact of these tools is considerable and seems likely to increase further in the near future. Therefore, it is mandatory to improve their reliability. The accuracy and robustness of these tools are controlled by many aspects, ranging from continuum mechanics, contact and friction, material behaviour modelling to numerical analysis. However, the quality of simulation results is strongly dependent on the accuracy of constitutive models to describe the thermo-mechanical behaviour of materials [2].

Constitutive modelling

Constitutive models provide the link between the deformations that a material undergoes and the resultant stresses. In the case of metal sheets, the thermo-mechanical behaviour is commonly described by phenomenological constitutive models which are of easy access in commercial simulation software. The complexity of these models depends on the type of phenomena they represent (e.g. hardening, anisotropy, temperature, and strain-rate dependence) and their flexibility to capture the exact behaviour of the material [3]. Therefore, phenomenological models can be complex non-linear equations with a large number of material-dependent parameters. Furthermore, constitutive models are not turn-key tools ready to be used in a numerical simulation tool. Indeed, a calibration process needs to be performed for the selected material, *i.e.* the material-dependent parameters need to be identified. As a result, the calibration process dictates the final accuracy of the constitutive model.

Calibration

The calibration process corresponds to the fitting of the response of the selected constitutive model to the experimental data representing the thermo-mechanical behaviour of the material. Consequently, the accuracy of the calibrated constitutive model is strictly related to the experimental data available for the process [4, 5]. In the context of non-linear constitutive models for the mechanical behaviour of

metal sheets, the classical procedures to acquire experimental data include tests of uniaxial tension, biaxial tension or hydraulic bulging and simple shear [2]. These tests are designed to have a single well-defined homogeneous strain state over a region of interest. Accordingly, it is straightforward to obtain the stress state that the material undergoes during the test. The main disadvantage of using these homogeneous tests is the required number of tests to collect a comprehensive experimental database. For example, anisotropic constitutive models or models that consider temperature and strain-rate effects require tests at different material orientations, or under different temperatures and strain-rates [6]. As a result, classical methods make the calibration process time consuming and costly. It is possible to resort to robot-assisted testing systems [7] to reduce the time, but this type of solutions requires a high initial investment and is not yet widespread in the field. Consequently, the unavailability of efficient procedures may precipitate numerical simulation software users to adopt erroneous solutions, such as using material parameters from a different material or material parameters from a calibration process with an insufficient amount of data. These solutions deteriorate the capabilities of constitutive models to represent the selected material and, consequently, the reliability of the simulation results [8].

New concept for calibration

There have been significant efforts to bring more efficient solutions to the problem of constitutive model calibration. The most promising solutions are based on the combination of full-field measurement techniques, heterogeneous tests, and inverse analysis [9]. This strategy relies on the fact that full-field measurement techniques have the ability to record the evolution of the displacements and strain fields at the surface of the specimens during a test. Additionally, heterogeneous tests, due to the non-uniform geometries or boundary conditions, may induce a large range of strains, strain-rates and temperatures in a specimen within a single test. The combination of full-field measurements and heterogeneous tests leads to more information on the thermo-mechanical behaviour of a material extracted from a single heterogeneous test when compared to classical procedures that use homogeneous tests. However, the analysis of heterogeneous displacements or strain fields requires inverse analysis methods to calibrate a constitutive model. These methods often rely on numerical simulation or principles from solid mechanics to transform the calibration process in an optimization problem [9, 10]. In addition to reducing the long experimental campaigns, this combination expands the analysis of experimental tests to higher levels of strain. This aspect is particularly important for accurate simulations in sheet metal forming processes. In this type of processes, the material undergoes high levels of deformation that go beyond the typical levels reached in homogeneous tests [11].

Challenges

Although significant progress has been made to prove the feasibility of this new calibration solution, there are still some challenges to be tackled in order to achieve widespread use in the scientific and industrial communities. The development of an efficient strategy to design heterogeneous tests is one of the challenges [12]. The objective is to reduce the number of experimental tests needed to calibrate a constitutive model without compromising the accuracy. Although some tests already presented in the literature offer a solution with reasonable results, there is still room for improvement and this is a research topic of growing interest [13–15]. The quantification of the sensitivity to measurement errors and how these errors propagate along the chain of the calibration process is also a challenge that remains unresolved. Finding a solution for this challenge is also an important aspect for the development of new tests and the assessment of the robustness of inverse analysis methods [16,17]. In the case of non-linear constitutive models, the calibration process ends with an optimisation problem, which typically is an ill-posed problem. Insufficient information in the experimental database contributes to this problem, but also the formulation of the constitutive models. In some cases, the universe of possible solutions for the material-dependent parameters includes solutions that violate physical constraints or represent homothetic solutions. Therefore, the identification of constraints to increase

the stability and robustness of the calibration results is also a problem that needs to be considered. The widespread of this solution is also hampered by complex implementation procedures in inverse methods and the absence of practical information. Currently, the inverse methods with the greatest impact are those that were born from simple ideas or those that the authors championed with the availability and dissemination of practical information on their implementation. Therefore, the development of practical guidelines and information on inverse methods is a topic of high importance to disseminate and have more acceptance in the scientific and industrial communities. Moreover, proving the relevance of this solution for constitutive models with increasing complexity, such as models that consider temperature and strain-rate effects, is also an open topic. To the best of author's knowledge, the combination of displacement or strain field measurements with temperature field measurements has not been largely explored.

1.2 Objectives and achievements

The driving force for the present thesis is the enhancement of the calibration process of constitutive models through the combination of full-field measurements, heterogeneous tests, and inverse analysis. Within this context, the aim of this thesis is the development of a calibration methodology for constitutive models that consider temperature and strain-rate effects on the mechanical behaviour of sheet metals. A thermo-mechanical heterogeneous test is analysed and coupled with two different inverse analysis methods, the Virtual Fields Method and Finite Element Model Updating.
However, on the way towards the main objective, some of the challenges mentioned above have been met. Therefore, this thesis also aims at contributing to the global issue of calibration of constitutive models with insights on the implementation and comparison of inverse analysis methods in the framework of linear elasticity and non-linear plasticity models. Furthermore, more focused on a specific inverse method, the Virtual Fields Method, this thesis aims at contributing to improve and expand the frontiers of application of this method. A new methodology to calibrate anisotropic plasticity models with a single biaxial test and the Virtual Fields Method is analysed. The application of constraints on constitutive models is also addressed in this analysis. Moreover, the selection of the number of virtual fields, a critical aspect of the method, is explored in the calibration of anisotropic plasticity models. A previously optimized heterogeneous test is coupled with the Virtual Fields Method to calibrate an anisotropic plasticity model.

1.3 List of publications and developed tools

This thesis is composed of six papers that represent contributions to the scientific community made via international journals and conference proceedings. These are listed below:

[**P1**] J.M.P. Martins, A. Andrade-Campos, S. Thuillier, Comparison of inverse identification strategies for constitutive mechanical models using full-field measurements, International Journal of Mechanical Sciences, 145, 330-345, 2018.

[**P2**] J.M.P. Martins, S. Thuillier, A. Andrade-Campos, Identification of material parameters for plasticity models: A comparative study on the finite element model updating and the virtual fields method, AIP Conference Proceedings, 1960(1), 110007, 2018.

[**P3**] J.M.P. Martins, A. Andrade-Campos, S. Thuillier, Calibration of anisotropic plasticity models using a biaxial test and the virtual fields method, International Journal of Solids and Structures, 172–173(1), 21-37, 2019.

[**P4**] J.M.P. Martins, S. Thuillier, A. Andrade-Campos, Calibration of Anisotropic Plasticity Models with an Optimized Heterogeneous Test and the Virtual Fields Method, Thermomechanics &

Infrared Imaging and Inverse Problems, Conference Proceedings of the Society for Experimental Mechanics Series, Springer, 6, 2020.

[**P5**] J.M.P. Martins, A. Andrade-Campos, S. Thuillier, Calibration of Johnson-Cook Model Using Heterogeneous Thermo-Mechanical Tests, Procedia Manufacturing, 47, 881-888, 2020.

[**P6**] J.M.P. Martins, S. Thuillier, A. Andrade-Campos, Calibration of a thermo-mechanical constitutive model using the VFM and a heterogeneous test. To be submitted.

This work also leaves a few contributions in terms of software tools, which constitute a solid base for future work. These contributions include subroutines written in fortran for the different inverse methods, Matlab scripts for post-processing of experimental data and UMAT subroutines for anisotropic elasto-plasticity models and thermo-elasto-plasticity models.

1.4 Structure of the thesis

Following this general introduction, this thesis is organized in five main chapters. Chapter 2 consists of a paper presenting an overview of four well-known inverse analysis methods, namely the Finite Element Model Updating, the Constitutive Equation Gap Method, the Equilibrium Gap Method, and the Virtual Fields Method [**P1**]. This paper provides a detailed discussion on the advantages and disadvantages of these methods, implementation details and a comparative study in the framework of infinitesimal strains for linear elasticity and non-linear plasticity. Chapter 3 is composed of three papers. The first section consists of a comparative study on the Finite Element Model Updating and the Virtual Fields Method, in the framework of finite strains for non-linear plasticity [**P2**]. The second and third sections focus exclusively on the Virtual Fields Method. In the second section, a single biaxial test and the Virtual Fields Method are analysed in the calibration of anisotropic plasticity models [**P3**]. In the third section, the combination of the Virtual Fields Method and a previously optimised heterogeneous test is also evaluated in the calibration of an anisotropic plasticity model [**P4**]. Chapter 4 is dedicated to the calibration of thermo-mechanical constitutive models using a thermo-mechanical heterogeneous test and two inverse analysis methods, the Virtual Fields Method and the Finite Element Model Updating. Two papers compose this chapter. The first section consists of a virtual analysis on the application of the Finite Element Model Updating to explore this heterogeneous test [**P5**]. The second section presents an experimental database obtained from this heterogeneous test. Its combination with the Virtual Fields Method to calibrate a modified version of the well-known Johnson-Cook model is analysed [**P6**]. Chapter 5 presents the conclusions and perspectives for future work on the topic of calibration of constitutive models.

Chapter 2

State-of-the-art on inverse analysis methods

The development of inverse analysis methods for the calibration of constitutive models has been a prolific research area, and as a result, an interesting number of methods based on full-field measurements was proposed. However, the dissemination and widespread use of inverse analysis methods need to be reinforced by bridging the gap between theory and implementation procedure. Moreover, a performance evaluation study under the same conditions is essential to guide the end-users in the selection of the proper method.

2.1 Comparison of inverse identification strategies for constitutive mechanical models using full-field measurements

This section provides an overview of four inverse analysis methods, namely the Finite Element Model Updating, the Constitutive Equation Gap Method, the Equilibrium Gap Method and the Virtual Fields Method. The implementation of each method is presented with the aid of flowcharts representing the algorithms. The pros and cons of each method are also discussed, and a comparative study on linear elasticity and non-linear plasticity under the same conditions is presented. This comparative study focuses on the accuracy of each method, with and without the presence of noise, and on computational performance. A simple numerical example is introduced to compare the methods.

International Journal of Mechanical Sciences 145 (2018) 330–345

Contents lists available at ScienceDirect

International Journal of Mechanical Sciences

journal homepage: www.elsevier.com/locate/ijmecsci

Comparison of inverse identification strategies for constitutive mechanical models using full-field measurements

J.M.P. Martins[a,b,*], A. Andrade-Campos[a], S. Thuillier[b]

[a] Centre for Mechanical Technology and Automation (TEMA), GRIDS Research Unit, Mechanical Engineering Department, University of Aveiro, Portugal
[b] Univ. Bretagne Sud, UMR CNRS 6027, Lorient, IRDL F-56100, France

ARTICLE INFO

MSC:
00-01
99-00

Keywords:
Parameter identification
Inverse problem
Full-field measurements
Finite element method
Linear elasticity
Elasto-plasticity

ABSTRACT

The calibration of phenomenological constitutive material models has been a constant need, because the parameters differ for each material and the ability of a model to mimic the real behaviour of a material is highly dependent on the quality of these parameters. Classically, the parameters of constitutive models are determined by standard tests under the assumption of homogeneous strain and stress fields in the zone of interest. However, in the last decade, Digital Image Correlation techniques and full-field measurements have enabled the development of new parameter identification strategies, such as the Finite Element Model Updating, the Constitutive Equation Gap Method, the Equilibrium Gap Method and the Virtual Fields Method. Although these new strategies have proven to be effective for linear and non-linear models, the implementation procedure for some of them is still a laborious task. The aim of this work is to give a detailed insight into the implementation aspects and validation of these methods. Detailed flowcharts of each strategy, focusing on the implementation aspects, are presented and their advantages and disadvantages are discussed. Moreover, these modern strategies are compared for the cases of homogeneous isotropic linear elasticity and isotropic plasticity with isotropic hardening. A simple numerical example is used to validate and compare the different strategies.

1. Introduction

With the innovation surge currently happening in industry, reliable and fast solutions for engineering problems are more important than ever. Numerical simulation has been a valuable tool for their resolution and is now well-established. However, it is essential for these tools to keep a continuous improvement of their predictive capabilities. One of the areas for potential improvement is mechanical modelling of materials and the respective calibration procedure. The quest for more accurate models has been particularly intense regarding the elasto-plastic behaviour of sheet metals. Indeed, many advanced and more complex mechanical models have been developed to accurately describe phenomena such as hardening and anisotropy. However, this increase in complexity usually means a tedious process of parameter calibration, due to long experimental campaigns. For example, the yield criterion Yld2000 [1] depends on 8 material parameters, which requires three uniaxial yield stresses and three uniaxial anisotropy coefficients, the biaxial yield stress and anisotropy coefficient. Consequently, in industrial practice, simpler models are still preferred to avoid such experimental campaign and complex identification process [2]. Therefore, there is a clear demand for new processes of calibration that can simplify the experimental campaign without compromising the accuracy of the models.

Nowadays, there are two main approaches to conduct the identification process: a classical approach and a more recent one based on full-field measurements [3,4]. The classical approach relies on simple tests, that provide near homogeneous strain and stress states over the zone of interest. It is taken advantage of this homogeneity to retrieve the material parameters from simple analytical solutions. This kind of approach has several drawbacks, i.e.: (i) the limited exploitation of experimental tests, since homogeneous stress and strain state assumption can no longer be used after the onset of necking; (ii) the large number of tests required when complex constitutive models have to be calibrated; and (iii) the stress and strain fields do not resemble the ones obtained in forming operations.

The second approach is increasingly being used, mainly because of the rapid development of full-field measurements techniques, such as digital image correlation [5]. These techniques allow a more flexible design of mechanical tests and take advantage of the heterogeneous displacement/strain fields [6]. Indeed, due to the heterogeneity, each material point experiences a different stress and strain history, hence the

* Corresponding author at: Centre for Mechanical Technology and Automation (TEMA), GRIDS Research Unit, Mechanical Engineering Department, University of Aveiro, Portugal.
E-mail addresses: joao.martins52@ua.pt (J.M.P. Martins), gilac@ua.pt (A. Andrade-Campos), sandrine.thuillier@univ-ubs.fr (S. Thuillier).

https://doi.org/10.1016/j.ijmecsci.2018.07.013
Received 20 February 2018; Received in revised form 11 July 2018; Accepted 14 July 2018
Available online 19 July 2018

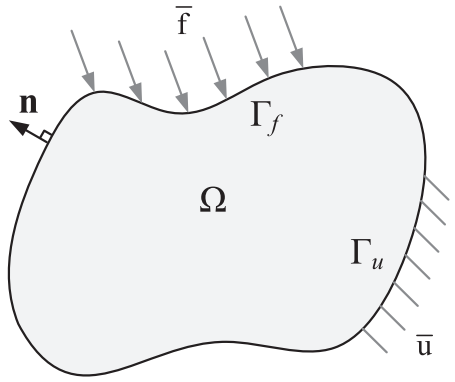

Fig. 1. Domain Ω with prescribed displacement and traction boundary conditions.

number of material parameters governing the field is generally greater than those driving homogenous strain fields [7]. Therefore, this second approach enables to reduce the number of experiments required to calibrate a model. Furthermore, it enables to extend the exploitation limits of a test, since the heterogeneous fields are no longer a problem. However, effective inverse strategies to extract the material parameters from full-field measurements are required.

Accordingly, the development of inverse strategies in computational mechanics has evolved rapidly in recent years, leading to an interesting number of strategies based on full-field measurements, e.g. [3,4,8,9]. The most well-known methods are the Finite Element Model Updating (FEMU) [10], the Constitutive Equation Gap Method (CEGM) [11], the Equilibrium Gap Method (EGM) [12,13] and the Virtual Fields Method (VFM) [14]. These four strategies prove to be effective in identifying parameters associated with linear and non-linear models and, therefore, these will be the focus of this work. However, it should also be mentioned that more strategies have emerged recently with promising results, such as the Constitutive Compatibility Method (CCM) [15], the Dissipation Gap Method [16], the Self-Optimizing Method (Self-OPTIM) [17] and the Integrated Digital Image Correlation Method (Integrated-DIC) [18].

To the best of the authors knowledge, studies on the implementation aspects of these strategies, as well as comparative studies, are rare, specially in elasto-plasticity. Since the mentioned strategies rely on different principles, it is interesting to evaluate their performance in the same conditions, as well as their sensitivity to noise. Thus, the aim of this study is to introduce the four strategies mentioned above, discuss the implementation details and finally, present a comparative study for quasi-static loading conditions. For the sake of simplicity, the scope of this study lies within the framework of infinitesimal small strains. The extension to large strains can be tedious [19,20], with the exception of FEMU, and is out of the scope of this article.

The outline of this work is as follows. A brief description of the inverse problem and the constitutive models used in this study is presented in Section 2. The four inverse strategies selected, FEMU, CEGM, EGM and VFM, are presented in Section 3, as well as flowcharts for each one and a discussion of the main advantages and drawbacks. Finally, in Section 4, the performance of these strategies is compared for two different constitutive models. This performance study starts with a simple case of an isotropic linear elastic model that is afterwards extended for an elasto-plastic model with isotropic non-linear hardening. Moreover, the comparative studies are performed with and without noise.

2. Identification/inverse problem

Consider a continuum solid body whose reference configuration occupies the domain Ω and is bounded by $\partial\Omega$ (see Fig. 1). It is assumed that the material within the domain Ω is homogeneous. The boundary of this body is composed of two sub-boundaries Γ_f and Γ_u, such that $\partial\Omega = \Gamma_f \cup \Gamma_u$ and $\Gamma_f \cap \Gamma_u = \emptyset$. A surface external force is prescribed over Γ_f, possibly with a null value, and a displacement field is prescribed over Γ_u. Neglecting the body forces and assuming static equilibrium, a linear elastic behaviour and infinitesimally small displacements, the mechanical state of the body is governed by three sets of equations: the equilibrium equations,

$$\begin{cases} \mathrm{div}\boldsymbol{\sigma} = 0 & \text{in } \Omega, \\ \boldsymbol{\sigma}\cdot\mathbf{n} = \bar{\mathbf{f}} & \text{on } \Gamma_f, \end{cases} \tag{1}$$

the kinematic compatibility equations,

$$\begin{cases} \boldsymbol{\varepsilon} = \frac{1}{2}\left(\nabla\mathbf{u}(\mathbf{x}) + \nabla^{\mathrm{T}}\mathbf{u}(\mathbf{x})\right) & \text{in } \Omega, \\ \mathbf{u} = \bar{\mathbf{u}} & \text{on } \Gamma_u, \end{cases} \tag{2}$$

and the constitutive equation,

$$\boldsymbol{\sigma} = \mathbf{C} : \boldsymbol{\varepsilon} \qquad \text{in } \Omega, \tag{3}$$

where $\boldsymbol{\sigma}$ denotes the Cauchy stress tensor, $\bar{\mathbf{f}}$ is the prescribed vector of external forces over Γ_f, $\mathbf{u}$ is the displacement vector field, $\bar{\mathbf{u}}$ is the prescribed displacement vector field over Γ_u, $\boldsymbol{\varepsilon}$ is the infinitesimal strain tensor and $\mathbf{n}$ the unit normal vector to $\partial\Omega$.

The stress and strain are related through Eq. (3), for which $\mathbf{C}$ is the constitutive material tensor. It is assumed to be function of a vector that gathers all the unknown constitutive material parameters $\boldsymbol{\xi} = \{\xi_1, \ldots, \xi_n\}$ (n is the number of material parameters). In case of isotropic linear elastic behaviour, $\mathbf{C}(\boldsymbol{\xi})$ represents the Hooke's elasticity tensor and $\boldsymbol{\xi}$ contains two parameters: Poisson's ratio ν and Young's modulus E, $\boldsymbol{\xi} = \{\nu, E\}$, respectively.

For the direct problem of continuum mechanics, the initial shape of the solid body, the material parameters and the set of boundary conditions, $\bar{\mathbf{f}}$ and $\bar{\mathbf{u}}$, are assumed to be known. Accordingly, the unknowns are the fields $(\mathbf{u}, \boldsymbol{\varepsilon}, \boldsymbol{\sigma})$, which must satisfy the three previous sets of Eqs. (1), (2) and (3). For the inverse problem of parameter identification using full-field measurements, the aim is to retrieve the material parameters given a discrete observation of the displacement field $\hat{\mathbf{u}}$ and information concerning the boundary conditions, $\bar{\mathbf{f}}$ and $\bar{\mathbf{u}}$. The measured displacement field $\hat{\mathbf{u}}$ can be obtained, for instance, through a non-contact measurement technique, such as DIC, and the strain field required to calculate the stress field can be calculated using Eq. (2). The idea behind the inverse problem is to explore an implicit relationship between the measured displacement field and the parameters of the constitutive model.

Typically, full-field measurements are performed on the surface of the body and this limits the identification through the volume. Therefore, the inverse problem in linear and non-linear cases is usually seen as a in-plane problem, for which the plane stress assumption can be adopted. This assumption implies that the body with domain Ω is a thin flat body, with volume V and a constant thickness t that is assumed much smaller than the other dimensions. Furthermore, the body only undergoes in-plane loading.

For the case of non-linear elasto-plastic behaviour, the linear relationship between stress and strain is no longer valid, and the constitutive equations are obtained within the classical incremental theory of plasticity. In the following, these equations are briefly recalled.

Consider the additive decomposition of the total strain tensor increment $d\boldsymbol{\varepsilon}$, in terms of elastic $d\boldsymbol{\varepsilon}^{\mathrm{e}}$ and plastic $d\boldsymbol{\varepsilon}^{\mathrm{p}}$ components, which can be written as

$$d\boldsymbol{\varepsilon} = d\boldsymbol{\varepsilon}^{\mathrm{e}} + d\boldsymbol{\varepsilon}^{\mathrm{p}}. \tag{4}$$

Moreover, consider an hypoelastic relationship to describe the stress-strain relation, as follows

$$d\boldsymbol{\sigma} = \mathbf{C} : \left(d\boldsymbol{\varepsilon} - d\boldsymbol{\varepsilon}^{\mathrm{p}}\right), \tag{5}$$

where $d\boldsymbol{\sigma}$ is the stress increment. The plastic strain increment $d\boldsymbol{\varepsilon}^{\mathrm{p}}$ can be defined by means of three key concepts: a yield criterion, a hardening

law and a plastic flow rule. The von Mises yield criterion is adopted here, thus the yield condition can be expressed as

$$f(\boldsymbol{\sigma}, \bar{\varepsilon}^{\mathrm{p}}) = \bar{\sigma}(\boldsymbol{\sigma}) - \sigma_y\left(\bar{\varepsilon}^{\mathrm{p}}\right) = 0, \tag{6}$$

where $\sigma_y(\bar{\varepsilon}^{\mathrm{p}})$ is the yield stress as a function of the equivalent plastic strain $\bar{\varepsilon}^{\mathrm{p}}$ and $\bar{\sigma}(\boldsymbol{\sigma})$ is the equivalent von Mises stress, which under plane stress conditions assumes the following form

$$\bar{\sigma}(\boldsymbol{\sigma}) = \sqrt{\frac{3}{2}\boldsymbol{\sigma}'(\boldsymbol{\sigma}) : \boldsymbol{\sigma}'(\boldsymbol{\sigma})} = \sqrt{\sigma_{xx}^2 + \sigma_{yy}^2 - \sigma_{xx}\sigma_{yy} + 3\sigma_{xy}^2}, \tag{7}$$

where $\boldsymbol{\sigma}'(\boldsymbol{\sigma})$ is the deviatoric stress tensor and σ_{xx}, σ_{yy} and σ_{xy} are the components of the stress tensor. The evolution of the yield stress is governed by the Swift's isotropic hardening law, with the following form

$$\sigma_y\left(\bar{\varepsilon}^{\mathrm{p}}\right) = K\left(\varepsilon_0 + \bar{\varepsilon}^{\mathrm{p}}\right)^n, \tag{8}$$

which depends on three material parameters, K, ε_0 and n.

The classical associated flow rule is adopted, which can be introduced as

$$d\boldsymbol{\varepsilon}^{\mathrm{p}} = d\lambda\frac{\partial f}{\partial \boldsymbol{\sigma}}, \tag{9}$$

it defines the plastic strain increment. The direction of the plastic flow is defined by the term $\partial f/\partial\boldsymbol{\sigma}$ and the magnitude is given by the plastic multiplier $d\lambda$. Based on this, Eq. (5), which gives the stress increment, can be updated to

$$d\boldsymbol{\sigma} = \mathbf{C} : \left(d\boldsymbol{\varepsilon} - d\lambda\frac{\partial f}{\partial \boldsymbol{\sigma}}\right). \tag{10}$$

For the von Mises yield criterion, the plastic multiplier is equivalent to the increment in the equivalent plastic strain $d\bar{\varepsilon}^{\mathrm{p}}$ [21], which is defined as

$$d\bar{\varepsilon}^{\mathrm{p}} = \sqrt{\frac{2}{3}d\boldsymbol{\varepsilon}^{\mathrm{p}} : d\boldsymbol{\varepsilon}^{\mathrm{p}}}. \tag{11}$$

The plastic multiplier is explicitly determined using the consistency condition, which imposes that the current stress state remains on the yield surface after yielding and can be written as

$$df = \frac{\partial f}{\partial \boldsymbol{\sigma}} : d\boldsymbol{\sigma} + \frac{\partial f}{\partial \bar{\varepsilon}^{\mathrm{p}}} : d\bar{\varepsilon}^{\mathrm{p}} = 0. \tag{12}$$

By replacing the stress increment (Eq. (10)) in the consistency condition (Eq. (12)) and after some algebra manipulation, the plastic increment can be explicitly obtained:

$$d\lambda = \frac{\frac{\partial f}{\partial \boldsymbol{\sigma}} : \mathbf{C} : d\boldsymbol{\varepsilon}}{\frac{\partial f}{\partial \boldsymbol{\sigma}} : \mathbf{C} : \frac{\partial f}{\partial \boldsymbol{\sigma}} - \frac{\partial f}{\partial \bar{\varepsilon}^{\mathrm{p}}}\sqrt{\frac{2}{3}\frac{\partial f}{\partial \boldsymbol{\sigma}} : \frac{\partial f}{\partial \boldsymbol{\sigma}}}} \tag{13}$$

Finally, Eq. (10) for the stress increment can be updated and gives

$$d\boldsymbol{\sigma} = \left(\mathbf{C} - \frac{\frac{\partial f}{\partial \boldsymbol{\sigma}} : \mathbf{C}\otimes\mathbf{C} : \frac{\partial f}{\partial \boldsymbol{\sigma}}}{\frac{\partial f}{\partial \boldsymbol{\sigma}} : \mathbf{C} : \frac{\partial f}{\partial \boldsymbol{\sigma}} - \frac{\partial f}{\partial \bar{\varepsilon}^{\mathrm{p}}}\sqrt{\frac{2}{3}\frac{\partial f}{\partial \boldsymbol{\sigma}} : \frac{\partial f}{\partial \boldsymbol{\sigma}}}}\right) : d\boldsymbol{\varepsilon} \tag{14}$$

or

$$d\boldsymbol{\sigma} = \mathbf{C}^{\mathrm{ep}} : d\boldsymbol{\varepsilon}, \tag{15}$$

where $\mathbf{C}^{\mathrm{ep}}$ is the so-called elasto-plastic tangent stiffness matrix. This matrix is a function of the unknown material parameters, so it can be defined as function of the material parameters $\mathbf{C}^{\mathrm{ep}}(\boldsymbol{\xi})$. For this elasto-plastic model, the material parameters vector gathers five parameters $\boldsymbol{\xi} = \{\nu, E, K, \varepsilon_0, n\}$.

In this case, the inverse problem must take into account the history dependent behaviour of plasticity. Therefore, deformation history during the experiment must be acquired, which means measurements of displacement field for different time instants $\hat{\mathbf{u}}(\mathbf{x}, t)$ (for which $t \in [0, T]$) must be performed and used to solve the inverse problem. Thus, the total strain is discretized along the time, as well as the boundary conditions.

3. Inverse strategies based on full-field measurements

3.1. Finite element model updating

Among all inverse strategies available for identifying material parameters, Finite Element Model Updating (FEMU) is the most used. Since the introduction of this strategy by Kavanag and Clough [10], a significant number of studies have been published. It was used with a wide range of models, e.g. elasticity [22,23], plasticity with emphasis on sheet metal forming [3,24–26] and viscoplasticity [27,28].

The idea behind this strategy is to infer the unknown material parameters after comparing numerical predictions with experimental measurements. Therefore, it requires a finite element (FE) model of the mechanical test, to generate numerical predictions of the response of the material. Based on the comparison between experimental and numerical data and by means of an optimization method, the material parameters are adjusted iteratively until the numerical results match the experimental ones as closely as possible.

The data used with this strategy can be of different kinds: displacements, strains, force, temperatures, etc. FEMU is easily adapted to the available experimental data. In fact, it is not mandatory to use full-field measurements with FEMU, partial measurements of the complete field can also be used. The choice of the data has been a widely discussed subject on this strategy and the literature reveals a lack of consensus [3]. Another widely discussed point is how the experimental data are compared with the numerical data. This comparison is usually performed using an objective function that evaluates the gap between experimental and numerical results. However, this objective function can assume different formulations [29,30]. An example of an objective function based on the measured strains on the surface of the sample can be defined as

$$\mathcal{F}_{\mathrm{FEMU}}(\boldsymbol{\xi}) = \sum_{i=1}^{n_{\mathrm{s}}}\sum_{j=1}^{n_{\mathrm{p}}}\left[\left(\hat{\varepsilon}_{xx} - \varepsilon_{xx}(\boldsymbol{\xi})\right)_j^2 + \left(\hat{\varepsilon}_{yy} - \varepsilon_{yy}(\boldsymbol{\xi})\right)_j^2 + \left(\hat{\varepsilon}_{xy} - \varepsilon_{xy}(\boldsymbol{\xi})\right)_j^2\right]_i. \tag{16}$$

This objective function is formulated based on the sum of the squares of the gap between experimental $(\hat{\varepsilon}_{xx}, \hat{\varepsilon}_{yy}, \hat{\varepsilon}_{xy})$ and numerical (ε_{xx}, ε_{yy}, ε_{xy}) data, considering the different components of the in-plane strain tensor. The experimental data (full strain field) are usually made of a discrete number of values representing the measurement points on the surface of the sample for different time instants ($\hat{\varepsilon}(\mathbf{x}, t)$). The variables n_{p} and n_{s}, in Eq. (16), represent the number of measurement points on the surface of the sample and the number of time instants for which measurements are performed, respectively.

It is a common practice to use weighting coefficients in the formulation of the objective function (e.g. [31]), but their selection is not intuitive and usually depends on the user [30]. Therefore, the use of weights will be avoided in this work.

Another important remark regarding the evaluation of the objective function is that the numerical data must be calculated at the exact same locations as the experimental points. Otherwise, the numerical data must be interpolated to match these locations.

A detailed flowchart for FEMU strategy is presented in Fig. 2. In the flowchart, B.C. stands for boundary conditions. It starts with an initial set of material parameters ($\boldsymbol{\xi}^{\mathrm{i}}$) arbitrarily chosen used to run the first FE analysis. The evaluation of the objective function is then performed. If the value of the objective function is above a threshold value, the iterative process starts and the optimization method generates a new (or updated) set of material parameters ($\boldsymbol{\xi}^{\mathrm{u}}$). The process is repeated until the value of the objective function reaches a value below the threshold or until the set of parameters stagnates. The threshold value is defined by the user and represents the admissible global gap between numerical and experimental results.

Within the iterative cycle of FEMU, the update of the material parameters is performed by searching for a minimum in the objective func-

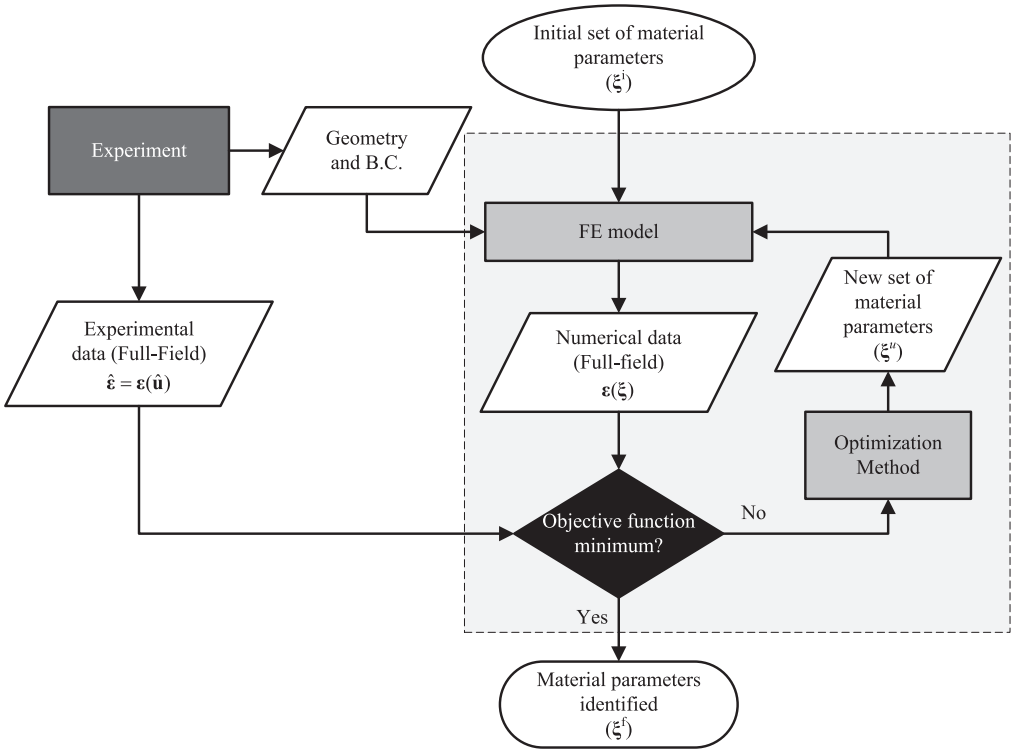

Fig. 2. Detailed flowchart for the FEMU.

tion. Coupling an optimization method with the objective function is the usual way to do it. The type of optimization methods used in this kind of problem lies within two main families: (i) the gradient-based methods (e.g. the Gauss-Newton method or the Levenberg–Marquardt method) and (ii) the direct methods (e.g. evolutionary and simplex) [3,30,32]. The first family of methods is the most used. It requires the value of the objective function and its gradient to take a decision, whereas the direct methods only use the value of the objective function. The use of gradient-based methods is related to its computational efficiency, since they usually require less evaluations of the objective function. However, this type of methods has a major disadvantage. They do not guarantee the location of the global minimum and depend on the initial set of material parameters chosen to initiate the identification procedure [25]. Other methods that will be described also require the coupling with optimization methods, so whenever invoked in the context of other methods the reader can review this section.

As mentioned before, FEMU is not limited to full-field measurements, which gives an even wider range of applications. Another important feature of FEMU is that it can be adapted to complex specimen shapes and loads. For instance, a curved sample cut from a coil steel [33]. These advantages and the ease of the implementation make FEMU very attractive. However, the major drawback that has been pointed out over the years and that motivated researchers to develop other strategies is the excessive computational cost (e.g. [34]), consequence of the FE analysis at each evaluation of the objective function. In addition, the analysis requires a FE model that represents the experimental test as close as possible to reality, which can be difficult to attain depending on the geometry and load conditions. However, it is strictly necessary to avoid undesired errors. Moreover, the results can also be mesh sensitive, which is an aspect inherent to every method that makes use of FE analysis.

3.2. Constitutive equation gap method

The Constitutive Equation Gap Method (CEGM) (also called as, Error in the Constitutive Equation) was first proposed by Ladevèze and Leguillon [11], as an error estimation procedure for FE analysis. It was applied in a variety of fields [35,36], before being adapted to identify material parameters of an elastic isotropic model based on full-field measurements [37], with significant efforts for heterogeneous materials [38,39]. More recently, Guchhait and Banerjee [40] extended it for anisotropic elasticity. Moreover, it has also been used in the field of plasticity [41] and damage [42].

CEGM objective function is based on the evaluation of the error between a statically admissible stress field, denoted $\boldsymbol{\tau}$, and a stress field calculated from a measured displacement/strain field $\hat{\boldsymbol{\varepsilon}} = \boldsymbol{\varepsilon}(\hat{\mathbf{u}})$ and a chosen constitutive model. This error is quantified by means of an energy norm. In the case of linear elasticity, it leads to the following objective function

$$\mathcal{F}_{\mathrm{CEGM}}(\boldsymbol{\tau}, \boldsymbol{\xi}) = \frac{1}{2}\int_{\Omega} [\boldsymbol{\tau} - \mathbf{C}(\boldsymbol{\xi}) : \hat{\boldsymbol{\varepsilon}}] : \mathbf{C}^{-1}(\boldsymbol{\xi}) : [\boldsymbol{\tau} - \mathbf{C}(\boldsymbol{\xi}) : \hat{\boldsymbol{\varepsilon}}] \mathrm{d}\Omega, \tag{17}$$

If the statically admissible stress field describes correctly the stress state of the body and the material parameters fit the description of the material behaviour, the objective function value should be close to zero.

The flowchart for the CEGM is presented in Fig. 3. The first step is to define an initial set of material parameters ($\boldsymbol{\xi}^{\mathrm{i}}$), followed by the determination of a statically admissible stress field with this initial set of material parameters. Then, the objective function is evaluated. If its value is above a threshold the optimization method generates a new set of material parameters ($\boldsymbol{\xi}^{\mathrm{u}}$). This process is repeated until the value of the objective function reaches a value below the threshold or until the process stagnation. After that, the statically admissible stress field is updated. It is updated in accordance with a user-defined criterion and using the new set of material parameters. The whole process is repeated again for the new statically admissible stress field. The convergence criterion for the statically admissible stress field can be checked by comparing the stress in the current and the last iteration [41].

The statically admissible stress field $\boldsymbol{\tau}$ is a key requisite of this strategy. This stress field must verify the force boundary conditions of the experimental test, as well as the equilibrium equation (Eq. (1)). It can be determined, for specific geometries and boundary conditions, by an an-

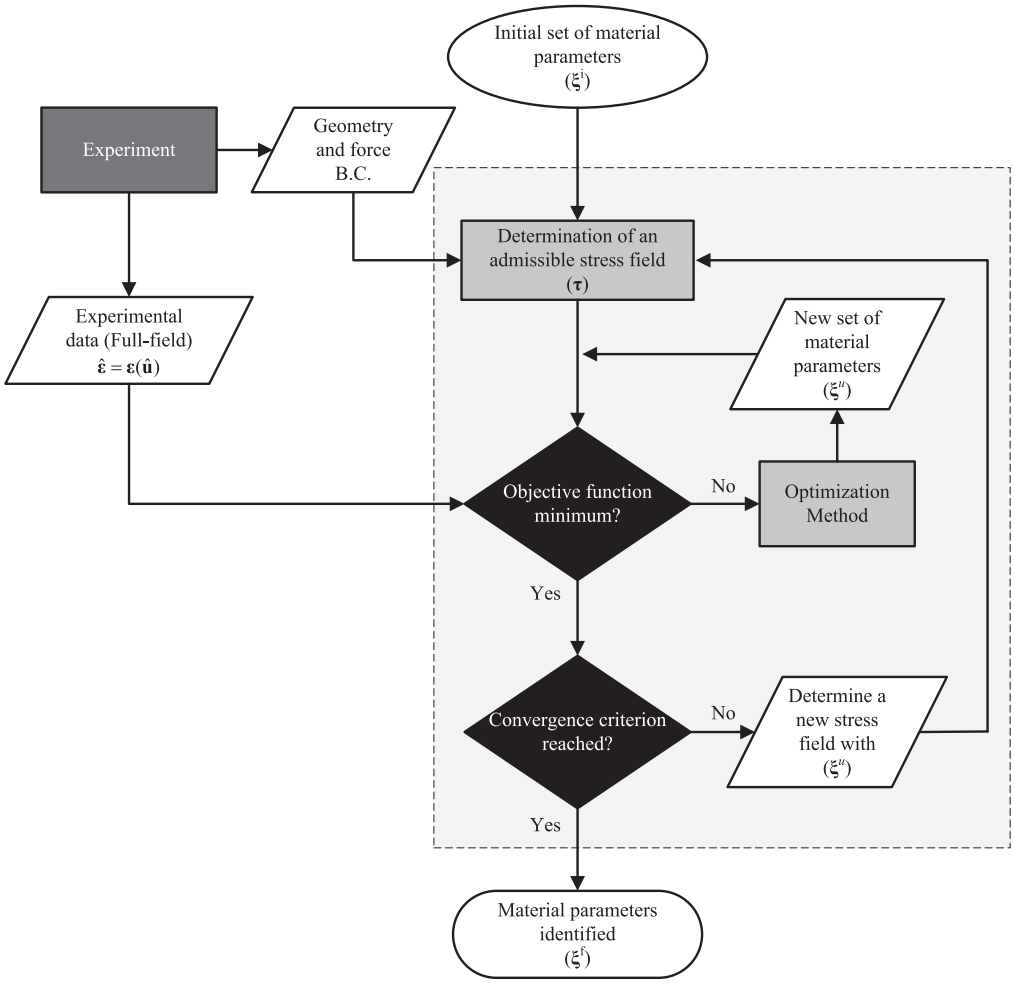

Fig. 3. Detailed flowchart for the CEGM.

alytic solution or, in a more general way, through a FE model [42]. Special techniques have also been developed to determine it when heterogeneous materials are analyzed [38,39]. In the present work, a FE model is adopted and the determination of the statically admissible stress field is performed before the minimization of the objective function (Fig. 3) . Note that, in case of homogeneous materials the admissible stress field is uniquely determined by the force boundary conditions, *i.e.*, it is independent of the material parameters. Therefore, it is not required to update it along the process.

Regarding the implementation of the CEGM, Eq. (17) can be converted into a more practical form which benefits from the discrete nature of experimental measurements acquired, for example, by DIC. In fact, displacements or strain fields are measured in a discrete number of points, which are usually associated with a mesh that results from a non-overlapping decomposition of the surface of the domain Ω. Therefore, each measurement point is representative of a small area or small element in this mesh. Moreover, measurements are acquired for a finite number of time instants during the experimental test. Considering this discrete nature of experimental measurements, the objective function (Eq. (17)) can be rewritten as follows

$$\mathcal{F}_{\mathrm{CEGM}}(\boldsymbol{\tau},\boldsymbol{\xi}) = \frac{1}{2}\sum_{i=1}^{n_s}\left[t\sum_{j=1}^{n_p} A_j \left\{\left[\boldsymbol{\tau}_j - \mathbf{C}(\boldsymbol{\xi}):\hat{\boldsymbol{\varepsilon}}_j\right]:\mathbf{C}^{-1}(\boldsymbol{\xi}):\left[\boldsymbol{\tau}_j - \mathbf{C}(\boldsymbol{\xi}) : \hat{\boldsymbol{\varepsilon}}_j\right]\right\}\right]_i, \tag{18}$$

where A_i is the representative area of each measurement point. Eq. (17) is integrated over the volume, but as plane stress conditions are assumed, the stress distribution is considered constant through the thickness t of the body. Note that the same mesh can be used to determine the statically admissible stress field, thus preventing an additional step for interpolation.

Until now CEGM has been described with focus on linear elasticity. Concerning the identification of material parameters for non-linear models, the determination or reconstruction of the stress field from the measured displacement/strain field is more challenging than in linear elasticity, due to the history dependent behaviour. In this case, a stress update algorithm to reconstruct the actual stress field is required. It is a common point with other identification strategies and FE codes, thus, different algorithms have been proposed, e.g. [9,20,43]. Here, considering the assumptions of Section 2 for plane stress elasto-plasticity, it will be adopted an implicit backward-Euler algorithm presented in [44]. This step is included in the evaluation of the objective function, hence the flowchart presented in Fig. 3 is also valid for the non-linear case. However, the objective function (Eq. (17)) assumes a different form, as follows

$$\mathcal{F}_{\mathrm{CEGM}}(\boldsymbol{\tau},\boldsymbol{\xi}) = \sum_{i=1}^{n_s}\left(\frac{1}{2}\int_{\Omega}[\boldsymbol{\tau} - \boldsymbol{\sigma}(\boldsymbol{\xi},\hat{\boldsymbol{\varepsilon}})] : \mathbf{C}^{-1} : [\boldsymbol{\tau} - \boldsymbol{\sigma}(\boldsymbol{\xi},\hat{\boldsymbol{\varepsilon}})]\mathrm{d}\Omega\right)_i. \tag{19}$$

The stress field $\boldsymbol{\sigma}(\boldsymbol{\xi},\hat{\boldsymbol{\varepsilon}})$ is now calculated by the stress update algorithm, taking into account the history dependent behaviour of plasticity. This formulation differs from the ones presented in [41], because it uses the inverse of the elastic stiffness matrix instead of the elasto-plastic tangent/secant stiffness matrices. This kind of formulation can be used when elastic material parameters are known *a priori*.

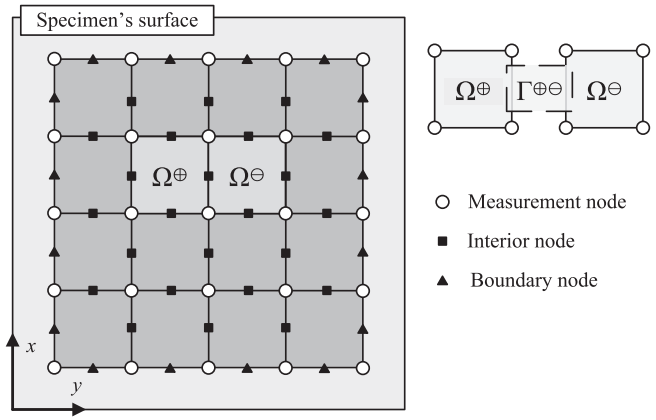

Fig. 4. Specimen's surface and measurement grid with the localization of the calculation points (adapted from [38]).

Regarding the advantages of CEGM, it can be applied to any constitutive model, although proper algorithms must be implemented to reconstruct the stress field from the measured data. Moreover, as FEMU, it is not restricted to full-field measurements [32]. The major drawback of CEGM is the calculation of a statically admissible stress field. It can be a laborious task, particularly when a heterogeneous distribution of the material properties is considered. When a FE model is used to generate this stress field, CEGM is affected by the same drawbacks related to the construction of a FE model. Compared with FEMU, it requires a lower number of simulations. Consequently, in terms of computational cost, CEGM is more efficient than FEMU. However, the implementation of the algorithm (Fig. 3) is not so intuitive as the one of FEMU (Fig. 2).

3.3. Equilibrium gap method

The Equilibrium Gap Method (EGM) was first proposed by Claire et al. [12,13] with the aim of identifying isotropic damage fields in heterogeneous materials resorting only to full-field measurements (the force boundary conditions were not taken into account). In this first attempt, the degradation of the elastic stiffness depended on a damage scalar variable [12,13]. Roux and Hild extended this method to more complex damage laws [45]. Later, Périé et al. [46] have proposed the extension of EGM to anisotropic damage. Moreover, Florentin and Lublineau [38] have used EGM as a reference to compare with CEGM in the identification of isotropic elastic parameters in heterogeneous materials. Although it has not yet been extended to elasto-plasticity, it could be performed by means of a method that captures the history dependent behaviour of non-linear models [45].

The implementation of the EGM can be performed following two different frameworks: finite-difference or finite element based formulations [47]. In this work, it is adopted a finite-difference version inspired from [38], which is adapted to homogeneous isotropic material behaviour.

To better describe the EGM, consider that the surface of a specimen is discretized in small subdomains that represent a measurement grid, as shown in Fig. 4. It is assumed that the experimental strain field ($\hat{\boldsymbol{\varepsilon}} = \boldsymbol{\varepsilon}(\hat{\mathbf{u}})$) is provided at the nodes of each subdomain (circles in Fig. 4). The EGM consists on the minimization of the gap in local equilibrium on the boundaries of each subdomain. The local equilibrium is expressed by assessing the continuity of the stress vector at the interfaces. For instance, considering the two subdomains $\Omega^{\oplus}$ and $\Omega^{\ominus}$ represented in Fig. 4, the local equilibrium for the boundary $\Gamma^{\oplus\ominus}$ can be expressed as

$$\boldsymbol{\sigma}^{\oplus} \cdot \mathbf{n}^{\oplus} + \boldsymbol{\sigma}^{\ominus} \cdot \mathbf{n}^{\ominus} = \mathbf{0}, \tag{20}$$

where $\mathbf{n}^{\oplus}$ and $\mathbf{n}^{\ominus}$ are the unit normal vectors to the boundaries of $\Omega^{\oplus}$ and $\Omega^{\ominus}$, respectively. $\mathbf{0}$ is the zero vector. For the elasticity case, $\boldsymbol{\sigma}^{\oplus}$ and $\boldsymbol{\sigma}^{\ominus}$ are calculated with Eq. (3) and the given measured strain field. Note that Eq. (20) results in two equations for each interface, one for each direction x and y.

A key point is that the strain measurements must be interpolated for the locations where the equilibrium is prescribed, i.e. the interfaces of the subdomains. In Fig. 4, the interface of each subdomain is marked with triangular and quadrangular marks. The interpolation can be performed using finite element shape functions [38].

In case of a boundary where a force boundary condition $\bar{\mathbf{f}}$ is prescribed, the equilibrium is prescribed as

$$\boldsymbol{\sigma} \cdot \mathbf{n} = \bar{\mathbf{f}}. \tag{21}$$

This condition can be difficult to impose since the distribution of the force needs to be known. However, there are other ways to verify the local equilibrium that, for example, make use of a weak form of Eq. (21). The weak form allows to use the resultant of the force $\bar{\mathbf{f}}$, but the left-hand side of Eq. (21) must be integrated over the boundary Γ_f [47].

In case of a free boundary, the force boundary condition is equal to zero ($\bar{\mathbf{f}} = \mathbf{0}$). For the boundaries with prescribed displacements (the imposed force is unknown), the stress vector continuity cannot be evaluated, hence these boundaries are not taken into account. Finally, the objective function can be written in a least-square based formulation, as follows

$$\mathcal{F}_{\mathrm{EGM}}(\boldsymbol{\xi}) = \sum_{i=1}^{n_s} \left[\sum_{j=1}^{n_d} \left\{ \left(\boldsymbol{\sigma}^{\oplus} \cdot \mathbf{n}^{\oplus} + \boldsymbol{\sigma}^{\ominus} \cdot \mathbf{n}^{\ominus}\right)_j \cdot \left(\boldsymbol{\sigma}^{\oplus} \cdot \mathbf{n}^{\oplus} + \boldsymbol{\sigma}^{\ominus} \cdot \mathbf{n}^{\ominus}\right)_j \right\} \right]_i + \sum_{i=1}^{n_s} \left[\sum_{i=1}^{n_b} \left\{ \left(\boldsymbol{\sigma} \cdot \mathbf{n} - \bar{\mathbf{f}}\right)_j \cdot \left(\boldsymbol{\sigma} \cdot \mathbf{n} - \bar{\mathbf{f}}\right)_j \right\} \right]_i, \tag{22}$$

where n_d and n_b are the number of interface/interior nodes within the domain Ω and at the boundary Γ, respectively.

Fig. 5 shows a flowchart for this strategy. The algorithm starts with an initial set of material parameters ($\boldsymbol{\xi}^{i}$) that can be arbitrarily chosen. Follows the interpolation of the strain field to the interface boundaries of each subdomain, which can be performed using finite element shape functions. Then, the equilibrium equations are written for each boundary and the objective function is evaluated. In case of reaching a minimum value of the objective function or the process stagnation, the algorithm is interrupted and the set of material parameters ($\boldsymbol{\xi}^{f}$) is determined. Otherwise, a new iteration is initiated and, by means of an optimization method, a new set of material parameters ($\boldsymbol{\xi}^{u}$) is determined.

Unlike the other methods, the EGM will not be extended to non-linear models. However, as mentioned before, the key point behind this process is to adopt a method that captures the history dependent behaviour of non-linear models, such as the stress update algorithm adopted for CEGM.

The EGM has a major advantage compared with FEMU and CEGM, it does not require the costly computations of a FE model. Consequently, it is less time consuming. Nevertheless, the implementation of this method is more laborious than in FEMU strategy. It also requires the availability of a strain field within the whole solid body (full-field measurements). Therefore, it is not so flexible as the FEMU and CEGM. In addition, the applied force distribution must be known, as for FEMU and CEGM, which can be difficult to obtain, unless the weak form of Eq. (21) is used.

3.4. Virtual fields method

The Virtual Fields Method (VFM) has received significant attention from the scientific community in the recent years. It was first introduced by Grédiac [14] and since then its effectiveness has been proved in a large range of applications. The complete theory of VFM and its applications can be found in [48]. The most recent applications, organized by

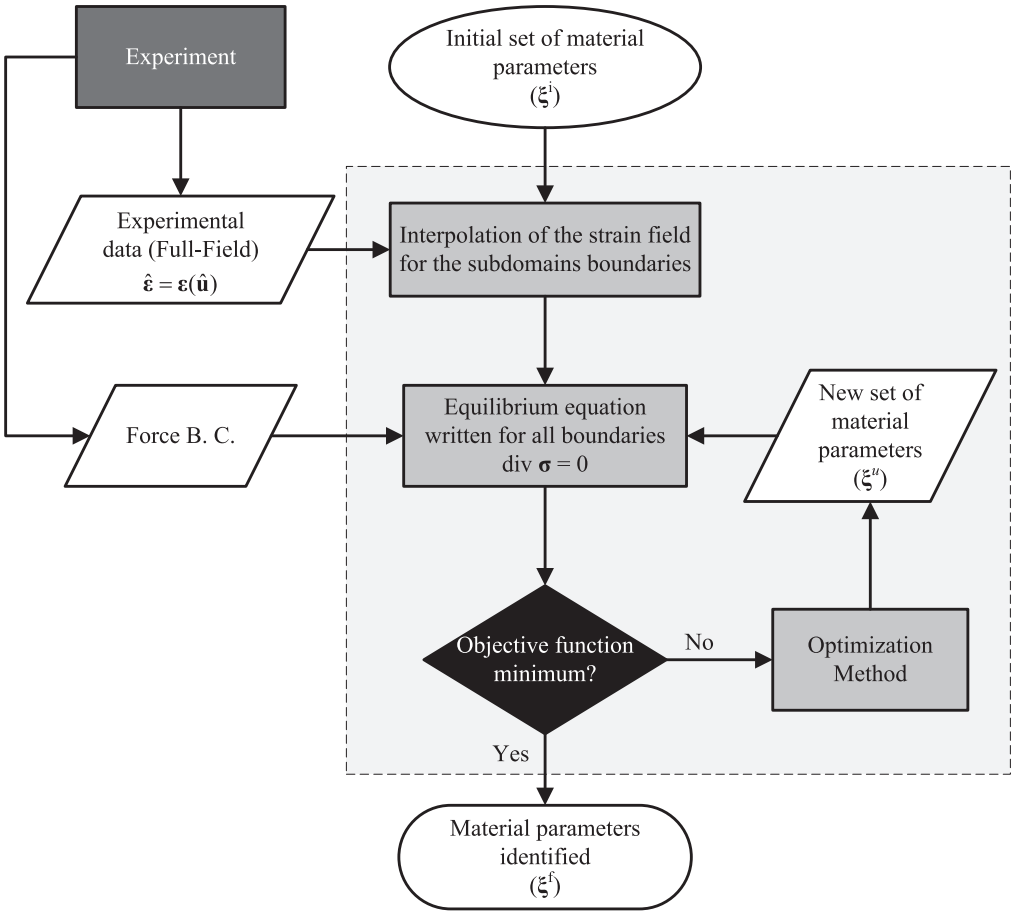

Fig. 5. Detailed flowchart for the EGM.

constitutive behaviours, are: anisotropic thermo-elasticity [49], hyper-elasticity [50], plasticity (anisotropic hardening, non-linear kinematic hardening and damage) [34,51,52], viscoplasticity [53] and temperature dependent viscoplasticity using isothermal tests [54].

The key elements behind VFM are the Principle of Virtual Work and a suitable choice of virtual fields. For the solid body shown in Fig. 1, in the absence of body-forces and assuming infinitesimal small displacements, the Principle of Virtual Work expresses that the internal virtual work must equal the external virtual work performed by the external forces and can be written as follows

$$\underbrace{\int_{\Omega} \boldsymbol{\sigma}(\xi, \hat{\boldsymbol{\varepsilon}}) : \boldsymbol{\varepsilon}^{\star} dV}_{\text{Internalwork}} = \underbrace{\int_{\Gamma_f} \bar{\mathbf{f}} \cdot \mathbf{u}^{\star} dS}_{\text{Externalwork}}, \tag{23}$$

where $\boldsymbol{\varepsilon}^{\star}$ is a virtual strain field and $\mathbf{u}^{\star}$ is a virtual displacement field. dV and dS are the infinitesimal volume and area for the current domain of the solid body, respectively. The principle of virtual work is independent of any constitutive model, which, theoretically, allows to apply VFM to all types of constitutive models. Furthermore, the force distribution ($\bar{\mathbf{f}}$) is not required. Instead, the resultant of the applied force can be used with a suitable choice of virtual fields. Thus, the only unknown of the problem is the Cauchy stress tensor $\boldsymbol{\sigma}(\xi, \hat{\boldsymbol{\varepsilon}})$, which depends on the set of material parameters. Considering elasticity case, the Cauchy stress tensor is computed using Eq. (3) and the measured displacement/strain field ($\hat{\boldsymbol{\varepsilon}} = \boldsymbol{\varepsilon}(\hat{\mathbf{u}})$). For this case, the material parameters can be evaluated directly from a system of equations. The system of equations has the same number of equations as number of unknown material parameters of the model.

For simplicity's sake, a different notation for the Eq. (3) is considered here [48,55]. Thus $\boldsymbol{\sigma}$ can be written in the matrix notation as

$$\begin{Bmatrix} \sigma_{xx} \\ \sigma_{yy} \\ \sigma_{xy} \end{Bmatrix} = \begin{bmatrix} Q_{xx} & Q_{xy} & 0 \\ Q_{yx} & Q_{yy} & 0 \\ 0 & 0 & Q_{ss} \end{bmatrix} \begin{Bmatrix} \hat{\varepsilon}_{xx} \\ \hat{\varepsilon}_{yy} \\ \hat{\varepsilon}_{xy} \end{Bmatrix}, \tag{24}$$

Replacing Eq. (24) in the principle of virtual work (Eq. (23)) and after some algebraic manipulation, it can be written

$$\begin{aligned} &Q_{xx} \int_{\Omega} \hat{\varepsilon}_{xx} \varepsilon^{\star}_{xx} dV + Q_{yy} \int_{\Omega} \hat{\varepsilon}_{yy} \varepsilon^{\star}_{yy} dV + Q_{xy} \int_{\Omega} \hat{\varepsilon}_{yy} \varepsilon^{\star}_{xx} dV \\ &\quad + Q_{yx} \int_{\Omega} \hat{\varepsilon}_{xx} \varepsilon^{\star}_{yy} dV + Q_{ss} \int_{\Omega} \hat{\varepsilon}_{xy} \varepsilon^{\star}_{xy} dV \\ &= \int_{\Gamma_f} \bar{f}_x \cdot u^{\star}_x dS + \int_{\Gamma_f} \bar{f}_y \cdot u^{\star}_y dS, \end{aligned} \tag{25}$$

where the variables Q_{xx}, Q_{yy}, Q_{xy}, Q_{yx}, Q_{ss} have been moved out of the integrals, since these are assumed as constants. In case of isotropic linear elasticity, the following relation exists between the terms: $Q_{yy} = Q_{xx}$, $Q_{yx} = Q_{xy}$ and $Q_{ss} = (Q_{xx} - Q_{xy})/2$. Accordingly, the Poisson's ratio and the Young's modulus can be expressed as $\nu = Q_{xx}/Q_{xy}$ and $E = Q_{xx}/(1 - \nu^2)$.

In order to retrieve the two unknown material parameters ($\xi = \{\nu, E\}$), it is required two independent virtual fields. The number of virtual fields must be equal to the number of unknown material parameters and Eq. (25) must be written for each selected virtual field. The calculation of integrals in Eq. (25) can be approximated by discrete sums, as performed for the CEGM (Section 3.2). The result is a linear system of two equations with two unknowns, Q_{xx} and Q_{xy}, respectively.

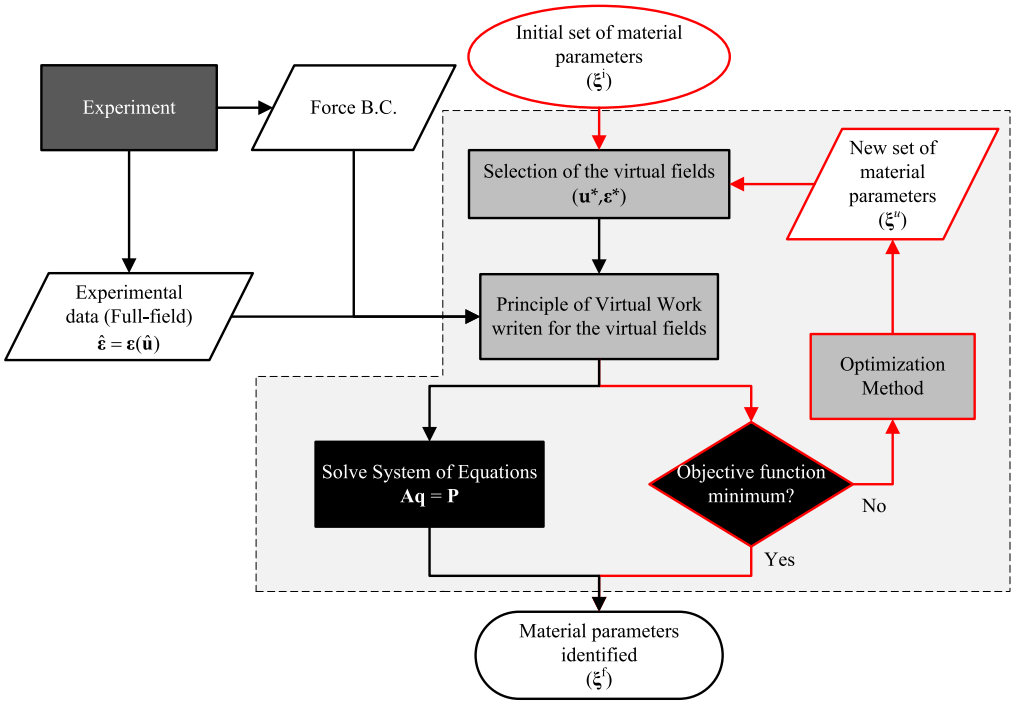

Fig. 6. Detailed flowchart for the VFM. Note that the red path is exclusive for non-linear constitutive models. (For interpretation of the references to colour in this figure legend, the reader is referred to the web version of this article.)

Provided that the measured strain field is heterogeneous and the chosen virtual fields are independent, the system of equations is linearly independent and can be written as

$$\mathbf{Aq} = \mathbf{P}, \tag{26}$$

where $\mathbf{A}$ is a square matrix composed by the strain terms, $\mathbf{q}$ is a vector of the unknown material coefficients $\{Q_{xx}, Q_{xy}\}$ and $\mathbf{P}$ is the vector of virtual external work of the applied forces. This linear system of equations is solved with a low computational cost.

For the case of a non-linear model, it is no longer possible to derive the linear system of equations and the identification process turns into an iterative procedure, which relies on the minimization of an objective function [48,56]. This objective function expresses the gap between the internal and the external virtual works and can be defined in a least square based formulation as

$$\mathcal{F}_{\mathrm{VFM}}(\boldsymbol{\xi}) = \sum_{i=1}^{n_s} \left(\int_{\Omega} \boldsymbol{\sigma}(\boldsymbol{\xi}, \hat{\boldsymbol{\varepsilon}}) : \boldsymbol{\varepsilon}^{\star} dV - \int_{\Gamma_f} \bar{\mathbf{f}} \cdot \mathbf{u}^{\star} dS \right)_i^2, \tag{27}$$

The calculation of the stress field is performed through a stress update algorithm, as the one adopted for CEGM [44].

A detailed flowchart for VFM is presented in Fig. 6. Two different paths are represented. The first one (black lines) includes the main steps for the identification of material parameters of linear models. As mentioned above, for linear constitutive models the material parameters are retrieved after solving a system of linear equations (Eq. (26)). The second path (red lines) corresponds to non-linear constitutive models. In this case, the material parameters are retrieved after the cost function value reached a minimum or the process stagnation. The search for the minimum value is performed by means of an optimization method.

The choice of the virtual fields is part of the VFM identification process. An infinite number of virtual fields can be used, but a proper choice facilitates the identification process and can improve the quality of the final set of parameters. The suitable choice of the virtual fields has been pointed out as the major weakness of VFM, specially in non-linear cases [3,25]. It should be emphasized that, the virtual displacement and strain fields are just mathematical test functions and can be seen as weights [48,57]. Moreover, they can be defined independently of the measured displacement/strain strain field [48]. However, due to a matter of convenience, the virtual fields are usually defined in accordance with two conditions. First, the displacement boundary conditions must be satisfied, *i.e.*, at the boundary Γ_u the virtual displacement field must be zero ($\mathbf{u}^{\star} = \mathbf{0}$) [32,48]. The second condition is related to the use of the resultant of the applied force, instead of its distribution. Therefore, the virtual displacement fields must be chosen in order to be constant along the boundary Γ_f and, to eliminate the components of the resultant force that are unknown, $\mathbf{u}^{\star}$ must be collinear with $\bar{\mathbf{f}}$ [48,52]. Moreover, it is required that the virtual fields assure a C^0 continuity. Regarding the use of the applied force in VFM, in special cases such as dynamic testing, obtaining accurate measurements of the applied force can be difficult. A different formulation of Eq. (23), which includes the virtual work of the inertial forces, can then be used and the external virtual work term can be cancelled out using suitable virtual fields [48,58,59]. This approach has been exclusively applied to the identification of dynamic mechanical characteristics, thus it will not be addressed in this work.

A great effort has been made to suppress the major weakness of VFM and currently there are three strategies available for the choice of the virtual fields, which are:

(i) *Manually defined virtual fields*: This procedure is the most used in non-linear cases [34,51,57]. Usually, polynomials or sine/cosine functions are used [48]. This strategy is the easiest to implement, but it is user-dependent. Therefore, the search for a function that meet the conditions mentioned above depends on the expertise of the user. Moreover, there is no guarantee that the chosen virtual fields produce the best results.

(ii) *Stiffness-based virtual fields*: This second procedure has been a great step to overcome the previous drawbacks. It was first proposed by Avril et al. [60] for anisotropic elasticity and then extended to elasto-plasticity [56]. In this case, the calculation of the virtual fields requires the derivation of the tangent stiffness-matrix (in elasto-plasticity, the tangent elasto-plastic stiffness matrix (Eq. (14)). This strategy relies on a statistical approach to

quantify the uncertainty of the identified parameters due to noise on the measurements. Based on this, an automatic procedure to derive virtual fields that minimizes the effect of noise is designed. However, the implementation is a cumbersome task due to the calculation of the tangent elasto-plastic stiffness matrix.

(iii) *Sensitivity-based virtual fields*: Recently proposed by Marek et al. [57], this strategy offers an easier implementation procedure. In this case, the virtual fields are determined according to a sensitivity stress map, i.e., the virtual fields are determined to give more weight to the locations of the specimen where more information about a parameter is encoded [57]. Thus, the sensitivity of the stress field to each parameter must be tested to define a virtual field for each unknown material parameter.

The major advantage of VFM is that it does not need FE analysis. Therefore, when compared with strategies such as FEMU and CEGM, a superior computational efficiency is expected. Indeed, Zhang et al. [50] reported a significant drop on the time required to retrieve the material parameters. In their case, the VFM was 125 faster than the FEMU. Another important advantage of VFM is that it does not require the exact distribution of the applied force on the boundary Γ_f. With a proper choice of virtual fields, it only requires the force resultant in one direction, which is usually measured during experiments.

Like EGM, the main disadvantage of VFM is that it requires full-field experimental data over the entire domain, which is not as flexible as FEMU and CEGM. Moreover, in non-linear cases, like CEGM, VFM requires a tool for the calculation of the stress field from the measured strain field, often based on return-mapping algorithm.

4. Comparison of the different inverse strategies

The aim of this section is to compare the inverse strategies described in Section 3. Robustness in the presence of noisy data and computational efficiency are the two main aspects to be evaluated. Full-field measurements are generated with the aid of the FE method and a single numerical test with a heterogeneous strain field is used.

This section is presented in two parts. In the first part, the different strategies are evaluated in isotropic linear elasticity, for which Young's modulus and Poisson's ratio ($\boldsymbol{\xi} = \{E, \upsilon\}$) are the unknown material parameters. In the second part, the different strategies are evaluated in isotropic elasto-plasticity for the model presented in Section 2, and the set of parameters $\boldsymbol{\xi} = \{K, \varepsilon_0, n\}$ is identified. For this last part, the elastic parameters are considered to be known *a priori*.

The analysis was carried out with a standard computer, with an Intel(R) Core(TM) i7-4770 (3.40 GHz) processor and 8.00 GB of RAM memory. The computational time presented for each strategy is the *wall-time* or *real-time clock*, which means the total time of a task including input/output activities.

4.1. Heterogeneous test

In order to easily and clearly compare the different strategies, a numerical test is designed to be simple, but also to generate a heterogeneous strain field. It consists of a solid with dimensions 3×3 mm^2 in-plane and thickness of $t = 0.1$ mm. The solid is discretized with 4-node bilinear elements, making a total of 9 plane-stress elements and 16 nodes. Fig. 7 (a) presents the initial geometry and the boundary conditions, as well as the finite element mesh. x and y are the local coordinates along the horizontal and vertical axes, according to the reference system. The boundaries $x = 0$ and $y = 0$ are fixed and the force boundary condition is applied on the boundary $x = 3$ mm. The force boundary condition has a non-uniform distribution along the $y-$coordinate and a single component in the $x-$direction. The distribution of this load changes linearly with y, as: $f_x(y) = my + b$. The variables m and b control the distribution. Although tension is the main stress state corresponding to this load, the other components of the stress tensor are also active.

Table 1
Identification results in elasticity.

	E [GPa]	ν	Iterations	Normalized wall-time
Reference parameters	210.00	0.3000		
FEMU	210.00	0.3000	10	1.000
CEGM	210.00	0.2993	12	0.444
EGM	210.97	0.2874	9	0.167
VFM	210.00	0.3000	(–)	(–)

Regarding the identification process, the force distribution is assumed to be known. This is useful to build up the FE model for FEMU and CEGM, and also for the EGM, since to establish the local equilibrium at the boundary Γ_f, Eq. (21) must be determined. In contrast, VFM does not require the force distribution, which is an important aspect to alleviate constraints in the design of a mechanical test.

4.2. Identification of material parameters using full-field measurements in linear elasticity

In this part, the reference material assumed for the model of Fig. 7 (a) is considered homogeneous and isotropic linear elastic. The reference material parameters, Poisson's ratio and Young's modulus, are $\nu = 0.3$ and $E = 210.00$ GPa, respectively. The distribution of the force boundary condition is defined by $m = 10$ Nmm^{-1} and $b = 50$ N. The numerical results are generated using an in-house FE code dedicated to linear elastic problems. The distribution of the components of the infinitesimal strain tensor are shown in Fig. 7 (b), (c) and (d). It can be seen that the test is heterogeneous, which results from the non-uniform distribution of the applied force. The strain tensor, used in the different strategies, is derived from the displacement field using the derivatives of the FE shape functions. It is calculated at the integration points and output at the nodes. This leads to an information at 16 points, instead of 9 if the centroid of the elements was used.

To perform the identification using FEMU, CEGM and EGM, an initial set of material parameters is required, so the following set was defined: $\boldsymbol{\xi} = \{E, \upsilon\} = \{0.2, 100.00 \text{ GPa}\}$. Regarding the determination of a statically admissible stress field for CEGM, the same initial set of material parameters is used. This stress field is not updated during the process, since the material properties are homogeneous over the body. A gradient-based optimization algorithm, called Generalized Reduced Gradient (GRG) [61], is chosen. The threshold value for the cost function and for the variation of each parameter between iteration is set to 1×10^{-8}.

In contrast to the former strategies, VFM does not require an optimization method, but requires a suitable choice of virtual fields. Following the manual approach (see Section 3.4), two different virtual fields are chosen, which can be written as

$$\mathbf{u}^{\star(1)} = \begin{Bmatrix} u_x^{\star(1)} = x \\ u_y^{\star(1)} = 0 \end{Bmatrix} \Rightarrow \quad \boldsymbol{\varepsilon}^{\star(1)} = \begin{Bmatrix} \varepsilon_{xx}^{\star(1)} = 1 \\ \varepsilon_{yy}^{\star(1)} = 0 \\ \varepsilon_{xy}^{\star(1)} = 0 \end{Bmatrix}, \tag{28}$$

$$\mathbf{u}^{\star(2)} = \begin{Bmatrix} u_x^{\star(2)} = 0 \\ u_y^{\star(2)} = y \end{Bmatrix} \Rightarrow \quad \boldsymbol{\varepsilon}^{\star(2)} = \begin{Bmatrix} \varepsilon_{xx}^{\star(2)} = 0 \\ \varepsilon_{yy}^{\star(2)} = 1 \\ \varepsilon_{xy}^{\star(2)} = 0 \end{Bmatrix}. \tag{29}$$

The selected virtual fields have the simplest possible form. Both virtual fields satisfy the displacement boundary conditions and the first one reduces the use of the applied force to its resultant along the $x-$direction. It is also noteworthy that, with the selected virtual fields, the same weight is given to each measurement point ($\varepsilon_{xx}^{\star(1)} = 1$ and $\varepsilon_{yy}^{\star(2)} = 1$).

The results of the identification process for each strategy are presented in Table 1. FEMU, CEGM and VFM accurately retrieve the material parameters. EGM leads to good results for Young's modulus, but the deviation for Poisson's ratio is around 4% . This small error can be

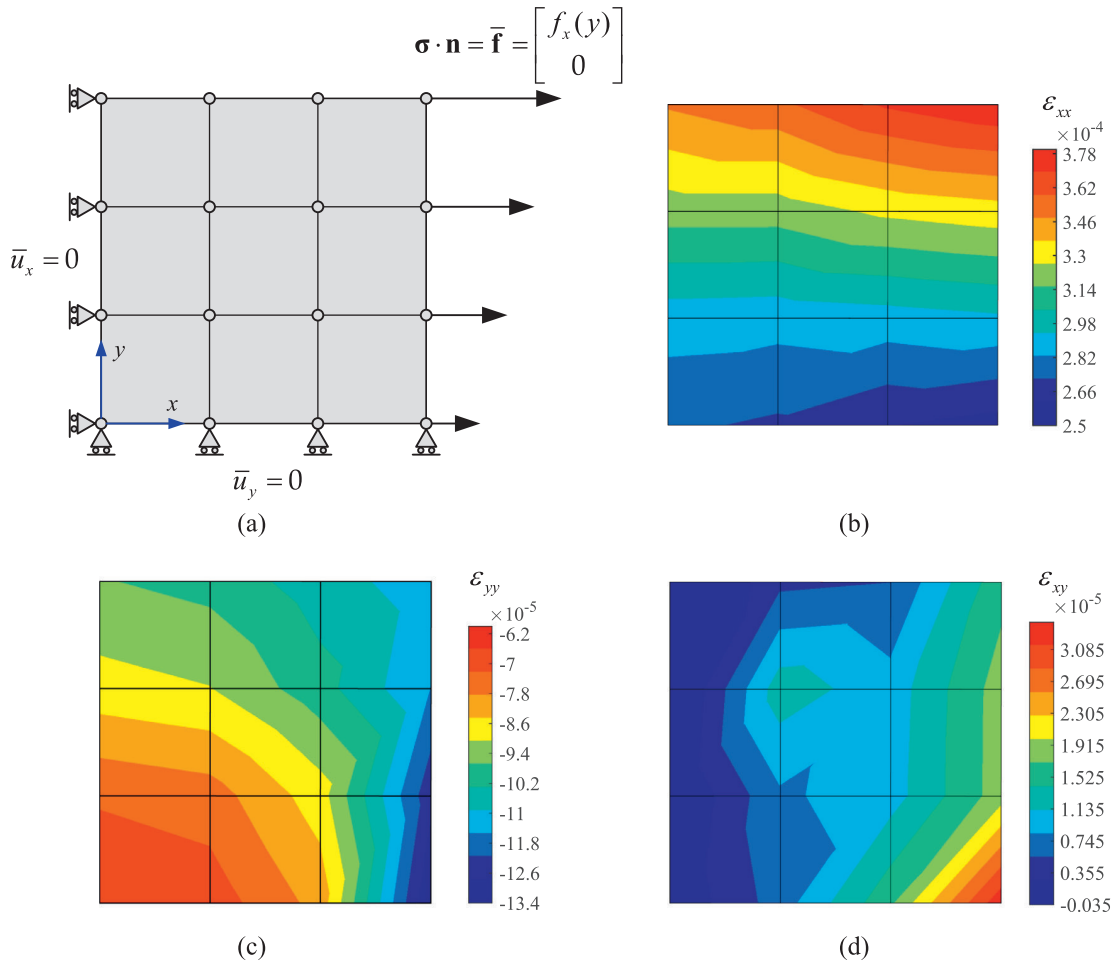

Fig. 7. Heterogeneous test: (a) initial geometry, mesh and boundary conditions of the test; and components of the infinitesimal strain tensor; (b) ε_{xx}, (c) ε_{yy} and (d) ε_{xy}.

attributed to the interpolation process. According to the presented results, it is possible to conclude that the four strategies were implemented correctly.

The number of iterations for each method is also evaluated and is presented in Table 1. CEGM requires a larger number of iterations than the other strategies. However, when compared with FEMU, CEGM requires a single FE simulation to determine the admissible stress field, whereas FEMU needs a FE simulation at each evaluation of the cost function. This is reflected in the normalized wall-time, also presented in Table 1. The wall-time of the FEMU strategy is used for normalization, since it has the highest value. The normalization is adopted here because the values are too low. In terms of the iterative strategies (FEMU, CEGM and EGM), EGM presents the lowest value for the wall-time. The wall-time for VFM is close to zero, indeed, it just requires time for the inversion of a 2×2 matrix and its multiplication by the vector of virtual external work (Eq. (26)), which are simple operations.

Experimental measurements acquired by DIC are inevitably affected by errors from different sources, such as out-of-plane movements, quality of the speckle, interpolation errors and so on. These errors have an important effect on the measured displacement field and then on the computed strain field. This affects the quality of the identified material parameters. Therefore, testing the robustness and stability of the identification strategies when fed with data corrupted with errors is an important aspect. To this purpose, Rossi et al. [62] proposed a simulator able to numerically reproduce the entire chain of acquisition of experimental measurements with DIC, which can be used to identify the effect of this errors in the identification process. Here, a simple approach, though enough to evaluate the performance of the identification strategies in the presence of errors, is adopted, which consists in adding a random error to the computed strain field. The random error with a zero-mean Gaussian distribution and standard deviation of 1 is added to the reference strain field used above. The magnitude of the error is of the order 1×10^{-6}. The results with noisy data are presented in Table 2. It is also presented the relative error for each parameter, which is calculated relatively to the reference values. The CPU normalized times for each strategy are similar to the one presented in Table 1.

Table 2
Identification results in elasticity with noisy data (error magnitude of 1×10^{-6}).

	E [GPa]	ν	E - Error[%]	ν - Error[%]
Reference parameters	210.00	0.3000		
FEMU	203.90	0.2706	2.90	9.798
CEGM	204.55	0.2728	2.59	9.058
EGM	195.10	0.2356	7.09	21.436
VFM	205.14	0.2753	2.31	8.207

Table 2 shows that EGM presents the highest level of error for both parameters, with almost 21% of error for Poisson's ratio and 7% for Young's modulus. EGM has the highest sensitivity to noise in this case. The other three strategies give similar results, with an error lower than 3% for Young's Modulus and lower than 10% for Poisson's ration. Nev-

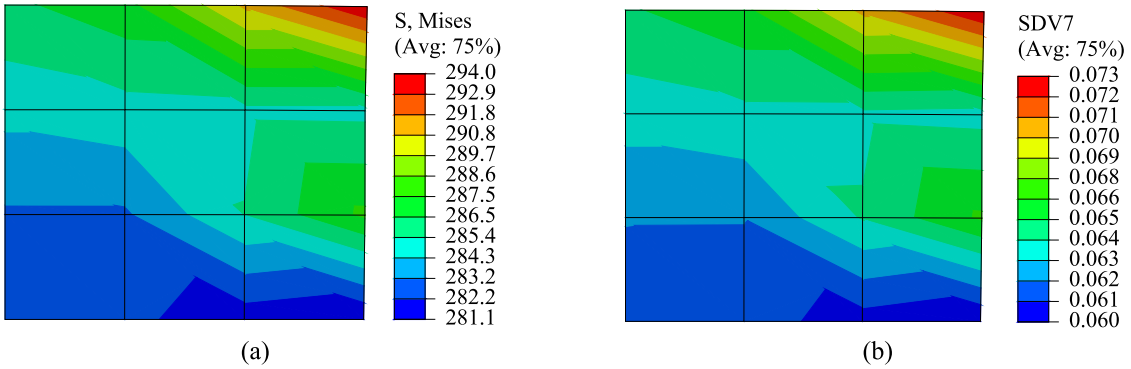

Fig. 8. (a) von Mises stress distribution and (b) equivalent plastic strain field at the end of the test.

ertheless, VFM presents the lowest level of error for both parameters, followed by CEGM and finally, FEMU. In conclusion, for this specific case, VFM is the most robust strategy in the presence of noisy data and EGM is the least robust.

Although not addressed in this study, it should be mentioned that the results obtained for noisy data with VFM, according to [48], could be improved through the use of stiffness-based virtual fields, which are specially designed to minimize the effect of noise (see Section 3.4).

4.3. Identification of material parameters using full-field measurements in elasto-plasticity

In this second part, it is addressed the identification of the material parameters for non-linear models, namely the isotropic elasto-plastic model presented in Section 2. The material parameters for the elastic part are the same of the last section ($E = 210$ GPa and $\nu = 0.3$) and it is assumed that they are known *a priori*. Thus, the material parameters to be identified are the parameters of the Swift's Law (Eq. (8)), for which the following reference values are adopted: $\boldsymbol{\xi} = \{K, \varepsilon_0, n\} = \{565\ \text{MPa}, 7.81 \times 10^{-3}, 0.26\}$. The numerical results are generated using the FE code ABAQUS standard. The numerical model is built up using an element CPS4 (bilinear shape functions and full integration) along with the mesh of Fig. 7 (a). A small displacement formulation is also adopted. Regarding the force boundary condition applied to the model, the following parameters are adopted: $m = 10\ \text{Nmm}^{-1}$ and $b = 270$ N.

The input data for all the methods is still the strain field, but the strain tensor is output at the centroid of the elements. Therefore, only 9 points are available. The force resultant is extracted on the boundary Γ_f.

The FE analysis is discretized in five equal increments, with a constant increment size of 0.2. As a result, five strain fields are available for the identification. For the first two increments, the body undergoes only elastic deformations and the yielding process starts in the third increment. The distributions of the von Mises stress and the equivalent plastic strain field at the end of the test are shown in Fig. 8.

Due to the non-linearity of the model, VFM assumes the form of the objective function presented in Section 3.4. Nevertheless, it requires the selection of a virtual field to write the principle of virtual work. Only one virtual field is chosen in order to keep the process as simple as possible. Hence, the first virtual field presented in Eq. (28) ($\mathbf{u}^{\star(1)}$) is adopted.

The objective functions of the different methods (FEMU, CEGM and VFM) are minimized with the Levenberg–Marquardt optimization method [63]. This is a least-square gradient-based optimization method which requires the derivative of the objective functions. Forward differences are adopted for the calculation of the derivatives. The convergence criterion is similar to the one used in Section 4.2, but with a value of 1×10^{-5}. Generally, constraints on the domain of the material parameters are assigned *a priori*. However, in this work, this will be avoided, unless required for a strategy to achieve a solution.

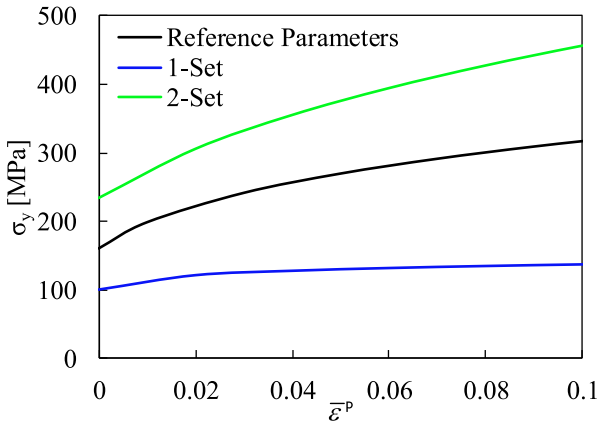

Fig. 9. Flow stress evolution according to the Swift's law for the initial sets of material parameters listed in Table 3.

Table 3
Initial sets of material parameters for the Swift's law (1-Set and 2-Set) used to start the identification process.

Parameters	K [MPa]	ε_0	n
Reference	565	7.81×10^{-3}	0.26
1-Set	165	2.00×10^{-3}	0.08
2-Set	965	1.76×10^{-2}	0.35

CEGM and VFM require the reconstruction of the stress field from the numerically generated strain field. For both strategies, it is adopted an implicit backward-Euler stress update algorithm presented in [44].

Such an identification is a more difficult process than the previously performed one, mainly due to the non-linear nature of the model, the coupling between the parameters and also the number of parameters. The presence of local minima in the objective function is one of the aspects that can stop the process and lead to erroneous solutions. Therefore, in order to evaluate the robustness of the presented strategies, two different initial sets of material parameters are arbitrarily selected. The two sets are presented in Table 3 and the respective flow stress curves given by Swift's law are presented in Fig. 9.

The results of the identification process for the different strategies are summarized in Table 4. CEGM and VFM correctly retrieve the three parameters, independently of the initial set of parameters. This indicates that the reference solution is a global minimum within the interval delimited by the selected initial sets (see Table 3). Figs. 10 and 11 present the evolution of the material parameters along the identification process, as well as the evolution of the value of the objective functions,

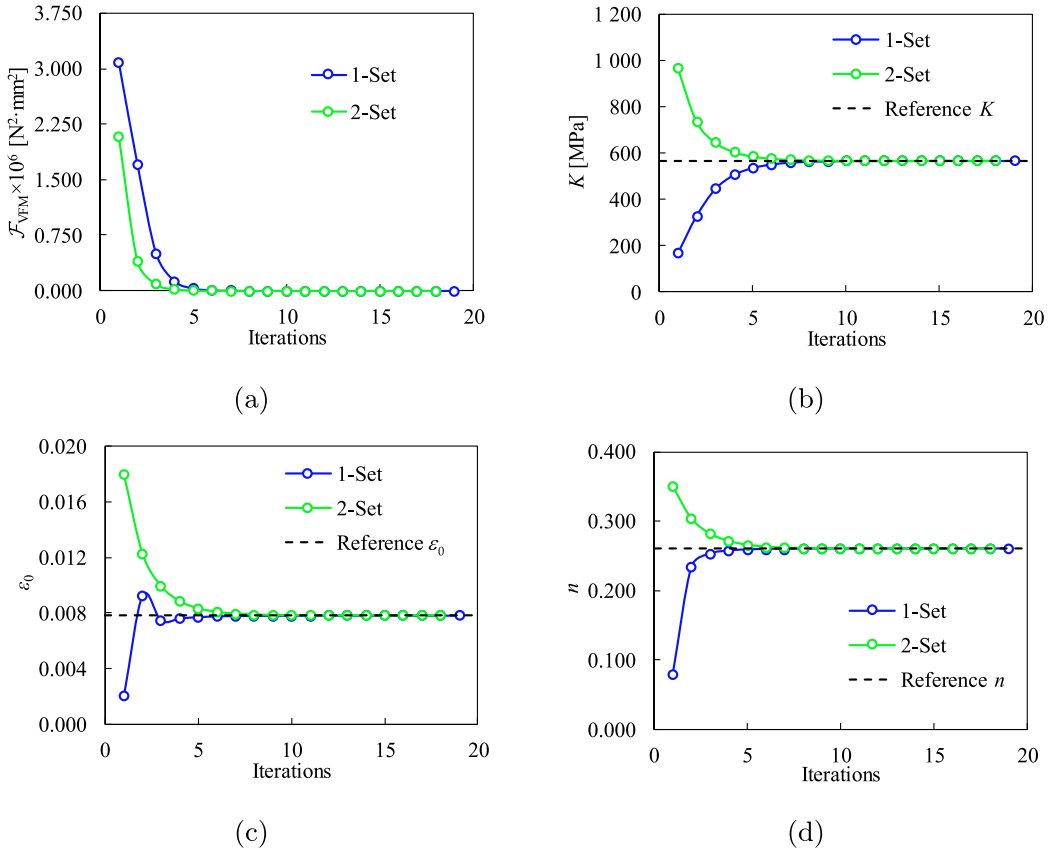

Fig. 10. Results of the identification process for VFM strategy: (a) objective function evolution; parameters (b) K; (c) ε_0 and (d) n evolutions.

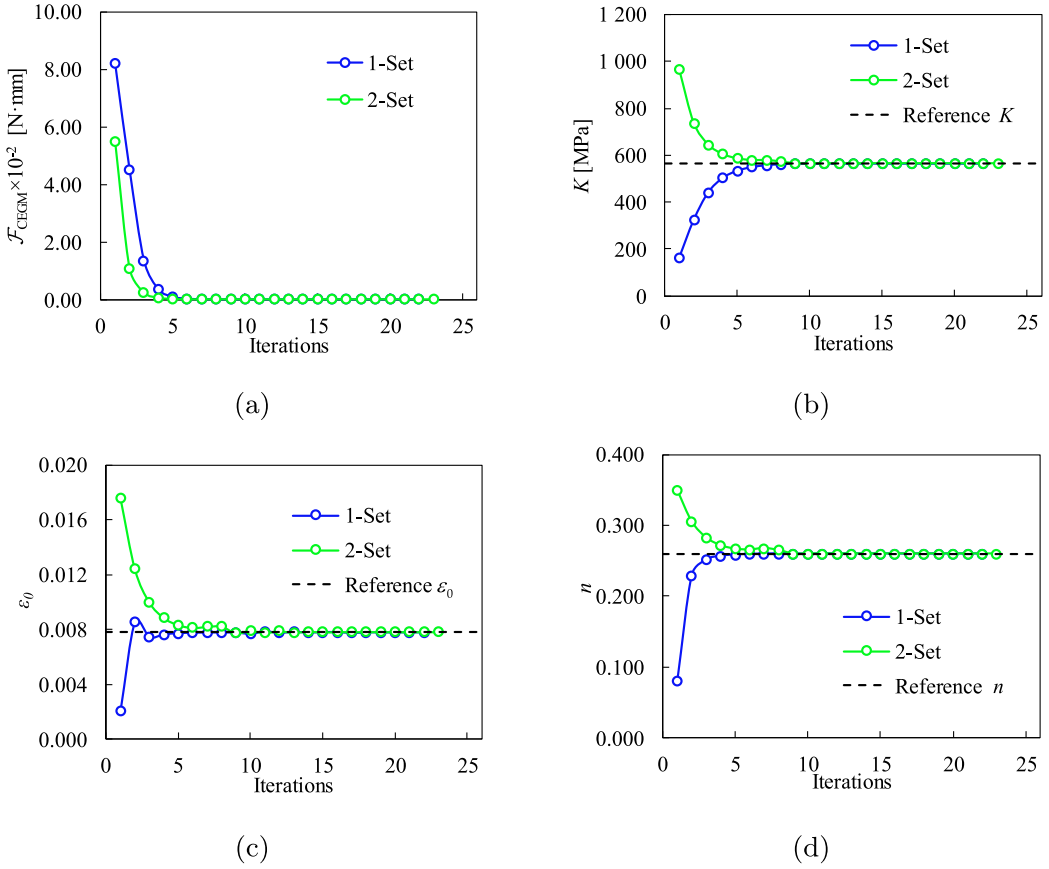

Fig. 11. Results of the identification process for CEGM strategy: (a) objective function evolution; parameters (b) K; (c) ε_0 and (d) n evolutions.

Table 4
Identification results in elasto-plasticity (isotropic hardening described by Swift's law).
*Constraint on the material parameters domain.

	Parameters	K [MPa]	ε_0	n	Iterations	Wall-time [s]
	Reference	565	7.810×10^{-3}	0.260		
FEMU	1-Set*	564.998	7.809×10^{-3}	0.259	41	4407.5
	2-Set	565.000	7.808×10^{-3}	0.260	20	2048.9
CEGM	1-Set	564.317	7.761×10^{-3}	0.259	22	38.5
	2-Set	564.985	7.819×10^{-3}	0.260	23	36.9
VFM	1-Set	565.080	7.795×10^{-3}	0.260	19	10.3
	2-Set	565.085	7.795×10^{-3}	0.260	18	7.8

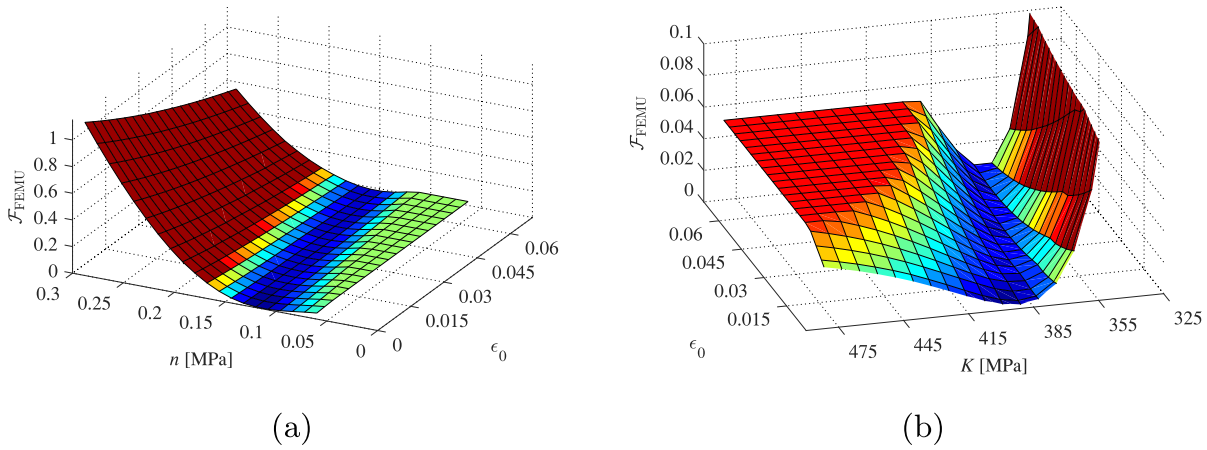

Fig. 12. Plots of the objective function of FEMU for: (a) $K = 386.691$ MPa; (b) $n = 0.113$.

for both strategies. These figures reveal that both strategies have fast convergence.

FEMU strategy is able to retrieve the material parameters when the identification starts from the 2-Set of initial parameters. However, for the 1-Set, the presence of a local minimum in the cost function for the values of the parameters $K = 386.691$ MPa and $n = 0.113$ leads to negative values of the parameter ε_0, which is not admissible for Swift's law. The presence of this local minimum can be seen in Fig. 12. Therefore, in order to guarantee positive values for the solution parameters, a constraint on the material parameters domain must be added and kept through the remaining part of this study. Besides, the convergence of FEMU is not so fast as in the case of CEGM and VFM, as can be observed in Fig. 13.

The iterations and wall-time are also presented in Table 4. VFM provides the lowest wall-time, with an average of 0.48 s per iteration. CEGM is more than 3 times slower than VFM and has an average of 1.7 s per iteration. FEMU presents the worst results for the wall-time. For the 1-Set, VFM is almost 428 times faster than FEMU and for the 2-Set, VFM is 263 times faster than FEMU, which are significant differences. The choice of the initial set of parameters strongly affects the wall-time in the case of FEMU, a consequence of the required number of iterations. The identification which starts from 1-Set is clearly hampered by the presence of local minima, which led to an increase of the iterations number and, consequently, to the increase of the wall-time.

As performed for the elastic case, the effect of noise on the identification process is also addressed in this case and the sensitivity of the different strategies is evaluated. A random error with a zero-mean Gaussian distribution and standard deviation of 1 is added to the reference strain fields used in the previous results. Two levels of noise are tested, the first one with a magnitude of order 1×10^{-5} and the other with a magnitude of order 1×10^{-4}. The results for each noise level are presented in Tables 5 and 6.

For the first level of noise (magnitude of order 1×10^{-5}, Table 5), the three strategies retrieve the material parameters with a good accuracy, independently of the initial set of parameters. This indicates that the reference set of parameters gives a global minimum. Nevertheless, VFM has a slight deviation on the parameter ε_0, but the error is below 1.4%.

For the second level of error (magnitude of order 1×10^{-4}, Table 6), FEMU correctly retrieves the material parameters, with errors below 0.5%. The initial set has no influence on the accuracy of the results. CEGM underestimates the values of the three parameters for both initial sets and has the highest error for the parameter ε_0, with an error around 97%. VFM has reasonable results for the parameters K and n, with errors below 4%. Nevertheless, it overestimates the parameter ε_0.

The parameter ε_0 dictates the beginning of the plastic regime, i.e., it defines the initial yield stress ($\sigma_0 = K\varepsilon_0^n$). As the number of time steps used is reduced and these do not capture the exact instant of transition between elastic and plastic regime, it can be difficult to retrieve this parameter. Nevertheless, using the results obtained with VFM to calculate the initial yield stress, the following values are obtained: 162.71 MPa and 162.84 MPa for the 1-Set and 2-Set, respectively. Comparing these with the reference value, which is 160 MPa, gives an error around 0.02%, which is admissible. It is also possible to see in Fig. 14 that the identified material parameters capture the correct evolution of the reference yield stress curve. In the case of CEGM, the obtained values for the initial yield stress are: 105.98 MPa and 107.87 MPa for the 1-Set and 2-Set, respectively. The errors for these two values are around 33%, which continues to be a significant difference. Moreover, the solutions obtained are also plotted in Fig. 14. It is possible to see the difference for the reference solution in the initial yield stress, but for higher values of equivalent plastic strain, the evolution of Swift's law is close to the reference one. For the case of FEMU the results are in good agreement with the reference, which is also highlighted in Fig. 14.

In Tables 5 and 6 is also presented the objective function value for the obtained solutions. Comparing the values of Table 5 with their counterparts in Table 6, an increase in the objective function value and parameters deviation with increasing values of noise can be observed. This is expected because the strain fields used as input data are no longer ex-

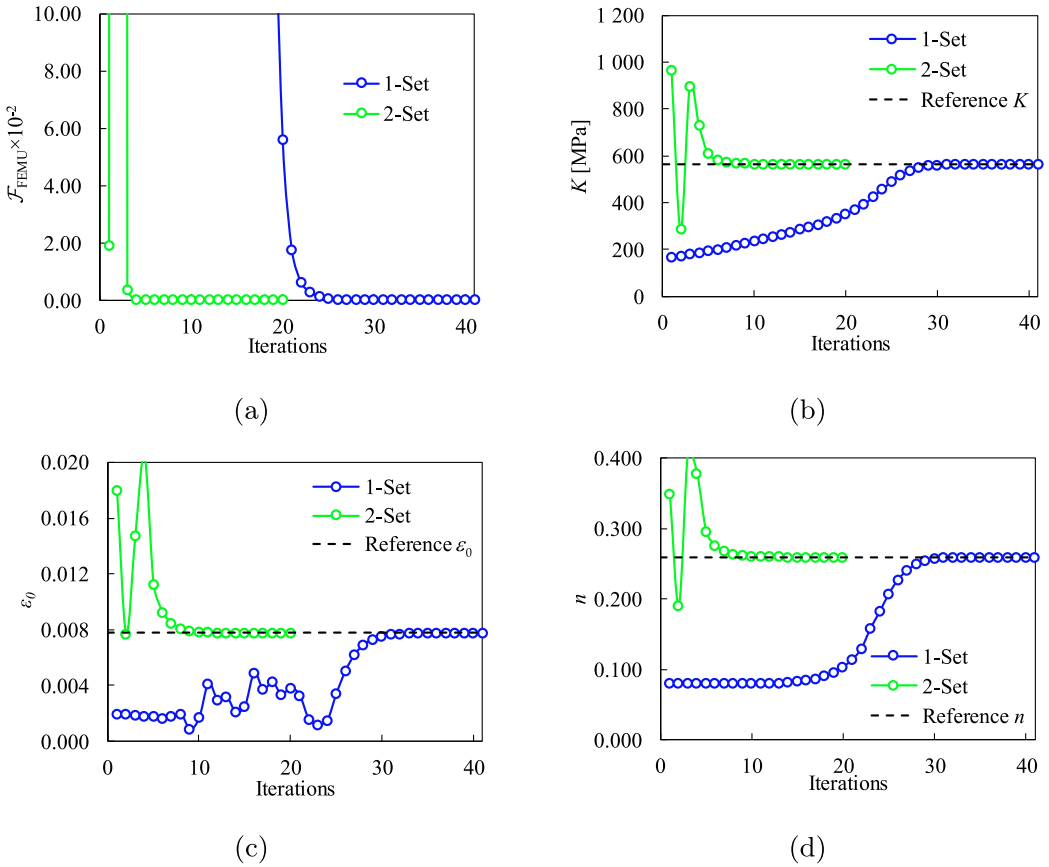

Fig. 13. Results of the identification process for FEMU strategy: (a) objective function evolution; parameters (b) K; (c) ε_0 and (d) n evolutions.

Table 5
Identification results in elasto-plasticity (isotropic hardening described by Swift's law) with noisy data (magnitude of order 1×10^{-5}). *Constraint on the material parameters domain.

		Parameters	K [MPa]	ε_0	n	Iterations	Obj. Func.
		Reference	565	7.810×10^{-3}	0.260		
FEMU		1-Set*	564.912	7.806×10^{-3}	0.259	42	1.29×10^{-8}
	Error		0.016%	0.051%	0.385%		
		2-Set	564.912	7.806×10^{-3}	0.259	18	1.29×10^{-8}
	Error		0.016%	0.051%	0.385%		
CEGM		1-Set	565.421	7.852×10^{-3}	0.260	34	4.36×10^{-5} N · mm
	Error		0.074%	0.537%	0.156%		
		2-Set	566.536	7.904×10^{-3}	0.261	20	4.36×10^{-5} N · mm
	Error		0.272%	1.203%	0.425%		
VFM		1-Set	566.135	7.915×10^{-3}	0.261	15	17.9 $N^2\cdot mm^2$
	Error		0.201%	1.344%	0.363%		
		2-Set	566.186	7.916×10^{-3}	0.261	13	17.9 $N^2\cdot mm^2$
	Error		0.209%	1.357%	0.367%		

act solutions of the direct problem and move away from this solution with the noise increase. The question that arises here is, for noisy data, whether the reference set remains a minimizer of the objective functions and whether the solutions obtained are only local minima. The results in Table 5 indicate that the reference set remains the global minimizer for the noise magnitude of 1×10^{-5}, since the reference set has been retrieved by the three strategies with small values of error, independently of the initial set of parameters. However, for Table 6, the results of CEGM and VFM have a higher error, particularly for CEGM. Therefore, in order to understand whether the reference solution remains a minimizer for this level of noise, the objective functions have been evaluated for the reference set and the values are: $\mathcal{F}_{FEMU}=1.284\times10^{-6}$, $\mathcal{F}_{CEGM}=3.243\times10^{-3}$ N · mm and $\mathcal{F}_{VFM}=2031.2$ $N^2\cdot mm^2$. The result for the objective function of FEMU is close to the ones presented in Table 6, which supports that for FEMU the reference set remains a minimizer for this level of error. For the other two strategies, these values of the objective functions are higher than the final values presented in Table 6, indicating that the reference set of material parameters is no longer the global minimizer in both strategies and the obtained results are the new ones. It means that higher values of noise can modify the objective functions of CEGM and VFM, thus preventing the correct parameters from being retrieved. As mentioned at the end of Section 4.2, the results of VFM could be improved if stiffness-based or sensitivity-based virtual fields had been used [57].

In conclusion, it seems that FEMU exhibits the lowest sensitivity to the presence of noisy data, in this example. The CEGM revealed the highest sensitivity to noise. The higher sensitivity to noise presented by CEGM and VFM when compared with FEMU, can be explained by

Table 6
Identification results in elasto-plasticity (isotropic hardening described by Swift's law) with noisy data (magnitude of order 1×10^{-4}). *Constraint on the material parameters domain.

		Parameters	K [MPa]	ε_0	n	Iterations	Obj. Func.
		Reference	565	7.810×10^{-3}	0.260		
FEMU		1-Set*	564.128	7.783×10^{-3}	0.259	38	1.29×10^{-6}
	Error		0.154%	0.345%	0.385%		
		2-Set	564.127	7.783×10^{-3}	0.259	16	1.29×10^{-6}
	Error		0.154%	0.345%	0.385%		
CEGM		1-Set	441.906	1.838×10^{-4}	0.166	62	2.96×10^{-3} N · mm
	Error		21.787%	97.646%	36.309%		
		2-Set	464.445	2.617×10^{-4}	0.177	143	3.08×10^{-3} N · mm
	Error		17.797%	96.649%	31.954%		
VFM		1-Set	576.854	9.203×10^{-3}	0.269	11	1796.1 $N^2 \cdot mm^2$
	Error		2.098%	17.839%	3.826%		
		2-Set	577.413	9.212×10^{-3}	0.270	10	1795.1 $N^2 \cdot mm^2$
	Error		2.197%	17.951%	3.866%		

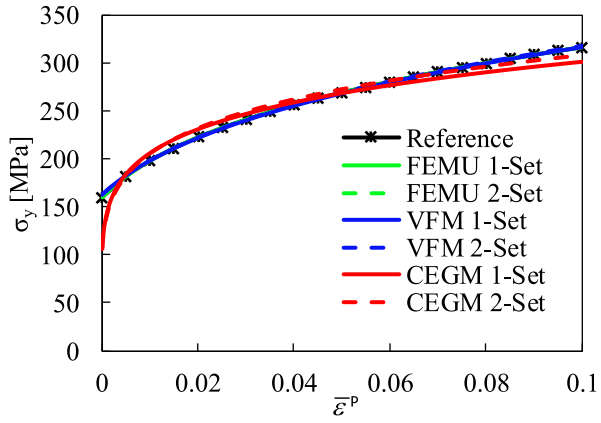

Fig. 14. Flow stress evolution according to Swift's law, for the identified sets of material parameters listed in Table 6.

the fact that, with FEMU the strain field is used directly to build up the objective function, whereas with CEGM and VFM, it is required the computation of the stress field that may lead to an amplification of the noise effect.

In terms of computational efficiency, the VFM has reached the best results with a significant margin for the other strategies, particularly for FEMU.

5. Conclusions

The calibration of constitutive models performed with full-field measurements is an increasingly used approach. Over the years, several strategies have been reported with successful results for linear and non-linear models. Therefore, it is important to understand and realize the advantages and drawbacks of each strategy, as well as their implementation aspects. This work is focused on four identification strategies based on full-field measurements, namely the Finite Element Model Updating (FEMU), the Constitutive Equation Gap Method (CEGM), the Equilibrium Gap Method (EGM) and the Virtual Fields Method (VFM). A brief overview of these strategies is presented, including their flowcharts and implementation details.

A comparative study is then performed. Two types of constitutive models are used: an isotropic linear elastic model and an elasto-plastic model with isotropic hardening described by Swift's law. In order to identify the material parameters of these two models, a FE model with a simple geometry is designed. The heterogeneous response of the FE model is generated by applying a non-uniform load distribution. The strain fields resultant from the solution of the direct problem are used as input for the different strategies. Hence, the four strategies are compared in the same conditions. Moreover, for both models, the robustness of the different strategies is tested against noisy data.

The results show an accurate performance of the different methods in elasticity, with the exception of EGM, which reveals a higher sensitivity to noise than the other methods. For the case of elasto-plasticity, FEMU achieves the most accurate results in the presence of data polluted with noise. Nevertheless, the computational time is significantly higher for FEMU. Moreover, in this specific case, it requires the use of constrains on the parameters domain to obtain admissible solutions. CEGM shows the highest sensitivity to noise, but in terms of computational cost, it is more efficient than FEMU. VFM has reasonable results in the presence of noise, and the best results for the computational cost. Moreover, improvements on VFM concerning noise sensitivity have already been performed and the results presented in this article could be further improved through the use of more advanced virtual fields. Therefore, VFM can be a perfect candidate when is expected a reasonable balance between quality of the identification procedure and computational cost.

Acknowledgements

The authors gratefully acknowledge the financial support of the Portuguese Foundation for Science and Technology (FCT) under the project P2020-PTDC/EMS-TEC/6400/2014 (POCI-01-0145-FEDER-016876) by UE/FEDER through the program COMPETE 2020 and UID/EMS/00481/2013-FCT under CENTRO-01-0145-FEDER-022083. The authors also would like to acknowledge the Région Bretagne (France) for its financial support. J.M.P. Martins is also grateful to the FCT for the PhD grant SFRH/BD/117432/2016.

References

[1] Barlat F, Brem J, Yoon J, Chung K, Dick R, Lege D, et al. Plane stress yield function for aluminum alloy sheets-part 1: theory. Int J Plast 2003;19(9):1297–319. doi:10.1016/S0749-6419(02)00019-0.
[2] Bruschi S, Altan T, Banabic D, Bariani P, Brosius A, Cao J, et al. Testing and modelling of material behaviour and formability in sheet metal forming. CIRP Ann 2014;63(2):727–49. doi:10.1016/j.cirp.2014.05.005.
[3] Prates P, Pereira A, Sakharova N, Oliveira M, Fernandes J. Inverse strategies for identifying the parameters of constitutive laws of metal sheets. Adv Mater Sci Eng 2016;2016:1–18. doi:10.1155/2016/4152963.
[4] Markiewicz E, Langrand B, Notta-Cuvier D. A review of characterisation and parameters identification of materials constitutive and damage models: from normalised direct approach to most advanced inverse problem resolution. Int J Impact Eng 2017;110:371–81. doi:10.1016/j.ijimpeng.2017.01.028.
[5] Sutton MA. Computer vision-based, noncontacting deformation measurements in mechanics: a generational transformation. Appl Mech Rev 2013;65(5):050802–050802–23. doi:10.1115/1.4024984.
[6] Zhang S, Leotoing L, Guines D, Thuillier S. Potential of the cross biaxial test for anisotropy characterization based on heterogeneous strain field. Exp Mech 2015;55(5):817–35. doi:10.1007/s11340-014-9983-y.
[7] Grédiac M, Hild F. Full-field measurements and identification in solid mechanics. John Wiley & Sons; 2012.

[8] Bonnet M, Constantinescu A. Inverse problems in elasticity. Inverse Probl 2005;21(2):R1.
[9] Avril S, Pierron F, Pannier Y, Rotinat R. Stress reconstruction and constitutive parameter identification in plane-stress elasto-plastic problems using surface measurements of deformation fields. Exp Mech 2008;48(4):403–19. doi:10.1007/s11340-007-9084-2.
[10] Kavanagh KT, Clough RW. Finite element applications in the characterization of elastic solids. Int J Solids Struct 1971;7(1):11–23. doi:10.1016/0020-7683(71)90015-1.
[11] Ladeveze P, Leguillon D. Error estimate procedure in the finite element method and applications. SIAM J Numer Anal 1983;20(3):485–509. doi:10.1137/0720033.
[12] Claire D, Hild F, Roux S. Identification of damage fields using kinematic measurements. Compt Rendus Mécanique 2002;330(11):729–34. doi:10.1016/S1631-0721(02)01524-3.
[13] Claire D, Hild F, Roux S. A finite element formulation to identify damage fields: the equilibrium gap method. Int J Numer Methods Eng 2004;61(2):189–208. doi:10.1002/nme.1057.
[14] Grédiac M. Principe des travaux virtuels et identification. Comptes rendus de l'Académie des sciences Série 2, Mécanique, Physique, Chimie, Sciences de l'univers, Sciences de la Terre 1989;309(1):1–5.
[15] Moussawi A, Lubineau G, Florentin E, Blaysat B. The constitutive compatibility method for identification of material parameters based on full-field measurements. Comput Methods Appl Mech Eng 2013;265:1–14. doi:10.1016/j.cma.2013.06.003.
[16] Blaysat B, Florentin E, Lubineau G, Moussawi A. A dissipation gap method for full-field measurement-based identification of elasto-plastic material parameters. Int J Numer Methods Eng 2012;91(7):685–704. doi:10.1002/nme.4287.
[17] Yun GJ, Shang S. A self-optimizing inverse analysis method for estimation of cyclic elasto-plasticity model parameters. Int J Plast 2011;27(4):576–95. doi:10.1016/j.ijplas.2010.08.003.
[18] Réthoré J. A fully integrated noise robust strategy for the identification of constitutive laws from digital images. Int J Numer Methods Eng 2010;84(6):631–60. doi:10.1002/nme.2908.
[19] Rossi M, Pierron F. Identification of plastic constitutive parameters at large deformations from three dimensional displacement fields. Comput Mech 2012;49(1):53–71. doi:10.1007/s00466-011-0627-0.
[20] Rossi M, Pierron F, Štamborská M. Application of the virtual fields method to large strain anisotropic plasticity. Int J Solids Struct 2016;97–98:322–35. doi:10.1016/j.ijsolstr.2016.07.015.
[21] Dunne F, Petrinic N. Introduction to computational plasticity. Oxford University Press on Demand; 2005.
[22] Lecompte D, Smits A, Sol H, Vantomme J, Van Hemelrijck D. Mixed numerical–experimental technique for orthotropic parameter identification using biaxial tensile tests on cruciform specimens. Int J Solids Struct 2007;44(5):1643–56. doi:10.1016/j.ijsolstr.2006.06.050.
[23] Bruno L, Felice G, Pagnotta L, Poggialini A, Stigliano G. Elastic characterization of orthotropic plates of any shape via static testing. Int J Solids Struct 2008;45(3):908–20. doi:10.1016/j.ijsolstr.2007.09.017.
[24] Kajberg J, Lindkvist G. Characterisation of materials subjected to large strains by inverse modelling based on in-plane displacement fields. Int J Solids Struct 2004;41(13):3439–59. doi:10.1016/j.ijsolstr.2004.02.021.
[25] Cooreman S, Lecompte D, Sol H, Vantomme J, Debruyne D. Identification of mechanical material behavior through inverse modeling and dic. Exp Mech 2008;48(4):421–33. doi:10.1007/s11340-007-9094-0.
[26] Pottier T, Toussaint F, Vacher P. Contribution of heterogeneous strain field measurements and boundary conditions modelling in inverse identification of material parameters. Eur J Mech A Solids 2011;30(3):373–82. doi:10.1016/j.euromechsol.2010.10.001.
[27] Kajberg J, Wikman B. Viscoplastic parameter estimation by high strain-rate experiments and inverse modelling–speckle measurements and high-speed photography. Int J Solids Struct 2007;44(1):145–64. doi:10.1016/j.ijsolstr.2006.04.018.
[28] Ghouati O, Gelin J-C. A finite element-based identification method for complex metallic material behaviours. Comput Mater Sci 2001;21(1):57–68. doi:10.1016/S0927-0256(00)00215-9.
[29] Cao J, Lin J. A study on formulation of objective functions for determining material models. Int J Mech Sci 2008;50(2):193–204. doi:10.1016/j.ijmecsci.2007.07.003.
[30] Andrade-Campos A, de Carvalho R, Valente R. Novel criteria for determination of material model parameters. Int J Mech Sci 2012;54(1):294–305. doi:10.1016/j.ijmecsci.2011.11.010.
[31] Mathieu F, Leclerc H, Hild F, Roux S. Estimation of elastoplastic parameters via weighted FEMU and integrated-DIC. Exp Mech 2015;55(1):105–19. doi:10.1007/s11340-014-9888-9.
[32] Avril S, Bonnet M, Bretelle A-S, Grédiac M, Hild F, Ienny P, et al. Overview of identification methods of mechanical parameters based on full-field measurements. Exp Mech 2008;48(4):381. doi:10.1007/s11340-008-9148-y.
[33] Denys K, Coppieters S, Cooreman S, Debruyne D. Alternative method for the identification of the strain hardening behaviour along the rolling direction of coil. Strain 2017;53(5) e12231–n/a. doi:10.1111/str.12231.
[34] Fu J, Barlat F, Kim J-H, Pierron F. Application of the virtual fields method to the identification of the homogeneous anisotropic hardening parameters for advanced high strength steels. Int J Plast 2017;93:229–50. doi:10.1016/j.ijplas.2016.07.013. Special Issue on Constitutive Descriptions of Plasticity at Various Scales in memory of Prof. José J. Grácio
[35] Bui H, Constantinescu A. Spatial localization of the error of constitutive law for the identification of defects in elastic bodies. Arch Mech 2000;52(4–5):511–22.
[36] Roux S, Hild F, Pagano S. A stress scale in full-field identification procedures: a diffuse stress gauge. Eur J Mech A Solids 2005;24(3):442–51. doi:10.1016/j.euromechsol.2005.02.002.
[37] Geymonat G, Hild F, Pagano S. Identification of elastic parameters by displacement field measurement. Comptes Rendus Mécanique 2002;330(6):403–8. doi:10.1016/S1631-0721(02)01476-6.
[38] Florentin E, Lubineau G. Identification of the parameters of an elastic material model using the constitutive equation gap method. Comput Mech 2010;46(4):521–31. doi:10.1007/s00466-010-0496-y.
[39] Florentin E, Lubineau G. Using constitutive equation gap method for identification of elastic material parameters: technical insights and illustrations. Int J Interact Des Manuf 2011;5(4):227–34. doi:10.1007/s12008-011-0129-5.
[40] Guchhait S, Banerjee B. Anisotropic linear elastic parameter estimation using error in the constitutive equation functional. Proc R Soc Lond A Math Phys Eng Sci 2016;472(2192). doi:10.1098/rspa.2016.0213.
[41] Latourte F, Chrysochoos A, Pagano S, Wattrisse B. Elastoplastic behavior identification for heterogeneous loadings and materials. Exp Mech 2008;48(4):435–49. doi:10.1007/s11340-007-9088-y.
[42] Merzouki T, Nouri H, Roger F. Direct identification of nonlinear damage behavior of composite materials using the constitutive equation gap method. Int J Mech Sci 2014;89:487–99. doi:10.1016/j.ijmecsci.2014.10.002.
[43] Coppieters S, Kuwabara T. Identification of post-necking hardening phenomena in ductile sheet metal. Exp Mech 2014;54(8):1355–71. doi:10.1007/s11340-014-9900-4.
[44] Crisfield M. Non-Linear finite element analysis of solids and structures, 1. John Wiley & Sons, Ltd.; 1991.
[45] Roux S, Hild F. Digital image mechanical identification (DIMI). Exp Mech 2008;48(4):495–508. doi:10.1007/s11340-007-9103-3.
[46] Périé JN, Leclerc H, Roux S, Hild F. Digital image correlation and biaxial test on composite material for anisotropic damage law identification. Int J Solids Struct 2009;46(11):2388–96. doi:10.1016/j.ijsolstr.2009.01.025.
[47] Amiot F, Périé J-N, Roux S. Equilibrium gap method. John Wiley & Sons, Inc.; 2012. p. 331–62. ISBN 9781118578469. doi:10.1002/9781118578469.ch12.
[48] Pierron F, Grédiac M. The virtual fields method: extracting constitutive mechanical parameters from full-field deformation measurements. Springer Science & Business Media; 2012.
[49] Ma Y, Yao X, Liu X, Hao W, Fang D. Inversion and decoupling of thermo-mechanical deformation in anisotropic materials using the virtual fields method. Proc R Soc Lond A Math Phys Eng Sci 2013;469(2154). doi:10.1098/rspa.2013.0124.
[50] Zhang L, Thakku SG, Beotra MR, Baskaran M, Aung T, Goh JCH, et al. Verification of a virtual fields method to extract the mechanical properties of human optic nerve head tissues *in vivo*. Biomech Model Mechanobiol 2017;16(3):871–87. doi:10.1007/s10237-016-0858-2.
[51] Fu J, Barlat F, Kim J-H, Pierron F. Identification of nonlinear kinematic hardening constitutive model parameters using the virtual fields method for advanced high strength steels. Int J Solids Struct 2016;102:30–43. doi:10.1016/j.ijsolstr.2016.10.020.
[52] Notta-Cuvier D, Langrand B, Lauro F, Markiewicz E. An innovative procedure for characterising a coupled elastoplastic damage model of behaviour using the virtual fields method. Int J Solids Struct 2015;69:415–27. doi:10.1016/j.ijsolstr.2015.05.009.
[53] Notta-Cuvier D, Langrand B, Markiewicz E, Lauro F, Portemont G. Identification of Johnson–Cook's viscoplastic model parameters using the virtual fields method: application to titanium alloy ti6al4v. Strain 2013;49(1):22–45. doi:10.1111/str.12010.
[54] Valeri G, Koohbor B, Kidane A, Sutton MA. Determining the tensile response of materials at high temperature using DIC and the virtual fields method. Opt Lasers Eng 2017;91:53–61. doi:10.1016/j.optlaseng.2016.11.004.
[55] Grediac M, Pierron F, Avril S, Toussaint E. The virtual fields method for extracting constitutive parameters from full-field measurements: a review. Strain 2006;42(4):233–53. doi:10.1111/j.1475-1305.2006.tb01504.x.
[56] Pierron F, Avril S, Tran VT. Extension of the virtual fields method to elasto-plastic material identification with cyclic loads and kinematic hardening. Int J Solids Struct 2010;47(22):2993–3010. doi:10.1016/j.ijsolstr.2010.06.022.
[57] Marek A, Davis FM, Pierron F. Sensitivity-based virtual fields for the non-linear virtual fields method. Comput Mech 2017. doi:10.1007/s00466-017-1411-6.
[58] Louëdec GL, Pierron F, Sutton MA, Siviour C, Reynolds AP. Identification of the dynamic properties of al 5456 FSW welds using the virtual fields method. J. Dyn. Behav. Mater. 2015;1(2):176–90. doi:10.1007/s40870-015-0014-6.
[59] Leem D, Kim JH, Barlat F, Song JH, Lee MG. Identification of dynamic flow stress curves using the virtual fields methods: theoretical feasibility analysis. Met Mater Int 2018;24(2):351–61. doi:10.1007/s12540-018-0024-8.
[60] Avril S, Grédiac M, Pierron F. Sensitivity of the virtual fields method to noisy data. Comput Mech 2004;34(6):439–52. doi:10.1007/s00466-004-0589-6.
[61] Lasdon LS, Waren AD, Jain A, Ratner M. Design and testing of a generalized reduced gradient code for nonlinear programming. ACM Trans. Math. Softw. (TOMS) 1978;4(1):34–50.
[62] Rossi M, Lava P, Pierron F, Debruyne D, Sasso M. Effect of DIC spatial resolution, noise and interpolation error on identification results with the VFM. Strain 2015;51(3):206–22. doi:10.1111/str.12134.
[63] Marquardt DW. An algorithm for least-squares estimation of nonlinear parameters. J. Soc. Ind. Appl. Math. 1963;11(2):431–41. doi:10.1137/0111030.

2.2 Final Remarks

This overview reveals some of the strengths and weaknesses of the four inverse methods analysed. The Finite Element Model Updating relies on an intuitive idea and therefore, it is often an easy choice. Though the other three methods outperform it in terms of computational efficiency, the complex algorithms hamper the use of these methods. Moreover, the Finite Element Model Updating, which relies on the comparison of experimental and numerical data, seems to be less affected by noise. Therefore, the other three methods require more careful treatment of experimental data. The Virtual Fields Method presents reasonable results in terms of accuracy and a minimal computational expense when compared to the Finite Element Model Updating. Moreover, the Virtual Fields Method is an interesting option when the distribution of the load along the boundary of the specimen is unknown. The Virtual Fields Method seems the best option to avoid the high computational expense of the Finite Element Model Updating.

Chapter 3

VFM - Single test calibration methodology

The interest in the Virtual Fields Method has increased in recent years. The Virtual Fields Method presents an interesting balance between the accuracy of the calibration results and computational cost. Therefore, it is often pointed out as an efficient alternative to Finite Element Model Updating. For the Virtual Fields Method to be a solid alternative to Finite Element Model Updating, the complexity of the method must be overcome by the pluses. Computational efficiency is an asset and not requiring the exact knowledge of boundary conditions is another plus. Nevertheless, it continues to be difficult to rank the robustness of these two methods even in the case of simple plasticity models.
Moreover, the calibration of anisotropic plasticity models due to a large number of material parameters worsens the computational expense of Finite Element Model Updating. The Virtual Fields Method can play an important role here. On the other hand, it is crucial to find a test that can generate the experimental database to perform the simultaneous identification of the multiple parameters that constitute these models and lead the process to a minimum number of tests. The biaxial test in a cruciform specimen is a strong candidate, the test presents a variety of strain paths with a large range of strain values. Nevertheless, it has never been combined with the Virtual Fields Method in this context. Similarly, a recently developed heterogeneous test, called the butterfly test, must be considered.

3.1 Identification of Material Parameters for Plasticity Models: A Comparative Study on the Finite Element Model Updating and the Virtual Fields Method

This section presents a comparative study focused on the accuracy of the Virtual Fields Method and the Finite Element Model Updating in plasticity models. The two methods are tested in the finite strain framework. A simple uniaxial test with varying cross-section is chosen. Swift's isotropic hardening law is the selected model.

Identification of Material Parameters for Plasticity Models: A Comparative Study on the Finite Element Model Updating and the Virtual Fields Method

J.M.P. Martins[1,2, a)], S. Thuillier[1, b)] and A. Andrade-Campos[2, c)]

[1] *Univ. Bretagne Sud, FRE CNRS 3744, IRDL, F-56100 Lorient, France.*
[2] *Centre for Mechanical Technology and Automation (TEMA), GRIDS Research Unit, Mechanical Engineering Department, University of Aveiro Campus Universitário de Santiago, 3810-193 Aveiro, Portugal.*

[a)] Corresponding author: *joao.martins52@ua.pt*
[b)] *sandrine.thuillier@univ-ubs.fr*
[c)] *gilac@ua.pt*

Abstract. The identification of material parameters, for a given constitutive model, can be seen as the first step before any practical application. In the last years, the field of material parameters identification received an important boost with the development of full-field measurement techniques, such as Digital Image Correlation. These techniques enable the use of heterogeneous displacement/strain fields, which contain more information than the classical homogeneous tests. Consequently, different techniques have been developed to extract material parameters from full-field measurements. In this study, two of these techniques are addressed, the Finite Element Model Updating (FEMU) and the Virtual Fields Method (VFM). The main idea behind FEMU is to update the parameters of a constitutive model implemented in a finite element model until both numerical and experimental results match, whereas VFM makes use of the Principle of Virtual Work and does not require any finite element simulation. Though both techniques proved their feasibility in linear and non-linear constitutive models, it is rather difficult to rank their robustness in plasticity. The purpose of this work is to perform a comparative study in the case of elasto-plastic models. Details concerning the implementation of each strategy are presented. Moreover, a dedicated code for VFM within a large strain framework is developed. The reconstruction of the stress field is performed through a user subroutine. A heterogeneous tensile test is considered to compare FEMU and VFM strategies.

INTRODUCTION

The reduction of the time and the costs to bring a new material or product to market is of primary importance for any industry. Numerical simulation tools have been exploited in this sense and nowadays, they play an important role in the design of a new component or manufacturing process. One of the key points for the success of the predictions of these tools has been the use of appropriate constitutive models and the respective calibration.

The description of the material behaviour has been an utmost problem for the community of solid mechanics and materials science and consequently, there is a wide range of material models available on the literature, especially for modelling the plastic response of a material. However, the accuracy of these models is strictly connected with the calibration process. The objective of the calibration process is to estimate the set of material parameters, which make part of the chosen model, to adjust the best as possible the model to the real response of the material.

The use of full-field measurements techniques (e.g. Digital Image Correlation) with the aim of calibrating material models is becoming more and more popular and one of the main advantages of using these techniques is the capability of exploring heterogenous strain or displacements fields. For an appropriate test geometry, the information contained in the measured heterogenous fields can be enough to identify several material parameters, thus reducing the number of required tests to calibrate a model. Consequently, different strategies to deal with this kind of data have emerged in

the recent years [1]. Among them, the ones that received more attention have been the Finite Element Model Updating and the Virtual Fields Method. These two strategies have been applied in the identification of different constitutive models, especially in the framework of plasticity (eg. [2, 3]). However, studies on the comparison of their performance in the framework of plasticity are rare. Therefore, when it comes time to choose which is the best strategy to deal with the conditions of a given application, there is no support. Thus, the objective of this work is to compare both strategies in the framework of plasticity and provide insight on the details of their application.

INVERSE METHODS

Finite Element Model Updating

The identification of material parameters with the Finite Element Model Updating (FEMU) relies on an intuitive idea, which is to adjust the material parameters from a Finite Element model in order to minimize the difference between experimental and numerical strain/displacements fields over a large area. This method has several advantages, but mainly its widespread application is due to the ease of implementation and the flexibility that it offers. It can easily be adapted to complex geometrical shapes and different kinds of data, e.g. displacements, strains or loads. In fact, this strategy does not require full-field measurements to be used, it can be used with just local measures. As for the disadvantages, this method requires a numerical model with a proper representation of the experimental test and for each evaluation of the objective function, it requires at least one run of this model, which can be time-consuming.

In the literature, a variety of objective function definitions can be found. It depends on the type of experimental test, the application and availability of experimental data. Some authors prefer the minimization of the gap between displacements, whereas others between strains. These can also be combined with the minimization of the gap between forces [3,4]. Here, a combination of strain components and forces is adopted. These two quantities have different units, which should not affect the optimization process, therefore these quantities are normalized. The chosen objective function can be written in a least-square sense as:

$$f(\boldsymbol{\xi}) = \frac{1}{n_\mathrm{s}} \sum_{i=1}^{n_\mathrm{s}} \left\{ \frac{1}{n_\mathrm{p}} \sum_{j=1}^{n_\mathrm{p}} \left[\left(\frac{\varepsilon_{xx}^{\mathrm{num}} - \varepsilon_{xx}^{\mathrm{exp}}}{\varepsilon_{xx}^{\mathrm{exp}}} \right)^2 + \left(\frac{\varepsilon_{yy}^{\mathrm{num}} - \varepsilon_{yy}^{\mathrm{exp}}}{\varepsilon_{yy}^{\mathrm{exp}}} \right)^2 + \left(\frac{\varepsilon_{xy}^{\mathrm{num}} - \varepsilon_{xy}^{\mathrm{exp}}}{\varepsilon_{xy}^{\mathrm{exp}}} \right)^2 \right]_j + \left(\frac{F^{\mathrm{num}} - F^{\mathrm{exp}}}{F^{\mathrm{exp}}} \right)^2 \right\}_i , \tag{1}$$

where $\boldsymbol{\xi}$ is the vector of material parameters, ε_{xx}, ε_{yy} and ε_{xy} are the in-plane components of the strain tensor and F is the force. The superscripts num and exp define the numerical and experimental data, respectively. n_s and n_p are the number of time steps and the number of in-plane measurement points, respectively.

Virtual Fields Method

The Virtual Fields Method (VFM) is based on the Principle of Virtual Work, which establishes the weak form of the equilibrium equations. This strategy allows the estimation of the material parameters through the minimization of the gap between internal and external virtual works. Both quantities are calculated based on the experimental measurements, therefore it avoids the use of numerical simulation tools. This is an advantage when compared with FEMU, because the computational cost of VFM is substantially lower. VFM requires the availability of full-field measurements to calculate the internal virtual work and as the full-field measurements are usually available for the surface of a specimen, it is necessary to assume that these measurements are known along the thickness. According to that, plane stress conditions are assumed. Moreover, in order to compute the external virtual work, it is required the knowledge of the resultant in-plane loading applied to the body.

In this study, the framework of finite strains theory is adopted, thus the Principle of Virtual Work is written using a Lagrangian (or material) description. Assuming static conditions and neglecting the body forces, the cost function has the following form

$$\varphi(\boldsymbol{\xi}) = \sum_{i=1}^{n_s} \left(\int_{\Omega_0} \mathbf{P}(\boldsymbol{\xi}, \boldsymbol{\varepsilon}^{\exp}) : \mathrm{Grad}\mathbf{u}^* \, dV - \int_{\partial\Omega_0} \overline{\mathbf{T}} \cdot \mathbf{u}^* \, dS_0 \right)_i^2 , \tag{2}$$

where $\mathbf{P}(\boldsymbol{\xi}, \boldsymbol{\varepsilon}^{\exp})$ is the first Piola-Kirchhoff stress tensor, which is a function of $\boldsymbol{\xi}$ and of the strain tensor $\boldsymbol{\varepsilon}^{\exp}$. This last one is derived from the measured displacement $\mathbf{u}^{\exp}$. The internal work is computed for the volume V occupied by the domain of the body Ω_0, in the reference configuration. $\overline{\mathbf{T}}$ is the prescribed first Piola-Kirchhoff traction vector on the boundary surface $\partial\Omega_0$, thus it is the measured force per unit of reference surface area. $\mathbf{u}^*$ is the virtual displacement field defined on the reference configuration. The Lagrangian description is a convenient description to write the Principle of Virtual Work, since for the computation of the internal and external work the geometric quantities are defined on the reference configuration. For more details on this formulation see [5,6].

The reconstruction of the stress field from the strain field is a key point for the calculation of the internal virtual work. Due to the non-linearity of the model, the stress reconstruction is performed recurring to an algorithm of the type Backward-Euler return [8].

The other key point of VFM is the selection of suitable virtual fields $\mathbf{u}^*$. This is frequently performed empirically, based on the experience of the user. However, it has been proposed recently an automatic strategy for the non-linear case [7]. Regarding the empiric approach, the virtual fields are selected in a convenient way. First, displacement boundary conditions must be satisfied, so they must be kinematically admissible ($\mathbf{u}^* = 0$ on the boundary with prescribed displacements). Moreover, to simplify the Principle of Virtual Work and calculate the external virtual work from the resultant of the applied force, the selected virtual field must be collinear with the applied force and constant on the boundary of application [6].

FEMU AND VFM COMPARISON: IDENTIFICATION OF THE PLASTIC RESPONSE

Material Model

For the present study, the material model chosen encompasses the following assumptions: (i) isotropic elastic behaviour described by the generalized Hooke's Law; (ii) isotropic von Mises yield criterion associated to isotropic hardening described by the Swift's law. Since the objective is the identification of the material parameters related with the plastic response, the elastic parameters, Young's modulus and Poisson's ratio are assumed as known quantities and take the following values: $E = 210$ GPa and $\nu = 0.3$, respectively. The remaining material parameters are the ones which govern the Swift's Law, given by:

$$\sigma_y = K\left(\varepsilon_0 + \bar{\varepsilon}^{\mathrm{p}}\right)^n \qquad \text{with} \qquad \varepsilon_0 = \left(\frac{\sigma_0}{K}\right)^{1/n} , \tag{3}$$

where σ_y is the flow stress, K is the hardening coefficient, n is the hardening exponent, σ_0 the initial yield stress and $\bar{\varepsilon}^{\mathrm{p}}$ denotes the equivalent plastic strain. The material parameters to be determined are K, n and σ_0.

Numerical Test

In order to compare the performance of the two inverse strategies, numerically emulated data are used. A specimen with varying cross-section is chosen [2]. The geometry of the specimen is depicted in Fig. 1 (a). This kind of geometry offers a heterogeneous strain field over a large area.

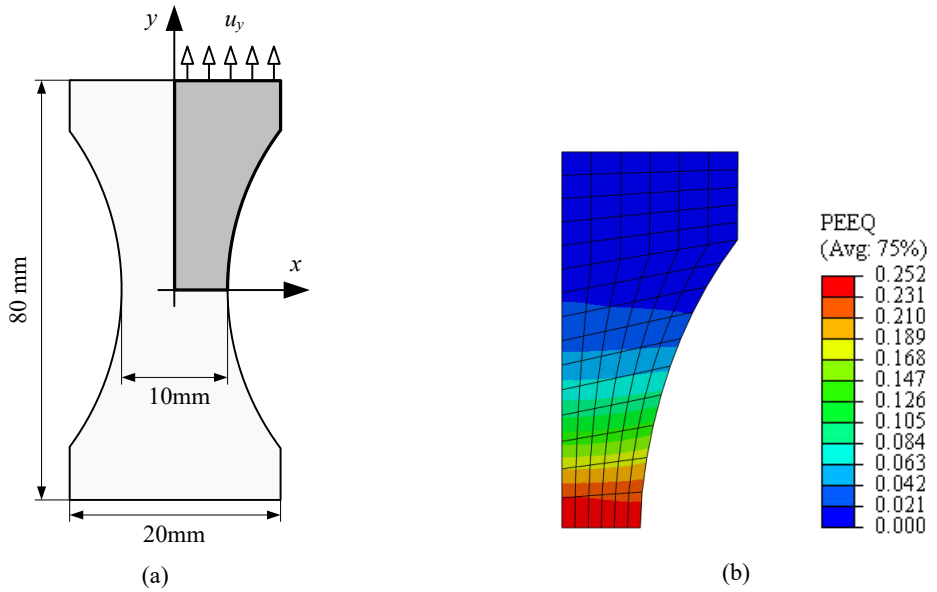

FIGURE 1. Specimen geometry (a) and corresponding finite element model (b). Equivalent Plastic strain distribution after a displacement of 3 mm

Exploiting the symmetries of the problem, only one-fourth of the sample is represented in the finite element model. The model is built up with ABAQUS standard assuming plane stress conditions and a large strain formulation. The mesh is defined as regular and the element CPS4 (bilinear shape functions and full integration) is chosen. A total of 112 elements are used. Symmetry boundary conditions are applied to the boundaries $x = 0$ and $y = 0$. A displacement boundary condition, with a total displacement of $u_y = 3$ mm, is applied along the y direction to the top boundary of the specimen. In order to emulate the full-field measurements, a reference set of material parameters is chosen for the Swift's law with the following values: $K = 565$ MPa, $n = 0.26$ and $\sigma_0 = 160$ MPa. The mesh is shown in Fig. 1 (b) as well as the equivalent plastic strain distribution at the maximum displacement. The maximum value of plastic deformation is $\bar{\varepsilon}^p = 0.252$ and it is localized in the centre of the specimen. The gradient of deformation is mainly along the y direction.

Optimization Procedures and Implementation Details

Both FEMU and VFM strategies require an optimization method to minimize the objective functions and consequently, find the best parameter set. In the literature, there is no consensus on each method should be used, but one of the most popular, belonging to the family of least-square gradient-based methods, is the Levenberg-Marquardt algorithm. Its low CPU cost and ease of implementation are the main advantages. However, it is common to reach a local minimum instead of a global one.

In this study, the Levenberg-Marquardt method is adopted to minimize the objective function of both inverse strategies. The Jacobian matrix is calculated by forward finite differences. A convergence criterion of 1×10^{-10} is chosen.

Regarding the implementation details of FEMU, the strain field used as input is extracted from the same mesh presented in Fig. 1 (b). The centroid of the elements is chosen as the location for the calculation of the logarithmic strain tensor. For VFM, the displacements field is the input data. However, the determination of the internal virtual work requires the derivation of the logarithmic strain tensor, which in this case, is calculated at the centroid of the finite elements by means of bilinear shape functions. All the calculations required for VFM are performed using the same mesh (see Fig. 1), avoiding extra interpolation errors. The reconstruction of the stress field, which is required

for VFM, is performed through a user subroutine. Regarding the selection of the virtual fields, the empirical approach is chosen, and the simplest virtual field is selected $\left(u_x^* = 0,\ u_y^* = y\right)$.

Results and Discussion

The numerical data generated by the model presented in Fig. 1 is used as representing the experimental data, thus the reference parameters are known *a priori* ($\xi^{\text{ref}} = \left(K = 565 \text{ [MPa]},\ n = 0.26,\ \sigma_0 = 160 \text{ [MPa]}\right)$). It should be mentioned that the reference simulation was run with the automatic increment control technique, provided by ABAQUS, resulting in a total of 30 increments (or time steps) to complete the simulation.

In order to evaluate the performance of both strategies and verify that the estimated solution is a global minimum, two initial sets of parameters are arbitrarily chosen to start the optimization process, namely $\xi^{\text{sup}} = \left(K = 965 \text{ [MPa]},\ n = 0.35,\ \sigma_0 = 234 \text{ [MPa]}\right)$ and $\xi^{\text{inf}} = \left(K = 165 \text{ [MPa]},\ n = 0.08,\ \sigma_0 = 100 \text{ [MPa]}\right)$. The results for both strategies are presented in Table 1, with the respective error for each parameter. It is also presented the final value of the objective function for each identification.

TABLE 1. Identified parameters for both strategies (FEMU and VFM) and for both initial solutions ξ^{sup} and ξ^{inf}.

Initial sets	K [MPa]	n	σ_0 [MPa]	**Objective Func.**
		VFM		
ξ^{sup} and ξ^{inf}	564.24	0.265	160.72	$\varphi = 2.29\times10^{5}$ N·mm
Error [%]	*0.134*	*2.084*	*0.456*	
		FEMU		
ξ^{sup}	686.23	0.343	174.99	$f = 7.62\times10^{-2}$
Error [%]	*21.457*	*32.072*	*9.371*	
ξ^{inf}	524.36	0.245	153.25	$f = 9.12\times10^{-3}$
Error [%]	*7.192*	*5.739*	*4.216*	
		FEMU (fixed increment size)		
ξ^{sup}	568.74	0.2633	160.36	$f = 5.97\times10^{-6}$
Error [%]	*0.662*	*1.270*	*0.228*	
ξ^{inf}	552.77	0.250	159.7	$f = 7.95\times10^{-5}$
Error [%]	*2.164*	*3.729*	*0.187*	

VFM strategy is able to retrieve the reference parameters with an error lower to 0.5% for the parameters K and σ_0. The parameter n has a higher error, around 2%, but still reasonable. These results are reached for the two initial sets, suggesting a global minimum for the set of parameters estimated.

FEMU strategy reaches different solutions for the two initial sets of parameters, indicating the presence of local minima. Moreover, when Swift's law is plotted for the different sets of parameters (see Fig. 2 (a)), it is possible to observe that both sets give a good description at small values of the equivalent plastic strain. This suggests that points with a low value of the equivalent plastic strain have a higher weight on the value of the objective function. This is in good agreement with Fig. 1 (b), where the spatial distribution of the equivalent plastic strain shows that most of the points have a low value of equivalent plastic strain at the end of the test. Fig. 2 (b) shows the evolution of the equivalent von Mises stress along the test for the centroid of the nearest element to the centre of the specimen (where the specimen has the highest values of equivalent plastic strain) and in this case, it is also possible to verify that more points are located within the interval from 0 to 0.05 of logarithmic strain than in other intervals. This last distribution of data points is a consequence of the automatic increment control technique. Therefore, the same test is simulated for a fixed increment size, much smaller, thus increasing the number of points and favouring an even distribution of the strain values in the input data of FEMU. In this case, the result FEMU strategy has succeeded in the identification process (see Table 1, FEMU (fixed increment size)), for both initial sets of material parameters. The maximum error is reached

for the parameter n, with a value of 3.7%, whereas the for the other parameters the error was lower than 2.2%. It highlights the influence of the cost function definition, where the relatively huge amount of considered data introduces indirectly weights.

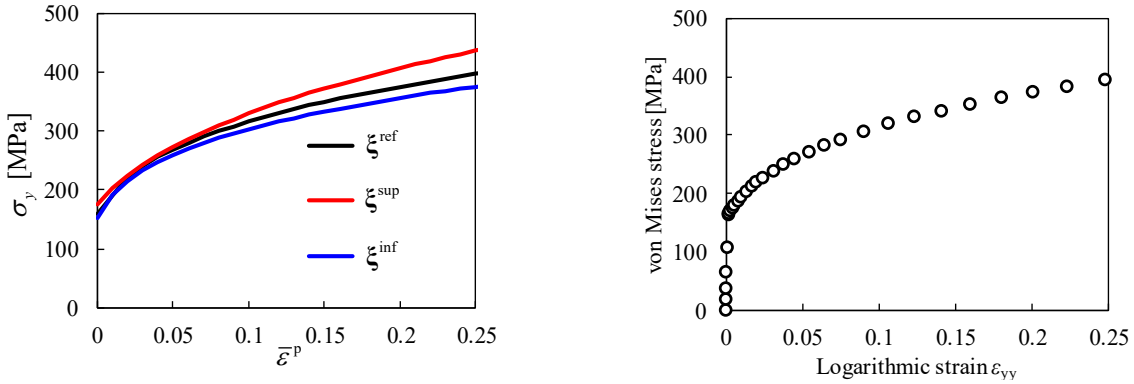

(a) (b)

FIGURE 2. Swift's law plotted for the solutions obtained with FEMU strategy (see Table 1) (a) and stress-strain curve obtained with the reference set of parameters for the nearest element to the centre of the specimen presented in Fig. 1(b).

CONCLUSIONS

FEMU and VFM inverse strategies have been compared in the framework of plasticity. In this case, the parameters of Swift's hardening law were identified with input data numerically generated. The results showed that VFM strategy was able to accurately retrieve the reference parameters for the given conditions, whereas FEMU strategy revealed sensitivity to the distribution of the input data for different levels of strain. For a more accurate identification with FEMU, equally distributed data for the different levels of strain should be used.

ACKNOWLEDGMENTS

The authors gratefully acknowledge the financial support of the Portuguese Foundation for Science and Technology (FCT) under the project P2020-PTDC/EMS-TEC/6400/2014 (POCI-01-0145-FEDER-016876) by UE/FEDER through the program COMPETE 2020. The authors also would like to acknowledge the Région Bretagne (France) for its financial support. J.M.P. Martins is also grateful to the FCT for the PhD grant SFRH/BD/117432/2016.

The authors would also like to thank Professor Fabrice Pierron and Mr. Aleksander Marek for the support in the development of the code for the Virtual Fields Method.

REFERENCES

1. S. Avril et al., Exp. Mech. **48**, pp.381–402 (2008).
2. J.-H. Kim et al., Int. J. Solids Struct. **50**, pp.3829–3842 (2013).
3. S. Cooreman et al., Exp. Mech. **48**, pp.421-433 (2008).
4. H. Haddadi and S. Belhabib, Int. J. Mech. Sci. **62**, pp.47-62 (2012).
5. M. Rossi et al., Int. J. Solids Struct. **97-98**, pp.322-335 (2016).
6. F. Pierron and M. Grédiac, The Virtual Fields Method – Extracting constitutive mechanical parameters from full-field deformation measurements, Springer, New York, 2012.
7. A. Marek et al., Comput. Mech. **60**, pp.409-431 (2017)
8. M. A. Crisfield, Non-linear Finite Element Analysis of Solids and Structures, vol.1, John Wile y& Sons, New York, 1991.

3.2 Calibration of anisotropic plasticity models using a biaxial test and the Virtual Fields Method

In this section, the combination of the Virtual Fields Method and a cruciform specimen in biaxial tension is explored. It is intended to propose a calibration methodology to simultaneously calibrate an isotropic hardening law and an anisotropic yield criterion. Three cruciform geometries are analysed as potential candidates to combine with the Virtual Fields Method. The study is performed with virtual experimental data and the reference parameters are known a priori, which allows to compare directly with the identification results and evaluate the quality of the information obtained from the test.

International Journal of Solids and Structures 172–173 (2019) 21–37

Contents lists available at ScienceDirect

International Journal of Solids and Structures

journal homepage: www.elsevier.com/locate/ijsolstr

Calibration of anisotropic plasticity models using a biaxial test and the virtual fields method

J.M.P. Martins[a,b,*], A. Andrade-Campos[a], S. Thuillier[b]

[a] Centre for Mechanical Technology and Automation (TEMA), GRIDS Research Unit, Mechanical Engineering Department, University of Aveiro, Portugal
[b] Univ. Bretagne Sud, UMR CNRS 6027, IRDL, Lorient, F-56100, France

ARTICLE INFO

Article history:
Received 30 November 2018
Revised 26 March 2019
Accepted 20 May 2019
Available online 22 May 2019

Keywords:
Anisotropic plasticity
Cruciform test
Full-field measurements
Parameter identification
Virtual fields method

ABSTRACT

The aim of the present study is to explore the combination of a biaxial test with a cruciform specimen and the virtual fields method to develop an efficient strategy for simultaneous identification of material parameters related with hardening and anisotropy in plasticity. In a first step, three cruciform geometries are evaluated as potential candidates to generate an experimental database for the calibration of the classical Hill'48 yield criterion and Swift's hardening law. In a second step, the geometry with the best results is used to calibrate YLD2000-2d yield criterion and Swift's hardening law. Numerical results are used as virtual experimental full-field measurements, which allows the comparison of the identified solution with the input material parameters. The accuracy of the identified material parameters is thoroughly assessed through the analysis of flow stress curve evolution, normalised yield stresses and plastic anisotropy coefficients, and for the last step, yield locus prediction. The results show the potential of this combination to identify simultaneously the material parameters related to hardening and anisotropy with a single test.

1. Introduction

The development of accurate and efficient models for the plastic behaviour of sheet metals has been crucial to improve components performance and to validate manufacturing processes through numerical simulation. In the last years, efforts have been oriented to provide models with more realistic descriptions of phenomena such as hardening and anisotropy (Bruschi et al., 2014). In the case of phenomenological models, which are usually preferred for Finite Element (FE) simulations, the improvement in accuracy has been associated to increased flexibility in the mathematical formulation, which has consequently led to an increase in the number of material parameters of the most recent models (Rabahallah et al., 2009). The increase in the number of parameters brought additional challenges for the identification of these parameters (or calibration process). The main challenge has been to gather the required data to properly identify the material parameters, which usually implies a time-consuming experimental campaign (Bandyopadhyay et al., 2018). Furthermore, the required data should be representative of the stress and strain states of the application that is intended to be simulated (Cooreman et al., 2008; Prates et al., 2014). These challenges have hampered the widespread use of more recent and accurate models (Bruschi et al., 2014).

The calibration process is the first step before any practical application of a constitutive model and it is directly related to its accuracy (Réthoré et al., 2013). Generally, a constitutive model to predict the plastic flow of sheet metals is defined by a hardening law and a yield criterion, within the framework of the associated flow rule. The calibration of both components is usually performed separately. For example, in the case of isotropic hardening, Swift's law (Swift, 1952) is traditionally calibrated by adjusting its prediction to stress-strain curves from uniaxial tensile tests or, when desired to extend the strain range, from hydraulic bulge tests (Tardif and Kyriakides, 2012). Regarding the yield criterion, modelling the anisotropic plastic behaviour of sheet metals has been a very active field and consequently, a large spectrum of yield criteria with different levels of complexity is available now. However, the criterion proposed by Hill (1948) (Hill'48 yield criterion) is still referred to as the most used yield criterion, a fact directly connected to the simplicity of both the formulation and the calibration process. In plane stress conditions, this criterion depends only on 4 parameters which can be analytically calculated using the plastic anisotropy coefficient (or Lankford's parameter)

* Corresponding author at: Centre for Mechanical Technology and Automation (TEMA), GRIDS Research Unit, Mechanical Engineering Department, University of Aveiro, Portugal.
E-mail addresses: joao.martins52@ua.pt (J.M.P. Martins), gilac@ua.pt (A. Andrade-Campos), sandrine.thuillier@univ-ubs.fr (S. Thuillier).

https://doi.org/10.1016/j.ijsolstr.2019.05.019
0020-7683/

in three different orientations i.e. rolling, diagonal and transverse ones, and the initial yield stress in the rolling direction. To collect this data, three uniaxial tensile tests at the three orientations are required. Nevertheless, its formulation lacks flexibility which restricts the representation of the mechanical behaviour of certain materials (Pearce, 1968), and also cannot predict both the initial yield stresses and the plastic anisotropy coefficients with the same accuracy (Banabic, 2010). Therefore, more flexible formulations have been proposed. Among others, the criterion proposed by Barlat et al. (2003) (YLD2000-2d) can be given as an example. The calibration of this yield criterion requires more information than Hill'48 yield criterion, namely, the plastic anisotropy coefficients and the yield stresses in different orientations of the sheet and also, the plastic anisotropic coefficient and yield stress from an equi-biaxial test. Moreover, the material parameters are identified using an optimisation procedure.

The examples presented above illustrate classical calibration procedures for the different components of a constitutive model. Nevertheless, the combination of full-field measurement techniques, such as digital image correlation (DIC), and the inverse methods developed to take full advantage of such data can simplify the calibration of classical plasticity models (Avril et al., 2008; Martins et al., 2018a). In this combined strategy, complex specimen geometries can be used in order to produce heterogeneous displacements/strain fields. An ideal geometry should produce heterogeneous displacement/strain fields that contain the required experimental data to calibrate a model and thereby, reduce the number of tests of the experimental campaign. Accordingly, the cruciform geometry has been investigated over the years (Prates et al., 2016). This type of geometry in biaxial tension is known for producing strain paths ranging from biaxial tension, at the centre of the specimen, to uniaxial tension, in the arms of the specimen (Zhang et al., 2014; Souto et al., 2015). Moreover, Zhang et al. (2014) through numerical analysis, showed that the prediction of the strain distribution in the central area of the specimen is dependent of the yield criterion selected.

The studies conducted on the biaxial test with the cruciform geometry are often based on inverse methods of a FEMU-based type. This type of inverse methods determines the best set of material parameters through the minimisation of a function representing the gap between numerical and experimental results. This function can be built based on strain or displacement fields or force values, or it can be a combination of these quantities. In the framework of plasticity, a thorough review of the combination of the biaxial test with the cruciform geometry and FEMU-based inverse methods can be found in (Prates et al., 2016). As an example of such studies, it can be mentioned the work of Zhang et al. (2014). These authors proposed a geometry for a cruciform specimen and succeeded to identify the material parameters of Bron and Besson yield criterion (Bron and Besson, 2004) (criterion with a total of 13 parameters). The function to be minimised was built using the major and minor strain distributions along a diagonal path in the central area of the specimen captured for a single time instant of the test. More recently, Coppieters et al. (2018) used a perforated cruciform specimen (Lecompte et al., 2007) to study the influence of boundary conditions, number of time instants and settings of DIC system on the identification of Hill'48 criterion's parameters using a FEMU inverse method. This study also reveals that such an inverse approach can give better results than a conventional identification procedure for Hill'48 yield criterion.

Although FEMU-based inverse methods can be considered a feasible tool for parameter identification, these are excessively time-consuming, a drawback attributed to the FE simulations required within the iterative process of identification. The virtual fields method (VFM) is an alternative to overcome this drawback (Martins et al., 2018a). This inverse method relies on the principle of virtual work and on the choice of a set of virtual fields (Pierron and Grédiac, 2012). In the framework of plasticity, the most recent applications of the VFM have been the simultaneous calibration of isotropic hardening and anisotropic yield criteria (Rossi et al., 2016; Marek et al., 2018), the calibration of kinematic hardening law (Fu et al., 2016) and a distortional hardening model (Fu et al., 2017). Rossi et al. Rossi et al. (2016) used a notched specimen to perform the simultaneous calibration of Swift's law and two criteria, namely *i.e.* Hill'48 yield criterion and YLD2000-2d yield criterion (Barlat et al., 2003). The obtained results were reasonable, although the authors suggested that a different specimen could improve the results. Marek et al. Marek et al. (2018) focused on the validation of a new strategy to automatically determine an optimal set of virtual fields for the calibration process. The results have been improved, but the same notched specimen was used.

The purpose of the present study is to explore the combination of the VFM and a cruciform specimen tested in biaxial tension for the simultaneous calibration of an isotropic hardening law and an anisotropic yield criterion. This combination has already been tested, but for the framework of hyperelasticity (Promma et al., 2009). In that case, the number of material parameters was just two, corresponding to the Mooney's hyperelastic model in plane stress conditions, and a linear version of the VFM was used (Pierron and Grédiac, 2012). The good results obtained proved the feasibility of this combination. Nevertheless, any study on this combination has been performed in the framework of anisotropic plasticity. The present study is performed with virtual experimental data and the reference parameters are known *a priori*, which allows to compare directly with the identification results and evaluate the quality of the information obtained from the test. In this first analysis, the evaluation of DIC settings and noise effect are out of the scope, though it will be required in further analysis. The outline of the article is as follows. Section 2 presents the VFM and a set of virtual fields that can be used with a cruciform specimen submitted to biaxial tension. Section 3 introduces the constitutive models addressed in this study, namely Swift's hardening law and the yield criteria Hill'48 and YLD2000-2d. In Section 4, three cruciform geometries are evaluated as potential candidates to combine with the VFM. A thorough evaluation of the generated strain and stress fields in these geometries is performed. Section 5 provides a detailed discussion regarding the identification results obtained, namely a comparison of the three cruciform geometry and the performance of the best geometry in the calibration of YLD2000-2d and Swift's law.

2. The virtual fields method

2.1. Theoretical background

The VFM is an inverse method for parameter identification based on full-field measurements which relies on the principle of virtual work, written in the framework of large strains in this study. This large strains formulation has been firstly applied to the calibration of hyperelastic models by Promma et al. (2009) and subsequently, adopted in several studies for the calibration of plasticity models (Rossi et al., 2016; Marek et al., 2018; Rossi and Pierron, 2012). Nevertheless, other formulations can be found in (Pierron and Grédiac, 2012; Pierron et al., 2010; Notta-Cuvier et al., 2015).

First, reference and current configurations of a continuum solid body Ω must be distinguished. Consider the reference or undeformed configuration Ω_0 occupied by the solid body at the beginning of the deformation process (time instant $t = 0$) and delimited by Γ_0. Also, consider that the boundary Γ_0 is composed of two sub-boundaries Γ_0^u and Γ_0^f, such that $\Gamma_0 = \Gamma_0^u \cup \Gamma_0^f$ and

$\Gamma_0^u \cap \Gamma_0^f = \emptyset$. Γ_0^u corresponds to the boundary with prescribed displacements and Γ_0^f the boundary with prescribed force. Moreover, the current or deformed configuration Ω_t is assumed as the region occupied by Ω after the deformation process at the time instant t. The position of a particle in the reference configuration Ω_0 is described by $\mathbf{X}$ relative to a reference frame and $\mathbf{x}(\mathbf{X}, t)$ gives the position of this same particle in the current configuration Ω_t. The displacement field which relates the position of this particle in the reference configuration and its position in the current configuration is given by $\mathbf{u}(\mathbf{X}, t) = \mathbf{x}(\mathbf{X}, t) - \mathbf{X}$.

Assuming quasi-static conditions and neglecting body forces, the principle of virtual work can be expressed in the reference configuration as:

$$-\underbrace{\int_{\Omega_0} \mathbf{P} : \text{grad}\ \mathbf{U}^* \mathrm{d}V}_{W_{\text{int}}} + \underbrace{\int_{\Gamma_0^f} \overline{\mathbf{T}} \cdot \mathbf{U}^* \mathrm{d}S}_{W_{\text{ext}}} = 0. \tag{1}$$

Here, $\mathbf{P}$ is the first Piola-Kirchhoff stress tensor, $\mathbf{U}^*$ is the virtual displacement vector defined in the reference configuration $\mathbf{X}$, as well as grad $\mathbf{U}^*$ (Holzapfel, 2000). $\overline{\mathbf{T}}$ is the first Piola-Kirchhoff stress vector prescribed on the boundary Γ_0^f with reference surface area S. Similarly, the first integral of Eq. (1) has to be computed over the reference volume V. The virtual displacement field ($\mathbf{U}^*$) must be a continuous and differentiable function and it is assumed, for a matter of convenience (Pierron and Grédiac, 2012; Holzapfel, 2000), that it vanishes on the boundary of applied displacements Γ_0^u (condition 1).

It is also useful to establish the link between reference and current configurations. Thus, the first Piola-Kirchhoff stress tensor can be defined in terms of the Cauchy stress tensor $\boldsymbol{\sigma}$ as

$$\mathbf{P} = \det(\mathbf{F})\boldsymbol{\sigma}\mathbf{F}^{-\mathrm{T}}, \tag{2}$$

where $\det(\mathbf{F})$ is the determinant of the deformation gradient $\mathbf{F}$ and $\mathbf{F}^{-\mathrm{T}}$ is the transpose of its inverse. The deformation gradient can be defined as

$$\mathbf{F} = \frac{\partial \mathbf{x}}{\partial \mathbf{X}} = \mathbf{I} + \frac{\partial \mathbf{u}}{\partial \mathbf{X}}, \tag{3}$$

where $\mathbf{I}$ is the second order unity tensor.

According to Eq. (1), the principle of virtual work states, for a body in equilibrium and for a continuous virtual field, that the internal virtual work W_{int} equals the external virtual work W_{ext} and this should be satisfied for every time instant t. The computation of the internal virtual work is, therefore, a key point that requires a constitutive model to establish the link between the stress field and the strain field. In the framework of elasto-plasticity, the relation between the stress field and the strain field is non-linear and history-dependent or path-dependent. Elasto-plastic constitutive models are commonly formulated in terms of the Cauchy stress tensor $\boldsymbol{\sigma}$. Therefore, the stress field corresponding to a defined time instant t is usually a function of the material parameters (consider $\boldsymbol{\xi}$ as the vector that gathers all material parameters) and the history of deformation, here denoted by $\boldsymbol{\varepsilon}|_{0\to t}$, and can be defined as

$$\boldsymbol{\sigma}^t = \boldsymbol{\sigma}^t\left(\boldsymbol{\xi}, \boldsymbol{\varepsilon}|_{0\to t}\right). \tag{4}$$

The principle of virtual work is the foundation for the VFM. In non-linear cases, to solve the inverse problem and find the best set of material parameters, the main idea behind the VFM is the minimisation of the difference between internal and external virtual work. The objective function is written in a least-square form as

$$\varphi\left(\boldsymbol{\xi}\right) = \left(W_{\text{int}}\left(\boldsymbol{\xi}\right) - W_{\text{ext}}\right)^2. \tag{5}$$

In practice, the internal and external virtual works are computed from measured quantities, namely the displacement fields and the resultant of the applied loads. The internal virtual work results from the reconstruction of the stress field, which in turn is performed using the strain fields and the adopted constitutive model. The strain fields are computed from the measured displacement fields $\mathbf{u}$ by means of the deformation gradient. Using the theorem of polar decomposition, the deformation gradient can be decomposed as

$$\mathbf{F} = \mathbf{V}\mathbf{R} \tag{6}$$

with $\mathbf{V}$ the left Cauchy stretch tensor and $\mathbf{R}$ is the orthogonal rotation tensor. The strain field can be computed for each time instant as the Hencky's strain tensor

$$\boldsymbol{\varepsilon} = \ln\mathbf{V}. \tag{7}$$

Moreover, the computation of the stress field is conventionally expressed in a local material frame free of rigid body rotations, thus the strain tensor in this local co-rotational frame can be computed as

$$\hat{\boldsymbol{\varepsilon}} = \mathbf{R}^{\mathrm{T}}\boldsymbol{\varepsilon}\mathbf{R}. \tag{8}$$

Full-field measurements are generally presented as a discrete number of measurements points on the surface of the specimen, and to apply the VFM, these points are usually fitted to a mesh of elements. Strain and stress tensors are then calculated at the centroid of these elements and become representative of the average strain and stress field in a specific element. This calculation can be performed, for example, by means of shape functions. This discrete form of the data allows to approximate the integral of the internal virtual work by a discrete sum as follows

$$W_{\text{int}}\left(\boldsymbol{\xi}, t\right) = \sum_{i=1}^{n_e} \mathbf{P}\left(\boldsymbol{\xi}, t\right) : \text{grad}\ \mathbf{U}^* A_i e_i. \tag{9}$$

where n_e represents the number of elements and A_i and e_i represent the area and the thickness of each element. The elemental area A_i and elemental thickness e_i do not depend on time, these quantities refer to the reference configuration Ω_0. This is one of the advantages of formulating the principle of virtual work in the reference configuration.

The formulation presented can be applied to three dimensional data. Indeed, there are a few attempts to use it with three dimensional measurements, such as (Rossi and Pierron, 2012; Rossi et al., 2018; Rahmani et al., 2014). Nevertheless, as mentioned before, full-field measurements are commonly available just on the surface of the specimen. To overcome the lack of information through-thickness, plane stress conditions are generally assumed which is reasonable when the specimen thickness is much smaller compared to the other dimensions. Nevertheless, the determination of the first Piola-Kirchhoff stress tensor requires additional assumptions (Marek et al., 2018), namely the determinant of the deformation gradient $\det(\mathbf{F})$, which can be seen as the local ratio of current to reference volume (Reddy, 2013). The determinant of the deformation gradient can be determined as

$$\det(\mathbf{F}) = F_{33} \cdot (F_{11}F_{22} - F_{12}F_{21}). \tag{10}$$

According to Marek et al. (2018), the determination of the component F_{33} of the deformation gradient for each instant can be calculated as

$$F_{33}(t) = 1 + \varepsilon_{33}(t) = 1 + \int_0^t \Delta\varepsilon_{33}\mathrm{d}t, \tag{11}$$

which leaves the increment of the out-of-plane strain component $\Delta\varepsilon_{33}$ to be calculated. In elasto-plasticity, assuming isotropic elastic behaviour, this component can be determined using Hooke's law and taking advantage of the isochoric character of plasticity as follows

$$\Delta\varepsilon_{33} = -\frac{\nu}{1-\nu}\left(\Delta\varepsilon_{11}^{\mathrm{e}} + \Delta\varepsilon_{22}^{\mathrm{e}}\right) - \left(\Delta\varepsilon_{11}^{\mathrm{p}} + \Delta\varepsilon_{22}^{\mathrm{p}}\right), \tag{12}$$

where $\Delta\varepsilon^{e}_{11}$ and $\Delta\varepsilon^{e}_{22}$ and $\Delta\varepsilon^{p}_{11}$ and $\Delta\varepsilon^{p}_{22}$ are the components of the elastic and plastic strain tensor, respectively, and ν is the Poisson's ratio.

The external virtual work is calculated based on the measured force during the test and constitutes a great asset for the VFM, because it is not required the distribution of the force. Choosing a virtual field constant along the boundary Γ_0^f (condition 2) simplifies the computation of the external virtual work as follows

$$W_{\text{ext}}(\mathbf{U}^*) = \mathbf{U}^* \cdot \int_{\Gamma_0^f} \overline{\mathbf{T}} \mathrm{d}S = \mathbf{U}^* \cdot \mathbf{F}^{\text{load}}. \tag{13}$$

Another important aspect in the calibration of non-linear constitutive models, such as elasto-plastic models, is the number of time instants taken into account to reconstruct the stress field. An accurate reconstruction of the stress field requires the use of several measures of the displacement field along the test. Therefore, Eq. (5) must be written as a sum of the principle of virtual work for each time instant. This is also a way to enrich the objective function. Finally, Eq. (5) can be written for different virtual fields in order to enrich the objective function and to explore the most relevant information from the reconstructed stress field. Hence, the objective function for the VFM can be written in a general form as

$$\varphi(\boldsymbol{\xi}) = \sum_{k=1}^{n_{\text{v}}} \sum_{j=1}^{n_{\text{t}}} \left(W_{\text{int}}\left(\boldsymbol{\xi}, \mathbf{U}^{*(k)}, t_j\right) - W_{\text{ext}}\left(\mathbf{U}^{*(k)}, t_j\right) \right)^2, \tag{14}$$

where n_{v} is the number of virtual fields selected and n_{t} the number of time steps considered. The identification of the material parameters is performed through the minimisation of Eq. (14). The minimum of the objective function is found when the identified material parameters in the selected constitutive model give rise to stress fields that minimise the difference between W_{int} and W_{ext} over the considered time instants. Generally, the reconstruction of the stress field for an elasto-plastic constitutive model requires an integration algorithm, in the same way as a finite element solver. There are several options for the integration algorithm, the classical one is based on the backward-Euler scheme combined with an elastic predictor/plastic corrector method to update the stress state. Examples of this kind of algorithm can be found in (Crisfield, 1991; Simo and Hughes, 1998). Nevertheless, other algorithms can be used, for instance, the one proposed by Rossi et al. (2016), called direct algorithm, which provides a faster reconstruction of the stress field.

2.2. Virtual fields definition and identification procedure

Defining a set of virtual fields is one of the main tasks before using VFM. In the framework of plasticity, three main strategies are currently available to select a suitable set of virtual fields (Marek et al., 2017). The most commonly used strategy is manually defined virtual fields. In this strategy, the user has to develop a continuous function adapted to the problem in hands (that depends on the experimental geometry and boundary conditions), that generates the value of the virtual field over the considered domain. Usually, the functions are of polynomial or periodical basis. This approach has the disadvantage of relying on the experience of the user to develop the function. Nevertheless, this approach is easy to implement. The other two strategies were developed to overcome the disadvantage of the previous one, allowing to obtain the virtual field set automatically with some user inputs (Pierron et al., 2010; Marek et al., 2017). Nevertheless, these two automatic strategies have the disadvantage of being more difficult to implement than the manual strategy and require a higher computational effort. Therefore, in the present study, the manual approach is chosen.

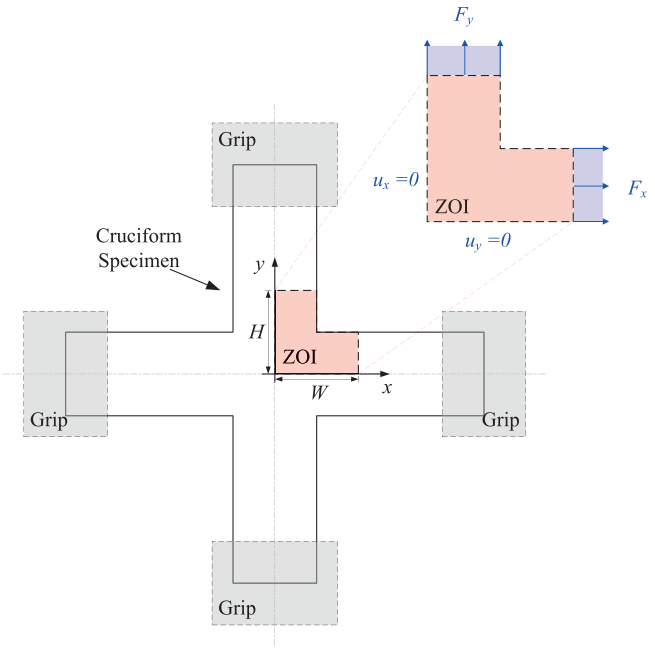

Fig. 1. Illustrative example of a biaxial test with a cruciform specimen and the respective zone of interest (ZOI) selected for the present study.

The set of virtual fields that will be presented can be used with any cruciform specimen. This set was developed to meet the above-mentioned conditions: to be null over the fixed boundaries (condition 1), where the prescribed displacement is zero, and constant over the boundaries at which the resultant of the applied force is known (condition 2). Consider the illustrative example of a general cruciform specimen under biaxial loading presented in Fig. 1. The set of developed virtual fields meets the above-mentioned conditions considering the zone of interest (ZOI) represented in Fig. 1, which corresponds to one-fourth of the central zone of the specimen. The boundaries with prescribed displacements ($u_x = u_y = 0$) are considered symmetry boundaries. For the boundaries marked with F_x and F_y, the resultant of the applied force is considered to be known for the respective direction.

The developed set of virtual field is the following:

$$\mathbf{U}^{*(1)} = \begin{cases} U_x^* = \frac{X}{W} \\ U_y^* = 0 \end{cases}, \tag{15}$$

$$\mathbf{U}^{*(2)} = \begin{cases} U_x^* = 0 \\ U_y^* = \frac{Y}{H} \end{cases}, \tag{16}$$

$$\mathbf{U}^{*(3)} = U_x^* = U_y^* = \sin\left(\frac{X}{W}\pi\right) \sin\left(\frac{Y}{H}\pi\right). \tag{17}$$

The constants W and H represent the height and width of the ZOI. X and Y represent the material coordinates in the global frame regarding the initial configuration. With this set of virtual fields, the objective function presented in Eq. (14) is written for $n_{\text{v}} = 3$. The first two virtual fields Eqs. (15) and (16) allow to writing the external virtual work for the applied force in the $x-$ and $y-$directions, which makes possible to use the force applied in each arm of the specimen. The third virtual field activates all the components of the stress tensor in the calculation of the internal virtual work since grad $\mathbf{U}^{*(3)}$ contains all the components active. Similar virtual fields can be found, for example, in (Rossi et al., 2016; Kim et al., 2014).

The objective function Eq. (14) is commonly normalised by the W_{ext}, but due to the selected virtual fields, this is not possible because the third virtual field Eq. (17) does not include the contribution of the W_{ext}. Therefore, Eq. (14) is normalised by the maximum W_{int}.

The theoretical background presented in this section, as well as the presented set of virtual fields, were implemented in an in-house code using the programming language Fortran. This code includes a gradient-based Levenberg-Marquardt optimisation method (Marquardt, 1963) used to minimise the objective function. The low computational cost and ease of implementation are the main assets of this gradient-based method. However, it is prone to reach local minima instead of a global one. In this study, the required Jacobian matrix for the Levenberg-Marquardt method is calculated by forward finite differences. The convergence criterion for this method was established as: the objective function becomes lower than a tolerance or the relative difference between parameters in consecutive iterations is lower than or equal to $\epsilon = 1 \times 10^{-10}$.

3. Material model

This section is dedicated to the elasto-plastic constitutive models used in this study. Two yield criteria are presented, Hill'48 and YLD2000-2d. In addition, as the present study is performed with virtual experimental data generated with two models which differ from each other in the adopted yield criterion, after presenting each yield criterion, the respective set of material parameters is also presented.

In this study, the elasto-plastic behaviour of sheet metals is modelled assuming additive decomposition of the strain rate tensor and associated flow rule (Cazacu et al., 2019). It is considered isotropic linear elastic behaviour described by Hooke's law and anisotropic plastic behaviour. The remaining elements, the yield surface and the hardening law, are presented below. It should be mentioned that all equations are presented in the orthogonal anisotropic frame (or material frame), which axes coincide with rolling, transverse and normal directions of the sheet plane. Moreover, the anisotropy frame is assumed to have a constant angle regarding the co-rotational frame along the deformation process.

The yield surface in plasticity, assuming isotropic hardening, can be written as

$$f = \overline{\sigma}(\boldsymbol{\sigma}) - \sigma_y\left(\overline{\varepsilon}^{\mathrm{p}}\right) = 0. \tag{18}$$

where $\overline{\sigma}(\boldsymbol{\sigma})$ is the equivalent stress defined by a yield criterion and $\sigma_y\left(\overline{\varepsilon}^{\mathrm{p}}\right)$ defines the flow stress. $\sigma_y\left(\overline{\varepsilon}^{\mathrm{p}}\right)$ is assumed as a function of a single internal variable, the equivalent plastic strain $\overline{\varepsilon}^{\mathrm{p}}$. Here, it is chosen the classical phenomenological Swift's law to describe the evolution of $\sigma_y\left(\overline{\varepsilon}^{\mathrm{p}}\right)$, which can be written as

$$\sigma_y\left(\overline{\varepsilon}^{\mathrm{p}}\right) = K\left(\varepsilon_0 + \overline{\varepsilon}^{\mathrm{p}}\right)^n, \qquad \varepsilon_0 = \left(\frac{\sigma_0}{K}\right)^{(1/n)} \tag{19}$$

σ_0, K and n are material parameters which must be identified according to the material. σ_0 is the initial yield stress and is assumed as a material parameter instead of ε_0, because when ε_0 is taken as the material parameter to be identified, the errors are usually high, due to the small order of magnitude of this parameter, but without significant impact on the initial yield stress (Martins et al., 2018a; Kim et al., 2013).

The first anisotropic yield criterion adopted is the quadratic criterion proposed by Hill (1948), which is commonly called Hill'48 yield criterion. Assuming plane stress condition, this criterion has the following form

$$\overline{\sigma}^2 = H(\sigma_{xx} - \sigma_{yy})^2 + G\sigma_{xx}^2 + F\sigma_{yy}^2 + 2N\sigma_{xy}^2. \tag{20}$$

H, G, F and N are the material parameters. σ_{xx}, σ_{yy} and σ_{xy} are the components of the Cauchy stress tensor in the anisotropic frame. It is often assumed, for matters of convenience, that the yield stress in the rolling direction corresponds to σ_y, leading to the condition $G + H = 1$. Following a direct procedure, the parameters G, F and N can be identified with closed-form solutions either as a function of the yield stresses or the plastic anisotropy coefficients. However, each approach gives different results (Banabic, 2010). The most common approach makes use of the plastic anisotropy coefficients (r_α) in directions 0°, 45° and 90° from the rolling direction. In this case, G, F and N are determined as

$$G = \frac{1}{1+r_0}; \qquad F = \frac{r_0}{r_{90}(1+r_0)}; \qquad N = \frac{(r_0+r_{90})(2r_{45}+1)}{2r_{90}(1+r_0)}. \tag{21}$$

Table 1
Parameters for Swift's law and Hill'48 yield, and normalized yield stress values (σ_α) and plastic anisotropy coefficients (r_α) for 0°, 45° and 90° according to the axis angle (α) between the rolling and tensile directions.

Swift's law			Hill'48 parameters		
σ_0 [MPa]	n	K [MPa]	F	G	N
160	0.26	565	0.2782	0.3731	1.5568
σ_α			r_α		
σ_0	σ_{45}	σ_{90}	r_0	r_{45}	r_{90}
1.000	1.030	1.051	1.680	1.890	2.253

In this study, Hill'48 yield criterion is combined with Swift's law to describe the behaviour of a typical mild steel. The reference material parameters associated with this model are presented in Table 1. The values of the elastic parameters are: Young's modulus $E = 210$ GPa and Poisson's ratio $\nu = 0.3$. Moreover, the normalised yield stress values (σ_α) and the plastic anisotropy coefficients (r_α) for different angles between the tensile and rolling direction ($\alpha = 0°, 45°$ and $90°$) are also presented in Table 1.

The second yield criterion adopted in this study is non-quadratic and was proposed by Barlat et al. (2003). Named YLD2000-2d, this yield criterion was formulated for plane stress conditions and can be expressed as

$$2\overline{\sigma}^a = |X_1' - X_2'|^a + |2X_2'' + X_1''|^a + |2X_1'' + X_2''|^a, \tag{22}$$

where a is a material parameter that usually assumes the value of 6 or 8, depending on the crystallographic structure of the material. X_1', X_2' and X_1'', X_2'' are the principal values of the tensors $\mathbf{X}'$ and $\mathbf{X}''$ obtained after two linear transformations on the deviatoric stress tensor. In a simple way, these can be determined directly from the Cauchy stress tensor as

$$\mathbf{X}' = \mathbf{L}'\boldsymbol{\sigma}; \qquad \mathbf{X}'' = \mathbf{L}''\boldsymbol{\sigma}, \tag{23}$$

where $\mathbf{L}'$ and $\mathbf{L}''$ can be defined based on eight parameters as

$$\begin{Bmatrix} L'_{11} \\ L'_{12} \\ L'_{21} \\ L'_{22} \\ L'_{66} \end{Bmatrix} = \begin{bmatrix} 2/3 & 0 & 0 \\ -1/3 & 0 & 0 \\ 0 & -1/3 & 0 \\ 0 & 2/3 & 0 \\ 0 & 0 & 1 \end{bmatrix} \begin{Bmatrix} \alpha_1 \\ \alpha_2 \\ \alpha_7 \end{Bmatrix} \quad \text{and} \tag{24}$$

$$\begin{Bmatrix} L''_{11} \\ L''_{12} \\ L''_{21} \\ L''_{22} \\ L''_{66} \end{Bmatrix} = \frac{1}{9}\begin{bmatrix} -2 & 2 & 8 & -2 & 0 \\ 1 & -4 & -4 & 4 & 0 \\ 4 & -4 & -4 & 1 & 0 \\ -2 & 8 & 2 & -2 & 0 \\ 0 & 0 & 0 & 0 & 9 \end{bmatrix} \begin{Bmatrix} \alpha_3 \\ \alpha_4 \\ \alpha_5 \\ \alpha_6 \\ \alpha_8 \end{Bmatrix}, \tag{25}$$

where α_k $(k = 1, \ldots, 8)$ are the parameters to be identified. The identification of the α_k parameters is conventionally performed

with the method proposed by Barlat et al. (2003) which requires the yield stresses σ_0, σ_{45} and σ_{90} and the plastic anisotropic coefficients r_0, r_{45} and r_{90}. Moreover, it also requires the biaxial yield stress σ_b and the biaxial anisotropy coefficient r_b. Using this data, α_k $(k = 1, \ldots, 8)$ can be identified using an optimisation method, such as the Newton-Raphson method as suggested by Barlat et al. (2003).

Similar to Hill'48, assuming σ_y as the yield stress in the rolling direction leads to the following condition

$$\left\{\frac{1}{2}\left[\left|\frac{2\alpha_1+\alpha_2}{3}\right|^a+\left|\frac{2(\alpha_3-\alpha_4)}{3}\right|^a+\left|\frac{4\alpha_5-\alpha_6}{3}\right|^a\right]\right\}^{(1/a)}=1. \tag{26}$$

This condition is not usually imposed, to the best of the authors' knowledge, except in (Guner et al., 2012).

The YLD2000-2d is combined with Swift's law to model the behaviour of an aluminium alloy AA6016 in T4 state (Yoon et al., 2004). The material parameters for this model are presented in Table 2. The elastic parameters are: $E = 70$ GPa and $\nu = 0.33$. Moreover, the normalised yield stress values and the plastic anisotropy coefficients are also presented (Yoon et al., 2004).

4. Cruciform geometries

In this section, three cruciform geometries used in biaxial tension are presented as well as the respective numerical models. Stress and strain fields are analysed for each geometry. In order to simplify the notation, the three geometries used in this work are called Cr1, Cr2 and Cr3. The first geometry selected was proposed by Zhang et al. (2014) to identify the material parameters of Bron and Besson yield criterion (Bron and Besson, 2004). The results of this study showed that the proposed geometry gives enough information for an accurate identification of a yield criterion. The dimensions and geometry of this specimen are presented in Fig. 2a. The other two geometries are adaptations of Cr1. The second

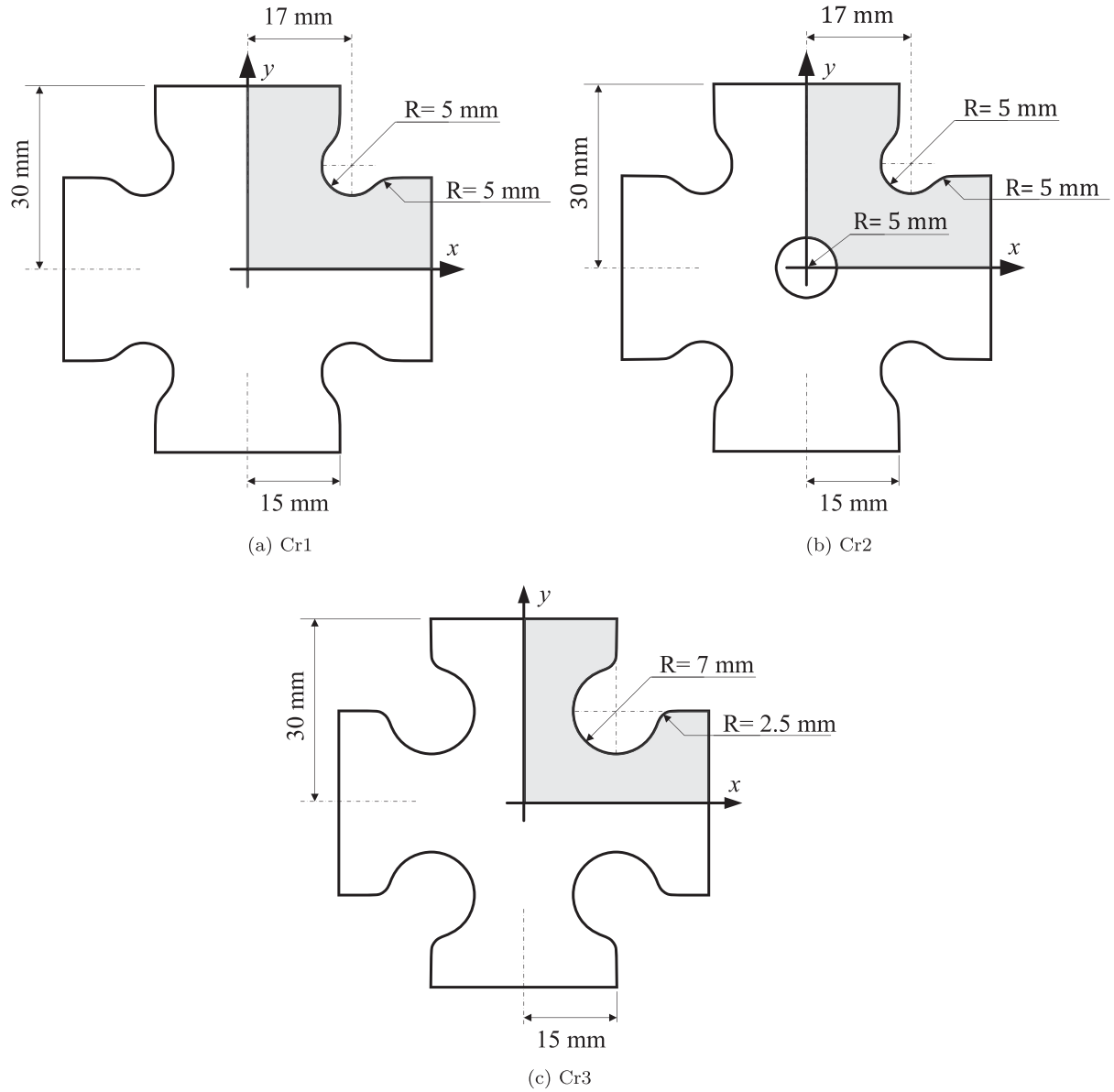

Fig. 2. Cruciform geometries: (a) Cr1 has been proposed by Zhang et al. (2014), (b) Cr2 and (c) Cr3 are adaptations of Cr1. The grey areas represent the geometry of the FE model.

Table 2
Parameters for Swift's law and YLD2000-2d yield criterion and normalized yield stress values (σ_α) and plastic anisotropy coefficients (r_α) for 0°, 45° and 90° according to the axis angle (α) between the rolling and tensile directions.

Swift's law			σ_α			r_α		
σ_0 [MPa]	n	K [MPa]	σ_0	σ_{45}	σ_{90}	r_0	r_{45}	r_{90}
212.03	0.239	385.47	1.0	0.984	0.944	0.94	0.39	0.64
YLD2000-2d parameters								
α_1	α_2	α_3	α_4	α_5	α_6	α_7	α_8	m
0.9580	1.045	0.9485	1.0568	0.9938	0.9397	0.9200	1.1482	8.0

geometry (Fig. 2b) has the same dimensions as Cr1, but contains a hole in the centre. The hole has the particular role of increasing the strain field heterogeneity and thus, increasing the sensitivity of the strain field to the material parameters. The inclusion of a hole in the geometry with this aim was reported in several studies such as, (Lecompte et al., 2007; Pottier et al., 2011; Schmaltz and Willner, 2014; Denys et al., 2016). For the third specimen (Fig. 2), the rounding radius at the intersection of the arms has been changed.

The three geometries are numerically tested in the same conditions. Due to the material and geometrical symmetries, the FE models represent one fourth of the respective specimen geometry (grey areas in Fig. 2). Moreover, plane stress conditions and constant thickness of the sheet are assumed. The simulation is displacement-driven, with a displacement of 2 mm applied to each arm of the specimen and symmetry boundary conditions. ABAQUS standard software is used to perform the numerical analysis. The element CPS4 (bilinear shape functions, full integration) is used, as well as a large strain formulation. The mesh density for the three geometries is selected based on a convergence study. High mesh densities have been tested without significant effect on the strain and stress distributions. Therefore, the chosen mesh density has an average size of the elements of 0.5 mm, which results in a total number of elements: 2480, 2089 and 2102 for Cr1, Cr2 and Cr3,

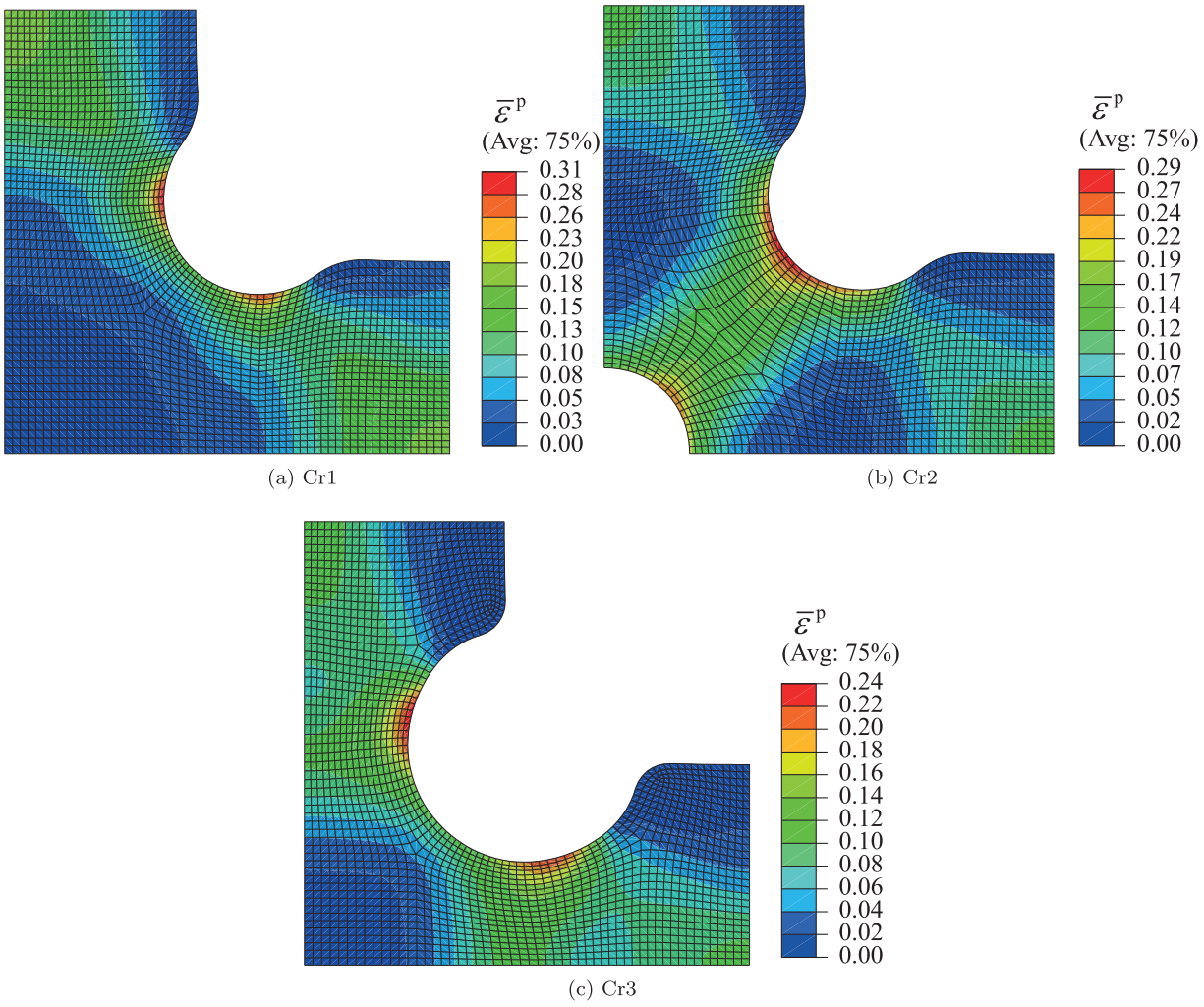

Fig. 3. Equivalent plastic strain distribution for the last increment and deformed FE mesh for the three geometries.

respectively. Indeed, similar mesh densities have been used in different works with cruciform specimens, for example (Prates et al., 2014; Zhang et al., 2014; Schmaltz and Willner, 2014).

The simulations are run with adaptive time stepping. The model composed by Swift's law and Hill'48 yield criterion is used, the material parameters for this constitutive model are presented in Table 1. For all the geometries it is assumed that rolling direction coincides with the *x*-axis represented in Fig. 2.

The equivalent plastic strain distribution at the last increment and the deformed FE meshes for the three geometries are presented in Fig. 3. Cr1 (Fig. 3a) contains the largest quasi-homogeneous area in the centre of the specimen, even though with lower values of equivalent plastic strain, which is a common characteristic of this kind of tests (Bruschi et al., 2014; Prates et al., 2016; Zhang et al., 2014). The highest values of the equivalent plastic strain are located in the arms and at the rounding radius at the

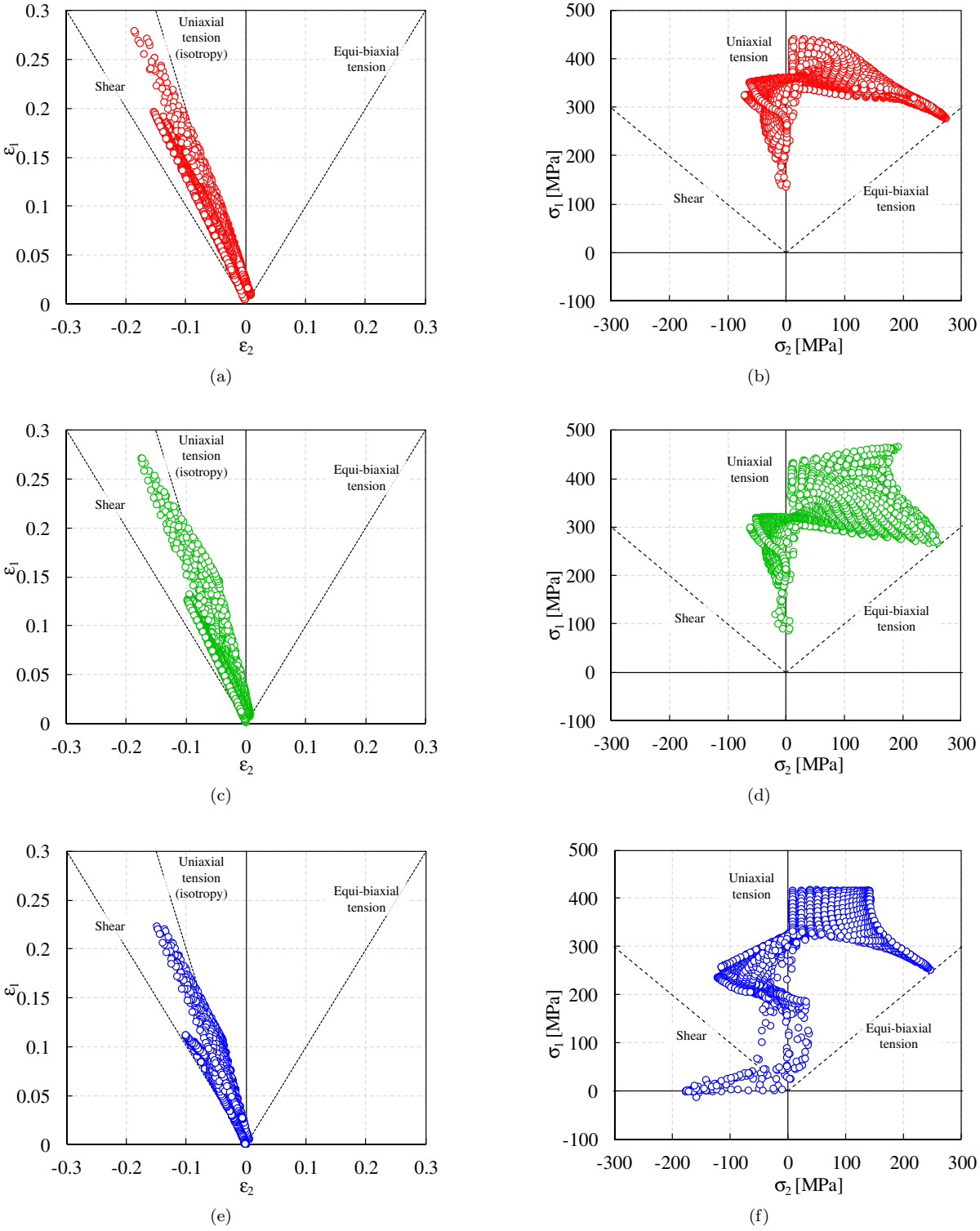

Fig. 4. Plot of the principal strain and stress fields at the end of the tests: (a) and (b) Cr1, (c) and (d) Cr2, and (c) and (d) Cr3.

J.M.P. Martins, A. Andrade-Campos and S. Thuillier / International Journal of Solids and Structures 172–173 (2019) 21–37 29

intersection of the two arms, with a maximum value of $\overline{\varepsilon}^{p} = 0.31$. Cr2 (Fig. 3b) loses completely the homogeneous area in the centre and has the highest concentration of equivalent plastic strain in the diagonal direction near the rounding radius at the intersection of the two arms and in the vicinity of the hole. The highest value is $\overline{\varepsilon}^{p} = 0.29$, slightly lower than for Cr1. In the case of Cr3 (Fig. 3c), a quasi-homogeneous area develops in the centre of the specimen, still with a smaller area than Cr1. The maximum value of equivalent plastic strain is lower in this case with $\overline{\varepsilon}^{p} = 0.24$. The range of plastic strain obtained in a specimen generally influences the identification results, specifically the identification of the hardening law.

The diversity of strain or stress states is also an important factor for an accurate calibration of a constitutive model, specially when a complex yield criterion has to be calibrated (Souto et al., 2015; Pottier et al., 2011; Kim et al., 2014). Therefore, the plot of the strain and stress states in the principal axes (in-plane) for the three geometries is presented in Fig. 4. ε_1 and ε_2 represent the major and minor strains, and σ_1 and σ_2 the major and minor stresses. It should be noted that in the three cases the whole specimen's surface is considered for these plots and for the remaining analysis. In the three cases, the stress states close to tension are predominant and the first quadrant in the principal stress space ($\sigma_1 > 0$ and $\sigma_2 > 0$) is the most populated one. Nevertheless, Cr3 (see Fig. 4(e-f)) shows the widest distribution of strain and stress states. It is possible to see an increase of points in the fourth quadrant in the principal stress space ($\sigma_1 > 0$ and $\sigma_2 < 0$) compared with the other two geometries, which gives weight to shear components in the identification procedure. In terms of spatial distribution, the region of equi-biaxial tension is located in the specimen centre, in the case of Cr1 and Cr3, whereas for Cr2, this region is divided in two and can be found near the vicinity of the hole. Along the arms of the specimens Cr1 and Cr2, the stress state evolves from equi-biaxial to tension, whereas for Cr3, stress states between simple shear and tension are also observed. A common feature of the three geometries is the equi-biaxial tension state represented by low values of strain, which is in accordance with the literature. Moreover, Fig. 5 shows the rotation angle (θ) between the principal stress base and material frame for Cr3. This measure can be used to highlight the sensitivity of the test to anisotropy. It can be seen that the cruciform specimen exhibits a rather wide distribution of the rotation angle. In particular, in the arms, where the equivalent plastic strain is the highest, values close to 0° and 90° are well represented, as well as two areas with values close to 45°.

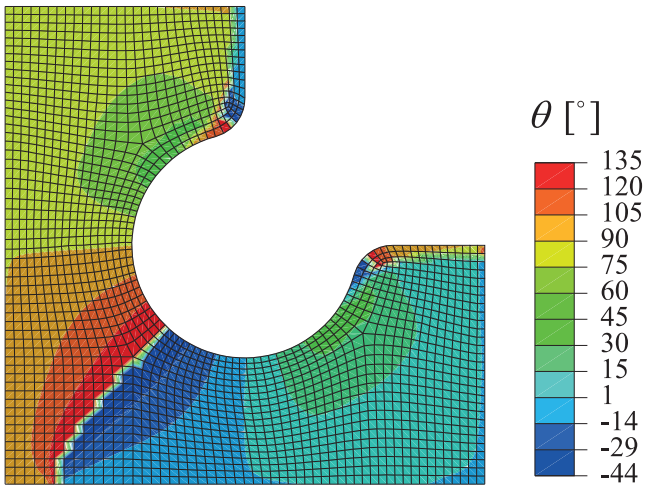

Fig. 5. Rotation angle between principal stress base and material frame for Cr3.

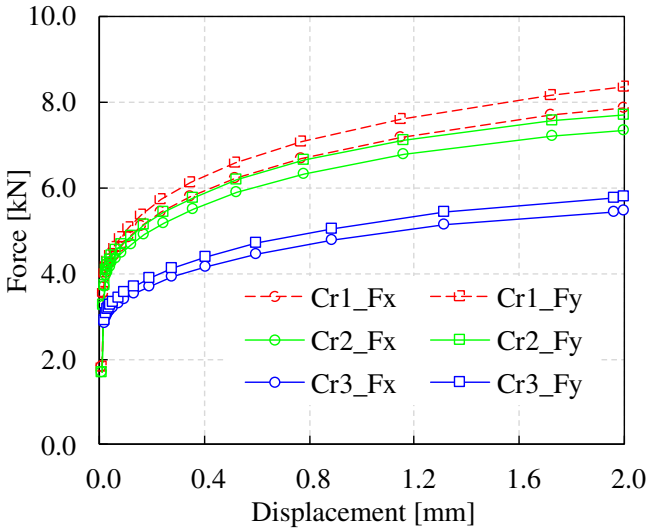

Fig. 6. Force vs displacement for the three geometries: Cr1, Cr2 and Cr3.

Such a distribution highlights the richness of the test for the prediction of the parameters related to anisotropy. Note that similar distributions of the rotation angle are obtained for the two other geometries.

The evolution of the force applied to the arms of the cruciform specimen is also presented in Fig. 6 for the three geometries. Due to the anisotropic behaviour of the material, there is a difference on the force applied to the horizontal and vertical arms. For the three geometries, the force applied in the $y-$direction is higher than in the $x-$direction.

5. Results

5.1. Hill'48 identification

In this first subsection, the three geometries presented in Section 4 are evaluated. The FE meshes presented in Fig. 3 are used with the VFM for the identification procedure. The model composed by Hill'48 yield criterion and Swift's law is selected to be calibrated. This model contains a total of 6 material parameters that are identified simultaneously using the displacement fields obtained for each cruciform geometry with the material parameters of Table 1. The accurate calibration of such a model can be hampered by the presence of local minima in the objective function, as reported by Kim et al. (2014). Hence, to check the presence of local minima, two initial sets of parameters are tested to initiate the optimisation problem. For the sake of simplicity, they are called *Sup_set* and *Inf_set* and are presented in Table 3. The two sets differ on the values of the hardening parameters, whereas the material parameters of Hill'48 yield criterion always start from the isotropic case. The two sets of hardening parameters represent flow curves above and below the reference one. The number of time steps n_t considered is the same required by ABAQUS to solve the FE simulation, which corresponds to 17, 19, and 17, for Cr1, Cr2 and Cr3, respectively. The distribution of the loading steps

Table 3
Reference parameters and two initial sets of parameters.

	σ_0 [MPa]	n	K [MPa]	F	G	N
Reference	160	0.26	565	0.2782	0.3731	1.5568
Sup_set	234	0.35	965	0.5	0.5	1.5
Inf_set	100	0.08	165	0.5	0.5	1.5

Table 4
Comparison of the three cruciform geometries (Fig. 2) in the calibration of Swift's law and Hill'48 yield criterion. The results are presented for the two different initial sets of parameters *Sup_set* and *Inf_set*.

		σ_0 [MPa]	n	K [MPa]	F	G	N
	Reference	160	0.26	565	0.2782	0.3731	1.5568
Cr1	*Sup_set*	160.35	0.262	566.11	0.2807	0.3758	1.9504
	Error	0.22%	0.85%	0.20%	0.87%	0.72%	25.29%
	Inf_set	160.38	0.263	566.40	0.2807	0.3758	1.9662
	Error	0.23%	0.99%	0.25%	0.88%	0.70%	26.30%
Cr2	*Sup_set*	160.66	0.258	566.07	0.2842	0.3786	1.6455
	Error	0.41%	0.76%	0.19%	2.15%	1.46%	5.70%
	Inf_set	160.51	0.258	565.62	0.2835	0.3779	1.6302
	Error	0.32%	0.67%	0.11%	1.89%	1.27%	4.72%
Cr3	*Sup_set*	159.76	0.261	566.40	0.2788	0.3735	1.5753
	Error	0.15%	0.44%	0.25%	0.22 %	0.10%	1.19%
	Inf_set	159.74	0.261	566.16	0.2788	0.3735	1.5707
	Error	0.16%	0.37%	0.21%	0.21%	0.09%	0.89%

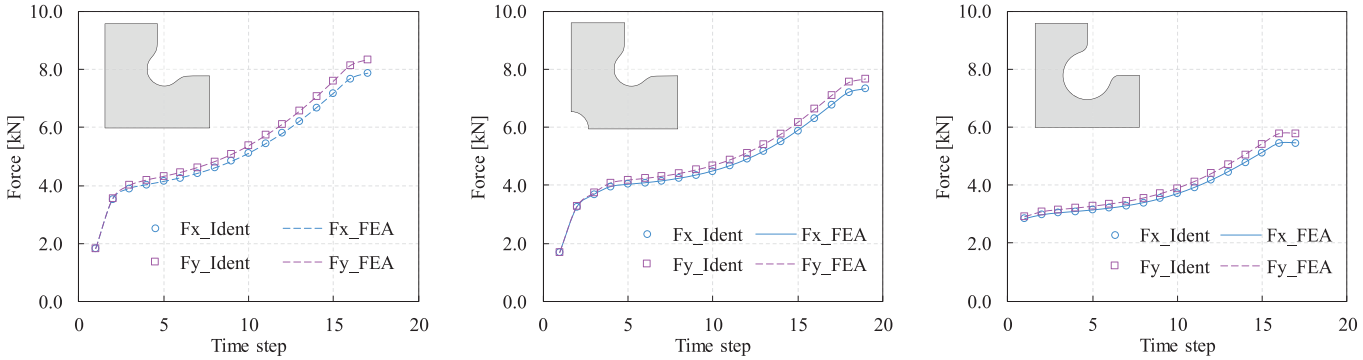

Fig. 7. Comparison between computed force from the identified parameters (Fx_Ident and Fy_Ident) and the resultant force from the FE analysis for the three geometries (Fx_FEA and Fy_FEA) for x and y−directions.

along the evolution of the applied displacement is represented in Fig. 6 by squares and circles. Note that the distribution of time steps is non-uniform. Nevertheless, it was shown previously that the VFM is not sensitive to the distribution of the time steps along the test, in contrast to the FEMU strategy (Martins et al., 2018b). Furthermore, the integration of the constitutive model for the reconstruction of the stress field in the VFM is performed using a backward-Euler algorithm, which was also implemented in a UMAT subroutine for ABAQUS standard.

The results of the identification process are presented in Table 4, as well as the absolute error calculated for each parameter. Regardless of the errors achieved, the identification process proved to be robust in finding a global minimum. Indeed, for each geometry, the two initial sets of parameters reach identical solutions.

The hardening parameters (σ_0, n and K) are accurately retrieved regardless of the geometry selected. Despite the fact that the three geometries reach different levels of equivalent plastic strain, there is no influence on the hardening behaviour identification, considering that the absolute error for σ_0, n and K is always lower than 1%. In certain cases, the range of equivalent plastic strain attained can be important for the identification process (Jones et al., 2018). Fig. 7 presents a comparison between the evolution of the applied force, shown in Fig. 6, and the computed force calculated on the basis of the internal virtual work and the material parameters identified. In this case, the solutions obtained with the *Inf_set* are used. The force can be calculated from the internal virtual work, since at the end of the optimisation, $W_{\text{int}} \approx W_{\text{ext}}$; combining this with Eq. (13), gives $W_{\text{int}} \approx W_{\text{ext}} \approx \mathbf{U}^* \cdot \mathbf{F}^{\text{load}}$ (Rossi et al., 2016). Considering the definition of the virtual fields 1 and 2, Eqs. (15) and (16), $W_{\text{int}} \approx F^{\text{load}}$. For the three geometries, there is a clear agreement between this load calculation and FE predictions, which means the identified material parameters are able to describe the force in x and y directions.

Nevertheless, the highest absolute errors come from the yield criterion parameters, particularly from the parameter N which is strictly related to the in-plane shear component σ_{xy}. The identifications performed with the data from Cr1 and Cr2 have the largest errors for parameter N, above 25% and 5%, respectively. Since the same identification procedure is used for the three geometries, the only thing that makes the difference, in this case, is the range of strain paths provided by each geometry. Looking back to Fig. 4, it is possible to see that Cr2 has a wider dispersion of strain and stress states than Cr1. Consequently, the error is reduced from 25% to 5% for the parameter N. Cr3 gives the lowest error for the parameter N, around 1%, which is a reasonable result. This can be explained by the fact that Cr3 has the widest dispersion in the fourth quadrant ($\sigma_1 > 0$ and $\sigma_2 < 0$) of the principal stress space (see Fig. 4f), which gives a higher weight to the shear component and, consequently, improves the identification of the parameter N.

In order to verify the validity of the identified yield criterion parameters presented in Table 4, the evolution of the normalised yield stress and plastic anisotropy coefficient (r_α) value as a function of α is assessed in Fig. 8. The results for each geometry are obtained with the solution corresponding to the parameter set *Inf_set*. Both the normalised yield stresses and plastic anisotropy coefficients are well described with the identified parameters from Cr3. However, it is possible to observe a slight underestimation of the normalised yield stress for the angles 30°, 45° and 60°, which is a consequence of the error in the parameter N. The same tendency

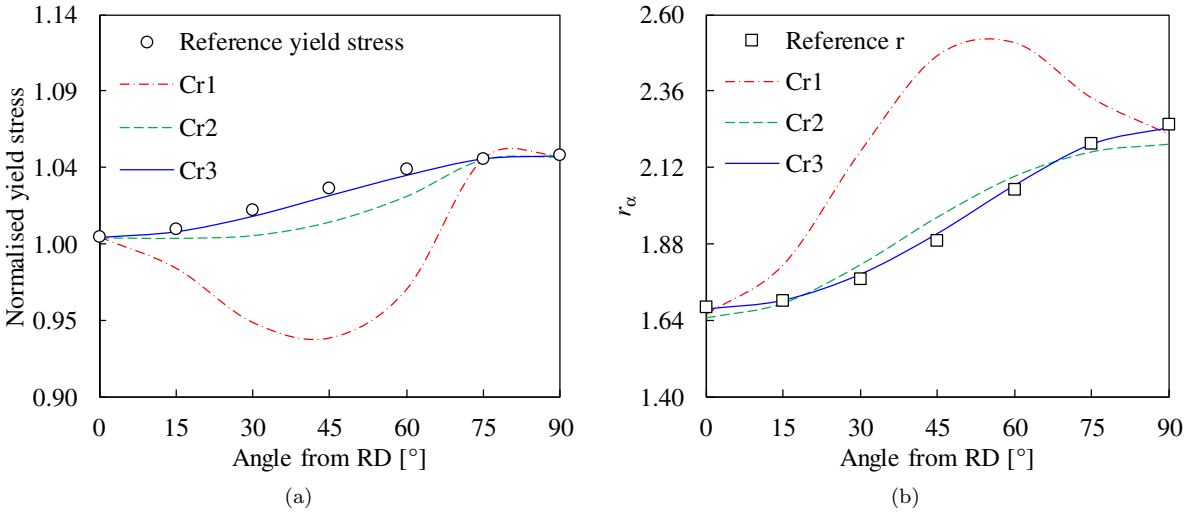

Fig. 8. Evolution of the (a) normalised yield stress and (b) plastic anisotropy coefficient according to the tension axis angle from the rolling direction for the identified parameters with Cr1, Cr2 and Cr3.

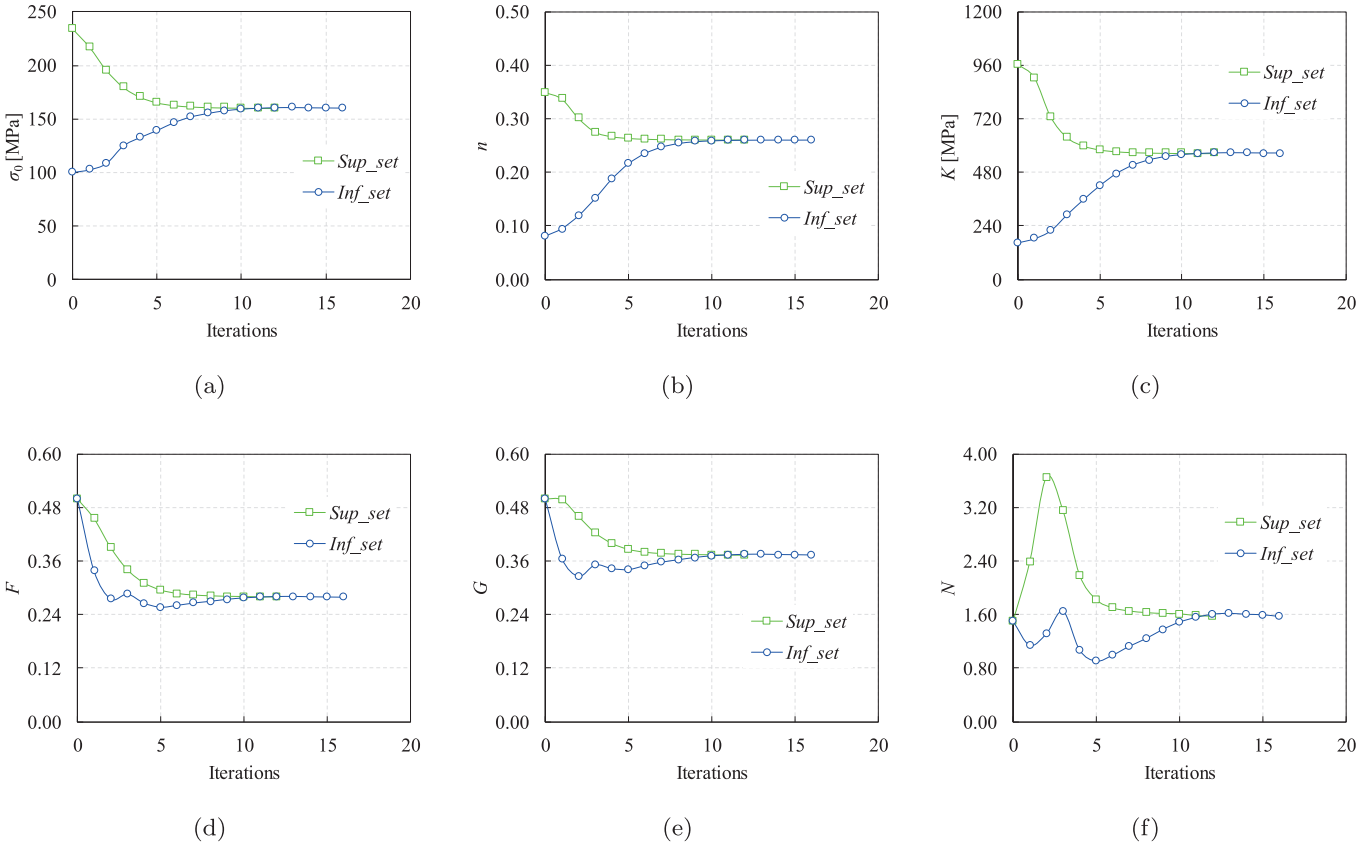

Fig. 9. Evolution of the identified parameters for Cr3 during the optimisation process.

is observed for the other two sets of parameters obtained with Cr1 and Cr2. In the case of the plastic anisotropy coefficient, the parameters obtained with the Cr1 and Cr2 overestimate this coefficient for the angles 30°, 45° and 60°, but tend to give better estimations near the angles 0° and 90°.

Since the results of Cr3 are the most accurate, the remaining analysis is focused on these results. Regarding the optimisation results, Fig. 9 presents the evolution of the material parameters during the iteration process, the evaluations of the objective function required for the Jacobian matrix calculation are not included. Despite the optimisation process stopped just after 12 and 16 iterations depending on the initial set of parameters, most of the parameters reach a convergence plateau after 10 iterations. The evolution of the parameter N shown in Fig. 9f, presents the most oscillating evolution. This fact can be caused by a lower sensitivity of the objective function to the parameter N.

Moreover, the identifications presented in this study were carried out with a standard computer, with an Intel(R) Core(TM) i7-6700 (2.60 GHz) processor and 16.00 GB of RAM memory. Depending on the initial set of parameters, the computational time is 57 s

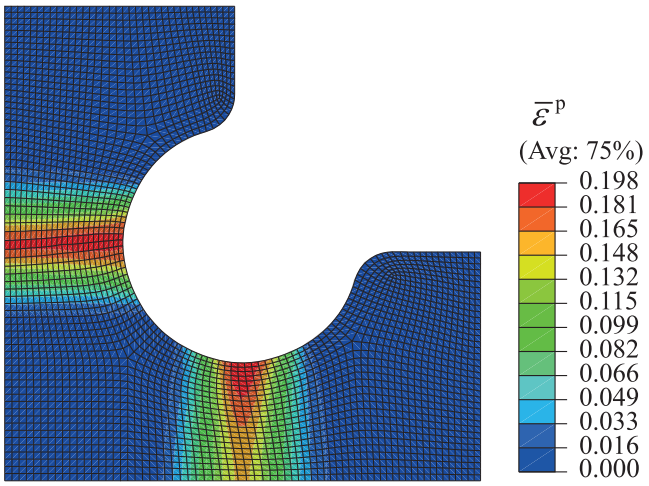

Fig. 10. Equivalent plastic strain distribution for the last increment and the deformed FE mesh for Cr3 using the YLD2000-2d yield criterion and the material parameters of Table 2.

for the *Sup_set* and 86 s for the *Inf_set*. The computational time is significantly low, because it is used just one test in the virtual database and regarding that test, the number of time steps and the number of spatial points for the computation of internal work are reasonable.

5.2. YLD2000-2d identification

In this section, the combination of the VFM with the cruciform specimen is tested in a model with a more complex yield criterion, the YLD2000-2d. This yield criterion is combined with Swift's hardening law, resulting in a total of 11 parameters to be identified. Once again, the identification of the hardening and yield criterion parameters is performed simultaneously. The reference material parameters, which correspond to an aluminium alloy AA6016 in T4 state (Yoon et al., 2004), are presented in Table 2. Cr3 provided the best results for the Hill'48 yield criterion, hence it is chosen for this analysis. The same FE model of Fig. 3c is used here. The simulation is displacement-driven, and 1 mm of displacement is applied to each arm of the specimen. This value is reduced in the present case to avoid exceeding the maximum force value. By means of a three-dimensional model, it has been confirmed that after the maximum force value, the normal stress through thickness exhibits a sudden increase, which invalidates the plane stress condition and consequently, limits the application of the VFM beyond this point. The number of elements is increased up to 3226 to better describe the strain gradients developed in the arms of the specimen. The methodology adopted in the VFM procedure uses shape functions and the displacement fields extracted from the FE model at the nodes, to compute the strain tensor at the centroid of the element (as explained in Section 2.1), which leads to an average strain tensor over the element. Thus, an increase in the number of elements mitigates the loss of information on the gradients present in the elements. In this case, an even finer mesh could be adopted, but no significant improvements in the results are noticed, whereas the computational time increases. Therefore, to have a computationally efficient mesh it is necessary to find a balance between identification results and computational time.

In this case, the integration of the constitutive model in the VFM is performed using a forward-Euler algorithm, which was also implemented in a UMAT subroutine for ABAQUS standard. This kind of integration scheme, despite requiring less computational time, requires a reduced increment size to prevent errors. Therefore, the number of time steps used in this simulation is 214. These are also the number of time steps n_t used in the identification process. The equivalent plastic strain distribution for the last increment and the deformed FE mesh are presented in Fig. 10. It is possible to observe that deformation concentrates on the smallest section of the specimen. The maximum equivalent plastic strain value is around $\overline{\varepsilon}^{p} = 0.198$. The plot of the principal strains and stresses for the last increment is presented in Fig. 11. The equivalent plastic strain distributions and the principal strain plots (respectively Figs. 10 and 11a for the aluminium alloy and Figs. 3c and 4e for the mild steel) exhibit significant differences for the two materials. It comes from the very beginning of the test, due to a strong localisation in the arms for the aluminium alloy, that would also appear for the mild steel if a large displacement was applied (above 4 mm). Therefore, the strain paths close to the shear region shown in Fig. 3c can no longer be seen in Fig. 11a. This tendency to localize is very strong for the aluminium alloy and starts almost at the beginning of plastic yielding. Indeed, for a maximum plastic strain of 0.01, the principal strain plots for the aluminium alloy and mild steel display some similarities in the shear-tension quadrant, though, for the aluminium alloy, there are already strain states in the tension-plane strain quadrant, due to a tendency to strain localisation. It emphasises the fact that the design of a heterogeneous test for material parameter should be checked against an instability criterion to limit the range of deformation, to

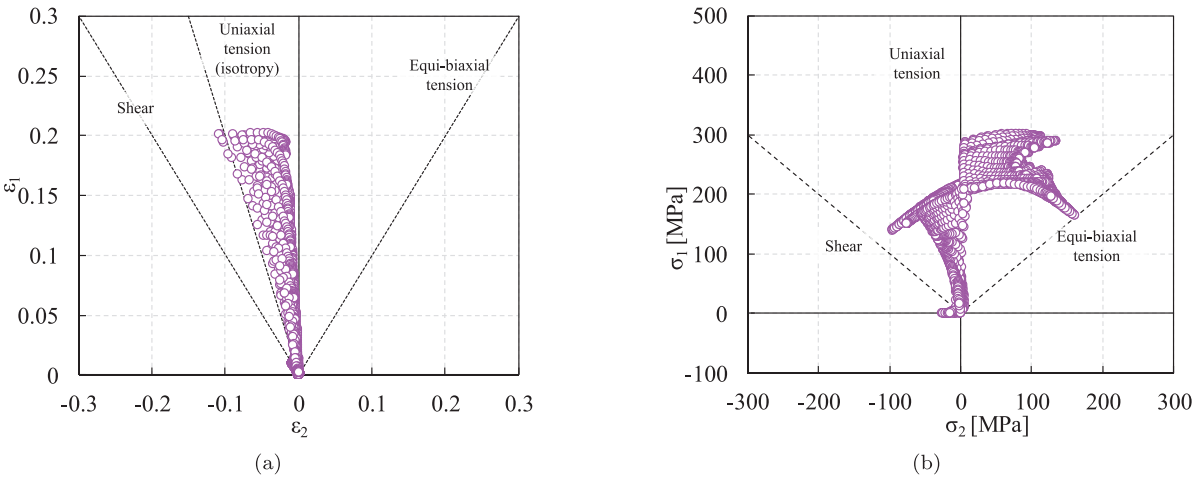

Fig. 11. Plot of the strain (a) and stress (b) fields at the end of the test in the principal axes, corresponding to the model of Fig. 10.

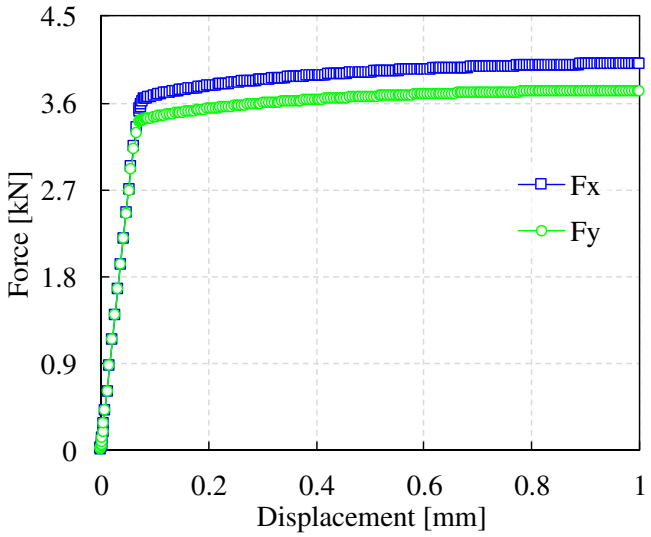

Fig. 12. Force vs displacement for the two arms of the model of Fig. 10.

avoid excessive localisation. In order to test the stability of geometry Cr3, material parameters for YLD2000-2d for the mild steel have been identified from the plastic anisotropy coefficients and stress ratios given in Table 1, with a calculated biaxial coefficient (Yoon et al., 2004). A similar equivalent plastic strain distribution as in Fig. 3c is obtained. Moreover, for the aluminium alloy, two sets of Hill'48 coefficients have been identified, either from the plastic anisotropy coefficients or from the normalised stress ratios given in Table 4. As for the mild steel, the equivalent plastic strain distribution is close to the one obtained with YLD2000-2d model. These results highlight the fact that the test is more sensitive to the material than to the mechanical model. However, it is interesting to note that for the numerical simulation with Hill'48 model, with parameters identified from the stress ratios, the projection of the yield surface in the $(\sigma_{xx}, \sigma_{yy})$ plane (material frame) is such that the plane strain point corresponds to a higher stress than the prediction based on Hill'48 model with parameters identified from the plastic anisotropy coefficients. This emphasises that the tendency to excessive localisation is also dependent on the model. It can be concluded that excessive localisation (or not) depends more significantly on the material than on the constitutive model.

As a consequence of the reduction of the applied displacement and strain localisation in the arms, a significant part of the stress points presented in Fig. 11b remains in the elastic regime or corresponds to a low value of equivalent plastic strain. The evolution of the resultant of the applied force for the two directions is presented in Fig. 12. The anisotropy effect is visible on the evolution of the force of the two arms. In this case, the force in the $y-$direction has the lowest value in the plastic regime.

As performed before, to check the presence of local minima in the objective function, two initial sets of parameters are tested which are presented in Table 5. The two sets differ on the values of the hardening parameters, whereas the α_i (i=1,..,8) parameters always start from 1.0, corresponding to the isotropic case. The elastic parameters are considered to be known *a priori*.

The condition described by Eq. (26) is imposed on YLD200-2d, as a constraint added to the optimisation problem, by means of a penalty function. Therefore, the objective function becomes

$$f = \varphi(\boldsymbol{\xi}) + \delta \cdot \Im(\boldsymbol{\xi}), \tag{27}$$

where the parameter δ is a penalty coefficient which assumes the value 1×10^4. The function $\Im(\boldsymbol{\xi})$ can be written as

$$\Im(\boldsymbol{\xi}) = \left\{ \left| \left[\frac{1}{2} \left(\left| \frac{2\alpha_1 + \alpha_2}{3} \right|^a + \left| \frac{2(\alpha_3 - \alpha_4)}{3} \right|^a + \left| \frac{4\alpha_5 - \alpha_6}{3} \right|^a \right) \right]^{(1/a)} - 1 \right| - tol \right\}^2. \tag{28}$$

The parameter *tol* is a tolerance added to the constraint in order to prevent errors in this specific case, since using the reference parameters in Eq. (26) the value of 1 is not exactly reached. *tol* assumes the value of 1×10^{-4}. It should be mentioned that the absence of this condition leads to multiple solutions and its adoption reveals essential to avoid this problem. This particular behaviour of YLD2000-2d yield criterion was also reported by Guner et al. (2012) and solved imposing the same constraint. Nevertheless, Guner et al. (2012) imposed exactly the constraint of Eq. (26) which allowed to reduce the number of optimisation variables.

The results obtained with the constrained objective function are presented in Table 6. The first thing to note is the fact that there is no sensitivity to the initial set of parameters, the two sets *Sup_set* and *Inf_set* converge on an identical solution, which suggests that the obtained set represents a global minimum. The results also show a good prediction of the initial yield stress σ_0, this is due to the constrained imposed. The remaining hardening parameters have higher errors, specially the hardening exponent. A plot of Swift's law for the reference and identified parameters as well as the force predicted based on the internal virtual work are presented in Fig. 13. The results for the force show a good match between the predicted and the reference (FE analysis). Moreover, despite the errors in the parameters K and n, the reference and the identified Swift's law have a good match. Even

Table 5
Reference parameters and initial parameter for Swift's law and YLD2000-2d yield criterion.

Swift's law			
	σ_0 [MPa]	n	K [MPa]
Reference	212.03	0.239	385.47
Sup_set	312	0.339	585
Inf_set	112	0.139	185

YLD2000-2d yield criterion									
	α_1	α_2	α_3	α_4	α_5	α_6	α_7	α_8	m
Reference	0.9580	1.045	0.9485	1.0568	0.9938	0.9397	0.9200	1.1482	8.0
Sup_set & *Inf_set*	1.0	1.0	1.0	1.0	1.0	1.0	1.0	1.0	8.0

Table 6
Results of the identification process for Swift's law and YLD2000-2d yield criterion.

Swift's law

	σ_0 [MPa]	n	K [MPa]
Reference	212.03	0.239	385.47
Sup_set	212.40	0.260	398.07
Error	0.17 %	10.77%	3.27%
Inf_set	212.40	0.260	398.07
Error	0.17 %	10.77%	3.27%

YLD2000-2d yield criterion (m=8)

	α_1	α_2	α_3	α_4	α_5	α_6	α_7	α_8
Reference	0.9580	1.045	0.9485	1.0568	0.9938	0.9397	0.9200	1.1482
Sup_set	0.9860	0.9959	0.9378	1.0647	0.9946	0.9491	1.0458	1.1963
Error	2.92%	4.70%	1.13%	0.75 %	0.08%	1.00%	13.67%	4.19%
Inf_set	0.9860	0.9958	0.9378	1.0647	0.9956	0.9491	1.0459	1.1962
Error	2.92%	4.71%	1.13%	0.75%	0.08%	1.00%	13.69%	4.19%

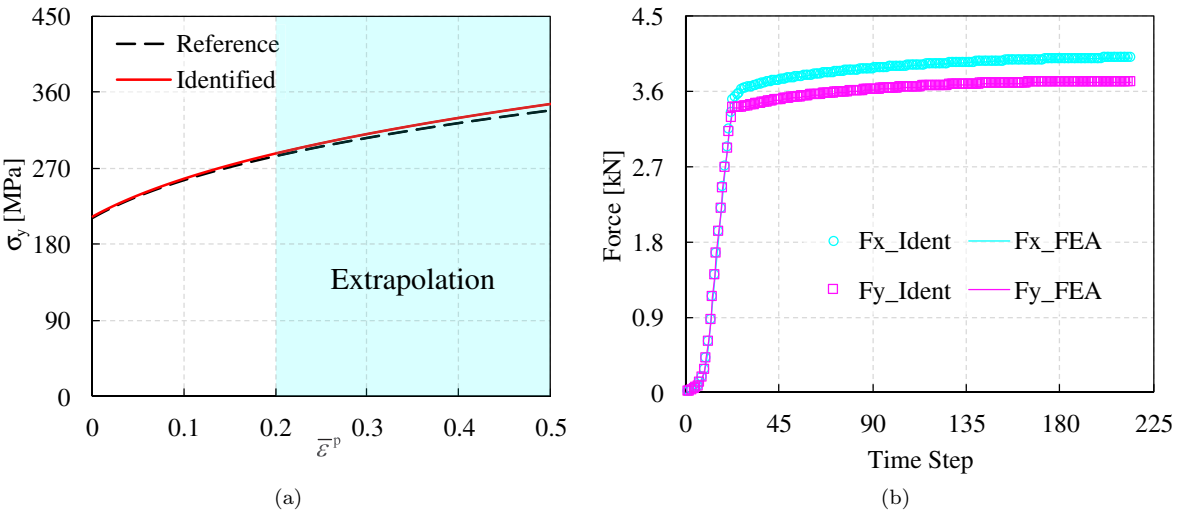

Fig. 13. Results obtained with the identified parameter set *Sup_set* of Table 6: (a) plot of Swift's law and (b) force prediction based on the internal work.

when the results are extrapolated to $\bar{\varepsilon}^p = 0.50$[1], there is only a slight overestimation of the flow stress.

For the yield criterion, the highest errors are reached for the parameters α_2, α_8 and above all α_7, the remaining have errors lower than 3%. The errors in the parameters α_7 and α_8 follow a similar tendency as the results presented for Hill'48 yield criterion since these parameters are strictly connected to the shear components. This is coherent with the results presented in Fig. 11b, which show the lack of information on the fourth quadrant ($\sigma_1 > 0$ and $\sigma_2 < 0$). This lack of data corresponds to lower weight of the shear stress state in the optimisation. In order to better understand the quality of these identifications, the results of the predicted yield locus with the identified parameters (*Sup_set*) for different values of the ratio σ_{xy}/σ_0 in the normalised plane (σ_{xx}/σ_0, σ_{yy}/σ_0) are presented in Fig. 14. The results show an accurate fit of the predicted yield locus for $\sigma_{xy}/\sigma_0 = 0.0$, revealing that the error of 4.7% in the parameter α_2 has a minor influence on the results. Nevertheless, with the increase of σ_{xy}/σ_0, the identified parameters underestimate the form of the yield locus, a consequence of the overestimation of the parameters α_7 and α_8. Moreover, the predicted normalised yield stress and the plastic anisotropy

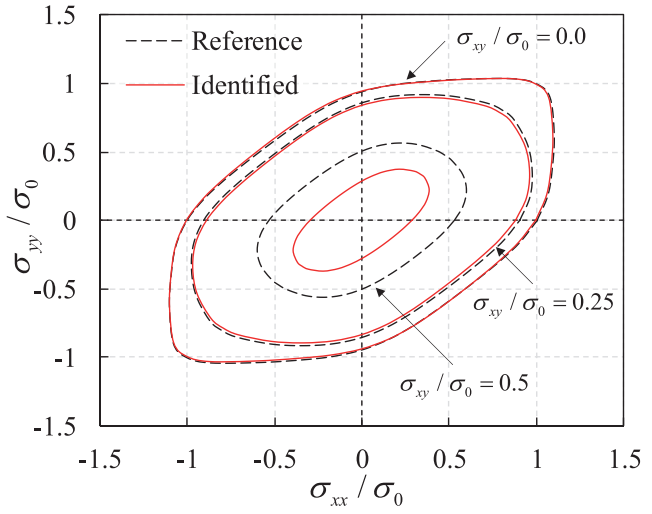

Fig. 14. Comparison of the reference yield locus with the identified yield locus for different levels of σ_{xy}/σ_0.

[1] Note that the cruciform test only reaches a maximum value of equivalent plastic strain of $\bar{\varepsilon}^p = 0.19$.

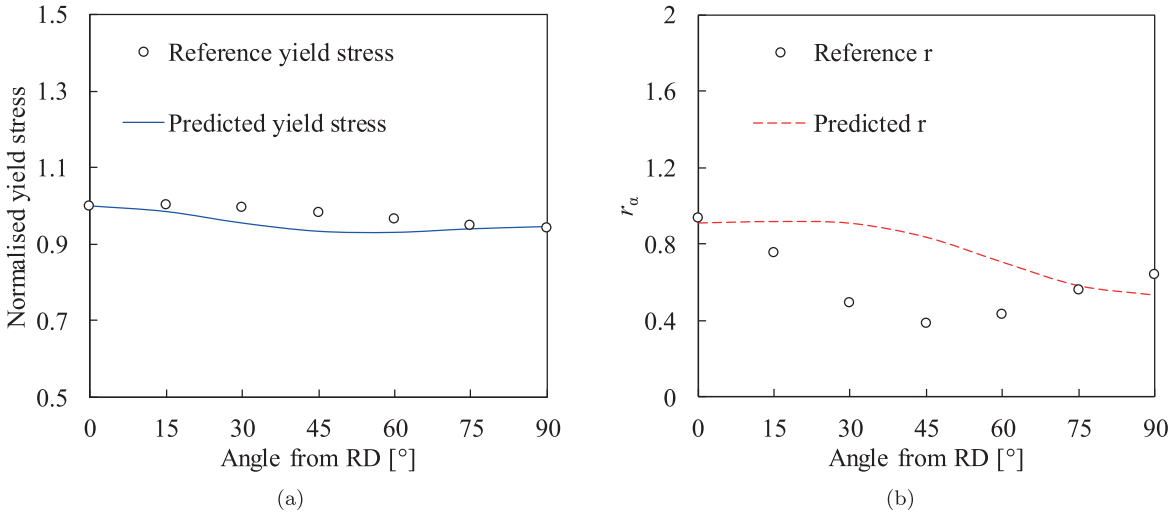

Fig. 15. Evolution of the (a) normalised yield stress and (b) plastic anisotropy coefficient according to the tension axis angle from the rolling direction for the parameters identified with Cr3 and the aluminium alloy.

Table 7
Results of the identification process for Swift's law and YLD2000-2d yield criterion using the constitutive parameters for the mild steel.

Swift's law			
	σ_0 [MPa]	n	K [MPa]
Reference	160.0	0.26	565.0
Sup_set	159.87	0.265	571.51
Error	0.08%	1.96%	1.15%
Inf_set	159.87	0.265	571.50
Error	0.08%	1.96%	1.15%

YLD2000-2d yield criterion ($m = 6$)								
	α_1	α_2	α_3	α_4	α_5	α_6	α_7	α_8
Reference	1.0840	0.9459	0.7961	0.8739	0.9159	0.8048	1.0090	0.9822
Sup_set	1.0831	0.9470	0.7955	0.8740	0.9150	0.8011	1.0088	0.9945
Error	0.09%	0.11%	0.07%	0.02%	0.09%	0.47%	0.02%	1.25%
Inf_set	1.0830	0.9470	0.7955	0.8741	0.9150	0.8011	1.0088	0.9945
Error	0.09%	0.11%	0.08%	0.02%	0.10%	0.47%	0.02%	1.25%

coefficient (r_α) with the identified parameters for different angles of the tension axis are presented in Fig. 15. Similarly to the results obtained for Hill'48 yield criterion, the normalised yield stress is well predicted for 0° and 90°, whereas it is underestimated for the remaining angles between 0° and 90°. Regarding the prediction of the plastic anisotropy coefficient, there is a significant error and the tendency is to overestimate, with the exception of the angle 0°. These results for the plastic anisotropy coefficient can be explained by the intrinsic nature of the VFM. The method *per se* searches the best stress field for each step to minimise the difference between internal and external virtual works, whereas the plastic deformation prediction is a result of this process of minimisation.

Finally, the capacity of Cr3 to retrieve a large number of material parameters, for YLD2000-2d criterion, is also investigated for the mild steel. As previously mentioned, YLD2000-2d parameters are calculated from the plastic anisotropy coefficients and normalised yield stress ratios given in Table 1 and are presented in Table 7 as the reference values. It should be emphasised that the equivalent plastic strain distribution and the stress and strain states in principal axes are very close to the ones presented in Figs. 3c, 4e and 4f. Therefore, the same procedure for the identification with the VFM is repeated. Two initial sets of parameters are used. The initial values for the hardening parameters are the ones presented in Table 2 and isotropic values are chosen for the yield criterion parameters. The results of these identifications are presented in Table 7.

As can be concluded from Table 7, the relative error in the retrieved material parameters is significantly lower compared to the aluminium alloy, specially for the parameters α_2, α_7 and, α_8. The predicted normalised yield stresses and the plastic anisotropy coefficients (r_α) with the retrieved parameters (*Sup_set*) for different angles of the tension axis are presented in Fig. 16. The results show a very good agreement with the reference values. These results obtained for 2 materials show that the quality and richness of the information encoded in the heterogeneous strain fields provided by Cr3 leads to a very good prediction of material parameters for YLD2000-2d criterion, as long as the excessive strain localisation is not reached.

Concerning the computation time, it depends slightly on the initial set of parameters, respectively 944 s and 827 s for *Sup_set* and *Inf_set*. Comparing to the identification of the model composed by Hill'48 yield criterion, there is an increase of one order of magnitude in the computational time. This can be attributed to the increase in the number of time steps and spatial integration points in the optimisation process.

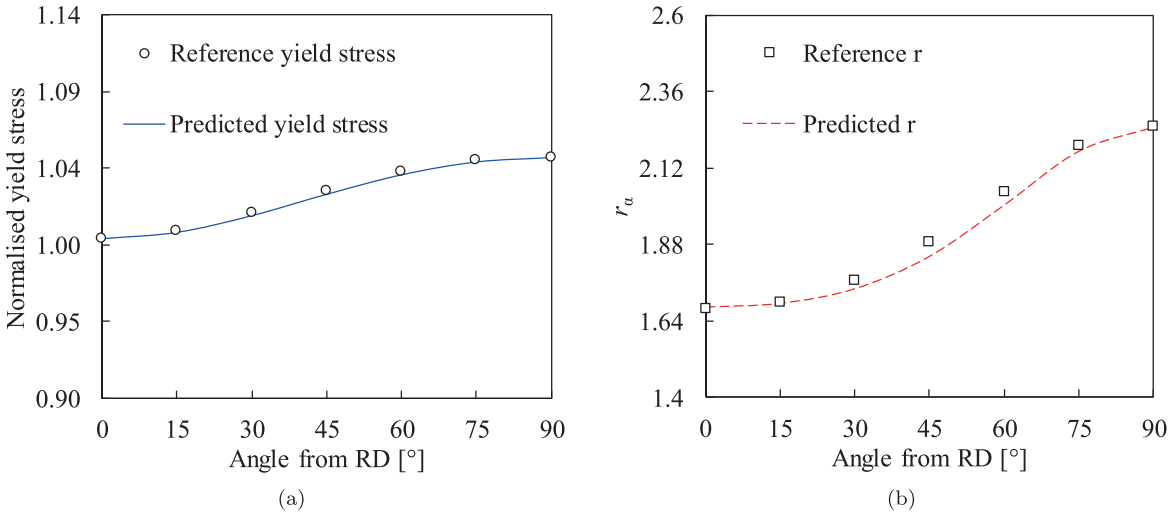

Fig. 16. Evolution of (a) the normalised yield stress and (b) plastic anisotropy coefficient according to the tension axis angle from the rolling direction for the parameters identified with Cr3 and mild steel.

6. Conclusion

The purpose of this study is to explore the cruciform specimen under biaxial tension as a potential test for the simultaneous identification of the parameters that govern an anisotropic yield criterion and a hardening law using the virtual fields method.

In a first step, three cruciform geometries are tested in the identification of the constitutive parameters of Hill'48 yield criterion and Swift's hardening law for a mild steel. The base for this study is the geometry proposed by Zhang et al. (2014) and the other two geometries are inspired by the first one, with simple geometrical adaptations to increase the strain and stress field heterogeneity. The comparison of the three geometries shows that the geometry proposed by Zhang et al. (2014), despite providing a wide spread of stress states, lacks on information for shear stress states. This affects the identification of the yield criterion parameters, namely the parameter related to the shear component. Therefore, the increase of heterogeneity with special emphasis on the presence of the shear stress states is essential to identify accurately the material parameters of Hill'48 yield criterion. Thus, the other two geometries present better results, especially the third geometry which produces a wider dispersion of stress states and gives more information in the shear region. Moreover, all the identifications performed reached a single solution for the 6 parameters with a single test, independently of the initial set of parameters. Nevertheless, from this comparison, it is concluded that the third geometry provides the best results, with a maximum error of 1% for all the parameters.

The second step addresses the identification of the material parameters of a more complex yield criterion, namely YLD2000-2d yield criterion, simultaneously with Swift's law. The third geometry analysed in the first step is chosen for this analysis. A reference set of constitutive parameters representing an aluminium alloy is selected. In this case, the objective function is modified to include a constraint on the YLD2000-2d criterion. In terms of the information provided by the test, it is observed that the test is sensitive to the material used. The plastic behaviour of the aluminium alloy leads to strain localization in the smallest section of the specimen, which increases the information near plane strain, but reduces the information in the shear region. Nevertheless, the identification results prove to be insensitive to the initial set of parameters. The hardening curve is identified with reasonable accuracy, but the yield criterion parameters, specially the ones directly related to shear, contain high errors. A detailed analysis of the results shows that the error in the yield criterion parameters is not significant for the prediction of the initial yield stresses, but it has a more pronounced effect on the plastic anisotropy coefficient prediction. Moreover, a second identification is performed for the same model but with the parameters of the mild steel used in the first step. In this case, the identification results have a reasonable error (maximum error lower than 2%), which emphasises the dependence on the chosen material.

In summary, the results of this second step show that is possible to identify all the material parameters from a constitutive model with a single test, but the accuracy of the identification is much dependent on the capability of the test to generate strain fields with relevant information. Moreover, it is highlighted that the information given by heterogeneous tests can be dependent on the material selected and this can affect the accuracy of the identification results. Therefore, the design methodologies of new heterogeneous tests should take into account the stability of the test when using different materials.

Finally, the computational cost should be highlighted. The combination of a single cruciform test, the VFM and the Levenberg-Marquardt method presented a reasonable computational time, difficult to achieve with other strategies, especially if compared with a FEMU-based inverse method. Even for a more complex model, such as YLD2000-2d yield criterion, the maximum time required for the simultaneous identification of all parameters was 944 s.

Acknowledgements

The authors gratefully acknowledge the financial support of the Portuguese Foundation for Science and Technology (FCT) under the projects CENTRO-01-0145-FEDER-029713, POCI-01-0145-FEDER-016876, POCI-01-0145-FEDER-031243 and POCI-01-0145-FEDER-030592 by UE/FEDER through the programs CENTRO 2020 and COMPETE 2020, and UID/EMS/00481/2013-FCT under CENTRO-01-0145-FEDER-022083. The authors also would like to acknowledge the Région Bretagne (France) for its financial support. J.M.P. Martins is also grateful to the FCT for the PhD grant SFRH/BD/117432/2016.

References

Avril, S., Bonnet, M., Bretelle, A.-S., Grédiac, M., Hild, F., Ienny, P., Latourte, F., Lemosse, D., Pagano, S., Pagnacco, E., Pierron, F., 2008. Overview of identification methods of mechanical parameters based on full-field measurements. Exp. Mech. 48 (4), 381–402. doi:10.1007/s11340-008-9148-y.

Banabic, D., 2010. Plastic Behaviour of Sheet Metal. Springer Berlin Heidelberg, Berlin, Heidelberg, pp. 27–140 doi:10.1007/978-3-540-88113-1_2.

Bandyopadhyay, K., Hariharan, K., Lee, M.-g., Zhang, Q., 2018. Robust multi objective optimization of anisotropic yield function coefficients. Mater. Des. 156, 184–197. doi:10.1016/j.matdes.2018.06.033.

Barlat, F., Brem, J., Yoon, J., Chung, K., Dick, R., Lege, D., Pourboghrat, F., Choi, S.-H., Chu, E., 2003. Plane stress yield function for aluminum alloy sheets - part i: theory. Int. J. Plast. 19 (9), 1297–1319. doi:10.1016/S0749-6419(02)00019-0.

Bron, F., Besson, J., 2004. A yield function for anisotropic materials application to aluminum alloys. Int. J. Plast. 20 (4), 937–963. doi:10.1016/j.ijplas.2003.06.001.

Bruschi, S., Altan, T., Banabic, D., Bariani, P., Brosius, A., Cao, J., Ghiotti, A., Khraisheh, M., Merklein, M., Tekkaya, A., 2014. Testing and modelling of material behaviour and formability in sheet metal forming. CIRP Ann. 63 (2), 727–749. https://doi.org/10.1016/j.cirp.2014.05.005.

Cazacu, O., Revil-Baudard, B., Chandola, N., 2019. Plasticity-Damage Couplings: From Single Crystal to Polycrystalline Materials, Vol. 253. Springer doi:10.1007/978-3-319-92922-4.

Cooreman, S., Lecompte, D., Sol, H., Vantomme, J., Debruyne, D., 2008. Identification of mechanical material behavior through inverse modeling and DIC. Exp. Mech. 48 (4), 421–433. doi:10.1007/s11340-007-9094-0.

Coppieters, S., Hakoyama, T., Debruyne, D., Takahashi, S., Kuwabara, T., 2018. Inverse yield locus identification using a biaxial tension apparatus with link mechanism and displacement fields. J. Phys. 1063, 012039. doi:10.1088/1742-6596/1063/1/012039.

Crisfield, M., 1991. Non-Linear Finite Element Analysis of Solids and Structures, Volume 1. John Wiley & Sons, Ltd..

Denys, K., Coppieters, S., Seefeldt, M., Debruyne, D., 2016. Multi-DIC setup for the identification of a 3d anisotropic yield surface of thick high strength steel using a double perforated specimen. Mech. Mater. 100, 96–108. doi:10.1016/j.mechmat.2016.06.011.

Fu, J., Barlat, F., Kim, J.-H., Pierron, F., 2016. Identification of nonlinear kinematic hardening constitutive model parameters using the virtual fields method for advanced high strength steels. Int. J. Solids Struct. 102–103, 30–43. doi:10.1016/j.ijsolstr.2016.10.020.

Fu, J., Barlat, F., Kim, J.H., Pierron, F., 2017. Application of the virtual fields method to the identification of the homogeneous anisotropic hardening parameters for advanced high strength steels. Int. J. Plast. 93, 229–250. doi:10.1016/j.ijplas.2016.07.013.

Guner, A., Soyarslan, C., Brosius, A., Tekkaya, A., 2012. Characterization of anisotropy of sheet metals employing inhomogeneous strain fields for Yld2000-2D yield function. Int. J. Solids Struct. 49 (25), 3517–3527. doi:10.1016/j.ijsolstr.2012.05.001.

Hill, R., 1948. A theory of the yielding and plastic flow of anisotropic metals. Proc. R. Soc. London A 193 (1033), 281–297. doi:10.1098/rspa.1948.0045.

Holzapfel, A.G., 2000. Nonlinear Solid Mechanics: A Continuum Approach for Engineering. John Wiley & Sons, LTD..

Jones, E., Carroll, J., Karlson, K., Kramer, S., Lehoucq, R., Reu, P., Turner, D., 2018. Parameter covariance and non-uniqueness in material model calibration using the virtual fields method. Comput. Mater. Sci. 152, 268–290. doi:10.1016/j.commatsci.2018.05.037.

Kim, J.-H., Barlat, F., Pierron, F., Lee, M.-G., 2014. Determination of anisotropic plastic constitutive parameters using the virtual fields method. Exp. Mech. 54 (7), 1189–1204. doi:10.1007/s11340-014-9879-x.

Kim, J.-H., Serpantié, A., Barlat, F., Pierron, F., Lee, M.-G., 2013. Characterization of the post-necking strain hardening behavior using the virtual fields method. Int. J. Solids Struct. 50 (24), 3829–3842. doi:10.1016/j.ijsolstr.2013.07.018.

Lecompte, D., Smits, A., Sol, H., Vantomme, J., Hemelrijck, D.V., 2007. Mixed numerical experimental technique for orthotropic parameter identification using biaxial tensile tests on cruciform specimens. Int. J. Solids Struct. 44 (5), 1643–1656. doi:10.1016/j.ijsolstr.2006.06.050.

Marek, A., Davis, F.M., Pierron, F., 2017. Sensitivity-based virtual fields for the non-linear virtual fields method. Comput. Mech. 60 (3), 409–431. doi:10.1007/s00466-017-1411-6.

Marek, A., Davis, F.M., Rossi, M., Pierron, F., 2018. Extension of the sensitivity-based virtual fields to large deformation anisotropic plasticity. Int. J. Mater. Form. doi:10.1007/s12289-018-1428-1.

Marquardt, D.W., 1963. An algorithm for least-squares estimation of nonlinear parameters. J. Soc. Ind. Appl.Math. 11 (2), 431–441. doi:10.1137/0111030.

Martins, J.M., Andrade-Campos, A., Thuillier, S., 2018. Comparison of inverse identification strategies for constitutive mechanical models using full-field measurements. Int. J. Mech. Sci. 145 (February), 330–345. doi:10.1016/j.ijmecsci.2018.07.013.

Martins, J.M.P., Thuillier, S., Andrade-Campos, A., 2018. Identification of material parameters for plasticity models: a comparative study on the finite element model updating and the virtual fields method. AIP Conf. Proc. 1960 (1), 110007. doi:10.1063/1.5034964.

Notta-Cuvier, D., Langrand, B., Lauro, F., Markiewicz, E., 2015. An innovative procedure for characterising a coupled elastoplastic damage model of behaviour using the virtual fields method. Int. J. Solids Struct. 69–70, 415–427. doi:10.1016/j.ijsolstr.2015.05.009.

Pearce, R., 1968. Some aspects of anisotropic plasticity in sheet metals. Int. J. Mech. Sci. 10 (12), 995–1004. doi:10.1016/0020-7403(68)90053-2.

Pierron, F., Avril, S., Tran, V.T., 2010. Extension of the virtual fields method to elasto-plastic material identification with cyclic loads and kinematic hardening. Int. J. Solids Struct. 47 (22), 2993–3010. doi:10.1016/j.ijsolstr.2010.06.022.

Pierron, F., Grédiac, M., 2012. The Virtual Fields Method: Extracting Constitutive Mechanical Parameters from Full-Field Deformation Measurements. Springer Science & Business Media.

Pottier, T., Toussaint, F., Vacher, P., 2011. Contribution of heterogeneous strain field measurements and boundary conditions modelling in inverse identification of material parameters. Eur. J. Mech. A/Solids 30 (3), 373–382. doi:10.1016/j.euromechsol.2010.10.001.

Prates, P., Oliveira, M., Fernandes, J., 2014. A new strategy for the simultaneous identification of constitutive laws parameters of metal sheets using a single test. Comput. Mater. Sci. 85, 102–120. doi:10.1016/j.commatsci.2013.12.043.

Prates, P.A., Pereira, A.F.G., Sakharova, N.A., Oliveira, M.C., Fernandes, J.V., 2016. Inverse strategies for identifying the parameters of constitutive laws of metal sheets. Adv. Mater. Sci. Eng. 2016 (Dic), 1–18. doi:10.1155/2016/4152963.

Promma, N., Raka, B., Grédiac, M., Toussaint, E., Cam, J.-B.L., Balandraud, X., Hild, F., 2009. Application of the virtual fields method to mechanical characterization of elastomeric materials. Int. J. Solids Struct. 46 (3), 698–715. doi:10.1016/j.ijsolstr.2008.09.025.

Rabahallah, M., Balan, T., Bouvier, S., Bacroix, B., Barlat, F., Chung, K., Teodosiu, C., 2009. Parameter identification of advanced plastic strain rate potentials and impact on plastic anisotropy prediction. Int. J. Plast. 25 (3), 491–512. doi:10.1016/j.ijplas.2008.03.006.

Rahmani, B., Ghossein, E., Villemure, I., Levesque, M., 2014. In-situ mechanical properties identification of 3d particulate composites using the virtual fields method. Int. J. Solids Struct. 51 (18), 3076–3086. doi:10.1016/j.ijsolstr.2014.05.006.

Reddy, J.N., 2013. An Introduction to Continuum Mechanics, 2 ed. Cambridge University Press doi:10.1017/CBO9781139178952.

Réthoré, J., Muhibullah, Elguedj, T., Coret, M., Chaudet, P., Combescure, A., 2013. Robust identification of elasto-plastic constitutive law parameters from digital images using 3D kinematics. Int. J. Solids Struct. 50 (1), 73–85. doi:10.1016/j.ijsolstr.2012.09.002.

Rossi, M., Cortese, L., Genovese, K., Lattanzi, A., Nalli, F., Pierron, F., 2018. Evaluation of volume deformation from surface DIC measurement. Exp. Mech. doi:10.1007/s11340-018-0409-0.

Rossi, M., Pierron, F., 2012. Identification of plastic constitutive parameters at large deformations from three dimensional displacement fields. Comput. Mech. 49 (1), 53–71. doi:10.1007/s00466-011-0627-0.

Rossi, M., Pierron, F., Štamborská, M., 2016. Application of the virtual fields method to large strain anisotropic plasticity. Int. J. Solids Struct. 97–98, 322–335. doi:10.1016/j.ijsolstr.2016.07.015.

Schmaltz, S., Willner, K., 2014. Comparison of different biaxial tests for the inverse identification of sheet steel material parameters. Strain 50 (5), 389–403. doi:10.1111/str.12080.

Simo, J.C., Hughes, T.J.R., 1998. Computational Inelasticity. Springer, New York, NY doi:10.1007/b98904.

Souto, N., Thuillier, S., Andrade-Campos, A., 2015. Design of an indicator to characterize and classify mechanical tests for sheet metals. Int. J. Mech. Sci. 101–102, 252–271. doi:10.1016/j.ijmecsci.2015.07.026.

Swift, H.W., 1952. Plastic instability under plane stress. J. Mech. Phys. Solids 1 (1), 1–18. doi:10.1016/0022-5096(52)90002-1.

Tardif, N., Kyriakides, S., 2012. Determination of anisotropy and material hardening for aluminum sheet metal. Int. J. Solids Struct. 49 (25), 3496–3506. doi:10.1016/j.ijsolstr.2012.01.011.

Yoon, J.-W., Barlat, F., Dick, R.E., Chung, K., Kang, T.J., 2004. Plane stress yield function for aluminum alloy sheets - part II: fe formulation and its implementation. Int. J. Plast. 20 (3), 495–522. doi:10.1016/S0749-6419(03)00099-8. Owen Richmond Memorial Special Issue.

Zhang, S., Leotoing, L., Guines, D., Thuillier, S., lai Zang, S., 2014. Calibration of anisotropic yield criterion with conventional tests or biaxial test. Int. J. Mech. Sci. 85, 142–151. doi:10.1016/j.ijmecsci.2014.05.020.

3.3 Calibration of anisotropic plasticity models with an optimized heterogeneous test and the Virtual Fields Method

In this section, a previously designed heterogeneous test is combined with the Virtual Fields Method. The heterogeneous test consists of a uniaxial standard test with an optimized specimen shape called butterfly shape. The sensitivity of the Virtual Fields Method to the number of virtual fields is analysed. The performance of this calibration methodology is analysed with experimental data previously acquired for a mild steel.

Chapter 5
Calibration of Anisotropic Plasticity Models with an Optimized Heterogeneous Test and the Virtual Fields Method

J. M. P. Martins, S. Thuillier, and A. Andrade-Campos

Abstract An accurate calibration of a constitutive model for finite element analysis is as important as an adequate choice of the constitutive model itself. The calibration strategy and the experimental database have determinant roles for the success of this stage. Over recent years, the increasing use of full-field measurement techniques has changed significantly the amount of data that compose the experimental database and suppressed some of the design constraints of the mechanical tests. These techniques enable to capture complete displacement/strain fields during a mechanical test, a feature that has been conveniently used to explore heterogeneous mechanical tests. The use of full-field measurements and heterogeneous tests has proven to be an interesting approach to calibrate complex models with a high number of material parameters, such as the case of anisotropic plasticity models. Usually, the inverse strategies selected to identify the material parameters from heterogeneous fields are based on the so-called finite element model updating (FEMU) method, which is known for being computationally demanding. Nevertheless, novel inverse strategies, such as the virtual fields method, have demonstrated much better results in terms of the computational cost without deterioration of the calibration results. Therefore, the aim of the present study, in the framework of full-field measurements, is to explore the combination of a previously designed heterogeneous test and the virtual fields method (VFM). The heterogeneous test consists of a uniaxial standard test with an optimized specimen shape, called butterfly shape. This specimen was specifically designed to obtain a wide range of strain paths and strain amplitudes and has given promising results when combined with a FEMU-based strategy. A set of virtual fields is developed to combine the butterfly test and the VFM. This set is tested with virtual experimental data generated and the sensitivity of the VFM to the number of virtual fields is confirmed. Moreover, experimentally acquired full-field measurements of butterfly test for a DC04 mild steel are used to assess the performance of this calibration strategy. An anisotropic plasticity model composed by Hill'48 and Swift's law is calibrated.

Keywords Calibration of constitutive models · Anisotropic metal plasticity · Heterogeneous test · Full-field measurements · Virtual fields method

Introduction

The use of numerical simulation tools to support the mechanical design of a manufacturing process or a part has long been employed by the industry. The demands for better accuracy of these tools led to the development of more and more complex constitutive models to mimic the real mechanical behaviour of materials. Nevertheless, before using any of these models, a calibration phase is required, in which the material parameters of the model are adjusted to have a close prediction of the material in hands. The predictive capabilities of constitutive models largely depend on this phase. Moreover, the applicability

J. M. P. Martins (✉)
Univ. Bretagne Sud, UMR CNRS 6027, IRDL, Lorient, France

Centre for Mechanical Technology and Automation (TEMA), University of Aveiro, Aveiro, Portugal
e-mail: joao.martins52@ua.pt

S. Thuillier
Univ. Bretagne Sud, UMR CNRS 6027, IRDL, Lorient, France
e-mail: sandrine.thuillier@univ-ubs.fr

A. Andrade-Campos
Centre for Mechanical Technology and Automation (TEMA), University of Aveiro, Aveiro, Portugal
e-mail: gilac@ua.pt

A. Baldi et al. (eds.), *Residual Stress, Thermomechanics & Infrared Imaging and Inverse Problems, Volume 6*,
Conference Proceedings of the Society for Experimental Mechanics Series, https://doi.org/10.1007/978-3-030-30098-2_5

of the models is also dependent on the experimental effort required for this phase. Frequently, the need for a large and diversified set of experimental tests to calibrate a constitutive model restrains the use of more advanced and accurate constitutive models [1].

The advent of full-field measurement techniques (e.g. Digital Image Correlation, DIC in short [2]) is changing significantly the calibration process of constitutive models. These techniques allow access to dense maps of data (displacements, strains, etc.) from a single mechanical test, which after post-treatment can be used to retrieve the material parameters of a selected constitutive model. Moreover, these techniques enable the use of complex sample geometries to test the mechanical behaviour of materials, which, if correctly designed, produce heterogeneous strain fields with enough information to extract several material parameters from a single test. However, to extract the material parameters from this type of data, it is required to solve an inverse problem that is time-consuming. Therefore, the quest for both efficient inverse methods and appropriate test geometries has been intense in the past few years. Nevertheless, inverse methods and new test geometries for mechanical testing are usually developed and validated separately and consequently, the symbiosis between these two is not fully explored.

In this work, a heterogeneous test specially optimized to calibrate constitutive models [3, 4] for sheet metal plasticity is combined with the Virtual Fields method (VFM) [5]. This heterogenous test, called butterfly test, is firstly presented as well as the experimental data previously acquired for a DC04 mild steel [4]. This study focuses on the selection of a set of virtual fields suitable for the above-mentioned test, as well as the influence of the number of virtual fields used. Finally, the performance of the VFM combined with the data acquired from a single butterfly test is assessed. An anisotropic model composed by Hill'48 yield criterion and Swift's hardening law is selected to be calibrated.

The Virtual Fields Method

The virtual fields method is an inverse method which relies on the principle of virtual work and kinematic full-field measurements to retrieve constitutive material parameters. Due to the nature of the principle of virtual work, this method can be applied to any constitutive model. In the case of non-linear models, such as elasto-plastic models, the inverse problem is solved by minimizing the squared difference of the gap between internal and external virtual work, with respect to the sought constitutive parameters and for different time steps. The objective function, in the large strain framework and assuming static equilibrium, can be written as:

$$\varphi(\boldsymbol{\xi}) = \frac{1}{n_{\mathrm{v}}}\sum_{i=1}^{n_{\mathrm{v}}}\frac{1}{n_{\mathrm{t}}}\sum_{j=1}^{n_{\mathrm{t}}}\left(\int_{\Omega_0}\mathbf{P}\left(\boldsymbol{\xi},\boldsymbol{\varepsilon}^{\mathrm{exp}}\right):\mathrm{Grad}\mathbf{U}^{*}\mathrm{d}V-\int_{\Gamma_0^{\mathrm{f}}}\overline{\mathbf{T}}\cdot\mathbf{U}^{*}\mathrm{d}S\right)^2, \tag{5.1}$$

where $\mathbf{P}$ is the first Piola-Kirchhoff stress tensor that is a function of the constitutive parameters $\boldsymbol{\xi}$ and the experimental strain field $\boldsymbol{\varepsilon}^{\mathrm{exp}}$. $\overline{\mathbf{T}}$ is the first Piola-Kirchhoff stress vector calculated on the boundary Γ_0^{f} where surface forces are applied. $\mathbf{U}^{*}$ can be any kinematically admissible virtual field and $\mathrm{Grad}\mathbf{U}^{*}$ is the respective gradient calculated with respect to the reference coordinates of the body. $\mathrm{d}V$ and $\mathrm{d}S$ are the infinitesimal volume and area of the body in the reference configuration Ω_0. n_{v} and n_{t} are the number of virtual fields selected and time steps considered, respectively. This large strain formulation is a convenient description to write the principle of virtual work, since for the computation of the internal and external work the geometric quantities are defined on the reference configuration. More details on this formulation can be found in [6].

One of the key parts of this method are the virtual fields selected to build the objective function, which can be any continuous and differentiable function. Nevertheless, these functions are usually selected from a set of kinematically admissible functions, i.e. it is required that the virtual fields vanish on the boundaries of prescribed displacement. In this work, the virtual fields are developed manually, which is addressed in the section Manually Defined Virtual Fields. The other key part of this method is the reconstruction of the stress field from the strain field $\boldsymbol{\varepsilon}^{\mathrm{exp}}$, which is derived from the measured displacement field. Usually, the displacement field is acquired on the surface of the specimen and, therefore, to reconstruct the stress field, the plane stress conditions are assumed. Moreover, to reconstruct the stress field, it is necessary to adopt *a priori* a constitutive model to make the link between strains and stresses. In this work, the adopted constitutive model is defined by: (1) linear isotropic elastic behavior (generalized Hooke's law) and; (2) plastic behaviour described by the orthotropic Hill'48 yield criterion and isotropic hardening (Swift's law). The calibration of the plastic part of the model is the focus of the present work, whereas the material parameters that govern elastic part are assumed to be known. Regarding the plastic behaviour, the equivalent Hill'48 yield criterion assumes the following form in plane stress conditions:

$$\bar{\sigma}^2 = F\sigma_{yy}^2 + G\sigma_{xx}^2 + H\left(\sigma_{xx} - \sigma_{yy}\right)^2 + 2N\sigma_{xy}^2, \tag{5.2}$$

where σ_{xx}, σ_{yy} and σ_{xy} are the components of the stress tensor with respect to the anisotropic material axes. F, G, H and N are the constitutive parameters that must be calibrated. Nevertheless, the relation $G + H = 1$ is assumed which leaves only F, G and N to be identified. The isotropic hardening law (Swift's law) has the following form:

$$\sigma_y\left(\bar{\varepsilon}^p\right) = K\left(\varepsilon_0 + \bar{\varepsilon}^p\right)^n, \varepsilon_0 = \left(\frac{\sigma_0}{K}\right)^{(1/n)} \tag{5.3}$$

where σ_0, K and n are the material parameters. $\bar{\varepsilon}^p$ is the equivalent plastic strain. Thus, the adopted model contains 6 material parameters which must be identified according to the studied material.

The methodology presented in this section was implemented in an in-house code using the programming language Fortran. This code contains bilinear shape functions to derive the strain field from the measured displacement field. Due to the non-linearity of the model, the stress reconstruction is performed using an algorithm of the type Backward-Euler return [7]. The minimization of the objective function is conducted by the gradient-based Levenberg-Marquardt optimization method.

The Butterfly Test

The butterfly test was first proposed by Souto et al. [3]. The geometry of the specimen was numerically designed through a shape optimization procedure which aimed a heterogeneous test to calibrate complex constitutive models for sheet metals. The optimization process was governed by an objective function that rated the information provided by the test in terms of range and diversity of strain states and strain level reached. The final geometry was able to produce a spectrum of strain states ranging from simple shear to plane strain. More recently, this final geometry was adapted by Aquino et al. [4] to facilitate the cutting process of the specimen. This adapted specimen was experimentally validated using special grips (Fig. 5.1a), and an attempt to calibrate a complex anisotropic constitutive model was performed through the inverse method FEMU. The specimen was obtained from 0.7 mm thick sheet metal of a DC04 mild steel. The tests were performed on a common tensile machine. The DIC-system employed to carried out the measurements was the ARAMIS 3D 5M system developed by GOM. Figure 5.1b shows the strain distribution in the principal strain space for a displacement of the tool equal to 7.1 mm. As can be seen, the adapted geometry produces a range of strains from simple shear to plane strain.

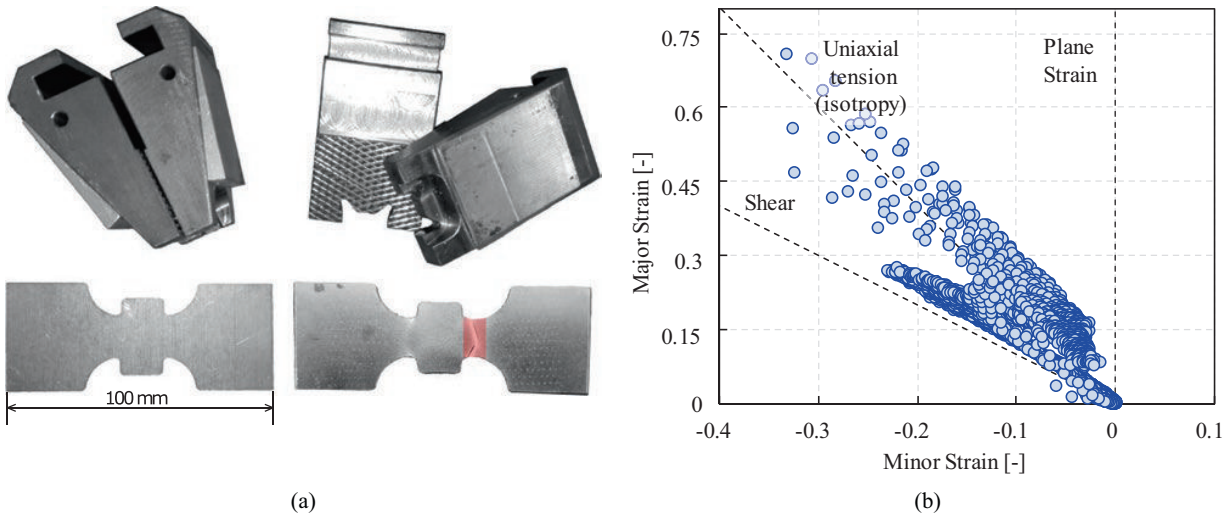

Fig. 5.1 (**a**) Grips and specimen used for the adapted butterfly test and (**b**) principal strains distribution for a tool displacement of 7.1 mm

In this work, the same experimental data used by Aquino et al. [4] is adopted. The displacement fields acquired for the specimen with the rolling direction orientated along the traction axis are used. These displacements fields are projected onto a 2D mesh generated by the Abaqus software (Fig. 5.2a) that represents one-fourth of specimen, in order to be processed by the VFM. A total of 398 steps from the load/displacement history of the grip are considered (Fig. 5.2b). Only the load history between the two red dots is considered, because most of the points in the early stages of the test have a low value of strain and were highly affected by noise. Yet, larger load histories were analysed, and the results were not significantly affected.

Manually Defined Virtual Fields

In non-linear cases, the VFM relies on the minimization of Eq. (5.1) to retrieve the constitutive parameters. As mentioned before, the virtual fields selected to build the objective function have a fundamental role in the results of the identification. Currently, there are three main approaches to select a suitable set of virtual fields, two of them rely on automatic procedures to select the virtual fields and require a low-level of user's intervention [6, 8]. The other approach, called manually defined virtual fields, depends exclusively on the user's intervention, since it is the user that must develop the suitable set according to the boundary conditions of the test. This last strategy has been the most used and its main advantages are the computational cost and the ease of implementation. For these reasons, this is the strategy adopted in the present work.

Generally, the manually defined virtual fields are developed using polynomial and/or periodic functions. These functions are manipulated to generate kinematically admissible virtual fields [5]. In terms of objective function, the components of the virtual field gradient can be seen as weights for the components of the stress tensor. Specially in anisotropic plasticity, all the components of the stress tensor contain information about the yield criterion, hence must be considered within the identification process. Based on these considerations, a set of 8 virtual fields is developed and the influence of the number of virtual fields on the identification results is assessed. The developed virtual fields can be written as:

$$\mathbf{U}^{*(1)} = \begin{cases} U_x^* = 0 \\ U_y^* = \dfrac{Y}{L}, \end{cases} \tag{5.4}$$

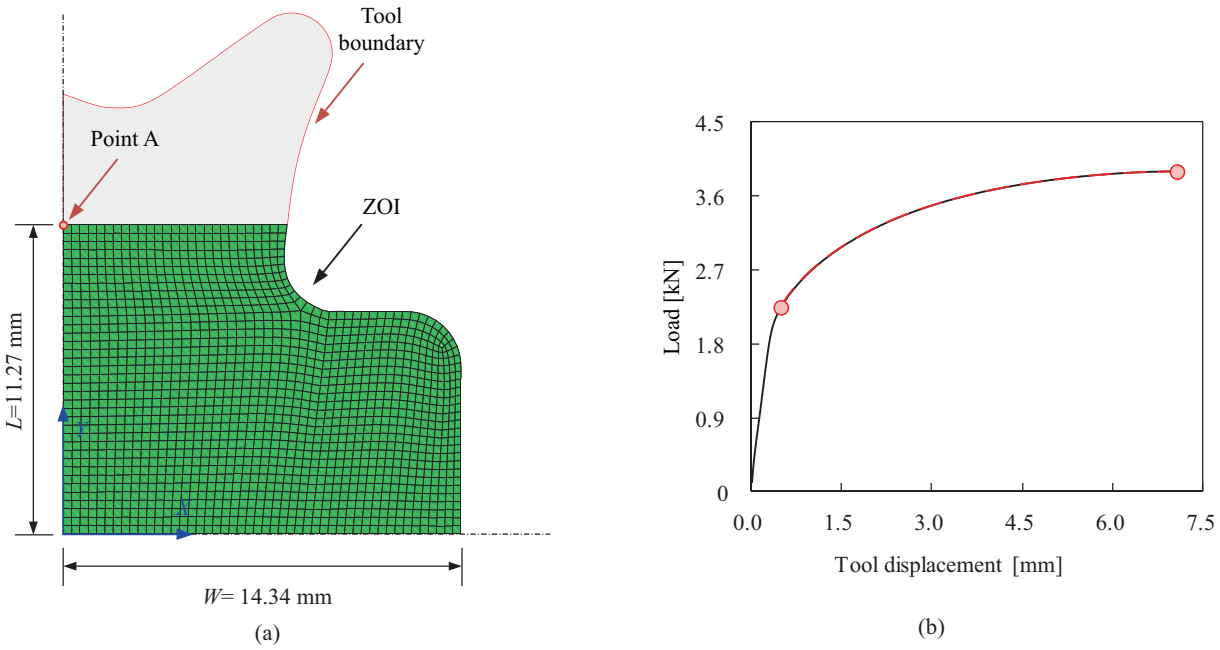

Fig. 5.2 (**a**) Zone of interest (ZOI) and regular mesh used for the VFM identification. (**b**) Load history for the butterfly test

$$\mathbf{U}^{*(2)} = \begin{cases} U_x^* = \dfrac{X\left(Y^2 - YL\right)}{WL^2} \\ U_y^* = 0 \end{cases}, \tag{5.5}$$

$$\mathbf{U}^{*(3)} = \begin{cases} U_x^* = \sin\left(\dfrac{X}{W}\pi\right)\sin\left(\dfrac{Y}{L}\pi\right) \\ U_y^* = 0 \end{cases}, \tag{5.6}$$

$$\mathbf{U}^{*(4)} = \begin{cases} U_x^* = 0 \\ U_y^* = \sin\left(\dfrac{X}{W}\pi\right)\sin\left(\dfrac{Y}{L}\pi\right) \end{cases}, \tag{5.7}$$

$$\mathbf{U}^{*(5)} = \begin{cases} U_x^* = 0 \\ U_y^* = \dfrac{XY\left(Y - L\right)}{WL^2} \end{cases}, \tag{5.8}$$

$$\mathbf{U}^{*(6)} = \begin{cases} U_x^* = 0 \\ U_y^* = \dfrac{Y^2\left(L - Y\right)}{L^3}\sin\left(\dfrac{\pi X}{W}\right) \end{cases}, \tag{5.9}$$

$$\mathbf{U}^{*(7)} = \begin{cases} U_x^* = \dfrac{L^3 - Y^3}{L^3}\sin\left(\dfrac{\pi X}{W}\right) \\ U_y^* = 0 \end{cases}, \tag{5.10}$$

$$\mathbf{U}^{*(8)} = \begin{cases} U_x^* = 0 \\ U_y^* = \dfrac{YL^2 - Y^3}{L^3}\sin\left(\dfrac{\pi X}{W}\right) \end{cases}, \tag{5.11}$$

where W and L are the maximum value of the width and length of the zone of interest (ZOI) of the specimen surface in the reference configuration (see Fig. 5.2a). X and Y are the coordinates in the reference configuration. In case of static equilibrium, the first virtual field is the only one that gives a non-zero value of internal virtual work, which should be balanced with the external virtual work. It also gives maximum weight to the normal component of the stress tensor in the y-direction and neglects the remaining components. The other virtual fields distribute the weight between two components, normal and shear components.

In order to assess the influence of the number of virtual fields in the identification process, virtual experimental data generated by finite element (FE) analysis is used. A two-dimensional FE model representing one-fourth of the butterfly test is built assuming plane stress conditions. A displacement of 1.5 mm is prescribed to a rigid tool, which is modelled assuming tie contact with the irregular boundary on top of the specimen (see Fig. 5.2a). A reference set of material parameters representing a mild steel is adopted and its values are listed in Table 5.1. The test is simulated in Abaqus standard software and the displacement field of a total of 375 load steps is retrieved to build the objective function (Eq. (5.1)).

A total of 8 identifications with an increasing number of virtual fields are performed. The presented virtual fields are added to the objective function in order to enrich the identification process. The results are presented in Fig. 5.3, in which the value of the optimized parameter is normalised by the respective reference value. The results show that for one virtual field (Eq. (5.4)) the errors are the highest, particularly for the yield criterion parameters. Nevertheless, the results are significantly improved when the second virtual field (Eq. (5.5)) is added and tend to stabilize for 5 virtual fields. For a total of 8 virtual fields, the maximum error attained is lower than 1.5% and corresponds to the parameter n.

This confirms that the number of virtual fields plays an important role in the accuracy of the VFM. Moreover, the set of the developed virtual fields is able to retrieve simultaneously the hardening law and yield criterion parameters using a single virtual butterfly test. This also demonstrates that the butterfly test provides a heterogenous strain field that contains enough information to identify the present model.

Table 5.1 Reference material parameters for Swift's hardening law and Hill'48 yield criterion

Swift's hardening law			Hill'48 yield criterion		
σ_0 (MPa)	n	K (MPa)	F	G	N
160	0.26	565	0.2782	0.3731	1.5568

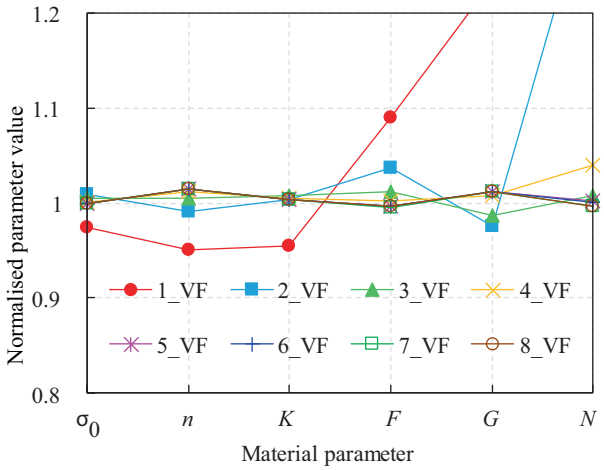

Fig. 5.3 Influence of the number of virtual fields on the identification results

Identification of Material Parameters: Results and Analysis

In this section, it is assessed the performance of the VFM combined with the experimental database acquired from the butterfly test to calibrate the constitutive model composed by Hill'48 yield criterion and Swift's hardening law. According to the results of the previous section, the 8 virtual fields presented are used to build the objective function. Moreover, since the optimization method is a gradient-based, the sensitivity to the initial set of parameters given to start the optimization process is also assessed. The initial sets are arbitrarily chosen.

The obtained set of parameters is presented in Table 5.2. Regardless of the initial set of parameters, the results converged always for the same solution set shown in Table 5.2. Moreover, Table 5.2 also shows the yield stress values and plastic anisotropic parameters calculated based on the retrieved parameters. The plastic anisotropic coefficient at 0 degrees (rolling direction) presents a value characteristic of mild steel [9], whereas the other two coefficients present values lower than the characteristic ones of this material.

The evolution of the internal virtual work calculated using the parameters of Table 5.2 and the first virtual field (Eq. (5.4)), and the evolution of the external virtual work calculated based on the measured load are presented in Fig. 5.4a. The evolutions of the internal and external virtual works show a good agreement. Nevertheless, the internal virtual work evolution suffers from minor oscillations, which can result from the presence of noise in the full-field measurements.

In order to check the validity of the retrieved parameters, the butterfly test is simulated with a two-dimensional FE model assuming plane stress conditions and using the retrieved parameters. The results of the force evolution for the FE model are compared with the measured load in Fig. 5.4b. Note that the results are plotted for the displacement of point A (see Fig. 5.4b), in order to minimise the impact of a possible sliding under the grips. Figure 5.4b shows a good agreement between the two load curves and a slight overestimation of the displacement at the end of the test. These results confirm that the material behaviour for the rolling direction is well captured by the constitutive model and its retrieved material parameters.

Table 5.2 Identification results for Swift's hardening law and Hill'48 yield criterion

Swift's hardening law			Hill'48 yield criterion		
σ_0 (MPa)	n	K (MPa)	F	G	N
166.4	0.31	593.9	0.5503	0.3439	1.4797
Normalised yield stresses σ_α			Plastic anisotropic coefficients r_α		
σ_0	σ_{45}	σ_{90}	r_0	r_{45}	r_{90}
1.0	1.02	0.91	1.90	1.15	1.19

Normalised yield stress values and plastic anisotropic coefficients calculated based on the obtained parameters

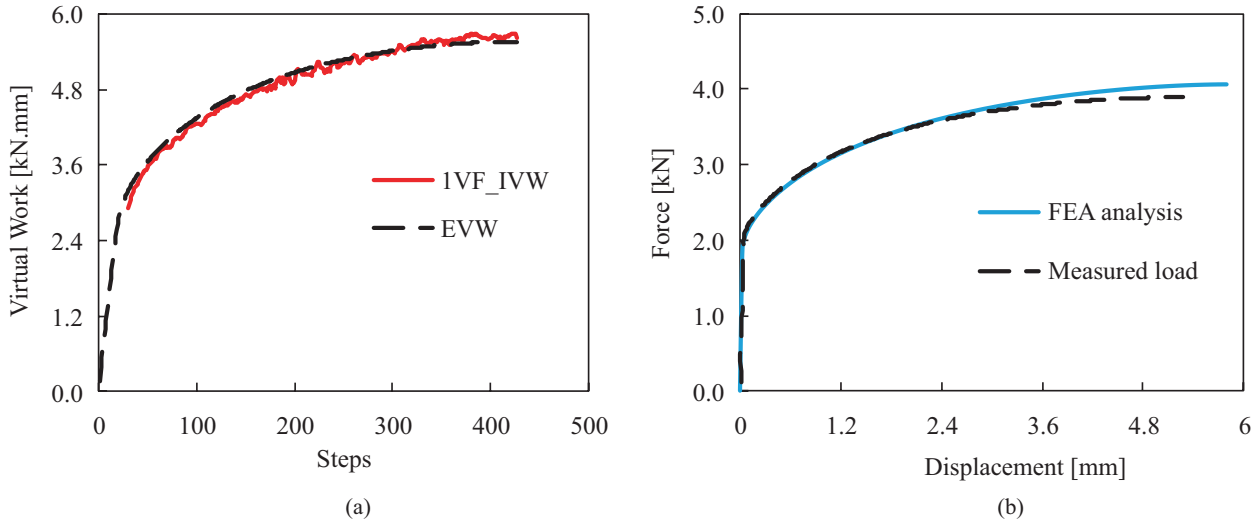

Fig. 5.4 (**a**) Evolution of the internal (virtual field of Eq. (5.4)) and external virtual work and (**b**) comparison of the measured load with the predicted load using FE analysis and the retrieved parameters presented in Table 5.2

Conclusions

The present work is a first attempt to link an optimized heterogenous mechanical test with VFM. The aim is to propose a strategy to identify all the parameters of an anisotropic constitutive model using a single test. A set of manually defined virtual fields to link the VFM and the butterfly test is proposed. This set is analysed using virtual experimental data, generated according to the adopted constitutive model. The analysis shows the dependence of the VFM on the number of virtual fields used to build the objective function. In this specific case, for a number superior to 5 virtual fields, there is a reasonable error (maximum error lower than 1.5%) in the identification results. Finally, the constitutive model composed by Hill'48 yield criterion and Swift's hardening law is calibrated using experimental data from a single test on a mild steel. The results revealed insensitivity of the VFM to the initial set of parameters used to start the identification process. Regarding the retrieved parameters, its performance is assessed through the predicted anisotropic plastic coefficients and FE analysis of the test. The predicted anisotropic plastic coefficient for the rolling direction is characteristic of mild steel, but the remaining coefficients suggest that the model was unable to predict them. The FE analysis of the test with the retrieved material parameters confirm this conclusion. The load curve predicted by the FE model shows a good agreement with the experimentally measured load, meaning that the overall behaviour of the material for the rolling direction was well captured. Nevertheless, a thorough study on the influence of the DIC parameters on the acquired data from the butterfly test should be performed.

Acknowledgements The authors acknowledge the financial support of FCT under the projects PTDC/EME-APL/29713/2017 (CENTRO-01-0145-FEDER-029713), PTDC/EMS-TEC/6400/2014 (POCI-01-0145-FEDER-016876), PTDC/EME-EME/31243/2017 (POCI-01-0145-FEDER-031243) and PTDC/EME-EME/30592/2017 (POCI-01-0145-FEDER-030592) by UE/FEDER through the programs CENTRO 2020 and COMPETE 2020, and UID/EMS/00481/2013-FCT under CENTRO-01-0145-FEDER-022083. The authors also would like to acknowledge the Région Bretagne (France) for its financial support. J.M.P. Martins is also grateful to the FCT for the PhD grant SFRH/BD/117432/2016.

References

1. S. Bruschi, T. Altan, D. Banabic, et al., Testing and modelling of material behaviour and formability in sheet metal forming. CIRP Ann. Manuf. Technol. **63**, 727–749 (2014)
2. M.A. Sutton, J.-J. Orteu, H. Schreier, *Image Correlation for Shape, Motion and Deformation Measurements* (Springer, Boston, 2009)
3. N. Souto, A. Andrade-Campos, S. Thuillier, Mechanical design of a heterogeneous test for parameters identification. Int. J. Mater. Form. **10**(3), 353–367 (2017)
4. J. Aquino, A. Andrade-Campos, S. Thuillier, Design of heterogeneous mechanical tests – numerical methodology and experimental validation. Strain **55**, e12313 (2019)
5. F. Pierron, M. Grédiac, *The Virtual Fields Method: Extracting Constitutive Mechanical Parameters from Full-Field Deformation Measurements* (Springer, New York, 2012)
6. A. Marek, F.M. Davis, M. Rossi, F. Pierron, Extension of the sensitivity-based virtual fields to large deformation anisotropic plasticity. Int. J. Mater. Form. **12**, 457–476 (2019)
7. M. Crisfield, *Non-Linear Finite Element Analysis of Solids and Structures*, vol 1 (Wiley, Chichester, 1991)
8. F. Pierron, S. Avril, V.T. Tran, Extension of the virtual fields method to elasto-plastic material identification with cyclic loads and kinematic hardening. Int. J. Solids Struct. **47**(22), 2993–3010 (2010)
9. S.L. Zang, S. Thuillier, A. Le Port, P.Y. Manach, Prediction of anisotropy and hardening for metallic sheets in tension, simple shear and biaxial tension. Int. J. Mech. Sci. **53**, 338–347 (2011)

3.4 Final Remarks

The present chapter is mainly dedicated to the Virtual Fields Method. It is shown that this method offers more than a reduced computational cost when compared to the Finite Element Model Updating. Its combination with two complex heterogeneous tests is analysed . On the overall, the Virtual Fields Method presented a robust response in the simultaneously calibration of the complete set of parameters of an anisotropic plasticity model. Moreover, as it does not require the exact knowledge of the boundary conditions eases the process of exploring a heterogeneous test. On the other hand, the selection of a suitable set of virtual fields is a downside. The design of a set of virtual fields to link the method with the butterfly test revealed that the number of virtual fields matters. An aspect that must be explored in the future. Apart form that, the calibration of complex anisotropic plasticity models revealed that constitutive models need to be prepared with constraints to reduce the non-uniqueness problem. This can also improve the convergence of the methods. Regarding the heterogeneous tests, the biaxial tension test in a cruciform specimen provides a large range of strain states and different levels of strain. Still, the geometry of a cruciform specimen can be enhanced to provide more information. The results from the optimised butterfly test show a good description of the material behaviour for the loading direction. Nevertheless, a test in a single loading direction seems insufficient to accurately capture the plastic anisotropy coefficients.

Intentionally blank page.

Chapter 4

Contributions to the calibration of thermo-mechanical constitutive models

The calibration of thermo-mechanical constitutive models is a demanding challenge that requires long experimental campaigns to create a database for a broad range of temperatures and strain rates. Moreover, the complexity of this process increases with the complexity of the constitutive model. Accordingly, the development of innovative calibration methodologies aiming at reducing the experimental campaigns is fundamental.

4.1 Calibration of Johnson-Cook Model Using Heterogeneous Thermo-Mechanical Tests

This section presents a calibration methodology based on the Finite Element Model Updating and a heterogeneous thermo-mechanical test performed on a Gleeble machine. The methodology is tested using virtually generated data.

Available online at www.sciencedirect.com

ScienceDirect

Procedia Manufacturing 47 (2020) 881–888

Procedia MANUFACTURING

www.elsevier.com/locate/procedia

23rd International Conference on Material Forming (ESAFORM 2020)

Calibration of Johnson-Cook Model Using Heterogeneous Thermo-Mechanical Tests

João Peixoto Martins[a,b,*], António Andrade-Campos[a], Sandrine Thuillier[b]

[a]*Centre for Mechanical Technology and Automation, Dep. Mechanical Engineering, University of Aveiro, Portugal*
[b]*Univ. Bretagne Sud, UMR CNRS 6027, IRDL, F-56100 Lorient, France*

* Corresponding author. *Tel.: +351-234-370-830; fax: +350-234-370-953. E-mail address:* joao.martins52@ua.pt

Abstract

In the present work, a calibration methodology based on full-field measurements from heterogeneous thermo-mechanical tests is introduced. In order to evaluate the feasibility of this methodology, the widely adopted Johnson-Cook model is chosen. This calibration methodology relies on the Finite Element Model Updating (FEMU) method to take full advantage of the information contained in full-field measurements and thus, simultaneously calibrate the three terms of the Johnson-Cook model regarding strain hardening, temperature and strain rate. A virtual experimental database composed of strain fields and load output from three heterogeneous tests performed at different average strain rates is used. The minimisation of the least-square objective function is performed by the gradient-based Levenberg-Marquardt optimisation algorithm. A detailed analysis of the virtual database and objective function is performed and discussed. Furthermore, the robustness of the proposed methodology is tested with noisy data.

Keywords: Calibration; FEMU; Heterogenous Thermo-Mechanical Test; Full-Field Measurements; Thermo-Elasto-Viscoplasticity

1. Introduction

The mechanical behaviour of metals is typically sensitive to strain, strain rate and temperature. In recent years, temperature and strain rate effects have gained more impact due to the increasing use of heat-assisted manufacturing processes (e.g. hot and warm forming [1,2]) and due to new generations of high strength steels, which, due to the heat generated by plastic deformation, reach higher temperatures than traditional steels during the deformation process [3, 4]. Therefore, an accurate prediction of the mechanical behaviour of metals under a wide range of temperatures and strain rates is essential for virtual manufacturing processes, crashworthiness tests, etc. Phenomenological thermo-elasto-viscoplastic constitutive models are usually applied to predict such behaviour. This type of models can be strongly non-linear and contains a large number of material parameters which often hamper their applicability.

According to classical calibration procedures, the identification of the material parameters of this type of models requires a long experimental campaign to create a database for a broad range of temperatures and strain rates. These classical procedures rely on uniaxial tests, whose strain and stress fields are analysed under the assumption of homogeneous conditions. As a consequence, a large number of tests is required to cover a wide range of temperatures and strain rates [5]. Moreover, the assumption of homogeneous strain/stress is very limiting in terms of maximum strain value and does not mimic the complex heterogeneous strain/stress fields which occur in real manufacturing processes.

Therefore, the solid mechanics' community has done a remarkable effort to reduce these long experimental campaigns using full-field measurement techniques, heterogeneous tests

10.1016/j.promfg.2020.04.274

and inverse methods. The main advantage of full-field measurement methods, such as Digital Image Correlation (DIC), is that complete deformation maps can be recorded from the surface of a specimen during a test. In the case of heterogeneous tests, a complete deformation map corresponds to a set of spatial points under different strain states, strain levels and strain rates. This information can also be enriched with temperature measurements, through thermographic cameras, for example. This data can be utilised as input for inverse methods and thus, used to retrieve the unknown material parameters. Currently, the Finite Element Model Updating (FEMU) method and the Virtual Fields Method (VFM) are the most used inverse methods [6, 7]. For example, Kajberg and Wikman [8] used a FEMU-based approach to calibrate the strain rate term of the Johnson-Cook model for high strain rates. Notta-cuvier et al. [9] proposed a methodology based on VFM and two tests to calibrate the same model. The calibration process was divided into two phases: first, the strain hardening term is calibrated resorting to a quasi-static test and then, the strain rate term is calibrated resorting to a dynamic test. Valeri et al. [10] have also proposed a methodology based on VFM to calibrate the temperature and strain rate terms of the Johnson-Cook model, using the data of several tensile tests performed at different temperatures. More recently, Jones et al. [11] analysed the simultaneous calibration of all parameters in a viscoplastic model using VFM. The non-uniqueness of the solution led the authors to analyse different strategies to tackle this issue.

In this work, a FEMU-based methodology is introduced to calibrate simultaneously the three terms of the Johnson-Cook model regarding strain hardening, strain rate and temperature. This methodology relies on heterogeneous thermo-mechanical tests performed for three different average strain rates. Full-field strain measurements and load signals are gathered in a database and combined with an accurate Finite Element (FE) model of the test. It is expected that this combination gathers sufficient information for the calibration of a thermo-elasto-viscoplastic model. Therefore, the sensitivity of the proposed methodology to the parameters of the Johnson-Cook model is assessed. This analysis is performed with virtual experiments that mimic the real ones. The real experiments were performed on Gleeble 3500 tensile testing machine and are detailed in [12].

2. Heterogeneous thermo-mechanical test: virtual experimental database

The experimental database is a key aspect of any constitutive model calibration. Gather all the essential information in the experimental database usually implies a lengthy experimental campaign. Nevertheless, full-field measurements and heterogeneous tests offer a different solution, eventually less lengthy. Based on this idea, an experimental database which relies on heterogeneous thermo-mechanical tests is proposed. These tests are performed on a Gleeble equipment and consist of tensile tests with a heterogeneous temperature field, which are performed at different average strain-rates. The Gleeble equipment contains a direct resistance heating system that allows to control the temperature in the centre of the specimen and hold it constant during the test, whereas the remaining part of the specimen undergoes a temperature gradient due to the water cooling system of the machine's grips. The asset of this procedure is the temperature gradient that triggers a heterogeneous deformation process and consequently, provides information on the mechanical behaviour of the material for different temperatures and strain rates.

In order to analyse the information encoded in the strain fields and load signals from these tests, it is used a virtual database generated by a FE model of the tests. The same specimen's geometry, represented in Fig. 1, is used in all the tests. Thus, the FE model represents the zone of interest (ZOI) in the tensile specimen and has the geometry depicted in Fig. 1. The thickness of the specimen is 1.75 mm.

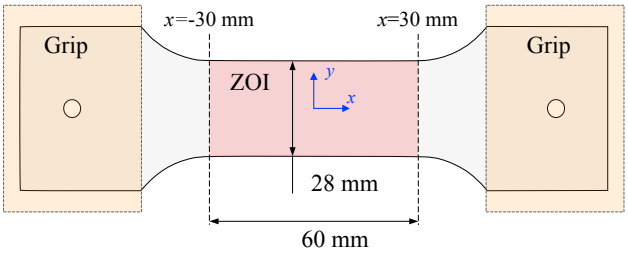

Fig. 1. Schematic representation of the specimen for the heterogeneous thermo-mechanical test and its respective ZOI.

Abaqus standard [13] is adopted to perform the FE analysis. An eight-node solid element with reduced integration is adopted to mesh the ZOI presented in Fig. 1. The final mesh is composed of a total of 1680 elements. The tests are performed for three different loading conditions in terms of time, which consist of different average strain rates; 10^{-4}, 10^{-3} and 10^{-2} s^{-1}. The boundary conditions are the displacements imposed on the boundaries $x = -30$ mm and $x = 30$ mm, based on the displacements measured with DIC during real tests for a DP980 steel sheet.

Generally, the temperature field generated during a test in the Gleeble equipment has a characteristic shape, which is symmetrical about the centre of the specimen and assumes a parabolic shape. An example of an experimental measurement of such a temperature field is presented in Fig. 2. The temperature value along a line on the specimen's surface (blue line in Fig. 2 a)) is presented in Fig. 2 b), as well as the measurements of three thermocouples, which confirm an approximate symmetrical and parabolic shape of the temperature profile along the length of the specimen. Moreover, it was confirmed that the temperature field is approximately constant during the test. Therefore, the measured temperature field is imposed in the FE model as an input variable and is considered constant for each node of the mesh along the deformation process. The temperature range investigated is then approximately [360°C,500°C].

Regarding the constitutive model, the widely used Johnson-Cook model is adopted. This model has a multiplicative formulation which decomposes the flow stress evolution in three terms regarding strain hardening, temperature and strain rate. It can be written in the following form:

$$\sigma_y = \left[A + B\left(\bar{\varepsilon}^{\mathrm{p}}\right)^n\right]\left[1-\left(\frac{T-T_{\mathrm{tr}}}{T_{\mathrm{m}}-T_{\mathrm{tr}}}\right)^m\right]\left[1+C\ln\left(\frac{\dot{\bar{\varepsilon}}^{\mathrm{p}}}{\dot{\varepsilon}_0}\right)\right] \quad (1)$$

where A, B and n are the material parameters which control the strain hardening effect, m, T_{tr} and T_{m} the temperature sensitivity and C and $\dot{\varepsilon}_0$ the strain rate sensitivity. T_{m} is usually defined as the melting temperature and T_{tr} as the transition temperature at or below which there is no temperature effect. $\dot{\varepsilon}_0$ is a threshold for strain-rate dependence, at or below which there is no strain-rate effect. $\bar{\varepsilon}^{\mathrm{p}}$ and $\dot{\bar{\varepsilon}}^{\mathrm{p}}$ are the equivalent plastic strain and strain rate, respectively.

In order to create the virtual experimental database, a reference set of material parameters is adopted. This reference set is characteristic of DP980 steel and is shown in Table 1 [14]. Anisotropic effects are not considered, and von Mises yield criterion is adopted. Moreover, isotropic elastic behaviour is defined. The calibration of the elastic constants is not part of this work and these are assumed to be known a priori, namely Young's modulus of 210 GPa and Poisson's ratio of 0.3.

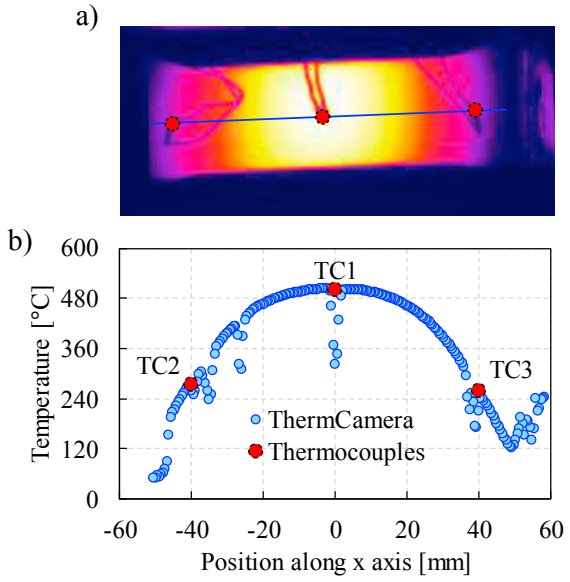

Fig. 2. Temperature field obtained during a test in a Gleeble equipment: a) thermographic camera measurement and b) temperature along a line and thermocouples measurements on the specimen's surface.

Table 1. Reference set of material parameters [14].

Strain hardening				
A [MPa]	B [MPa]	n		
205.21	1124.0	0.092		
Temperature and strain rate sensitivity				
m	T_{tr} [°C]	T_{m} [°C]	C [-]	$\dot{\varepsilon}_0$ [s^{-1}]
1.36	25	1000	0.05	0.001

The virtual load signals for the three tests performed at different average strain rates (10^{-4}, 10^{-3} and 10^{-2} s^{-1}) are shown in Fig. 3. Note that 29 time instants are selected to build the virtual database and their position is illustrated in Fig. 3 by the dots. The distribution of points gives a low weight to the beginning of the test. Nevertheless, it will be shown that, due to the heterogeneity of the test, even with such distribution of time instants, low values of strain and strain rate are also present in the database. Moreover, as can be seen from Fig. 3, the load signal is sensitive to the strain rate level. The increase in strain rate leads to an increase in the load value.

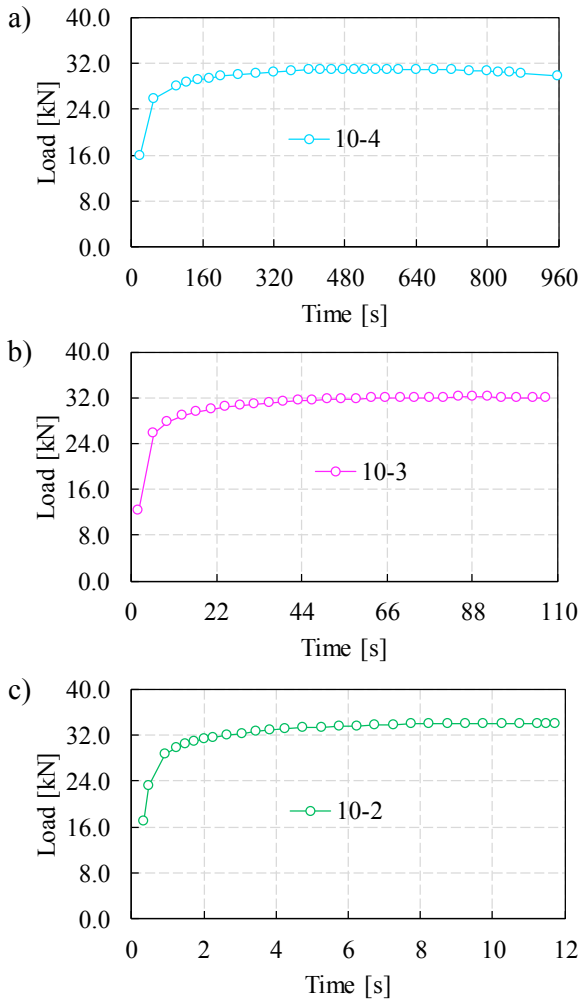

Fig. 3. Load signals of the heterogeneous thermo-mechanical tests performed at three different average strain rates: a) 10^{-4} s^{-1}, b) 10^{-3} s^{-1} and c) 10^{-2} s^{-1}.

In Fig. 4, the equivalent plastic strain distribution is presented for the last instant of each test, which correspond to 958 s, 107s and 11.75 s. The increase in average strain rate leads to lower values of equivalent plastic strain and delays the strain localization. In Fig. 5, a map of the occurrences in terms of equivalent plastic strain rate *versus* equivalent plastic strain for the complete deformation process shows the diversity of information available in these virtual tests. Fig. 5 highlights the fact that, independent of the average strain rate of each test, a significant range of equivalent plastic strain rate values are covered in each test, which is a consequence of the heterogeneity of the tests.

The virtual database is built with the complete strain fields for the ZOI (in-plane components of the strain tensor ε_{xx}, ε_{yy} and ε_{xy}) and load signals of 29 instants of three average strain-rates. It should be noted that only the in-plane strains at the top surface of the specimen are considered since only the strains at the surface of the specimen can be measured in a real experiment. Moreover, the strain fields are extracted from the centroid of each element.

3. FEMU-based approach and optimisation method

The Finite Element Model Updating (FEMU) relies on the simple idea of adjusting the unknown material parameters of a Finite Element (FE) model to minimise the difference between experimental and numerical results. Due to this straightforward idea, combined with the ease of implementation and flexibility in terms of usable data, this method has widespread adoption in many different applications.

The objective function that represents the idea behind FEMU can be built with different data, namely strain/displacements fields or load signals, or even a combination of both types of data. This flexibility in terms of data has contributed to increase the number of formulations presented in the literature. Nevertheless, it should be highlighted that the most recent ones have in common taking advantage of full-field measurements. In the present work, the adopted objective function relies on this common point and can be written as

$$\varphi(\boldsymbol{\chi}) = \frac{1}{n_{\text{tests}}}\sum_{i=1}^{n_{\text{tests}}}\left\{\frac{1}{n_{\text{ti}}}\sum_{j=1}^{n_{\text{ti}}}\left[\frac{1}{3\cdot n_{\text{p}}}\sum_{k=1}^{n_{\text{p}}}\left[\left(\frac{\varepsilon_{xx}^{\text{num}}(\boldsymbol{\chi})-\varepsilon_{xx}^{\text{exp}}}{\varepsilon_{\text{max}}^{\text{exp}}}\right)^2+\left(\frac{\varepsilon_{yy}^{\text{num}}(\boldsymbol{\chi})-\varepsilon_{yy}^{\text{exp}}}{\varepsilon_{\text{max}}^{\text{exp}}}\right)^2+\left(\frac{\varepsilon_{xy}^{\text{num}}(\boldsymbol{\chi})-\varepsilon_{xy}^{\text{exp}}}{\varepsilon_{\text{max}}^{\text{exp}}}\right)^2\right]_k+\left(\frac{F^{\text{num}}(\boldsymbol{\chi})-F^{\text{exp}}}{F_{\text{max}}^{\text{exp}}}\right)^2\right]_j\right\}_i \tag{2}$$

$\boldsymbol{\chi}$ is the vector of unknown material parameters and F is the load signal. The superscripts "num" and "exp" define the numerical and experimental data, respectively. n_{tests}, n_{ti} and n_{p} are the number of tests, time instants and number of in-plane measurement points, respectively. $F_{\text{max}}^{\text{exp}}$ is the maximum load value for each test and $\varepsilon_{\text{max}}^{\text{exp}}$ is the maximum strain value of all in-plane components for each test.

The Levenberg-Marquardt optimisation method is selected to minimise the objective function (Eq. 2). This method is a gradient-based method which resorts to the information of the approximated Hessian and Jacobian matrixes. The Levenberg-Marquardt method has the following form

$$\left\{\mathbf{H}(\boldsymbol{\chi}_\alpha)+\lambda\,\text{diag}\left(\mathbf{H}(\boldsymbol{\chi}_\alpha)\right)\right\}\Delta\boldsymbol{\chi}^{\text{LM}} = -\left[\mathbf{J}(\boldsymbol{\chi}_\alpha)\right]^{\text{T}}\mathbf{r}(\boldsymbol{\chi}_\alpha) \tag{3}$$

$\Delta\boldsymbol{\chi}^{\text{LM}}$ is the increment of the parameter vector $\mathbf{H}(\boldsymbol{\chi}_\alpha)$ is the Hessian matrix and $\mathbf{r}(\boldsymbol{\chi}_\alpha)$ is the residuals vector computed for the current solution of the material parameters set $\boldsymbol{\chi}_\alpha$. λ is a damping parameter used to stabilise the method in the vicinity of a minimum. Note that the residuals vector $\mathbf{r}(\boldsymbol{\chi}_\alpha)$ contains a number of lines equal to the number of residuals of each strain component, for each spatial point and time instant of each test, plus the number of load residuals for each time instant of each test. The Hessian matrix is approximated by

$$\mathbf{H}(\boldsymbol{\chi}_\alpha) = \left[\mathbf{J}(\boldsymbol{\chi}_\alpha)\right]^{\text{T}}\mathbf{J}(\boldsymbol{\chi}_\alpha) \tag{4}$$

where $\mathbf{J}(\boldsymbol{\chi}_\alpha)$ is the Jacobian matrix, that is computed by forward finite-differences [15]. The new set of material parameters for the iteration $\alpha+1$ is obtained through the updating of the previous one

$$\boldsymbol{\chi}_{\alpha+1} = \boldsymbol{\chi}_\alpha + \Delta\boldsymbol{\chi}^{\text{LM}} \tag{5}$$

The optimisation process stops when one of the following convergence criteria is attained: the objective function value is below $tol = 1\times10^{-12}$ or the parameter set reaches a stagnation plateau

$$\left(\left[\Delta\boldsymbol{\chi}^{\text{LM}}\right]^{\text{T}}\Delta\boldsymbol{\chi}^{\text{LM}}\right)^{1/2} \le tol \tag{6}$$

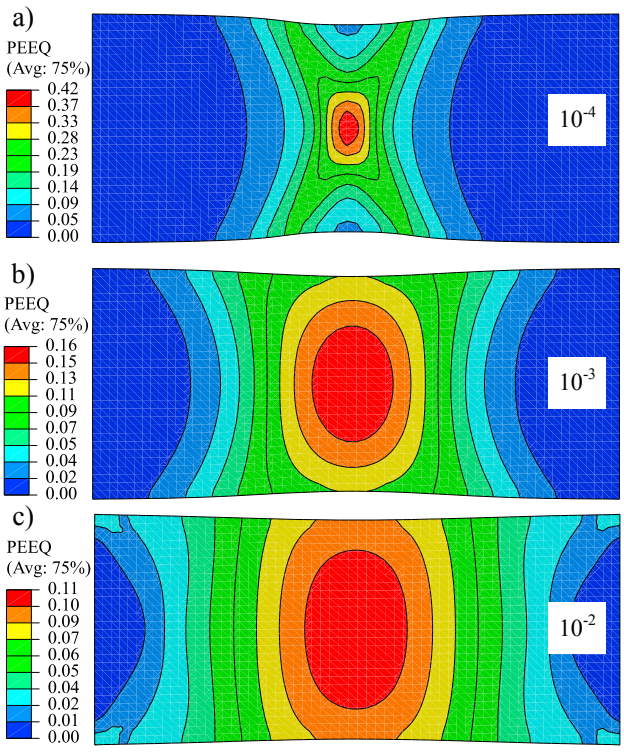

Fig. 4. Equivalent plastic strain (PEEQ) distribution for the last instant of each test, which correspond to 958 s, 107s and 11.75 s. Three different average strain rates: a) 10^{-4} s^{-1}, b) 10^{-3} s^{-1} and c) 10^{-2} s^{-1}.

4. Results

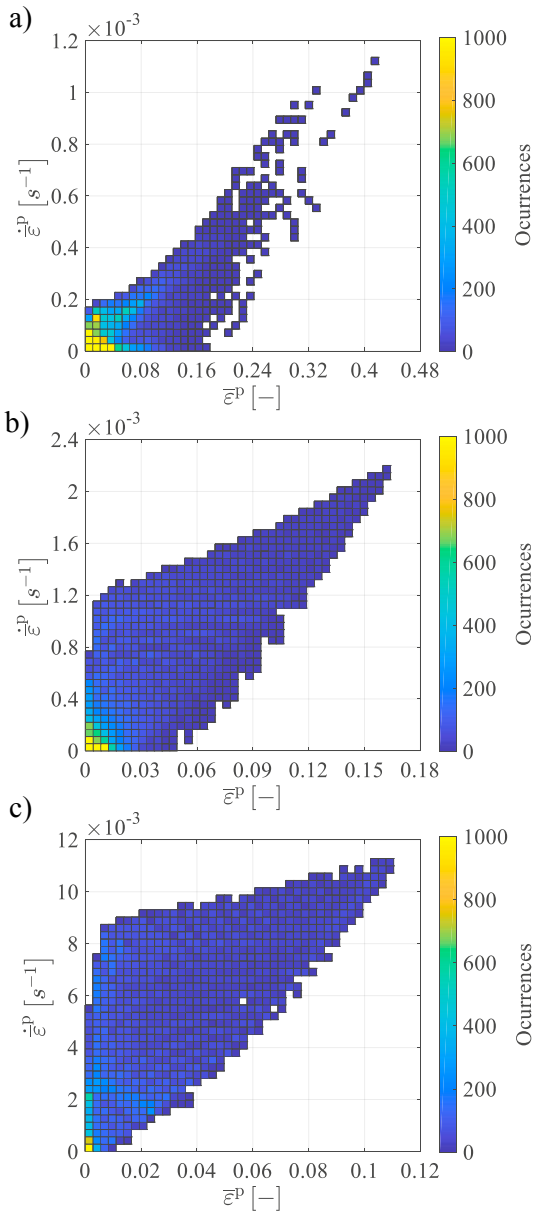

Fig. 5. Equivalent plastic strain rate *versus* equivalent plastic strain for the complete deformation process of the heterogeneous tests. Three different average strain rates: a) 10^{-4} s^{-1}, b) 10^{-3} s^{-1} and c) 10^{-2} s^{-1}.

In this section, the proposed methodology is analysed. The virtual database described in section 2 is combined with the objective function of section 3, to calibrate the Johnson-Cook model (Eq. 2). This analysis is structured into two subsections. In the first subsection, the Johnson-Cook model is calibrated using the virtual database without noise. The reference parameter set of Table 1, which represents the minimum of the objective function, is expected to be retrieved in this phase.

In the second subsection, the virtual database is polluted with normally distributed random noise, which includes both the strain fields and the load signals. In this case, the robustness of the present methodology is assessed.

Regarding the material parameters to be calibrated, only the parameters A, B, n, m and C are defined as optimisation variables, whereas the melting temperature T_m, the transition temperature T_{tr} and the parameter $\dot{\varepsilon}_0$ are considered known variables and kept fixed during the optimisation process. These three parameters are kept fixed because the first two have specific physical meaning and the third one may increase the problem of non-uniqueness of the solution [9].

In both subsections, the calibration results are presented for two initial sets of parameters. The two sets are named *Inf_set* and *Sup_set* and correspond to the reference parameters with 50% of their value subtracted or added, respectively.

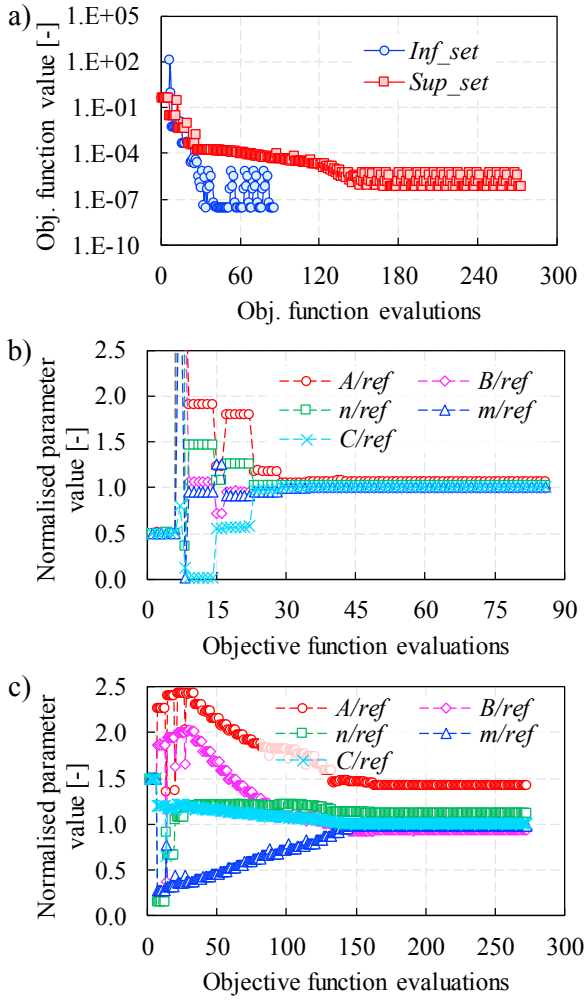

Fig. 6. Results for the identification with a virtual database without noise: a) evolution of the objective function for two different initial sets, b) and c) evolution of the material parameters for the *Inf_set* and *Sup_set* initial sets, respectively.

4.1. Virtual database without noise

The results for the virtual database without noise are presented in Fig. 6. The evolution of the objective function during the optimisation process is presented in Fig. 6. a). The

initial values of the objective function are 0.40 and 0.36 according to the initial set of parameters, *Inf_set* or *Sup_set*, and the final values are 7.45×10^{-9} and 3.97×10^{-7}, respectively. The final values are different which reveals the sensitivity to the initial parameter set. Moreover, none of the solutions is exactly the reference set of parameters, which indicates the presence of local minima or low sensitivity of the parameters in the vicinity of the minimum. Figs. 6 b) and c) show the evolution of the material parameters from the initial set to the final solution. Note that the actual value is normalized by the reference one. In both cases, the parameter *A* is the last one to converge to a stagnation value and retains the highest absolute error value: 5% and 42%, depending on the initial set. Moreover, in both cases, the parameters *m* and *C* reach the reference solution with an error below 1.5%. In both cases, the parameter *n* shows a comparatively stable convergence behaviour, whilst the parameter *B* presents some oscillations for the initial iterations.

According to these results, the identification of parameters *n*, *m* and *C* seems easier when compared to the other parameters, which means that the proposed database contains enough information for these three parameters. Nevertheless, the parameter A appears to be the most difficult to identify. This parameter represents the initial yield stress value, which seems to have a low impact on the objective function value in the vicinity of the minimum. Moreover, the identification process of the parameter *B* reveals also an unstable convergence behaviour, which means low sensitivity of the objective function to this parameter.

The approximate Hessian matrix (Eq. 4) can also be used to extract more information on the objective function's sensitivity to the material parameters. This matrix is symmetrical and represents the second order-partial derivative of the objective function with respect to the material parameters in the following order $\boldsymbol{\chi}=\{A,B,n,m,C\}$. Below, it is presented the Hessian matrix (Eq. 4) computed for the reference set (Table 1).

$$\mathbf{H}\left(\boldsymbol{\chi}^{\text{ref}}\right)=\begin{bmatrix} 8.2\times10^{-7} & 6.0\times10^{-7} & -2.2\times10^{-3} & 3.5\times10^{-4} & 4.7\times10^{-4} \\ \vdots & 4.4\times10^{-7} & -1.5\times10^{-3} & 2.6\times10^{-4} & 3.6\times10^{-4} \\ \vdots & \vdots & 7.1\times10^{0} & -9.4\times10^{-1} & -1.2\times10^{0} \\ \vdots & sym. & \vdots & 1.5\times10^{-1} & 2.2\times10^{-1} \\ \vdots & \vdots & \vdots & \vdots & 9.8\times10^{-1} \end{bmatrix}$$

The diagonal terms of this matrix have differences of several orders of magnitude. The highest values, 7.1×10^{0}, 9.8×10^{-1} and 1.5×10^{-1} correspond to parameters *n*, *C* and *m*, and the lowest values 8.2×10^{-7} and 4.4×10^{-7} correspond to *A* and *B*. This means that the sensitivity of the last two parameters in the vicinity of the reference values is much lower than for the other three parameters. According to this, more difficulties are expected in the identification of *A* and *B*. Moreover, the condition number of the Hessian matrix is 1.97×10^{10}, which means the problem is ill-conditioned and sensitive to small perturbations in the input data.

4.2. Virtual database with noise

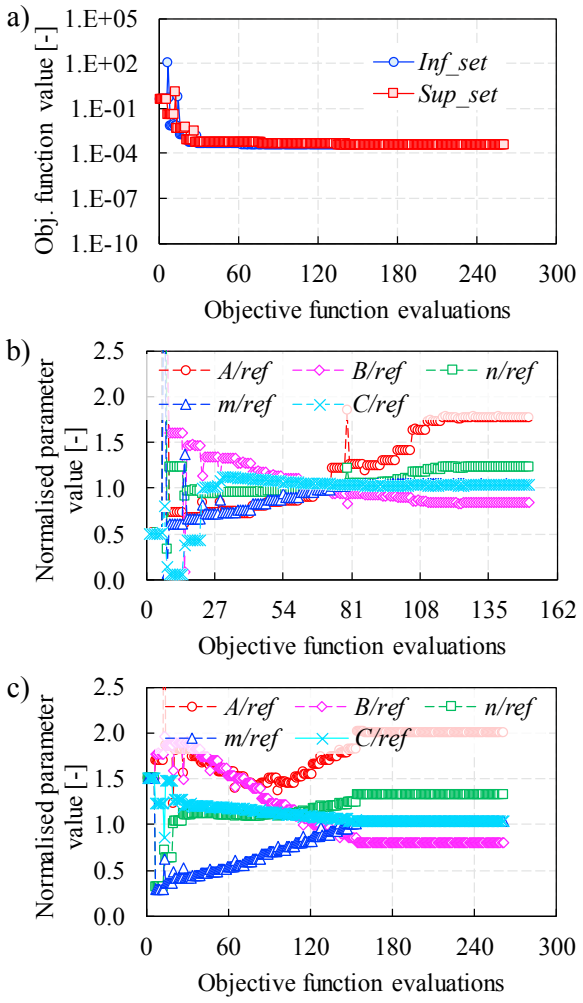

Fig. 7. Results for the identification with a virtual database with noise: a) evolution of the objective function for two different initial sets, b) and c) evolution of the material parameters for the *Inf_set* and *Sup_set* initial sets, respectively.

The results for the virtual database polluted with noise are presented in Fig. 7. The evolution of the objective function value is presented in Fig. 7 a), which at the end of the optimisation process, has approximately the same value, around 3.74×10^{-4}, for both initial sets. Due to the presence of noise, this value is much higher than the values obtained in the previous subsection. Fig. 7 b) and c) show the evolution of the material parameters for the *Inf_set* and *Sup_set*, respectively. Once again, the parameter *A* has the highest error, around 77% and 100% for the *Inf_set* and *Sup_set*, respectively. *C* and *m* have the lowest errors. In addition, although the two solutions have the same final value of the objective function, parameters *A*, *B* and *n* have different final values for the two solutions, which suggests the presence of local minima.

Based on these analyses, one can conclude that the results of this methodology are sensitive to noise, especially because there is no unique solution. The non-uniqueness of the solution is a major obstacle because it raises the question of what would

be the best parameter set to extrapolate the model capabilities. Therefore, a common strategy to overcome this obstacle is to exclude the parameters with the lowest sensitivities from the calibration process. Based on the previous results, the parameter *A* is the obvious candidate and can be assumed as a known variable.

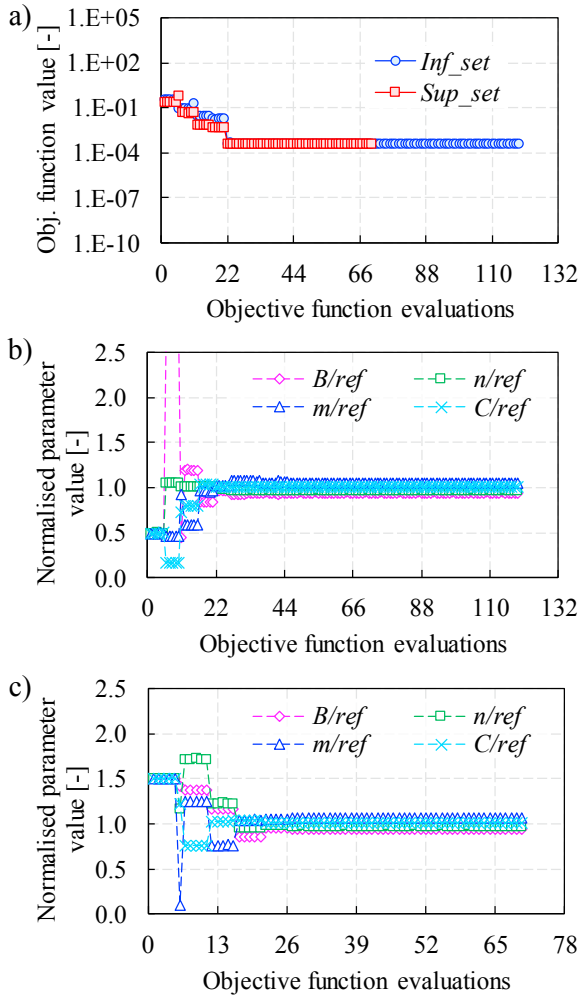

Fig. 8. Results for the identification with a virtual database with noise, assuming a fixed value for parameter *A*: a) evolution of the objective function for two different initial sets, b) and c) evolution of the material parameters for the *Inf_set* and *Sup_set* initial sets, respectively.

In the following analysis, the parameter *A* is fixed to the reference value, 205.21 MPa (see Table 1). Fig. 8 shows the results for this case. In Fig. 8 a), the final value of the objective function for the two solutions is approximately the same: 3.79×10^{-4}. The significant improvement is shown in Fig. 8 b) and c). In both cases, the material parameters converge for similar values, which are very close to the reference ones. The maximum error value is 7% for the parameter *m*. Moreover, the convergence behaviour of the material parameters is substantially more stable and faster for all material parameters.

Excluding parameter *A* of the calibration process solves the non-uniqueness problem and improves the stability of the problem. In addition, the retrieved parameters are closer to the reference set, which means an improvement of the robustness of the methodology.

5. Conclusions

In this work, a methodology to calibrate thermo-elasto-viscoplastic constitutive models based on full-field data combined with a FEMU-based approach is proposed. The goal of this methodology is to reduce the number of tests involved in this type of calibration and make the process more straightforward. Therefore, heterogeneous thermo-mechanical tests performed at different average strain rates on a Gleeble tensile testing equipment are utilised to build the database required for the calibration process.

The analysis of this new methodology based on virtual tests revealed that the simultaneous calibration of all the terms in the Johnson-Cook model is possible. The temperature and strain rate terms are easily calibrated. Nevertheless, low sensitivity to parameter *A* (initial yield stress) has been revealed, which also has led to the non-uniqueness of the final solution. Therefore, the possibility of considering this parameter as a known variable was tested, which indeed solved the obstacle of non-uniqueness of the solution. Moreover, this scenario improves the robustness of the proposed methodology in the presence of noise.

Based on these promising results, the next step is to evaluate the performance of the proposed methodology with real experimental data.

Acknowledgements

The authors acknowledge the financial support of FCT under the projects PTDC/EME-APL/29713/2017 (CENTRO-01-0145-FEDER-029713), PTDC/EME-EME/31243/2017 (POCI-01-0145-FEDER-031243) and PTDC/EME-EME/30592/2017 (POCI-01-0145-FEDER-030592) by UE/FEDER through the programs CENTRO 2020 and COMPETE 2020, and UID/EMS/00481/2013-FCT under CENTRO-01-0145-FEDER-022083. The authors also would like to acknowledge the Région Bretagne (France) for its financial support. J.M.P. Martins is also grateful to the FCT for the PhD grant SFRH/BD/117432/2016.

References

[1] Karbasian H, Tekkaya AE. A review on hot stamping. J Mater Process Tech 2010; 210:2103-18.
[2] Martins JMP, Alves JL, Neto DM, Oliveira MC, Menezes LF. Numerical analysis of different heating systems for warm sheet metal forming. Int J Adv Manuf Tech 2016; 83:897-909.
[3] Sung JH, Kim JH, Wagoner RH. A plastic constitutive equation incorporating strain, strain-rate, and temperature. Int J Plasticity 2010; 26: 1746-71.
[4] Bruschi S, Altan T, Banabic D, Bariani PF, Brosius A, Cao J, Tekkaya A E, et al. Testing and modelling of material behaviour and formability in sheet metal forming. CIRP Annals 2014; 63:727-49.
[5] Markiewicz É, Langrand B, Notta-Cuvier D. A review of characterisation and parameters identification of materials constitutive and damage models: From normalised direct approach to most advanced inverse problem resolution. Int J Impact Eng 2017; 110:371-81.

[6] Avril S, Bonnet M, Bretelle AS, Grédiac M, Hild F, Ienny P, Pierron F, et al. Overview of identification methods of mechanical parameters based on full-field measurements. Exp Mech 2008; 48:381-402.
[7] Martins JMP, Andrade-Campos A, Thuillier S. Comparison of inverse identification strategies for constitutive mechanical models using full-field measurements. Int J Mech Sci 2018; 145:330-45.
[8] Kajberg J, Wikman B. Viscoplastic parameter estimation by high strain-rate experiments and inverse modelling-Speckle measurements and high-speed photography. Int J Solids Struct 2007; 44:145-64.
[9] Notta-Cuvier D, Langrand B, Markiewicz E, Lauro F, Portemont G. Identification of Johnson-Cook's Viscoplastic Model Parameters Using the Virtual Fields Method: Application to Titanium Alloy Ti6Al4V. Strain 2013; 49:22-45.
[10] Valeri G, Koohbor B, Kidane A, Sutton MA. Determining the tensile response of materials at high temperature using DIC and the Virtual Fields Method. Opt and Laser Eng 2017; 91:53-61.
[11] Jones EMC, Carroll JD, Karlson KN, Kramer SLB, Lehoucq RB, Reu PL, Turner DZ. Parameter covariance and non-uniqueness in material model calibration using the Virtual Fields Method. Comp Mater Sci 2018; 152: 268-90.
[12] Martins JMP, Thuillier S, Andrade-Campos A. On the use of non-homogeneous thermo-mechanical fields to characterize DP980 steel sheets. In: 1st Iber Conf Theoret and Exp Mech and Mat11th Nat Cong Exp Mech; 2018. p 203-4.
[13] SIMULIA, Dassault Systèmes, 2017, "Abaqus 2017x documentation".
[14] Erice B, Roth CC, Mohr D. Stress-state and strain-rate dependent ductile fracture of dual and complex phase steel. Mech Mat 2018; 116:11-32.
[15] Nocedal J, Wright S. Numerical Optimization, 2nd ed. Springer-Verlag New York; 2006.

4.2 Calibration of a thermo-mechanical constitutive model using the VFM and a heterogeneous test

In this section, the Virtual Fields Method is applied to the calibration of a thermo-mechanical constitutive model. The heterogeneous thermo-mechanical test performed on a Gleeble machine is analysed. The experimental database is generated for a high strength steel. The temperature and kinematic fields of this test constitute this experimental database.

Calibration of a thermo-mechanical constitutive model using the VFM and a heterogeneous test

J.M.P. Martins[a,b,*], S. Thuillier[b], A. Andrade-Campos[a]

[a] *Centre for Mechanical Technology and Automation, Dep. Mechanical Engineering, University of Aveiro, Portugal*
[b] *Univ. Bretagne Sud, UMR CNRS 6027, IRDL, F-56100 Lorient, France*

Abstract

Phenomenological thermo-elasto-viscoplastic constitutive models are usually applied to predict the thermo-mechanical behaviour of sheet metals. Classical calibration procedures imply a large number of tests to identify all the parameters of this type of models, which usually leads to long experimental campaigns. In the present work, a calibration methodology which aims at reducing the number of tests to calibrate thermo-elasto-viscoplasticity constitutive models is proposed. This methodology relies on full-field measurements from a heterogeneous thermo-mechanical test and the Virtual Fields Method. The heterogeneous test is performed on a Gleeble 3500 machine, for a DP980 steel. The feasibility of this methodology is evaluated for a modified Johnson-Cook (J-C) model. This model has a multiplicative formulation composed of three terms, namely the strain-hardening, temperature, and strain-rate terms. The analysis of the heterogeneous test shows that it provides information on the thermo-mechanical behaviour of the material for a range of temperatures in between 360 to 500 °C. The strain and strain-rate field have a similar shape, with the highest values localised at the centre of the specimen. The calibration of the complete model with a single test revealed that it is possible to have a reasonable description of the flow stress for the conditions of the test, but the strain-rate term of J-C is not activated. However, when the database is composed of three tests at different displacements rates, the three terms of the model are activated.

Keywords: Calibration, Virtual Fields Method, Heterogenous Thermo-Mechanical Test, Full-Field Measurements, Thermo-Elasto-Viscoplasticity

1. Introduction

Temperature and strain-rate have a significant influence on the flow stress of sheet metals. A precise description of their role is essential for numerical simulation of manufacturing processes, e.g. in the simulation of hot and warm forming processes [1, 2]. Furthermore, in standard manufacturing processes, new generations of high strength steels reach high temperatures due to the heat generated by plastic deformation, which turns the effects of temperature and strain-rate imperative to be known [3, 4].

Phenomenological thermo-elasto-viscoplastic constitutive models are usually applied to predict the thermo-mechanical behaviour of metals. Different formulations can be assumed depending many aspects, such as material behaviour, the range of strain, strain-rate and temperature, the computational cost, etc. A comprehensive review of these models can be found at [4]. Typically, phenomenological thermo-elasto-viscoplastic models are strongly non-linear and contain many material parameters that need to be calibrated. Classical calibration procedures at low to medium strain-rates usually rely on tensile tests performed at different strain-rates and temperatures [5, 6]. Other less used tests are strain-rate jump tests [4, 7] or torsion tests [8].

*Corresponding author
Email addresses: joao.martins52@ua.pt (J.M.P. Martins), sandrine.thuillier@univ-ubs.fr (S. Thuillier), gilac@ua.pt (A. Andrade-Campos)

November 9, 2020

In classical procedures, the data collected from tensile tests are analysed under the assumption of homogeneous strain in the gage length, leading to a single stress-strain curve output from each test, corresponding to a given temperature and strain-rate. To cover a certain number of temperatures and strain-rates, at least an equal number of tests is required, which leads to long experimental campaigns.

Therefore, there has been a remarkable effort to reduce the number of tests by replacing classic procedures with a combination of full-field measurement techniques, heterogeneous tests and inverse methods. Full-field measurement techniques, such as Digital Image Correlation (DIC), allow to record complete displacement/strain maps at the surface of a specimen during a test, which combined with heterogeneous tests, can provide a set of spatial points under different strain states, strain levels and strain rates. This information can also be enriched with temperature measurements from the same test, obtained with a thermographic camera, for example. Thus, the experimental database that used to be obtained through long experimental campaigns can now be collected from a few heterogeneous tests. Nevertheless, the complexity of the loading conditions and the heterogeneity implies a new way of analysing this data. The calibration of a constitutive model using data from a heterogeneous test requires inverse methods [9, 10]. Currently, the Finite Element Model Updating (FEMU) and the Virtual Fields Method (VFM) are the most used inverse methods. In FEMU, a finite element (FE) model of the heterogeneous test configuration is built up, and through an iterative procedure that consists in minimizing the difference between experimental and numerical fields, the selected constitutive model is calibrated. Although this method is quite popular, it has a major drawback. The large number of FE analyses required leads to a high computational cost. Alternatively, the VFM provides a more efficient solution in terms of computational cost [11, 12, 13]. This inverse method, derived from the principle of virtual works, drives the calibration process through the balance between internal and external work, quantities computed from the measured displacements field and measured load [11]. Since the pioneering work of Grédiac [14] to characterize material properties of composites materials, the VFM has been explored and consequently adapted to calibrate different types of constitutive models. Nowadays, it is an appealing solution for calibrating non-linear constitutive models, such as plasticity [15, 16, 17] and viscoplasticy [18, 19, 20] constitutive models. In the framework of low strain-rate values, the work of Gramma et al. [18] aims at the simultaneous calibration of all the parameters of the Anand model with a single test. The authors analyse the sensitivity of the procedure to different loading ratios and rates in order to design a test with the necessary information. Jones et al. [19] investigated the calibration of the Bammann-Chiesa-Johnson viscoplastic model using a heterogeneous test with a specimen geometry similar to a capital letter "D". The simultaneous calibration of the full set of parameters raise the problem of non-uniqueness of the solution. Nevertheless, the authors have reached valid solutions, which were considered functionally equivalent for the loading conditions present in the test. Enrichment of the database with more tests was the solution pointed out by the authors to mitigate the non-uniqueness problem. Valeri et al. [20] proposed a methodology based on the VFM to calibrate the thermo-viscoplastic Johnson-Cook model. In the proposed methodology, the strain-hardening term is calibrated following a classical procedure and then only the temperature and strain-rate terms are calibrated using the VFM. The temperature, the averaged strain and strain-rate obtained from uniaxial tests performed at uniform temperatures composed the experimental database. The authors reached accurate descriptions of the flow stress from room temperature up to 900 °C.

In the present work, it is intended to step forward in the calibration of thermo-mechanical constitutive models. Therefore, the VFM is combined with a heterogeneous thermo-mechanical test. The heterogeneous thermo-mechanical test is performed on a Gleeble thermo-mechanical simulator. At this early stage, the objective lies more on the proof of concept regarding the combination of the VFM and this test and less on reaching bulletproof identifications. As will be shown, more experimental data and a more complex constitutive model would be required. Section 2 presents the heterogeneous thermo-mechanical test. The test was performed for three different average strain-rates, which are analysed in terms of strain, strain-rate and temperature fields. The selected constitutive model is presented in section 3. The VFM and the selected virtual fields, along with the calibration procedure are presented in Section 4. In Section 5, the combination of VFM and the three tests is analysed. This last section is divided into two parts. In the first part, the model is calibrated using a single test and in the second part, the model is calibrated using the three tests. In section 6, concluding remarks close the article.

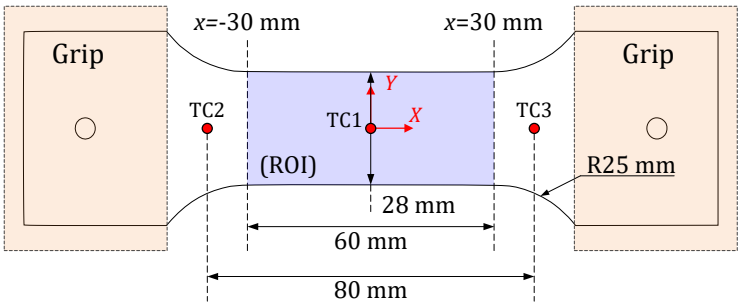

Figure 1: Geometry of the tensile specimen, region of interest (ROI) and position of the thermocouples.

2. Heterogeneous thermo-mechanical test

To accurately calibrate a thermo-viscoplasticity model for a given material, information on the mechanical behaviour of the material for different temperatures and strain-rates is required. This would imply a laborious experimental campaign if classical methods were used. Fortunately, the combination of full-field measurements and heterogeneous tests offers a more efficient alternative. In this case, the heterogeneous test must include an overlap of heterogeneous temperature and strain fields. With this idea in mind, a heterogeneous thermo-mechanical test performed on Gleeble 3500 thermo-mechanical simulator is explored in this work. It is expected that this test can provide information on the mechanical behaviour of the material for a considerable range of temperatures and strain-rates.

2.1. Gleeble machine

The Gleeble 3500 thermo-mechanical simulator combines a hydraulic servo system able to impose tension or compression forces and a direct resistance heating system. The direct resistance heating system is controlled using a thermocouple signal that provides accurate temperature control in a region of the specimen. Usually, the temperature is imposed at the centre of the specimen and held constant during the mechanical test, whereas a temperature gradient is developed from the centre to the extremities of the specimen due to the water-cooled jaws carriers [21]. This gradient, frequently deemed as adverse, is an asset for the present work. It triggers a heterogeneous deformation process that generates information on the mechanical behaviour of the material for different temperatures and strain rates.

2.2. Material and specimen geometry

A Dual-phase steel DP980 was considered for this study [22]. Tensile specimens from a rolled sheet with thickness 1.75 mm were used, the geometry of the specimen is depicted in Fig. 1. The longitudinal direction (x-direction in Fig. 1) of the specimens was aligned with the rolling direction of the sheet.

2.3. Experimental procedure and data acquisition

The specimens were loaded under constant displacement rate. Three displacement rates evenly distributed in the logarithmic scale were selected to conduct the tensile test: 0.006, 0.06 and 0.6 $\mathrm{mm\,s^{-1}}$. According to the length of the region with constant cross-section, these displacement rates correspond respectively to nominal strain-rates of $1.0 \cdot 10^{-4}$, $1.0 \cdot 10^{-3}$ and $1.0 \cdot 10^{-2}$ $\mathrm{s^{-1}}$. For the thermal field, 500 °C was the chosen temperature to impose at the centre of the specimens. Note that the displacement is imposed

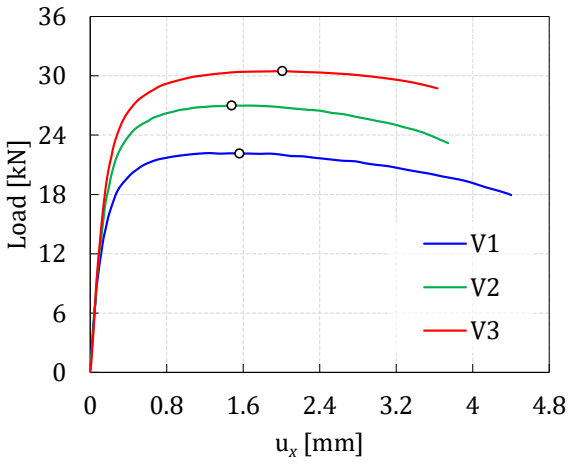

Figure 2: Load *vs* displacement (u_x) curves for the three displacement rates: 0.006, 0.06 and 0.6 mm s^{-1}, which correspond to V1, V2 and V3, respectively.

after a heating phase which ensures that the reference value of 500 °C has been reached in the specimen centre. The local kinematic measurements were acquired through a DIC system GOM-Aramis. Regarding the temperature field, monitored through three thermocouples (TC1, TC2 and TC3), which were welded in the specimens as depicted in Fig. 1, were used to monitor the temperature, as well as a FLIR thermal camera X6580SC. This last equipment gives the spatial distribution of the temperature through the complete surface of the specimens. To help the post-treatment of temperature field, the thermocouples (see Fig. 1) were used as references for the coordinate system as well as to determine the emissivity of the surface of the specimens.

2.4. Experimental results

Fig. 2 presents the load *vs* displacement curves up to rupture for the three displacement rates. These tests are named V1, V2 and V3, which correspond to 0.006, 0.06 and 0.6 mm s^{-1}, respectively. The material shows a significant sensitivity to strain-rate. The maximum load value indicated by the black circles corresponds to 22.3, 27.0 and 30.5 kN, for the tests V1, V2 and V3, respectively. The displacement (u_x) was calculated as the difference of the average displacement value at the boundaries x= −30 mm and x= 30 mm of the region of interest (ROI) (see Fig. 1). The displacement values at maximum load are 1.56, 1.48 and 2.0 mm. Note that, although only a single curve is presented for each displacement rate, the tests were repeated three times and reproducibility was observed.

The temperature measurements for the three thermocouples (TC1, TC2 and TC3) for each test are shown in Fig. 3. Throughout the duration of each test, the temperature remains nearly the same. This is a result of Gleeble's very precise control system, which preserves the temperature at the TC1 thermocouple, and due to the thermal conductivity of the material, the other two thermocouples maintain approximately the same temperature. The spatial distribution of the temperature varies mainly along the longitudinal direction of the specimen (x-direction), while the high conductivity of the steel leads to meaningless differences along the transversal direction (y-direction), less than 2 %. Therefore, these differences will be neglected in the analysis of the tests, as well as in the calibration procedure.

Fig. 4 shows the spatial distribution of temperature for the beginning of each test for a line passing through mid-plane of the specimens ($y = 0$ mm), as shown in Fig. 5. The red squares represent the thermocouples measurements, and the colour dots represent the thermal camera measurements. For the positions of the thermocouples, the measurements of the thermal camera show abrupt temperature drops. This is caused by the different emissivity of the thermocouples when compared with the surface of the specimens. For

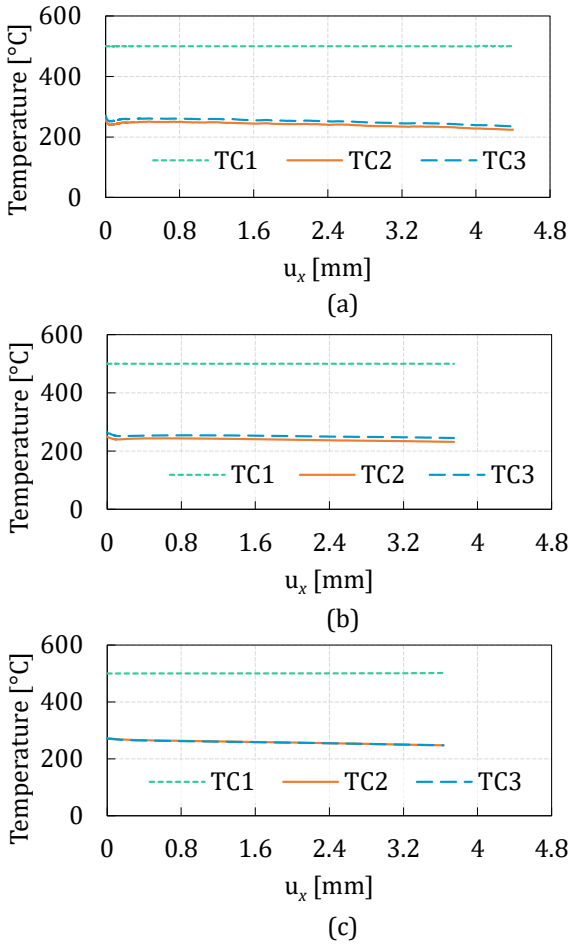

Figure 3: Temperature measurements acquired by the three thermocouples TC1, TC2 and TC3, for the tests: a) V1, b) V2 and c) V3.

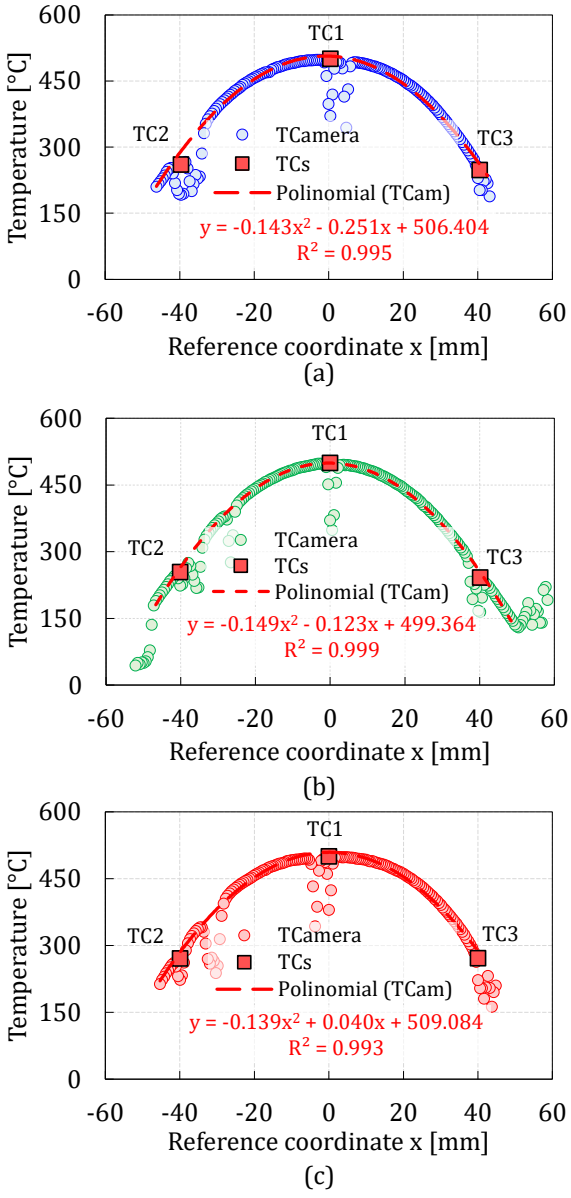

Figure 4: Spatial temperature distribution along a line passing through the mid-plane of the specimen($y = 0$ mm) (see Fig. 5) for each test: a) V1, b) V2 and c) V3.

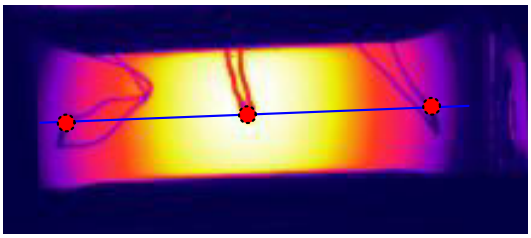

Figure 5: Temperature field for the test V2 captured by the thermal camera. The highest temperatures are represented in yellow and the lowest by the violet. The line passing through the mid-plane of the specimen ($y = 0$ mm) is represented in blue and the thermocouples position by the red circles.

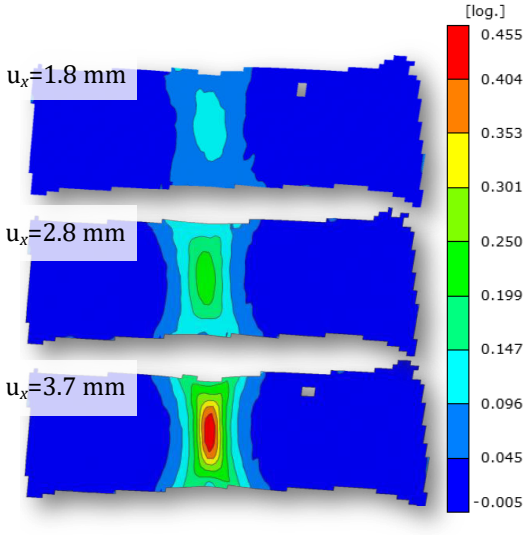

Figure 6: Major strain distribution for the test V2.

the three cases, the temperature field reaches its maximum value at the centre of the specimens. From the centre to the boundaries of the specimens, it is observed the decrease of temperature that leads to values around 360 °C for the boundaries of the ROI ($x = -30$ and $x = 30$ mm). This temperature distribution can be described by a 2$^{\text{nd}}$ order polynomial, as can be seen in Fig. 4. The squared values of the correlation coefficient (R^2) are around 1, which shows a very good agreement of the 2$^{\text{nd}}$ order polynomial.

During the tensile tests, the temperature gradient undergone by each specimen triggers a heterogeneous deformation process. The evolution of this process ends with strain localization at the centre of the specimen, which can be observed for the test V2 in Fig. 6. These three steps presented in this figure are beyond the maximum load value for the test V2, and it can be observed that the strain is localized in a small region [23, 24]. Using such an extension of data can lead to inaccuracies in the computation of the stress field since the strain field computation can be degraded. Additionally, the plane stress condition, which is required for the stress computation in VFM, can cause deviations in the computation. Therefore, for the VFM calibration, it is only considered the data up to the maximum load value, which is analysed in the following.

The evolution of the major strain along the mid-plane $y = 0$ mm is presented in Fig. 7 a1, b1 and c1 in the ROI, up to the maximum load. The spatial distribution shows a maximum strain value at the centre of the specimen and a decreasing trend from the centre to the ends of the ROI. The maximum values of major strains are 0.093, 0.086 and 0.109 for the tests V1, V2 and V3, respectively. Moreover, it seems that after a displacement of 0.8 mm the evolution of the strains field occurs only between $x = -15$ and $x = 15$ mm, which reduces the information for the thermo-viscoplastic regime in terms of strain and temperature. In terms of temperature, the range is between 460 to 500 °C. Moreover, in Fig. 7 a2, b2 and c2, it is shown the major *vs* minor strain distribution for the three tests at the instant of maximum load value, the strain state is mainly a uniaxial tensile state.

The strain-rate field can be considered as another source of information for the calibration of a constitutive model that takes into account the strain-rate effect. Fig. 8 shows the evolution of the strain-rate field ($\dot{\varepsilon}_{xx}$) up to the maximum load value for the same mid-plane. It was computed from the logarithmic strain in the x-direction through forward finite-differences. The maximum values of strain-rate are $4.13 \cdot 10^{-4}$, $3.69 \cdot 10^{-3}$ and $4.16 \cdot 10^{-2}$ s^{-1}. These are in the same order of magnitude as the nominal strain-rate of each test. The heterogeneity of the tests provides a wide dispersion of points, with a spatial distribution similar to the strain field.

A stress evaluation for the central region of the specimen is presented in Fig. 9. It was assumed a uniaxial

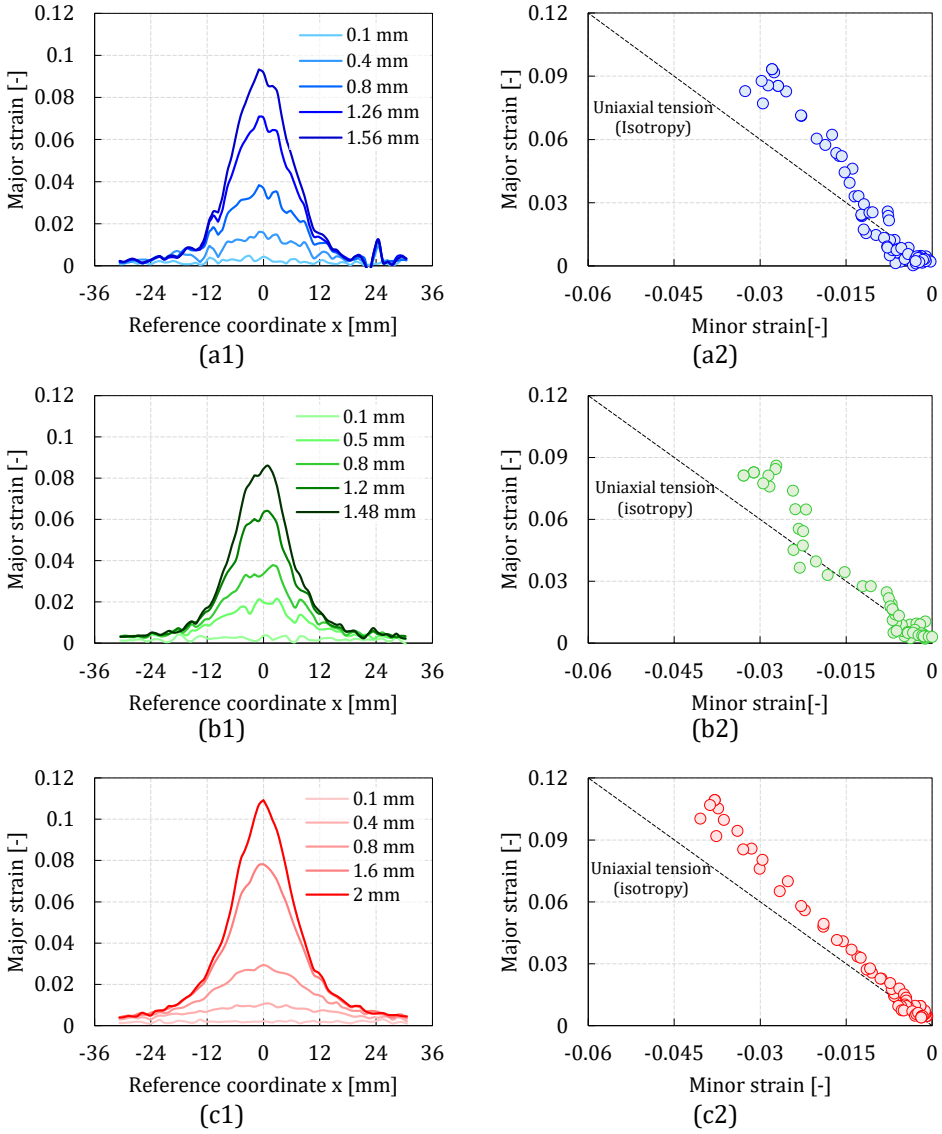

Figure 7: Major strain distribution and major strain *vs* minor strain along the mid-plane y =0 mm for the ROI, for the tests a) V1, b) V2 and c) V3.

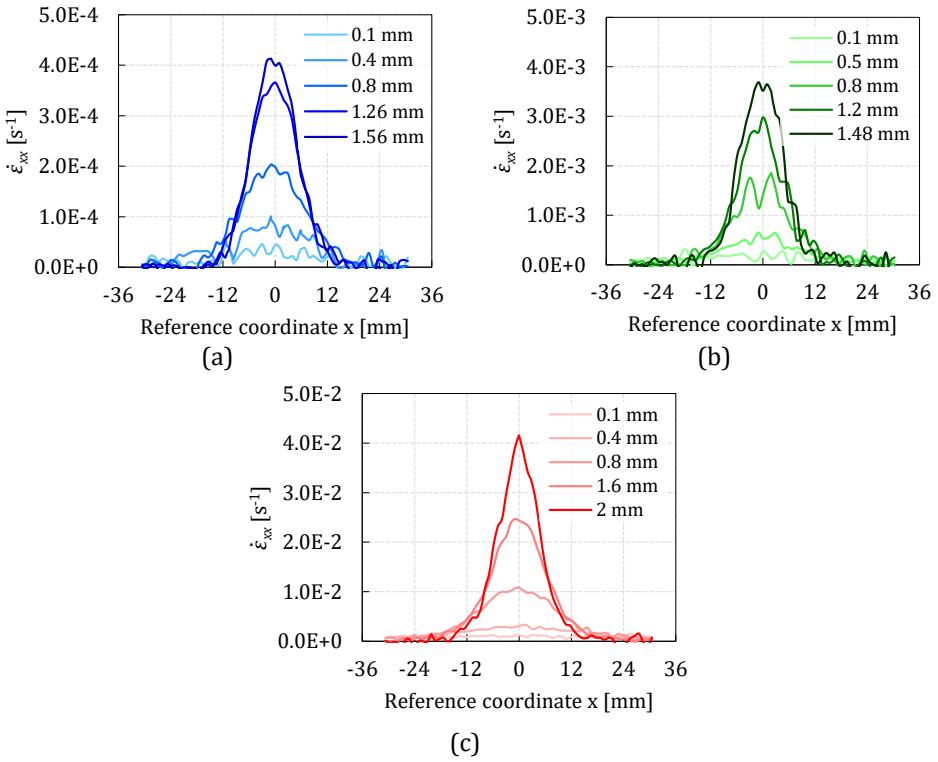

Figure 8: Strain-rate ($\dot{\varepsilon}_{xx}$) distribution along the mid-plane y =0 mm in the ROI and, for the tests a) V1, b) V2 and c) V3.

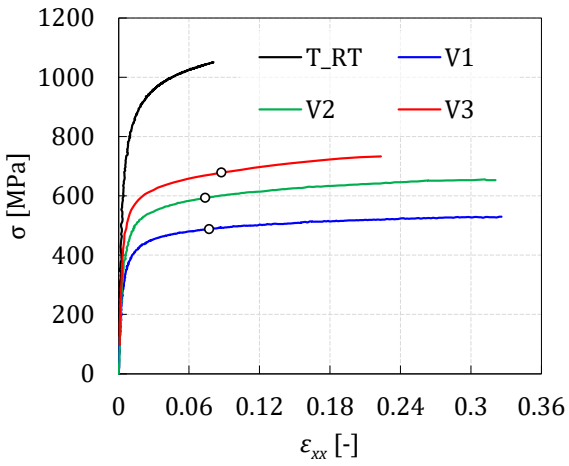

Figure 9: Stress *vs* strain curves computed for a central section of the specimens. The colour lines correspond to 500 °C. The black curve (T_RT) corresponds to room temperature obtained from a homogeneous tensile test [22].

stress state with homogeneous deformation for the central section of the specimens in between $x = -2$ and $x = 2$ mm. Based on that, the stress Cauchy (σ) was computed from the measured load and considering the actual cross-sectional area of the specimen. The actual cross-sectional area was computed assuming volume conservation. ε_{xx} is the average logarithmic strain tensor component for that central region. It can be assumed that these curves correspond to the temperature of 500 °C. It is also plotted in the same figure the stress curve for the same material at room temperature for a strain-rate of $1.0 \cdot 10^{-3}$ s^{-1}. The room temperature curve was obtained from a homogeneous tensile test in the same material [22]. From the beginning of the deformation process, the three curves at 500 °C show a positive sensitivity to strain-rate, which is also observed in the load curves, Fig. 2. The negative sensitivity to temperature is also clear when these curves are compared with the one at room temperature.

In conclusion, the three tests conducted for a DP980 compose the database to be used with VFM. It is observed that the three tests provide a collection of points with different temperatures ranging from 360 °C to approximately 500 °C for the ROI. The strain and strain-rate fields present different magnitudes with localization of the highest values at the centre of the specimen. The material behaviour has a positive sensitivity to strain-rate and a negative sensitivity to temperature.

It must be mentioned that the effect of temperature on the kinematic measurements is not explored in this work, but its impact can be important and should be analysed in the future.

3. Constitutive model

The purpose of this work is to evaluate the combination of an experimental database composed by heterogenous thermo-mechanical tests and the VFM to fully calibrate a thermo-elasto-viscoplastic constitutive model. For this purpose, a modified version of the phenomenological Johnson-Cook (J-C) model is selected. The original version of J-C model [8] is widely adopted to represent the response of metals under a wide range of temperatures and strain-rates. However, the original formulation of the J-C model lacks flexibility and several modifications have been proposed [25]. Instead of the original power term to describe the strain-hardening behaviour, many authors have proposed a combined Swift-Voce term [4, 3]. Therefore, the modified version of the J-C model selected for this work assumes the following form

$$\sigma_y = H\left(\bar{\varepsilon}^{\mathrm{p}}\right) \cdot G\left(T\right) \cdot F\left(\dot{\bar{\varepsilon}}^{\mathrm{p}}\right), \tag{1}$$

where,

$$H\left(\bar{\varepsilon}^{\mathrm{p}}\right) = \alpha \cdot \left[K \cdot \left(\varepsilon_0 + \bar{\varepsilon}^{\mathrm{p}}\right)^n\right] + \left(1-\alpha\right) \cdot \left[\sigma_0 + \left(\sigma_{\mathrm{sat}} - \sigma_0\right) \cdot \left(1 - \exp\left(-C_y \cdot \bar{\varepsilon}^{\mathrm{p}}\right)\right)\right], \tag{2}$$

$$G\left(T\right) = \left[1 - \left(\frac{T - T_{\mathrm{tr}}}{T_{\mathrm{m}} - T_{\mathrm{tr}}}\right)^m\right], \tag{3}$$

and

$$F\left(\dot{\bar{\varepsilon}}^{\mathrm{p}}\right) = \left[1 + C \ln\left(\frac{\dot{\bar{\varepsilon}}^{\mathrm{p}}}{\dot{\varepsilon}_0}\right)\right]. \tag{4}$$

According to this modified version of the J-C model, the flow stress (σ_y) is composed by three functions, $H\left(\bar{\varepsilon}^{\mathrm{p}}\right)$, $G\left(T\right)$ and $F\left(\dot{\bar{\varepsilon}}^{\mathrm{p}}\right)$, which represent the strain-hardening, temperature and strain-rate effects. These three terms are governed by the internal variables: equivalent plastic strain $\bar{\varepsilon}^{\mathrm{p}}$, temperature T and equivalent plastic strain-rate $\dot{\bar{\varepsilon}}^{\mathrm{p}}$. The strain-hardening term contains seven material parameters, α, K, ε_0, n, σ_0, σ_{sat} and C_y. Nevertheless, ε_0 is assumed as a function of σ_0, the initial yield stress, and can be computed from $\varepsilon_0 = \left(\sigma_0/K\right)^{1/n}$. The term $G\left(T\right)$ contains three parameters T_{tr}, T_{m} and m, and it is only active when the actual temperature T is above the transition temperature T_{tr}. The term $F\left(\dot{\bar{\varepsilon}}^{\mathrm{p}}\right)$ contains two parameters C and $\dot{\varepsilon}_0$. To have this term active, $\dot{\bar{\varepsilon}}^{\mathrm{p}}$ must be above $\dot{\varepsilon}_0$.

A common approach to calibrate the J-C model is to divide the process into three steps, each corresponding to the individual calibration of one term. In this work, the simultaneous calibration of the three terms is analysed. Nevertheless, some parameters are assumed to be known a priori. T_{tr} is fixed to 25 and T_{m} to 1000 °C which is common value for DP980 [3]. Moreover, the assumed value for T_{tr} was selected with the

intent of reaching a model calibration for a large range of temperatures. The parameter $\dot{\varepsilon}_0$ is also fixed to the value of $1.0 \cdot 10^{-5}$ s^{-1}. Such a low value was defined because the positive effect of strain-rate occurs very early in the deformation process of DP980, which implies the activation of the strain-rate term for low values of the equivalent plastic strain-rate. Moreover, it also mitigates the problem of multiple solutions [26]. The value of α is defined to be equal to 0.5. Note that setting α as a parameter to be identified is useless because K also weights the hardening terms.
Moreover, the models is developed within the framework of associated flow rule, the von Mises yield criterion and isotropic linear elasticity described by the generalized Hooke's law. The identification of the elastic parameters is not part of this work, thus based on the literature the value of 0.3 is assumed for the Poisson's ratio [22]. Concerning Young's modulus, a dependence on the temperature was observed. An average value of 106 GPa is determined at 500 °C using the curves presented in Fig. 9 and for room temperature the value determined is 185 GPa. Since no other values were available in this range of temperatures, it was defined a bilinear-piecewise equation for the Young's modulus. The objective was to have a better fit of the beginning of the load curves of the heterogeneous tests.

4. Virtual fields method

The idea behind the VFM is to use the principle of virtual work (PVW) and combine it with full field kinematic measurements and the load acquired during a mechanical test, to calibrate a constitutive model. This is performed through the enforcement of the equilibrium condition between the external and internal virtual work. In the framework of finite strain theory, assuming body forces as null and quasi-static conditions, the PVW can be written in the reference configuration as follows

$$\underbrace{\int_{\Omega_0} \mathbf{P} : \mathbf{grad}\ \mathbf{U}^* \mathrm{d}V}_{W_{\mathrm{int}}} - \underbrace{\int_{\Gamma_0^f} \overline{\mathbf{T}} \cdot \mathbf{U}^* \mathrm{d}S}_{W_{\mathrm{ext}}} = 0, \tag{5}$$

where $\mathbf{P}$ is the first Piola-Kirchhoff stress tensor, $\mathbf{U}^*$ is the virtual displacement vector expressed in the reference configuration ($\mathbf{U}^* = \mathbf{U}^*(\mathbf{X})$), as well as $\mathbf{grad}\ \mathbf{U}^*$. $\overline{\mathbf{T}}$ is the first Piola-Kirchhoff stress vector prescribed on the boundary Γ_0^f with the reference surface area S. Similarly, the first integral of Eq. 5 is written over the reference volume V. The virtual displacement field ($\mathbf{U}^*$) must be kinematically admissible, continuous and differentiable [11, 27].
The first Piola-Kirchhoff stress tensor $\mathbf{P}$ is obtained through the Piola transformation as

$$\mathbf{P} = \det(\mathbf{F})\boldsymbol{\sigma}\mathbf{F}^{-\mathrm{T}}, \tag{6}$$

where $\det(\mathbf{F})$ is the determinant of the deformation gradient $\mathbf{F}$ and $\mathbf{F}^{-\mathrm{T}}$ is the transpose of its inverse. The Cauchy stress tensor $\boldsymbol{\sigma}$ is computed from the strain tensor $\boldsymbol{\varepsilon}$, which is determined through the kinematic full-field measurements, and by means of previously selected constitutive model with an initial set of material parameters $\boldsymbol{\xi}$. In the present case, the assumed thermo-viscoplastic constitutive model (Eq. 1) takes into account temperature and strain-rate effects, which brings to the problem two more variables, time t and temperature T. Therefore,

$$\boldsymbol{\sigma} = \boldsymbol{\sigma}(\boldsymbol{\varepsilon}, \boldsymbol{\xi}, t, T). \tag{7}$$

The strain fields are computed from the measured displacement fields $\mathbf{u}$ by means of the deformation gradient $\mathbf{F}$. Using the theorem of polar decomposition, the deformation gradient can be decomposed as

$$\mathbf{F} = \mathbf{VR}, \tag{8}$$

where $\mathbf{V}$ is the left Cauchy stretch tensor and $\mathbf{R}$ is the orthogonal rotation tensor. The strain field can be computed for each time instant as the Hencky strain tensor

$$\boldsymbol{\varepsilon} = \ln\mathbf{V}. \tag{9}$$

Moreover, the computation of the Cauchy stress tensor is conventionally expressed in a local material frame free of rigid body rotations, thus the strain tensor in this local co-rotational frame can be computed as

$$\hat{\boldsymbol{\varepsilon}} = \mathbf{R}^{\mathrm{T}} \boldsymbol{\varepsilon} \mathbf{R}. \tag{10}$$

Full-field measurements are usually obtained as a discrete number of material points in a ROI belonging to the surface of the specimen. The computation of kinematic quantities can then be carried out using, for example, shape functions for discrete points in the ROI. The stress tensor and the virtual fields are also computed for the same locations and become representative of the average quantities for small regions. Moreover, as the through thickness information is not usually available, a plane stress state is assumed. The thickness estimation, which is required for the Piola transformation, is computed through the Poisson's ratio and the assumption of incompressible plasticity. For further details on these assumptions, the reader is referred to [28, 29].
Based on this discrete form of the data, the integral of the internal virtual work (Eq. 5) is approximated by a discrete sum as follows

$$W_{\mathrm{int}}\left(\boldsymbol{\xi}\right) = \sum_{i=1}^{n_{\mathrm{e}}} \mathbf{P}\left(\boldsymbol{\varepsilon}_i, \boldsymbol{\xi}, t, T_i\right) : \mathbf{grad}\ \mathbf{U}_i^* A_i e_i, \tag{11}$$

where n_{e} represents the number of points and A_i and e_i are the representative area and the thickness of these points. Note that adopting the reference configuration brings the advantage that the area A_i and thickness e_i do not need to be updated as the deformation process evolves. The same happens with the computation of the virtual fields that is only performed for the reference configuration.
The external virtual work is computed from the load acquired during the mechanical test. This computation can be simplified through the proper choice of the virtual fields. The selected virtual fields must be constant on the boundary Γ_0^f, which simplifies the computation of the second integral in Eq. 5 as follows

$$W_{\mathrm{ext}} = \mathbf{U}^* \cdot \int_{\Gamma_0^f} \overline{\mathbf{T}} \mathrm{d}S = \mathbf{U}^* \cdot \mathbf{F}^{\mathrm{load}}, \tag{12}$$

where $\mathbf{F}^{\mathrm{load}}$ is the resultant of the force acting on the boundary. This simplification is a major asset of VFM because it is not required the distribution of the force vector on the boundary.

4.1. Objective function

The PVW can be written for different time steps and also for different virtual fields in order to enrich the objective function. Relevant information from the history of the mechanical test and from different points in the spatial domain of the ROI can thus be explored. Hence, the objective function for the VFM can be written in a least-square framework as

$$\varphi\left(\boldsymbol{\xi}\right) = \sum_{k=1}^{n_{\mathrm{vf}}} \frac{1}{n_{\mathrm{vf}}} \left\{ \sum_{j=1}^{n_{\mathrm{t}}} \frac{1}{n_{\mathrm{t}}} \left[\sum_{i=1}^{n_{\mathrm{e}}} \mathbf{P}\left(\boldsymbol{\varepsilon}_{ij}, \boldsymbol{\xi}, t_j, T_{ij}\right) : \mathbf{grad}\ \mathbf{U}_{ik}^* A_i e_{ij} - \mathbf{U}_k^* \cdot \mathbf{F}_j^{\mathrm{load}} \right] \right\}^2, \tag{13}$$

where n_{vf} is the number of virtual fields selected and n_{t} the number of time steps considered. The calibration of the constitutive model is performed through the minimisation of the cost function given by Eq. 13. The material parameters $\boldsymbol{\xi}$ are found when the stress fields minimise the difference between W_{int} and W_{ext} for all time steps and virtual fields. Moreover, several tests be used, and in that case, the objective function is the sum of Eq. 13 computed for the different tests.

4.2. Virtual fields selection and identification procedure

One of the key elements of VFM is the selection of a set of virtual fields. The virtual fields must be kinematically admissible and can be any continuous and differentiable function. However, for practical reasons these should be constant on the boundaries where forces are applied. For the calibration of nonlinear constitutive models, there are three approaches to select a suitable set of virtual fields. Two of these approaches are automatic strategies and require a low level of user intervention [30, 28]. The other approach, called manual defined virtual fields, depends exclusively on user intervention, since it is the user who must develop the appropriate set according to the boundary conditions of the test. Compared to the other strategies, manually defined virtual fields strategy has the main advantages of low computational cost and ease of implementation. For these reasons, this is the strategy adopted in the present work.

Recently, it was confirmed that the number of virtual fields plays an important role in the accuracy of the VFM [31, 17]. Increase the number of virtual fields in Eq. 13 is just a way of improving the objective function with more information on the stress fields that are computed from a set of parameters. A total of 9 virtual fields are selected for this work. Note that $n_{\text{vf}} > \dim(\boldsymbol{\xi})$. The selected set is defined as the following

$$
\begin{aligned}
\mathbf{U}_1^* &= \begin{cases} U_X^* = \frac{X}{L} \\ U_Y^* = 0 \end{cases} & \mathbf{U}_2^* &= \begin{cases} U_X^* = 0 \\ U_Y^* = \cos\frac{\pi X}{2L} \end{cases} \\
\mathbf{U}_3^* &= \begin{cases} U_X^* = 0 \\ U_Y^* = \frac{Y}{W}\cos\frac{\pi X}{2L} \end{cases} & \mathbf{U}_4^* &= \begin{cases} U_X^* = \sin\frac{\pi X}{L}\sin\frac{\pi Y}{L} \\ U_Y^* = \sin\frac{\pi X}{L}\sin\frac{\pi Y}{L} \end{cases} \\
\mathbf{U}_5^* &= \begin{cases} U_X^* = 0 \\ U_Y^* = \sin\frac{\pi X}{L}\sin\frac{\pi Y}{L} \end{cases} & \mathbf{U}_6^* &= \begin{cases} U_X^* = 0 \\ U_Y^* = \frac{Y(|X|-L)}{WL} \end{cases} \\
\mathbf{U}_7^* &= \begin{cases} U_X^* = \frac{Y\left(X^2-L^2\right)}{L^2W} \\ U_Y^* = 0 \end{cases} & \mathbf{U}_8^* &= \begin{cases} U_X^* = 0 \\ U_Y^* = \frac{Y^2}{W^2}\sin\frac{\pi X}{L} \end{cases} \\
\mathbf{U}_9^* &= \begin{cases} U_X^* = \left[\exp\left(\frac{H^2-X^2}{H^2}\right)-1\right]\sin\frac{\pi X}{L} \\ U_Y^* = 0 \end{cases} .
\end{aligned}
\tag{14}
$$

The constants L and W represent half the length and width of the ROI, respectively. X and Y are the coordinates in the reference frame. Note that the reference frame is located in the specimen centre as shown in Fig. 1.

In the case of static equilibrium, the first virtual field is the only one that gives a non-zero value in the internal virtual work. The component $\partial U_X^*/\partial X$ of the gradient for this virtual field is the only one with non-zero value and constant distribution in ROI ($\partial U_X^*/\partial X = 1/L$). In this case, the internal virtual work is balanced with the external virtual work computed from the measured load. The other virtual fields have non-constant spatial distributions and distribute the weight between normal and shear components.

Another key element of the VFM is the reconstruction of the stress field. In case of non-linear constitutive models, such as the case of the model under study, it is required a stress integration algorithm. There are several options for the integration algorithm. The classical one is based on a backward-Euler scheme combined with a predictor/corrector method to update the stress state. Examples of this kind of algorithms can be found in [32, 33].

An in-house code for VFM was developed using Fortran programming language. A gradient-based Levenberg-Marquardt optimisation method [34] is used to solve the optimisation process. The required Jacobian matrix for the Levenberg-Marquardt method is calculated by forward finite differences. The convergence criteria for this method were established as: the objective function becomes lower than a tolerance or the relative difference between parameters in consecutive iterations is lower than or equal to $1.0 \cdot 10^{-10}$.

Regarding the treatment of the experimental data, the raw full-field displacements data obtained by DIC, using the ARAMIS system, are post-treated into Matlab. The displacement fields corresponding to each time step are interpolated onto a rectangular grid covering the entire area of the ROI. The grid is divided into regular elements with an area of 1 mm^2, which makes a total of 1769 data points for the spatial domain

	σ_0 [MPa]	K [MPa]	n [-]	σ_{sat} [MPa]	C_{y} [-]	m [-]	C [-]	φ_{ini} [-]·10^6	φ_{fin} [-]·10^6	Iter. [-]
Initial	*600*	*900*	*0.060*	*1200*	*20*	*1.00*	*0.0*	-	-	-
V1	641	1044	0.033	1147	34	0.99	$4.0{\cdot}10^{-8}$	1.2	0.4	28
V2	697	1388	0.054	1060	53	1.10	$1.3{\cdot}10^{-7}$	5.3	0.5	11
V3	616	1637	0.068	997	69	1.17	$2.6{\cdot}10^{-8}$	9.8	1.0	13

Table 1: Results of the calibration with a single test. φ_{ini}, φ_{fin} are the initial and final values of the objective function and Iter. is number of iterations in the Levenberg-Marquardt method.

corresponding to the nodes of the grid.
After interpolation, the displacements are smoothed through space and time. The spatial smoothing is performed through a moving average method and the temporal smoothing is performed using the Savitzky-Golay method. After completing this procedure, a reduced number of time steps, up to the maximum load value, is selected for each test and become the input data for VFM computations. The reduced number of time steps decreases the computational time and increases the size of the strain increments, which mitigates the impact of strain noise on the computation of the stress field. The strain field is computed for the centre of the elements using shape functions.
The temperature field is also an input for the reconstruction of the stress field. The polynomial functions presented in Fig. 4 are employed to impose the measured temperature values to each element of the grid. Note that only the gradient along the longitudinal direction (x-direction) of the specimen is considered. Moreover, as shown in Fig. 3, the temperature for the positions of the thermocouples is almost constant during the tests. Therefore, it is assumed that the elements of the grid hold the same temperature value for all the selected time steps.

5. Results of the calibration of the modified J-C model

In this section, the calibration of the modified J-C model performed with the VFM and the experimental data from the heterogeneous thermo-mechanical tests is presented. This analysis is divided into two parts. In the first part, the model is calibrated using each test individually, to capture the mechanical behaviour of the material for the specific conditions of each test and hence understand if the calibration process and the chosen constitutive model lead to a good description of these conditions. In the second part, the modified J-C model is calibrated using the three tests simultaneously. In this case, the model is calibrated for a wider range of conditions, and once again the validity of the obtained parameters is analysed. A finite element (FE) model of the heterogeneous test [31] is also presented and used to analyse the validity of the obtained parameters sets.
Note that a total of 7 parameters need to be identified, namely σ_0, K, n, σ_{sat}, C_{y}, m and C, whereas the remaining parameters are known a priori: $\alpha = 0.5$, $T_{\text{tr}} = 25\,^{\circ}\text{C}$, $T_{\text{m}} = 1000\,^{\circ}\text{C}$ and $\dot{\varepsilon}_0 = 1.0 \cdot 10^{-5}\ \text{s}^{-1}$. In the optimisation procedure, only one constraint is applied. This constraint concerns the universe of solutions for each parameter, limiting the admissible solutions to positive values only.

5.1. Calibration with a single test

The same initial set of parameters is used for the three calibrations, this set has characteristic parameter values for high strength steels, except for the parameter C, to which is attributed the zero value as an initial guess. The results of the identifications are presented in Table 1.
The obtained parameters show significant differences from the initial set, which reveals that the objective function and experimental database provide information sensitive to the parameters during the optimisation process. The exception is the parameter C, whose values are very close to zero, the initial value. The value close to zero means that the strain-rate term (Eq. 4) in the modified J-C has a null impact.

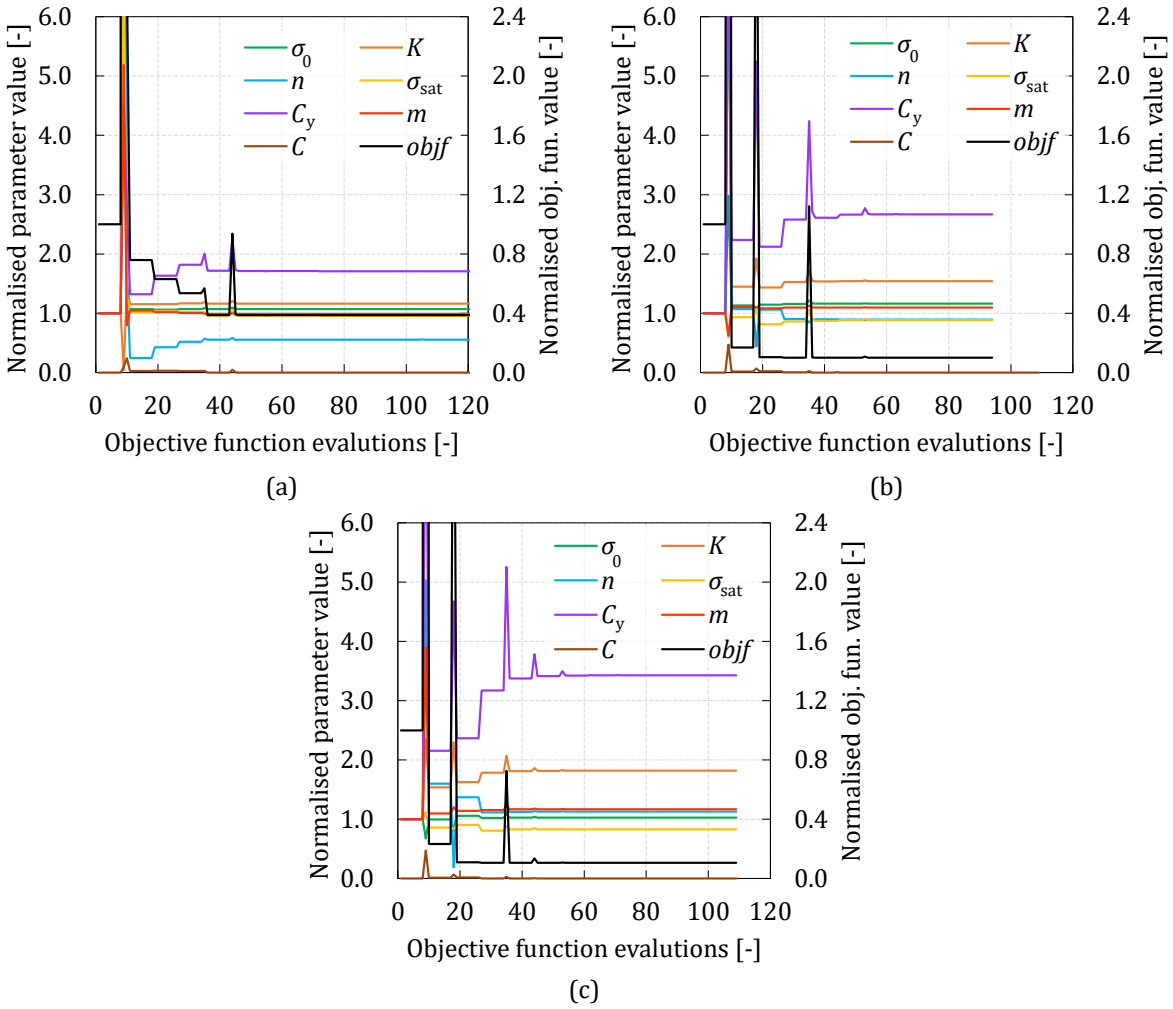

Figure 10: Evolution of the material parameters and objective function value (*objf*) during the calibration process: (a) V1, (b) V2 and (c) V3. The value of the parameters and objective function are normalised by the initial value, except for the case of the parameter C.

The values of objective function computed with the initial set (φ_{ini}) and the final set (φ_{fin}) are also shown in Table 1. The initial values have been reduced by around 90 % for the tests V2 and V3 and 68 % for the test V1. The number of iterations for the test V1 is higher than for the 2 other tests. Fig. 10 shows the evolution of the parameters and objective function value for the three cases during the calibration process. As can be seen, for the three cases, after 60 evaluations the process is stable and almost reached stabilised values.

Fig. 11 presents a comparison between internal and external virtual works. The internal virtual work is computed for the first virtual field $\mathbf{U}_1^*$ and using the initial (IVW_ini) and the finial (IVW_fin) sets of parameters. The external virtual work is computed using the measured load. It is notorious the difference between the initial solution and the final one and it is shown that the obtained parameters provide a good match between internal and external virtual works.

In Fig. 12 each term of the modified J-C model is individually plotted for the initial set and the final sets of parameters. Fig. 12a shows the strain-hardening term (Eq. 2) evolution with the increase in the equivalent plastic strain value ($\bar{\varepsilon}^{\text{p}}$). The obtained parameters lead to distinct strain-hardening curves which, in terms

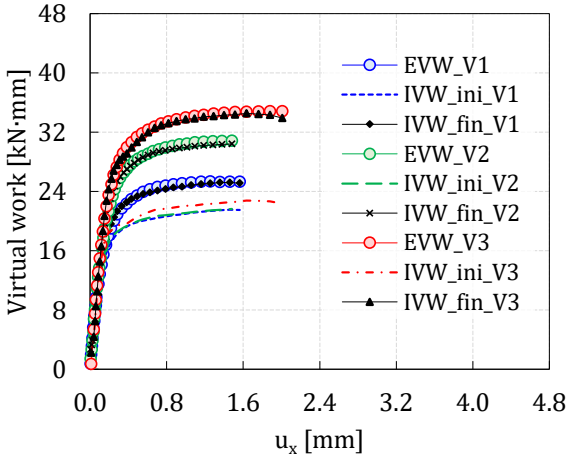

Figure 11: Internal virtual work (IVW) vs external virtual work (EVW). The IVW is plotted for the initial (IVW_ini) and final (IVW_fin) sets of parameters using the first virtual field $\mathbf{U}_1^*$.

of stress values, are ordered according to the displacement rate of the test used in the calibration. Hence, the highest stress values are found for the strain-hardening curve obtained with V3. The three curves have high strain-hardening rates for low values of equivalent plastic deformation and tend to a stress saturation value for high values of equivalent plastic deformation.

Fig. 12b presents the temperature term (Eq. 3) evolution up to 500 °C. This term shows a considerable impact of the temperature on the flow stress evolution. For example at 500 °C, this term reaches values of about 0.50, which means that the stress values are reduced to almost an half with an increase of temperature from 25 to 500 °C. This is consistent with the curves presented in Fig. 9. Moreover, similarly to the strain-hardening term, the impact of this term is ordered according to the displacement rate of the test used in the calibration.

As mentioned before, the obtained values for the parameter C are almost zero, thus the strain-rate term (Eq. 4) becomes equal to 1.0 for the three cases as can be confirmed in Fig. 12c. This means that the range of strain-rates found in each test is not sufficient to activate this term, and the positive effect of the strain-rate seen in Fig. 2 is not captured in any of the calibrations with a single test. Note that a different choice of initial value for the parameter C, would lead to a different solution for the remaining parameters, but the sensitivity to C would not change and positive effect of the strain-rate would be conditioned by this initial value.

Fig. 13 presents the strain-hardening term affected by the temperature term at 500 °C. As the predominant stress state is uniaxial tension in the three tests, Fig. 13 and 9 can be compared. The level of flow stress for each curve is similar to the level of stress for the respective counterpart in Fig. 9. According to this result, the magnitude of the flow stress for each test seems to be well described by the respective set of parameters.

To analyse the validity of the final sets of parameters presented in Table 1, these should be tested as input data for the simulation of the heterogeneous tests. The parameters should give at least a good representation of the test that provided the information for calibration. Therefore, a 3D FE model of the heterogeneous tests was built in Abaqus® standard. This model was previously presented in [31]. The FE model represents the ROI in the tensile specimen, as the geometry depicted in Fig. 1. An eight-node solid element with reduced integration (C3D8R) is adopted for the mesh, which is composed by $60 \times 28 \times 3$ regular elements. The modified J-C model presented in section 3 was implemented in a UMAT subroutine. The simulations of the tests are performed for the respective loading conditions in terms of time, which consist of different average strain rates: $1.0 \cdot 10^{-4}$, $1.0 \cdot 10^{-3}$ and $1.0 \cdot 10^{-2}$ s^{-1}. The boundary conditions are the displacements imposed on the boundaries $x = -30$ and $x = 30$ mm, which were extracted from the DIC measurements of each test. The temperature maps used in the calibrations are also imposed on the models. The simulation of each test

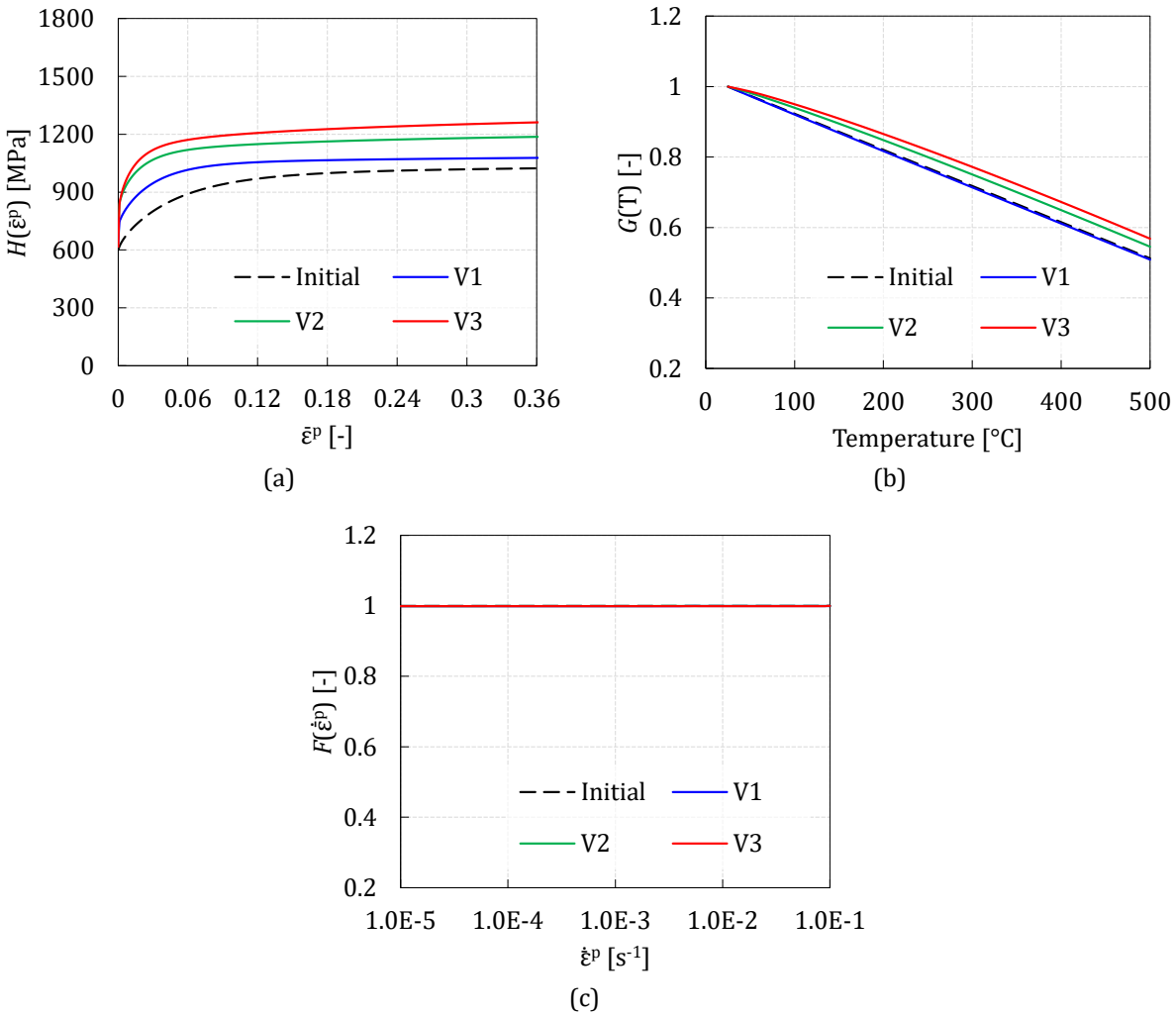

Figure 12: Evolution of three terms that compose the modified J-C model using the obtained sets of parameters presented in Table 1: (a) strain-hardening term (Eq. 2), (b) temperature term (Eq. 3) and (c) strain-rate term (Eq. 4).

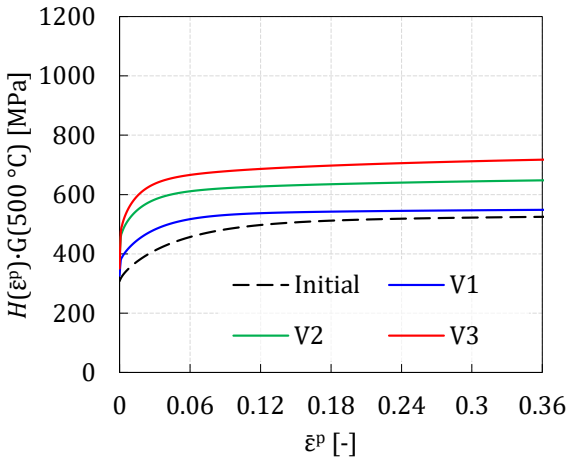

Figure 13: Evolution of the strain-hardening term (Eq. 3) affected by the temperature term (Eq. 3) at 500 °C for the final sets of parameters presented in Table 1.

is performed with the respective set of parameters (Table 1). Moreover, it is included in these simulations the time steps beyond the maximum load value to evaluate the accuracy of the parameters when the results are extrapolated.

Fig. 14 presents the comparison of the numerical and the experimental load curves for the three tests. The three sets of parameters provide reasonable results up to the maximum load value. The parameters of the test V3 (Fig. 14c) provide the best results, even in the extrapolation domain. In the other two cases (Fig. 14a and b), there is a slight overestimation for the maximum load value that propagates for the extrapolation domain.

In Fig. 15, the results for the logarithmic strain in the x-direction are presented for the three tests. The experimental results are labelled as Exp and the numerical ones as Num. Mload and Rup represent the time steps of maximum load and the last step before rupture (the last step of the simulation). The results for the test V3 (Fig. 15 c) are the most accurate ones. In this case, the finite element model and the parameters describe very well the bell-shaped curve of the strain distribution. In the extrapolation domain, the maximum strain value is overpredicted and the strain localisation is more severe than in the experimental results. Regarding Fig. 15 a and b, the localisation of strain is underestimated and a more uniform distribution of the strain field is obtained, but the trend is well captured. In the extrapolation domain, in both cases V1 and V2, the strain value at the centre of the specimen is overestimated.

5.2. Calibration with multiple tests

In this part, the results for the calibration of the modified J-C model using the three tests simultaneously are presented. Here, the goal is to reach a set of parameters that enables the representation of the conditions of the three tests through the modified J-C model. This is a more demanding problem than the previous one because the strain-rate range is enlarged by the inclusion of the three tests in the same experimental database and the model is forced to capture the positive sensitivity of the material to strain-rate.

The results for a single initial set are presented in Table 2. All the parameters were activated in the optimisation and the initial value of the objective function decreased by 54%. The number of iterations for the optimisation Levernberg-Marquardt method is 12. The evolution of the parameters and objective function value along the calibration is presented in Fig. 16. In this case, the problem seems more stable for the beginning of the optimisation.

Fig. 17 shows the comparison between internal and external virtual works. The internal virtual work is computed for the first virtual field $\mathbf{U}_1^*$ and using the initial (IVW_ini) and the final (IVW_fin) parameters set. The external virtual work is computed from the measured load. An underestimation of the IVW_fin for

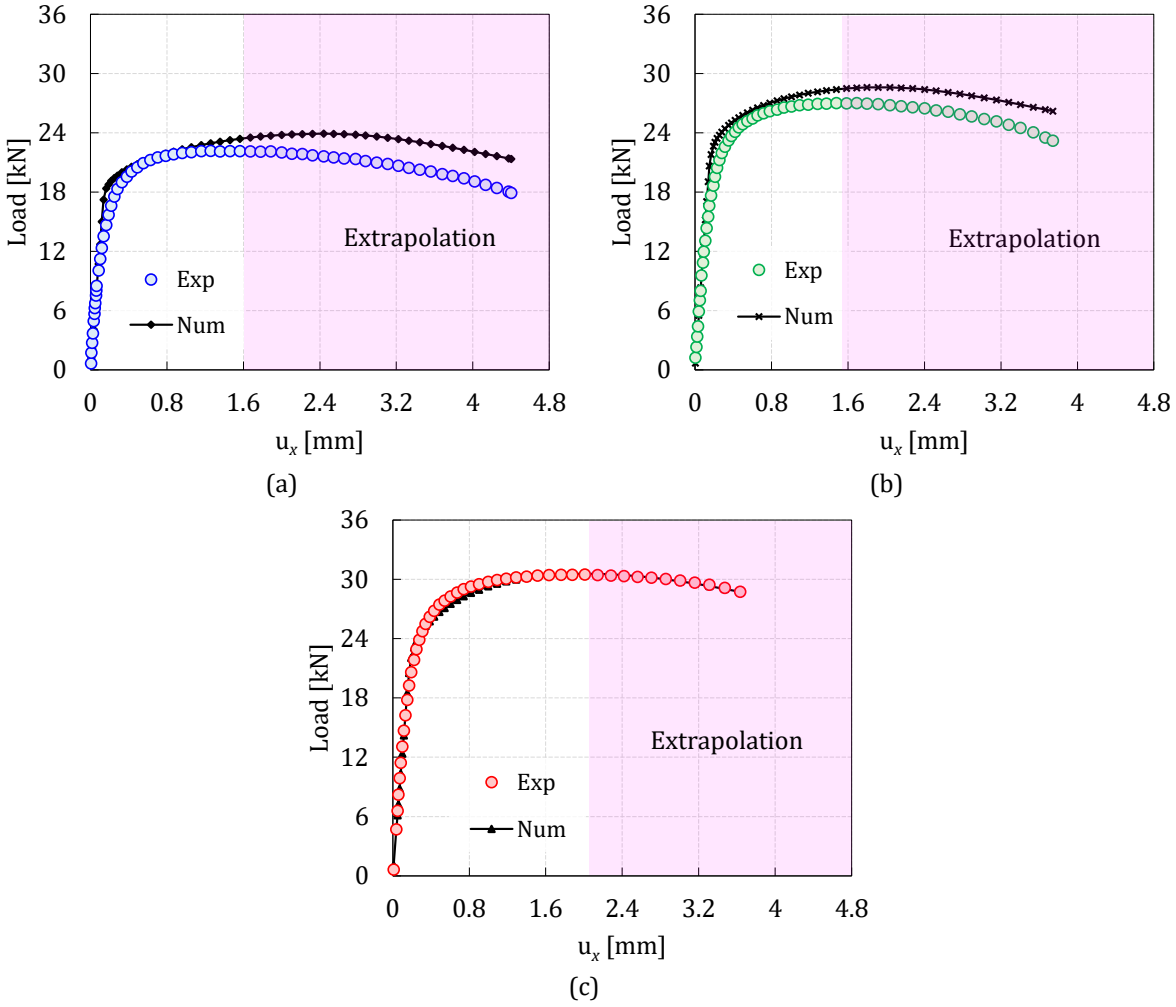

Figure 14: Comparison of experimental (Exp) and numerical (Num) load curves. The numerical load curves are obtained through FE analysis with the final sets of parameters presented in Table 1: (a) V1, (b) V2 and (c) V3.

	σ_0 [MPa]	K [MPa]	n [-]	σ_{sat} [MPa]	C_{y} [-]	m [-]	C [-]	φ_{ini} [-]·10^6	φ_{fin} [-]·10^6	Iter. [-]
Initial	*327*	*966*	*0.070*	*513*	*81*	*1.19*	*0.11*	-	-	-
Final	342	924	0.017	603	131	1.27	0.07	1.7	0.8	12

Table 2: Results of the calibration with three tests. φ_{ini}, φ_{fin} are the initial and final of values of the objective function and Iter. is number of iterations in the Levenberg-Marquardt method.

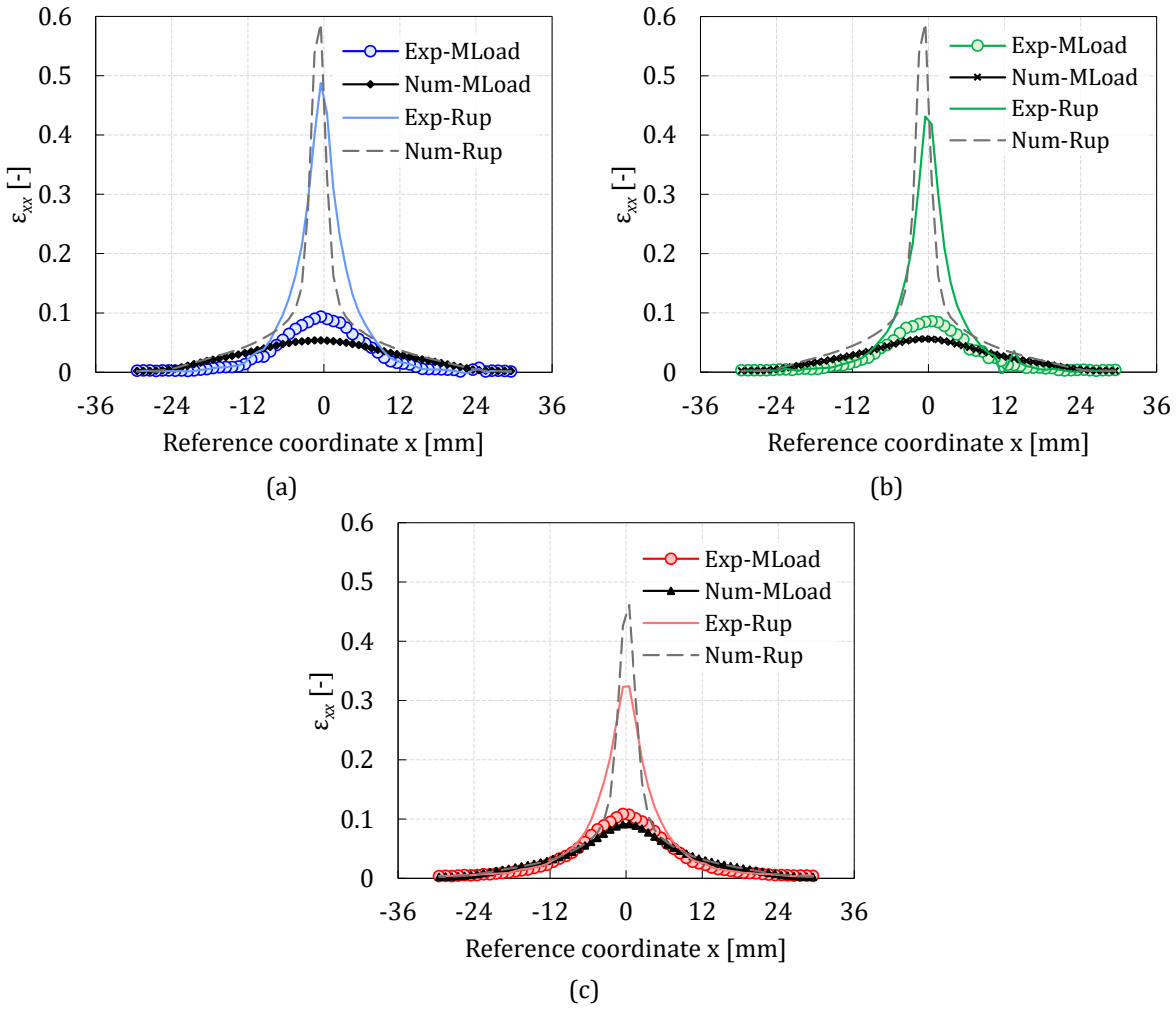

Figure 15: Comparison of experimental (Exp) and numerical (Num) spatial distribution of the logarithmic strain along the x-direction. The numerical results are obtained through FE analysis with the obtained sets of parameters presented in Table 1: (a) V1, (b) V2 and (c) V3.

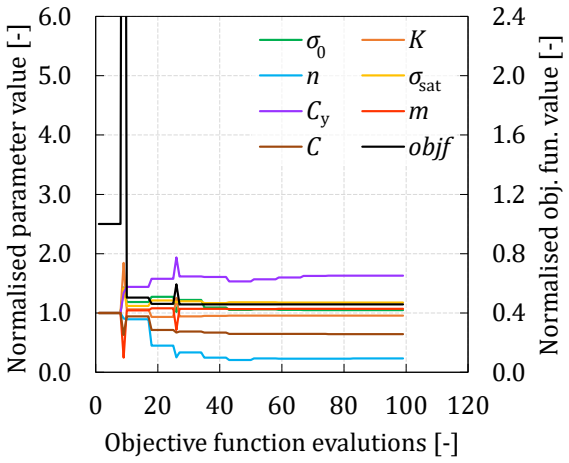

Figure 16: Evolution of the material parameters and objective function value (*objf*) during the calibration process for the experimental database composed by three tests. The values of the parameters and objective function are normalised by the initial value.

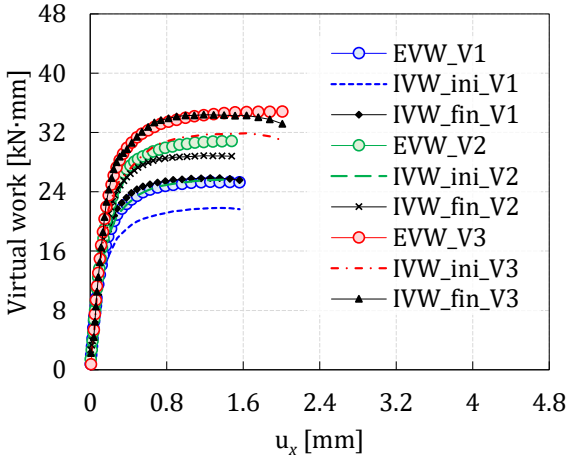

Figure 17: Internal virtual work (IVW) vs external virtual work (EVW). The IVW is plotted for the initial (IVW_ini) and final (IVW_fin) sets of parameters using the first virtual $\mathbf{U}_1^*$.

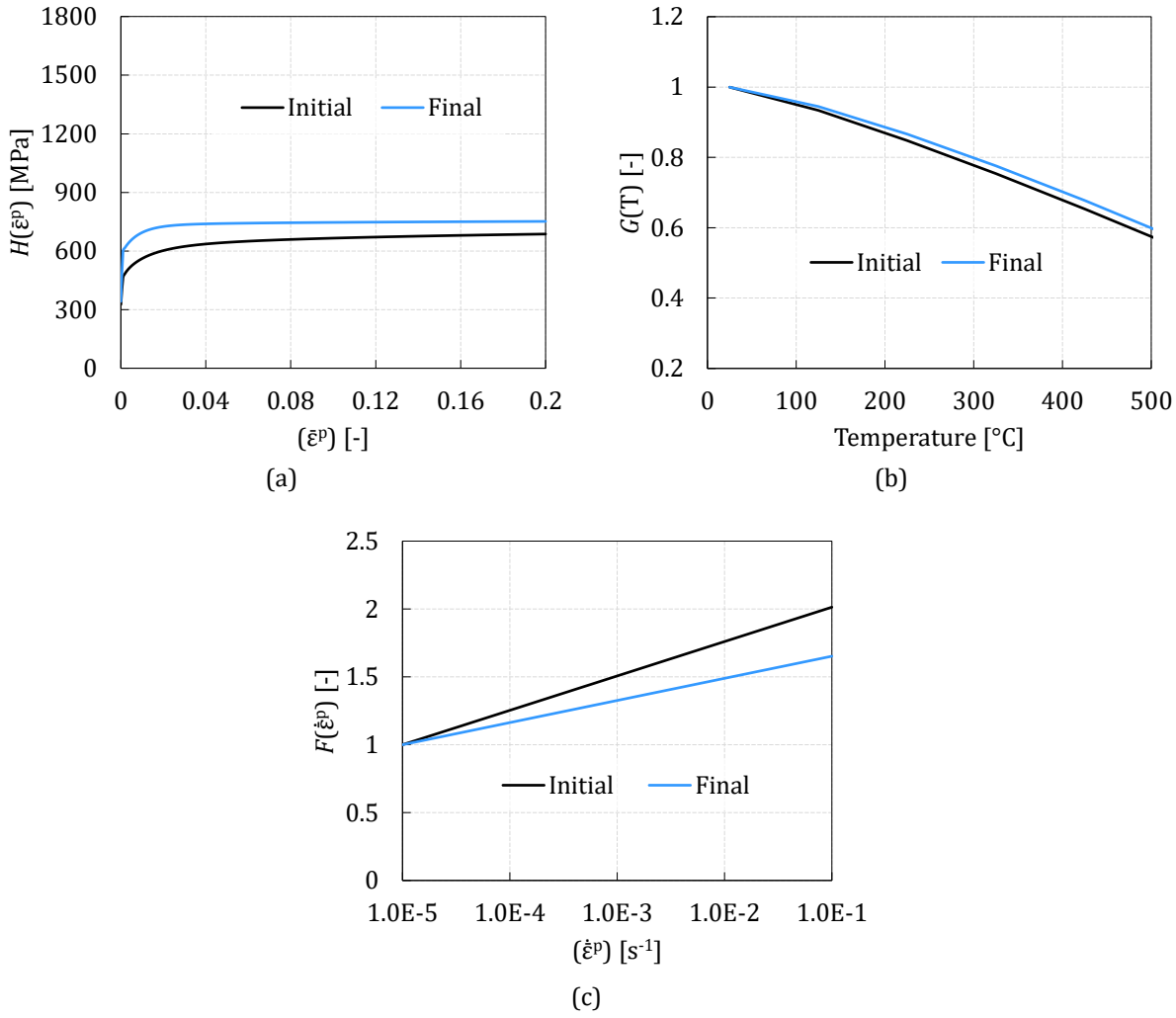

Figure 18: Evolution of three terms that compose the modified J-C model using the final set of parameters presented in Table 2: (a) strain-hardening term (Eq. 2), (b) temperature term (Eq. 3) and (c) strain-rate term (Eq. 4).

V2 is observed, which is not observed in Fig. 11. There is also a slight underestimation for V3 in the final time steps.

Fig. 18 shows the individual plot of the terms of the modified J-C model. In this case, the strain-hardening term (Fig. 18a) converges quickly to the stress saturation value, a consequence of the low value of the parameter n and the high value of the parameter C_y. The impact of the temperature continues to be significant (Fig. 18b), and the strain-rate has now an important role. Since the strain-hardening term converges to the saturation value very quickly, the strain-rate term assumes the leading role in the hardening process, imposing the increase in the flow stress through the positive effect of strain-rate.

The validity of the obtained set of parameters is tested in the numerical simulation of the three tests. Fig. 19 presents the results for the load prediction using the FE model previously described and the obtained set of parameters. From these figures, it is possible to conclude that parameter C captures the positive effect of strain-rate. Nevertheless, the results for the test V1 (Fig. 19a) and V2 (Fig. 19b) are overestimated. Although a slight overestimation for the higher values of displacement occurs, the results for the test V3 (Fig. 19c) are the most accurate ones.

In terms of strain field, the results presented in Fig. 20 show a deterioration of the predictions. Still,

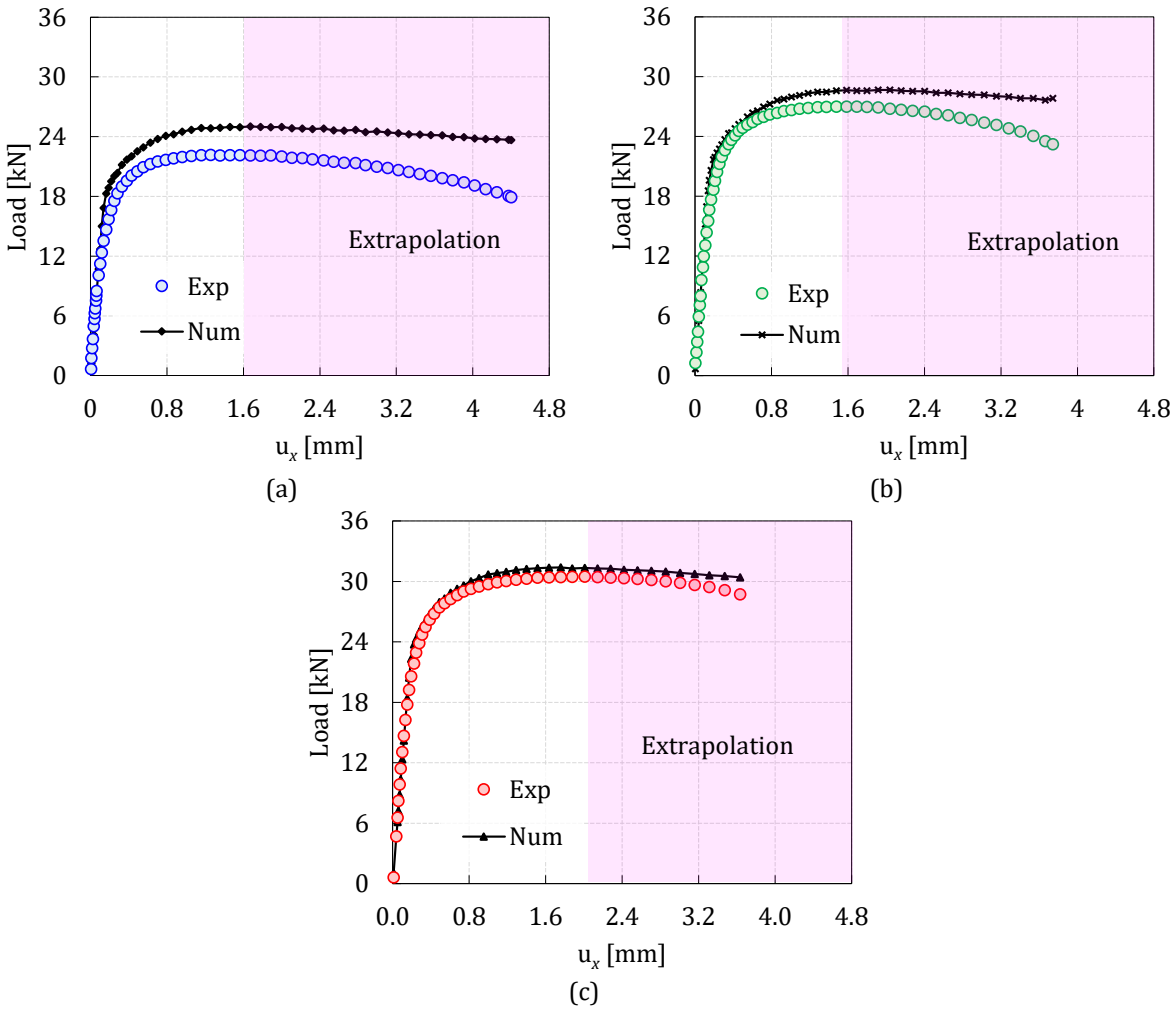

Figure 19: Comparison of experimental (Exp) and numerical (Num) load curves. The numerical load curves are obtained through FE analysis with the final set of parameters presented in Table 2: (a) V1, (b) V2 and (c) V3.

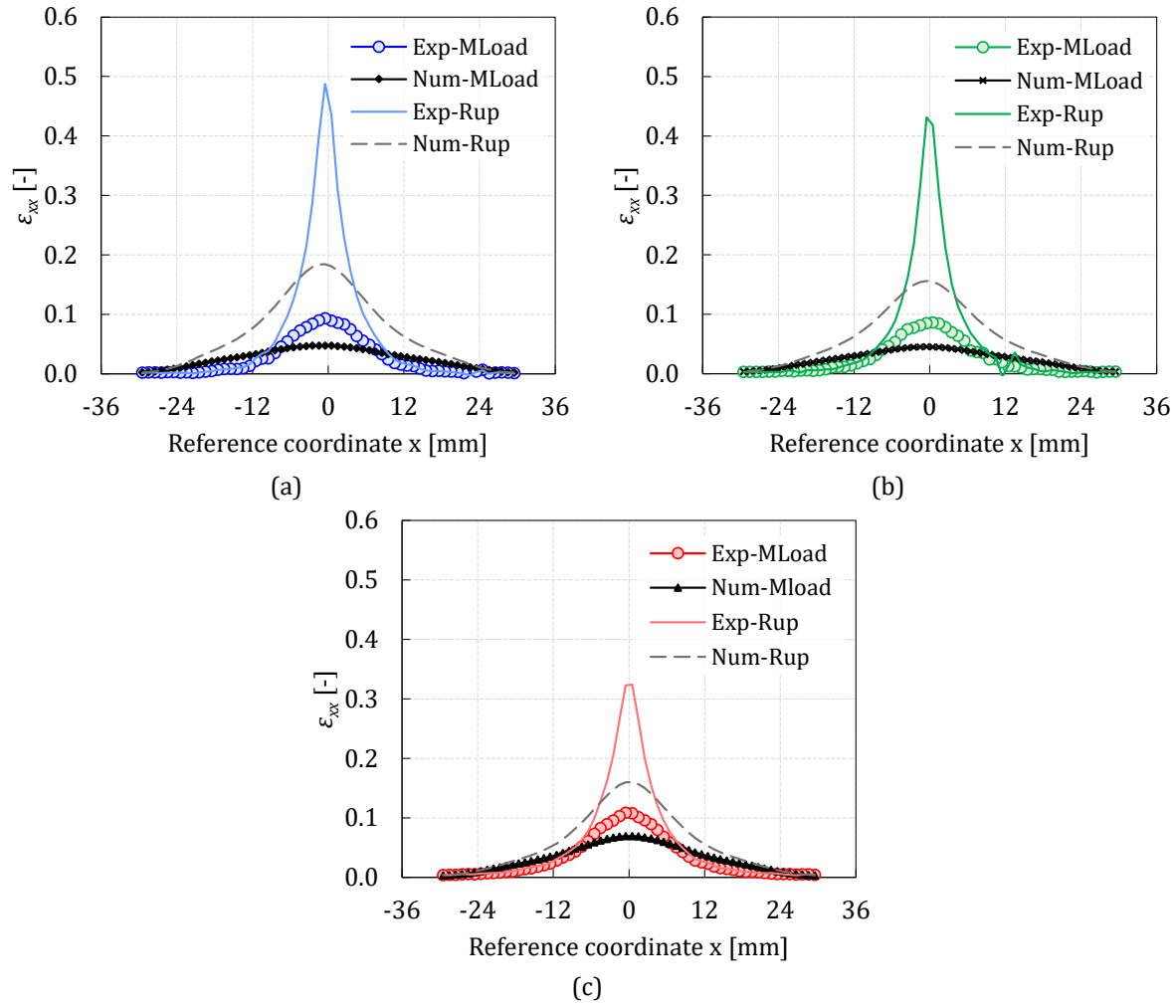

Figure 20: Comparison of experimental (Exp) and numerical (Num) spatial distribution of the logarithmic strain in the x-direction. The numerical results are obtained through FE analysis with the final set of parameters presented in Table 2: (a) V1, (b) V2 and (c) V3.

the best results are achieved for the test V3 (Fig. 20c). The predictions show a strain distribution more uniformly distributed and less localized. Consequently, the maximum strain value is underestimated. In the extrapolation domain, the numerical predictions tend to underestimate the strain localisation and present much lower strain values at the centre of the specimen.

5.3. Discussion

The results for the first part of this section include the calibration of the model using each test individually, which resulted in three distinct parameters sets. The validation of the obtained sets shows a reasonably well prediction of the numerical load, which means that the stress level is well predicted. However, the obtained sets have almost zero values for the parameter C, which means that the strain-rate effect was not captured by the strain-rate term. The results suggest that the effect of strain-rate, for the conditions of each test, is captured by the other two terms, which lead to significant differences in the obtained parameters from test to test. This limits the applicability of the these sets of parameters only to the conditions present in the respective test used in the calibration.

Furthermore, for the test with the highest strain-rate (V3), the prediction of the strain field is in very good agreement with the experimental measurements, but in the other two cases, the maximum strain value is underestimated and the distribution is less localised at the centre of the specimen. The temperature plays an important role in the strain localisation and these results suggest that the impact of the temperature term is underestimated for the tests with the lowest strain-rates.

In the second part of this section, the three tests were combined in a single database to calibrate the modified J-C model. The results show that three tests bring sufficient information to calibrate the parameter C, and the positive effect of strain-rate is captured through the strain-rate term. Nevertheless, the results show a lack of flexibility of the model to fit the experimental data provided by the three tests. This is observed directly by the results in the internal virtual work computation at the end of the optimisation (Fig. 17). Moreover, there is a significant deterioration of the strain field prediction. The high impact of the strain-rate term, which brings a positive effect on the flow stress, balances the negative effect of the temperature term. Consequently, the localisation of the deformation at the centre of the specimen is attenuated and more uniform distributions of the strain field are obtained.

Regarding the optimisation process, in both analyses, just one set of initial parameters was presented. Nevertheless, it was observed that the problem is sensitive to the initial set of parameters and multiple solutions are found. This reveals that the experimental database lacks information for some of the parameters. There are two potential solutions, the parametrisation of the model can be reduced, or the experimental database can be improved with more tests. Regarding the first solution, some parameters of the model have a specific meaning, like σ_0 that represents the initial yield stress. This parameter can be identified a priori, helping to reduce the number of variables in the optimisation process. For the second solution, including more tests in the database is also the path to more accurate results and to expand the validity of the obtained parameters. Moreover, the lack of flexibility of the model implies that more parameters are required to fit the mechanical behaviour of this material, thus it is reasonable to explore this solution.

The obtained results also give some indications that the chosen model needs to be enhanced to accurately describe the mechanical behaviour of the DP980 under such temperature and strain-rate conditions. The actual formulation of the J-C model can be a limitation. This formulation is usually called decoupled formulation because each term corresponds to an isolated effect (e.g. strain-hardening, temperature or strain-rate). However, coupled formulations in which the different effects interact with each other may be more suitable for the material and conditions under study. The results for the single test calibrations showed that all the parameters of the model could depend on the strain-rate effect, and also show a monotonic evolution for almost all parameters (except for the parameter σ_0). Therefore, the parameters n and C_y could be a function of the strain-rate effect.

6. Conclusions

The purpose of this work is to present a calibration methodology for thermo-mechanical constitutive models. This methodology combines a thermo-mechanical heterogenous test and the VFM. A modified J-C

model model is selected to test this methodology. The heterogenous test is performed on a Gleeble thermo-mechanical simulator and the material is a DP980. In order to capture different orders of magnitude in terms of strain-rate, the test is performed for three displacement rates.

The first part of this work presents the analysis of the test in terms of temperature, strain and strain-rate information. The analysis shows that the test provides a range of temperatures from 360 °C to 500 °C. The temperature field is nearly constant during the test. The highest values of the strain field are localised at the centre of the specimen due to the temperature distribution. The strain field distribution gives a wide range of values at each instant of the test. Nevertheless, due to the localised strain distribution, the information for the viscoplastic regime is reduced in terms of temperature. The strain-rate field presents a similar shape to the strain field. The strain-rate range of each test is in the same order of magnitude as the nominal strain-rate of the test.

Regarding the calibration results, these are analysed in two parts. In the first part, the calibration with a single test is analysed. Thus, the calibration is performed for each test corresponding to a different displacement rate. The results suggest that the flow stress is well described for the three cases. Nevertheless, the results also reveal that the experimental database composed by a single test performed for a displacement rate lacks information to calibrate the three terms of the modified J-C model. In the second part, the calibration is performed using the information of the three displacement rates. The combination of these three tests increases the range of strain-rate and consequently, provides sufficient information to calibrate the three terms of the model. The positive sensitivity of the material to strain-rate is captured by the strain-rate term. However, the results expose the lack of flexibility of the modified J-C model to capture the material behaviour under such range of strain-rates. The numerical simulations of the tests show overestimation of the load and underestimation of the strain localisation.

The proposed methodology presents reasonable results and represents a potential alternative to classical procedures. The main advantage is that a considerable range of temperatures and strain-rates is collected from a single test. Nevertheless, there is substantial room for improvement. For instance, the experimental database can be enhanced with different temperature ranges. Moreover, the lack of flexibility of the modified J-C model demands for a more complex model to describe the thermo-mechanical behaviour of the DP980 steel. Therefore, more information for different temperatures and strain-rates will be essential.

7. Acknowledgments

This project has received funding from the Research Fund for Coal and Steel under grant agreement No 888153. The authors also gratefully acknowledge the financial support of the Portuguese Foundation for Science and Technology (FCT) under the projects PTDC/EME-APL/29713/2017 (CENTRO-01-0145-FEDER-029713), PTDC/EME-EME/31243/2017 (POCI-01-0145-FEDER-031243) and PTDC/EME-EME/30592/2017 (POCI-01-0145-FEDER-030592) by UE/FEDER through the programs CENTRO 2020 and COMPETE 2020, and UID/EMS/00481/2013-FCT under CENTRO-01-0145-FEDER-022083. The authors also would like to acknowledge the Région Bretagne (France) for its financial support. J.M.P. Martins is also grateful to the FCT for the PhD grant SFRH/BD/117432/2016.

References

[1] H. Karbasian, A. Tekkaya, A review on hot stamping, Journal of Materials Processing Technology 210 (15) (2010) 2103 – 2118. doi:https://doi.org/10.1016/j.jmatprotec.2010.07.019.
URL http://www.sciencedirect.com/science/article/pii/S092401361000213X

[2] S. Toros, F. Ozturk, I. Kacar, Review of warm forming of aluminum–magnesium alloys, Journal of Materials Processing Technology 207 (1) (2008) 1 – 12. doi:https://doi.org/10.1016/j.jmatprotec.2008.03.057.
URL http://www.sciencedirect.com/science/article/pii/S092401360800318X

[3] B. Erice, C. Roth, D. Mohr, Stress-state and strain-rate dependent ductile fracture of dual and complex phase steel, Mechanics of Materials 116 (2018) 11 – 32, iUTAM Symposium on Dynamic Instabilities in Solids. doi:https://doi.org/10.1016/j.mechmat.2017.07.020.
URL http://www.sciencedirect.com/science/article/pii/S0167663616305361

[4] J. Sung, J. Kim, R. Wagoner, A plastic constitutive equation incorporating strain, strain-rate, and temperature, International Journal of Plasticity 26 (12) (2010) 1746 – 1771. doi:https://doi.org/10.1016/j.ijplas.2010.02.005.
URL http://www.sciencedirect.com/science/article/pii/S0749641910000276

[5] L. Gambirasio, E. Rizzi, On the calibration strategies of the johnson–cook strength model: Discussion and applications to experimental data, Materials Science and Engineering: A 610 (2014) 370 – 413. doi:https://doi.org/10.1016/j.msea.2014.05.006.
URL http://www.sciencedirect.com/science/article/pii/S0921509314005875

[6] E. Markiewicz, B. Langrand, D. Notta-Cuvier, A review of characterisation and parameters identification of materials constitutive and damage models: From normalised direct approach to most advanced inverse problem resolution, International Journal of Impact Engineering 110 (2017) 371 – 381, special Issue in honor of Seventy Fifth Birthday of Professor N. K. Gupta. doi:https://doi.org/10.1016/j.ijimpeng.2017.01.028.
URL http://www.sciencedirect.com/science/article/pii/S0734743X16307746

[7] A. Smith, Z. Chen, J. Lee, M. Lee, R. Wagoner, Effective method for fitting complex constitutive equations, International Journal of Plasticity 58 (2014) 100 – 119, in Honor of Kwansoo Chung. doi:https://doi.org/10.1016/j.ijplas.2014.01.005.
URL http://www.sciencedirect.com/science/article/pii/S074964191400014X

[8] G. Johnson, W. H. Cook, A constitutive model and data for metals subjected to large strains, high strain rates and high temperatures, in: Proceedings of the 7th International Symposium on Ballistics, Vol. 21, The Netherlands, 1983, pp. 541–547.

[9] S. Avril, M. Bonnet, A.-S. Bretelle, M. Grédiac, F. Hild, P. Ienny, F. Latourte, D. Lemosse, S. Pagano, E. Pagnacco, et al., Overview of identification methods of mechanical parameters based on full-field measurements, Experimental Mechanics 48 (4) (2008) 381.

[10] M. Grédiac, F. Hild, Full-field measurements and identification in solid mechanics, Wiley Online Library, 2013.

[11] F. Pierron, M. Grédiac, The virtual fields method: extracting constitutive mechanical parameters from full-field deformation measurements, Springer Science & Business Media, 2012.

[12] L. Zhang, S. Thakku, M. Beotra, M. Baskaran, T. Aung, J. Goh, N. Strouthidis, M. Girard, Verification of a virtual fields method to extract the mechanical properties of human optic nerve head tissues in vivo, Biomechanics and Modeling in Mechanobiology 16 (3) (2017) 871–887.

[13] J. Martins, A. Andrade-Campos, S. Thuillier, Comparison of inverse identification strategies for constitutive mechanical models using full-field measurements, International Journal of Mechanical Sciences 145 (2018) 330 – 345. doi:https://doi.org/10.1016/j.ijmecsci.2018.07.013.
URL http://www.sciencedirect.com/science/article/pii/S0020740318305836

[14] M. Grédiac, Principe des travaux virtuels et identification, Comptes rendus de l'Académie des sciences. Série 2, Mécanique, Physique, Chimie, Sciences de l'univers, Sciences de la Terre 309 (1) (1989) 1–5.

[15] A. Lattanzi, F. Barlat, F. Pierron, A. Marek, M. Rossi, Inverse identification strategies for the characterization of transformation-based anisotropic plasticity models with the non-linear vfm, International Journal of Mechanical Sciences 173 (2020) 105422. doi:https://doi.org/10.1016/j.ijmecsci.2020.105422.
URL http://www.sciencedirect.com/science/article/pii/S0020740319328826

[16] A. Marek, F. Davis, J.-H. Kim, F. Pierron, Experimental validation of the sensitivity-based virtual fields for identification of anisotropic plasticity models, Experimental Mechanics (2020) 1–26.

[17] J. Fu, W. Xie, J. Zhou, L. Qi, A method for the simultaneous identification of anisotropic yield and hardening constitutive parameters for sheet metal forming, International Journal of Mechanical Sciences (2020) 105756.

[18] S. Grama, S. Subramanian, F. Pierron, On the identifiability of anand visco-plastic model parameters using the virtual fields method, Acta Materialia 86 (2015) 118 – 136. doi:https://doi.org/10.1016/j.actamat.2014.11.052.
URL http://www.sciencedirect.com/science/article/pii/S1359645414009057

[19] E. Jones, J. Carroll, K. Karlson, S. Kramer, R. Lehoucq, P. Reu, D. Turner, Parameter covariance and non-uniqueness in material model calibration using the virtual fields method, Computational Materials Science 152 (2018) 268 – 290. doi:https://doi.org/10.1016/j.commatsci.2018.05.037.
URL http://www.sciencedirect.com/science/article/pii/S0927025618303501

[20] G. Valeri, B. Koohbor, A. Kidane, M. Sutton, Determining the tensile response of materials at high temperature using dic and the virtual fields method, Optics and Lasers in Engineering 91 (2017) 53 – 61. doi:https://doi.org/10.1016/j.optlaseng.2016.11.004.
URL http://www.sciencedirect.com/science/article/pii/S0143816616304109

[21] J. Coër, C. Bernard, H. Laurent, A. Andrade-Campos, S. Thuillier, The effect of temperature on anisotropy properties of an aluminium alloy, Experimental Mechanics 51 (7) (2011) 1185–1195.

[22] A. Mishra, Experimental investigation and numerical prediction of rupture in bending of metallic sheets, Ph.D. thesis, Lorient (2013).

[23] J.-H. Kim, A. Serpantié, F. Barlat, F. Pierron, M.-G. Lee, Characterization of the post-necking strain hardening behavior using the virtual fields method, International Journal of Solids and Structures 50 (24) (2013) 3829 – 3842. doi:https://doi.org/10.1016/j.ijsolstr.2013.07.018.
URL http://www.sciencedirect.com/science/article/pii/S0020768313002989

[24] S. Coppieters, J.-H. Kim, K. Denys, S. Cooreman, D. Debruyne, On complete solutions for the problem of diffuse necking in sheet metal, Procedia Engineering 207 (2017) 2012 – 2017, international Conference on the Technology of Plasticity, ICTP 2017, 17-22 September 2017, Cambridge, United Kingdom. doi:https://doi.org/10.1016/j.proeng.2017.10.1060.
URL http://www.sciencedirect.com/science/article/pii/S1877705817358551

[25] L. Gambirasio, E. Rizzi, An enhanced johnson–cook strength model for splitting strain rate and temperature effects on lower yield stress and plastic flow, Computational Materials Science 113 (2016) 231 – 265. doi:https://doi.org/10.1016/j.commatsci.2015.11.034.
URL http://www.sciencedirect.com/science/article/pii/S0927025615007417

[26] D. Notta-Cuvier, B. Langrand, E. Markiewicz, F. Lauro, G. Portemont, Identification of johnson–cook's viscoplastic model parameters using the virtual fields method: Application to titanium alloy ti6al4v, Strain 49 (1) (2013) 22–45. arXiv:https://onlinelibrary.wiley.com/doi/pdf/10.1111/str.12010, doi:10.1111/str.12010.
URL https://onlinelibrary.wiley.com/doi/abs/10.1111/str.12010

[27] A. Holzapfel, Nonlinear Solid Mechanics: A Continuum Approach for Engineering, John Wiley & Sons, LTD., 2000.

[28] A. Marek, F. Davis, M. Rossi, F. Pierron, Extension of the sensitivity-based virtual fields to large deformation anisotropic plasticity, International Journal of Material Forming 12 (3) (2019) 457–476.

[29] E. Jones, K. Karlson, P. Reu, Investigation of assumptions and approximations in the virtual fields method for a viscoplastic material model, Strain 55 (4) (2019) e12309, e12309 10.1111/str.12309. arXiv:https://onlinelibrary.wiley.com/doi/pdf/10.1111/str.12309, doi:10.1111/str.12309.
URL https://onlinelibrary.wiley.com/doi/abs/10.1111/str.12309

[30] F. Pierron, S. Avril, V. T. Tran, Extension of the virtual fields method to elasto-plastic material identification with cyclic loads and kinematic hardening, International Journal of Solids and Structures 47 (22) (2010) 2993 – 3010. doi:https://doi.org/10.1016/j.ijsolstr.2010.06.022.
URL http://www.sciencedirect.com/science/article/pii/S002076831000243X

[31] J. Martins, S. Thuillier, A. Andrade-Campos, Calibration of anisotropic plasticity models with an optimized heterogeneous test and the virtual fields method, in: Residual Stress, Thermomechanics & Infrared Imaging and Inverse Problems, Volume 6, Springer, 2020, pp. 25–32.

[32] M. Crisfield, Non-Linear Finite Element Analysis of Solids and Structures, Volume 1, John Wiley & Sons, Ltd., 1991.

[33] J. Simo, T. Hughes, Computational inelasticity, Springer, New York, NY, 1998. doi:https://doi.org/10.1007/b98904.

[34] D. Marquardt, An algorithm for least-squares estimation of nonlinear parameters, Journal of the society for Industrial and Applied Mathematics 11 (2) (1963) 431–441. doi:10.1137/0111030.

4.3 Final Remarks

This chapter proposes two methodologies for the calibration of thermo-mechanical constitutive models. Both rely on the same heterogeneous test, which is performed on a Gleeble machine. This test presents a considerable range of temperatures, strain values and strain-rates. The thermo-mechanical behaviour of the material is then exposed to a wide range of conditions, which results in a robust experimental database. The first methodology, which combines this test and the Finite Element Model Updating, is tested with virtually generated data. A detailed analysis of the sensitivity of the material parameters of the Johnson-Cook model shows that the complete calibration of the model is possible. Nevertheless, the initial yield stress revealed a low sensitivity. The second methodology is evaluated with experimental data obtained for a high strength steel. The Virtual Fields Method is combined with this experimental database. The results show that the experimental database information is sufficient to have reasonable results in the calibration of a thermo-elasto-viscoplasticity model. Nevertheless, the sensitivity of some parameters seems reduced. Although the results are very promising, there is plenty of room for improvement. In conclusion, both methodologies constitute potential candidates to replace classical procedures. The thermo-mechanical test covers a range of information that in classical procedures would require a large number of tests, that represents an important aspect to simplify the calibration of thermo-mechanical models.

Intentionally blank page.

Chapter 5

Conclusions and Perspectives

5.1 Conclusions

The ultimate objective of this thesis is to propose an efficient calibration methodology for thermo-mechanical models. This methodology is intended to be an alternative to classical procedures. It relies on full-field measurements, heterogeneous tests, and inverse analysis. These three elements all together form a new concept in the field of calibration of constitutive models, which has the potential to reduce the experimental campaigns and simplify the process. Consequently, this new concept has attracted a growing interest in the field. Full-field measurement techniques reached a level of maturity that allowed the shift of focus to the other two elements. A remarkable number of inverse analysis methods were proposed over the years. The selection of a proper heterogeneous test has also assumed a preponderant role. Thereby, the present thesis can also be seen as a collection of works focused on the simplification of the calibration process in different frameworks, in which different inverse methods are explored, as well as complex heterogeneous tests.
The starting point of this thesis is an overview of four inverse analysis methods, the Finite Element Model Updating (FEMU), the Constitutive Equation Gap Method (CEGM), the Equilibrium Gap Method (EGM) and the Virtual Fields Method (VFM). These seem the most promising methods so far. The focus is to understand the advantages and disadvantages of each strategy, as well as their implementation aspects. This study culminates in a comparative study of the different methods, in which two types of constitutive models are used: an isotropic linear elasticity model and an isotropic elasto-plasticity model. The sensitivity of the methods to the presence of noise in the full-field data is analysed. This overview shows that the CEGM, the EGM, and the VFM have algorithms significantly more complex than the FEMU. Thereby, FEMU continues to be the most used method. The results of the comparative study show similar performances in elasticity. The exception is the EGM, which presents a higher sensitivity to noise than the other methods. In elasto-plasticity, FEMU achieves the most accurate results in the presence of noise. Nevertheless, this superior performance in terms of accuracy has a considerable computational expense. The CEGM presents the highest sensitivity to noise, but in terms of computational cost, it is more efficient than FEMU. The VFM reaches reasonable results in the presence of noise, and the best results for the computational performance. These results suggest that among the four methods, the VFM provides the best balance between the quality of the calibration procedure and the computational cost.
A second study focused on the comparison between FEMU and VFM in more complex conditions is presented. The formulation is extended to finite strains. The goal is the comparison of the accuracy of the two methods in the calibration of an isotropic plasticity model. The results indicate that FEMU is sensitive to the distribution of the input data. The strain values with more representation in the database of the test have more impact on the calibration results. Thus, a more accurate identification with FEMU requires equally distributed data for the different levels of strain. Nevertheless, in the same conditions, the VFM does not show this sensitivity and presents a more accurate response. This suggest that VFM can offer more than a lower computational cost when compared to FEMU.

Following this analysis, the VFM is combined with a biaxial tension test of a cruciform specimen. The objective of this study is to propose a single test calibration methodology for anisotropic plasticity models. The biaxial tension test of a cruciform specimen brings valuable mechanical information for sheet metals, due to the variety of strain paths and a large range of strain values reached during the test. Three geometries of the cruciform test are explored in this study. These geometries include simple geometric perturbations that promote heterogeneity in the strain fields. The analysis of the respective strain and stress fields reveal that the simplest geometry has less information for the shear stress component, which leads to a less accurate calibration in the yield criterion. Nevertheless, the inclusion of geometric perturbations brings more heterogeneity and enhances the information for that component. Moreover, the calibration results demonstrate that the geometry with the widest distribution of stress and strain states provides sufficient information to calibrate all the parameters of the Hill'48 yield criterion and Swift's law with a maximum error of 1%. Although the analysis is based on virtual experimental data, the results are very promising.
The test is also analysed for a different material, which exposes the material sensitivity of the test. The information provided by the test is affected by the material under study. Regarding the calibration process, a more complex yield criterion, with a higher number of material parameters, is also tested. An additional constraint is required to mitigate the problem of multiple solutions. This constraint establishes in the yield criterion, that the yield stress in the rolling direction must equal the flow stress described by the hardening law. This leads to the conclusion that constitutive models need to be prepared with additional constraints for this new concept.
With the same objective of proposing a single test calibration methodology for anisotropic plasticity models, the VFM is combined with an optimised heterogeneous test. Contrary to the biaxial test, this test can be performed on a classical tensile machine and offers a wide range of strain states. Nevertheless, the results of the calibration indicate that a heterogeneous test performed in a single orientation of the material seems insufficient to accurately capture the plastic anisotropy coefficients. In the same study, the analysis of the number of virtual fields proves the dependence of the method. The results show that a number superior to 5 virtual fields stabilises the error in the calibrated parameters below 1.5%, for a constitutive model composed by Hill'48 yield criterion and Swift's hardening law.
The last part of this thesis concerns the calibration of thermo-mechanical constitutive models. A thermo-mechanical heterogeneous test performed on a Gleeble thermo-mechanical is proposed to generate the experimental database. The analysis of the test shows that a range of temperatures from 360 to 500 °C is covered and this temperature field is nearly constant during the test. The strain field distribution contains a wide range of values at each instant of the test. Nevertheless, the temperature distribution promotes localisation of the strain field at the centre of the specimen, which reduces the information for the viscoplastic regime in terms of the temperature range. The strain-rate field presents a similar shape to the strain field and the range of values is in the same order of magnitude of the nominal strain-rate of the test.
The FEMU is combined with a virtual database of the test and the calibration of the Johnson-Cook model is analysed. The results show that the parameters related to temperature and strain rate are easily calibrated. However, low sensitivity to the parameter representing the initial yield stress is observed. This low sensitivity to the initial yield stress leads to the appearance of local minima. A possible solution to mitigate this scenario is studied, which considers the initial yield stress as a know variable. This also improves the robustness of the proposed methodology in the presence of noise.
The test is also explored with the VFM to calibrate the modified J-C model. In a first attempt, only the information of a single test performed at a constant displacement rate is used. The results suggest a good description of the flow stress of the material, but only for the same conditions of the test. This means that the experimental database composed by a single test lacks information to calibrate the three terms of the modified J-C model, more specifically the strain-rate term. To improve these results, a second analysis with data of three tests at different displacement rates is performed. The combination of these three tests increases the range of strain-rate and consequently, provides sufficient information to calibrate the three terms of the model. The positive effect of the strain-rate on the flow

stress of the material is captured. However, the results suggest a lack of flexibility from the modified J-C model to capture the material behaviour of DP980 steel under such range of strain-rates.
Overall, the results obtained with this heterogeneous thermo-mechanical test are very positive and a more efficient alternative to long experimental campaigns can be envisaged. Both the VFM and FEMU analysis demonstrate the potential of the test. It would be interesting, as future work, to combine different ranges of temperature to enhance the experimental database and test more complex constitutive models.

5.2 Perspectives for future work

It is expected that in the near future the topic of calibration of constitutive models receives more attention due to the exciting challenges that remain to be dealt with. Some of the works initiated during this PhD intended to tackle some of the challenges in this field, and therefore deserve to be further studied. Moreover, several tools that were developed constitute a solid base for future work. For further research, the following recommendations are given:

- Regarding the inverse methods, the overview presented at the beginning of this thesis shows that FEMU has a major disadvantage compared to the remaining methods, which is the computational cost. This is caused by the excessive number of FE simulations that are required. However, if the convergence of this method is improved, this problem will be attenuated. It can be achieved by combining the FEMU with another inverse method in a single objective function. This can also bring benefits in the case of multiple solutions and ill-posedness of the inverse problem.

- The objective of identifying simultaneously all the parameters of an anisotropic plasticity model remains one of the most challenging topics in the field. Despite the complexity and variables that affect the problem, it should not be discarded. The biaxial test on a cruciform specimen shows interesting results. Therefore, the study initiated in this PhD should be experimentally validated.

- Moreover, the calibration of complex constitutive models frequently raises the problem of multiple solutions. Some of these solutions have no physical meaning or represent homothetic solutions that must be excluded from the universe of admissible solutions. This can be accomplished by employing optimisation constraints, which consider the formulation of the constitutive model. Formulate such constraints will require an individual analysis of each constitutive model.

- The VFM is a method with a growing interest in the community of solid mechanics. The recent progress in the method aimed at the development of automatic strategies to define the virtual fields. Nevertheless, the developed automatic strategies have some downsides, such as complex implementation procedures or high computational cost. Therefore, the development of an automatic strategy that mitigates those problems remain to be dealt with. The sensitivity of the method to the number of virtual fields can be a starting point to developed a new strategy.

- The work initiated in this thesis on the calibration of thermo-mechanical models has plenty of room for improvement. In terms of experimental measurements, heat waves may influence the accuracy of the displacement/strain measures. That should be analysed in the case of the proposed heterogeneous test. Moreover, the evolution of the deformation process leads to highly localised strain fields. The 3D effects may have an important role here, which must be understood in the future.

Intentionally blank page.

References

[1] D. Banabic. *Sheet metal forming processes: constitutive modelling and numerical simulation*. Springer Science & Business Media, 2010.

[2] S. Bruschi, T. Altan, D. Banabic, P.F. Bariani, A. Brosius, J. Cao, A. Ghiotti, M. Khraisheh, M. Merklein, and A.E. Tekkaya. Testing and modelling of material behaviour and formability in sheet metal forming. *CIRP Annals*, 63(2):727–749, 2014.

[3] J.L. Chaboche. A review of some plasticity and viscoplasticity constitutive theories. *International Journal of Plasticity*, 24(10):1642 – 1693, 2008. Special Issue in Honor of Jean-Louis Chaboche.

[4] A. Khalfallah, J.L. Alves, M.C. Oliveira, and L.F. Menezes. Influence of the characteristics of the experimental data set used to identify anisotropy parameters. *Simulation Modelling Practice and Theory*, 53:15 – 44, 2015.

[5] T. Pottier, F. Toussaint, and P. Vacher. Contribution of heterogeneous strain field measurements and boundary conditions modelling in inverse identification of material parameters. *European Journal of Mechanics - A/Solids*, 30(3):373 – 382, 2011.

[6] E. Markiewicz, B. Langrand, and D. Notta-Cuvier. A review of characterisation and parameters identification of materials constitutive and damage models: From normalised direct approach to most advanced inverse problem resolution. *International Journal of Impact Engineering*, 110:371 – 381, 2017. Special Issue in honor of Seventy Fifth Birthday of Professor N. K. Gupta.

[7] B. Jordan, M.B. Gorji, and D. Mohr. Neural network model describing the temperature- and rate-dependent stress-strain response of polypropylene. *International Journal of Plasticity*, 135:102811, 2020.

[8] C. Ilg, K. Witowski, D. Koch, P.R. Suanno, and A. Haufe. Constitutive model parameter identification via full-field calibration. In *IOP Conference Series: Materials Science and Engineering*, volume 651, page 012070. IOP Publishing, 2019.

[9] M. Grédiac and F. Hild. *Full-field measurements and identification in solid mechanics*. Wiley Online Library, 2013.

[10] S. Avril, M. Bonnet, A.-S. Bretelle, M. Grédiac, F. Hild, P. Ienny, F. Latourte, D. Lemosse, S. Pagano, E. Pagnacco, et al. Overview of identification methods of mechanical parameters based on full-field measurements. *Experimental Mechanics*, 48(4):381, 2008.

[11] S. Coppieters, S. Cooreman, H. Sol, P. Van Houtte, and D. Debruyne. Identification of the post-necking hardening behaviour of sheet metal by comparison of the internal and external work in the necking zone. *Journal of Materials Processing Technology*, 211(3):545 – 552, 2011.

[12] F. Pierron and M. Grédiac. Towards material testing 2.0. a review of test design for identification of constitutive parameters from full-field measurements. *Strain*, n/a(n/a):e12370. e12370 10.1111/str.12370.

[13] B. Barroqueiro, A. Andrade-Campos, J. Dias de Oliveira, and R.A.F. Valente. Design of mechanical heterogeneous specimens using topology optimization. *International Journal of Mechanical Sciences*, 181:105764, 2020.

[14] A. Maček, B. Starman, N. Mole, and M. Halilovič. Calibration of advanced yield criteria using uniaxial and heterogeneous tensile test data. *Metals*, 10(4):542, 2020.

[15] L. Chamoin, C. Jailin, M. Diaz, and L. Quesada. Coupling between topology optimization and digital image correlation for the design of specimen dedicated to selected material parameters identification. *International Journal of Solids and Structures*, 193-194:270 – 286, 2020.

[16] M. Rossi and F. Pierron. On the use of simulated experiments in designing tests for material characterization from full-field measurements. *International Journal of Solids and Structures*, 49(3):420 – 435, 2012.

[17] M. Rossi, P. Lava, F. Pierron, D. Debruyne, and M. Sasso. Effect of dic spatial resolution, noise and interpolation error on identification results with the vfm. *Strain*, 51(3):206–222, 2015.

Appendix A

Copyright agreements

Comparison of inverse identification strategies for constitutive mechanical models using full-field measurements

Author: J.M.P. Martins,A. Andrade-Campos,S. Thuillier

Publication: International Journal of Mechanical Sciences

Publisher: Elsevier

Date: September 2018

LICENSE TO PUBLISH AGREEMENT FOR CONFERENCE PROCEEDINGS

This License to Publish must be signed and returned to the Proceedings Editor before the manuscript can be published. If you have questions about how to submit the form, please contact the AIP Publishing Conference Proceedings office (confproc@aip.org). For questions regarding the copyright terms and conditions of this License, please contact AIP Publishing's Office of Rights and Permissions, 1305 Walt Whitman Road, Suite 300, Melville, NY 11747-4300 USA; Phone 516-576-2268; Email: rights@aip.org.

Article Title ("Work"):
Identification of Material Parameters for Plasticity Models: A Comparative Study on the Finite Element Model Updating and the Virtual Fields Method
(Please indicate the final title of the Work. Any substantive changes made to the title after acceptance of the Work may require the completion of a new agreement.)

All Author(s):
J.M.P. Martins, S. Thuillier, A. Andrade-Campos
(Please list **all** the authors' names in order as they will appear in the Work. All listed authors must be fully deserving of authorship and no such authors should be omitted. For large groups of authors, attach a separate list to this form.)

Title of Conference: ESAFORM 2018

Name(s) of Editor(s) _____

All Copyright Owner(s), if not Author(s):

_____

(Please list **all** copyright owner(s) by name. In the case of a Work Made for Hire, the employer(s) or commissioning party(ies) are the copyright owner(s). For large groups of copyright owners, attach a separate list to this form.)

Copyright Ownership and Grant of Rights

For the purposes of this License, the "Work" consists of all content within the article itself and made available as part of the article, including but not limited to the abstract, tables, figures, graphs, images, and multimedia files, as well as any subsequent errata. "Supplementary Material" consists of material that is associated with the article but linked to or accessed separately (available electronically only), including but not limited to data sets and any additional files.

This Agreement is an Exclusive License to Publish not a Transfer of Copyright. Copyright to the Work remains with the Author(s) or, in the case of a Work Made for Hire, with the Author(s)' employer(s). AIP Publishing LLC shall own and have the right to register in its name the copyright to the proceedings issue or any other collective work in which the Work is included. Any rights granted under this License are contingent upon acceptance of the Work for publication by AIP Publishing. If for any reason and at its own discretion AIP Publishing decides not to publish the Work, this License is considered void.

Each Copyright Owner hereby grants to AIP Publishing LLC the following irrevocable rights for the full term of United States and foreign copyrights (including any extensions):

1. The exclusive right and license to publish, reproduce, distribute, transmit, display, store, translate, edit, adapt, and create derivative works from the Work (in whole or in part) throughout the world in all formats and media whether now known or later developed, and the nonexclusive right and license to do the same with the Supplementary Material.
2. The right for AIP Publishing to freely transfer and/or sublicense any or all of the exclusive rights listed in #1 above. Sublicensing includes the right to authorize requests for reuse of the Work by third parties.
3. The right for AIP Publishing to take whatever steps it considers necessary to protect and enforce, at its own expense, the exclusive rights granted herein against third parties.

Author Rights and Permitted Uses

Subject to the rights herein granted to AIP Publishing, each Copyright Owner retains ownership of copyright and all other proprietary rights such as patent rights in the Work.

Each Copyright Owner retains the following nonexclusive rights to use the Work, without obtaining permission from AIP Publishing, in keeping with professional publication ethics and provided clear credit is given to its first publication in an AIP Publishing proceeding. Any reuse must include a full credit line acknowledging AIP Publishing's publication and a link to the Version of Record (VOR) on AIP Publishing's site.

Each Copyright Owner may:

1. Reprint portions of the Work (excerpts, figures, tables) in future works created by the Author, in keeping with professional publication ethics.
2. Post the Accepted Manuscript (AM) to their personal web page or their employer's web page immediately after acceptance by AIP Publishing.
3. Deposit the AM in an institutional or funder-designated repository immediately after acceptance by AIP Publishing.
4. Use the AM for posting within scientific collaboration networks (SCNs). For a detailed description of our policy on posting to SCNs, please see our Web Posting Guidelines (https://publishing.aip.org/authors/web-posting-guidelines).
5. Reprint the Version of Record (VOR) in print collections written by the Author, or in the Author's thesis or dissertation. It is understood and agreed that the thesis or dissertation may be made available electronically on the university's site or in its repository and that copies may be offered for sale on demand.
6. Reproduce copies of the VOR for courses taught by the Author or offered at the institution where the Author is employed, provided no fee is charged for access to the Work.
7. Use the VOR for internal training and noncommercial business purposes by the Author's employer.
8. Use the VOR in oral presentations made by the Author, such as at conferences, meetings, seminars, etc., provided those receiving copies are informed that they may not further copy or distribute the Work.
9. Distribute the VOR to colleagues for noncommercial scholarly use, provided those receiving copies are informed that they may not further copy or distribute the Work.
10. Post the VOR to their personal web page or their employer's web page 12 months after publication by AIP Publishing.
11. Deposit the VOR in an institutional or funder-designated repository 12 months after publication by AIP Publishing.
12. Update a prior posting with the VOR on a noncommercial server such as arXiv, 12 months after publication by AIP Publishing.

Author Warranties

Each Author and Copyright Owner represents and warrants to AIP Publishing the following:

1. The Work is the original independent creation of each Author and does not infringe any copyright or violate any other right of any third party.
2. The Work has not been previously published and is not being considered for publication elsewhere in any form, except as a preprint on a noncommercial server such as arXiv, or in a thesis or dissertation.
3. Written permission has been obtained for any material used from other sources and copies of the permission grants have been supplied to AIP Publishing to be included in the manuscript file.
4. All third-party material for which permission has been obtained has been properly credited within the manuscript.
5. In the event that the Author is subject to university open access policies or other institutional restrictions that conflict with any of the rights or provisions of this License, such Author has obtained the necessary waiver from his or her university or institution.

This License must be signed by the Author(s) and, in the case of a Work Made for Hire, also by the Copyright Owners. One Author/Copyright Owner may sign on behalf of all the contributors/owners only if they all have authorized the signing, approved of the License, and agreed to be bound by it. The signing Author and, in the case of a Work Made for Hire, the signing Copyright Owner warrants that he/she/it has full authority to enter into this License and to make the grants this License contains.

1. The Author must please sign here (*except* if an Author is a U.S. Government employee, then please sign under #3 below):

Author(s) Signature	Print Name	Date
João Miguel Pereira Martins	J.M.P. Martins	15/02/2018

2. The Copyright Owner (if different from the Author) must please sign here:

Name of Copyright Owner	Authorized Signature and Title	Date

3. If an Author is a U.S. Government employee, such Author must please sign below.
The signing Author certifies that the Work was written as part of his/her official duties and is therefore not eligible for copyright protection in the United States.

Name of U.S. Government Institution (e.g., Naval Research Laboratory, NIST)

Author Signature	Print Name	Date

PLEASE NOTE: NATIONAL LABORATORIES THAT ARE SPONSORED BY U.S. GOVERNMENT AGENCIES BUT ARE INDEPENDENTLY RUN ARE NOT CONSIDERED GOVERNMENT INSTITUTIONS. (For example, Argonne, Brookhaven, Lawrence Livermore, Sandia, and others.) Authors at these types of institutions should sign under #1 or #2 above.

If the Work was authored under a U.S. Government contract, and the U.S. Government wishes to retain for itself and others acting on its behalf, a paid-up, nonexclusive, irrevocable, worldwide license in the Work to reproduce, prepare derivative works from, distribute copies to the public, perform publicly, and display publicly, by or on behalf of the Government, please check the box below and add the relevant Contract numbers.

☐ Contract #(s) _____ [1.16.1]

LICENSE TERMS DEFINED

Accepted Manuscript (AM): The final version of an author's manuscript that has been accepted for publication and incorporates all the editorial changes made to the manuscript after submission and peer review. The AM does not yet reflect any of the publisher's enhancements to the work such as copyediting, pagination, and other standard formatting.

arXiv: An electronic archive and distribution server for research article preprints in the fields of physics, mathematics, computer science, quantitative biology, quantitative finance, and statistics, which is owned and operated by Cornell University, http://arxiv.org/.

Commercial and noncommercial scholarly use: *Noncommercial* scholarly uses are those that further the research process for authors and researchers on an individual basis for their own personal purposes. They are author-to-author interactions meant for the exchange of ideas. *Commercial* uses fall outside the author-to-author exchange and include but are not limited to the copying or distribution of an article, either in hard copy form or electronically, for resale or licensing to a third party; posting of the AM or VOR of an article by a site or service where an access fee is charged or which is supported by commercial paid advertising or sponsorship; use by a for-profit entity for any type of promotional purpose. Commercial uses require the permission of AIP Publishing.

Embargo period: The period of time during which free access to the full text of an article is delayed.

Employer's web page: A web page on an employer's site that highlights the accomplishments and research interests of the company's employees, which usually includes their publications. (See also: Personal web page and Scholarly Collaboration Network).

Exclusive License to Publish: An exclusive license to publish is a written agreement in which the copyright owner gives the publisher exclusivity over certain inherent rights associated with the copyright in the work. Those rights include the right to reproduce the work, to distribute copies of the work, to perform and display the work publicly, and to authorize others to do the same. The publisher does not hold the copyright to the work, which continues to reside with the author. The terms of the AIP Publishing License to Publish encourage authors to make full use of their work and help them to comply with requirements imposed by employers, institutions, and funders.

Full Credit Line: AIP Publishing's preferred format for a credit line is as follows (you will need to insert the specific citation information in place of the capital letters): "Reproduced from [FULL CITATION], with the permission of AIP Publishing." A FULL CITATION would appear as: Journal abbreviation, volume number, article ID number *or* page number (year). For example: Appl. Phys. Lett. 107, 021102 (2015).

Institutional repository: A university or research institution's digital collection of articles that have been authored by its staff and which are usually made publicly accessible. As authors are encouraged and sometimes required to include their published articles in their institution's repository, the majority of publishers allow for deposit of the Accepted Manuscript for this purpose. AIP Publishing also allows for the VOR to be deposited 12 months after publication of the Work.

Journal editorial office: The contact point for authors concerning matters related to the publication of their manuscripts. Contact information for the journal editorial offices may be found on the journal websites under the "About" tab.

Linking to the Version of Record (VOR): To create a link to your article in an AIP Publishing journal or proceedings, you need to know the CrossRef digital object identifier (doi). You can find the doi on the article's abstract page. For instructions on linking, please refer to our Web Posting Guidelines at https://publishing.aip.org/authors/web-posting-guidelines.

National Laboratories: National laboratories are sponsored and funded by the U.S. Government but have independent nonprofit affiliations and employ private sector resources. These institutions are classified as Federally Funded Research and Development Centers (FFRDCs). Authors working at FFRCs are not considered U.S. Government employees for the purposes of copyright. The Master Government List of FFRDCs may be found at http://www.nsf.gov/statistics/ffrdclist/.

Personal web page: A web page that is hosted by the author or the author's institution and is dedicated to the author's personal research interests and publication history. An author's profile page on a social media site or scholarly collaboration network site is *not* considered a personal web page. (See also: Scholarly Collaboration Network; Employer's web page).

Peer X-Press: A web-based manuscript submission system by which authors submit their manuscripts to AIP Publishing for publication, communicate with the editorial offices, and track the status of their submissions. The Peer X-Press system provides a fully electronic means of completing the License to Publish. A hard copy of the Agreement will be supplied by the editorial office if the author is unable to complete the electronic version of the form. (Conference Proceedings authors will continue to submit their manuscripts and forms directly to the Conference Editors.)

Preprint: A version of an author's manuscript intended for publication but that has not been peer reviewed and does not reflect any editorial input or publisher enhancements.

Professional Publication Ethics: AIP Publishing provides information on what it expects from authors in its "Statement of ethics and responsibilities of authors submitting to AIP Publishing journals" (http://publishing.aip.org/authors/ethics). AIP Publishing is also a member of the Committee on Publication Ethics (COPE) (http://publicationethics.org/), which provides numerous resources and guidelines for authors, editors, and publishers with regard to ethical standards and accepted practices in scientific publishing.

Scholarly Collaboration Network (SCN): Professional networking sites that facilitate collaboration among researchers as well as the sharing of data, results, and publications. SCNs include sites such as Academia.edu, ResearchGate, and Mendeley, among others.

Supplementary Material: Related material that has been judged by peer review as being relevant to the understanding of the article but that may be too lengthy or of too limited interest for inclusion in the article itself. Supplementary Material may include data tables or sets, appendixes, movie or audio clips, or other multimedia files.

U.S. Government employees: Authors working at Government organizations who author works as part of their official duties and who are not able to license rights to the Work, since no copyright exists. Government works are in the public domain within the United States.

Version of Record (VOR): The final published version of the article as it appears in the printed journal/proceedings or on the Scitation website. It incorporates all editorial input, is formatted in the publisher's standard style, and is usually viewed in PDF form.

Waiver: A request made to a university or institution to exempt an article from its open-access policy requirements. For example, a conflict will exist with any policy that requires the author to grant a nonexclusive license to the university or institution that enables it to license the Work to others. In all such cases, the Author must obtain a waiver, which shall be included in the manuscript file.

Work: The "Work" is considered all the material that comprises the article, including but not limited to the abstract, tables, figures, images, multimedia files that are directly embedded within the text, and the text itself. The Work does not include the Supplementary Material (see Supplementary Material above).

Work Made for Hire: Under copyright law, a work prepared by an employee within the scope of employment, or a work that has been specially ordered or commissioned for which the parties have agreed in writing to consider as a Work Made for Hire. The hiring party or employer is considered the author and owner of the copyright, not the person who creates the work.

Calibration of anisotropic plasticity models using a biaxial test and the virtual fields method

Author: J.M.P. Martins,A. Andrade-Campos,S. Thuillier

Publication: International Journal of Solids and Structures

Publisher: Elsevier

Date: 1 November 2019

Copyright Transfer Agreement

2019 Conference and Exposition on Experimental & Applied Mechanics
June 3–6, 2019 | Peppermill Resort | Reno, NV

The copyright to this submission is transferred to the Society for Experimental Mechanics, Inc. (for U.S. Government employees: to the extent transferable). The author warrants that his/her contribution is original and that he/she has full power to make this grant. The author signs for and accepts responsibility for releasing this material on behalf of any and all coauthors. The copyright transfer covers the exclusive right to reproduce and distribute the submission, including, but not limited to, the right to publish, republish, transmit, sell, distribute and otherwise use the submission in whole or in part in electronic and print editions.

If the submission was written by the author(s) in the course of the author's employment (as a "work-made-for-hire" in the course of employment), the submission is owned by the company/employer which must sign this Agreement (in addition to the author's signature) in the space provided below. In such case, the company/employer hereby assigns to the Society, during the full term of copyright, all copyright in and to the Contribution for the full term of copyright throughout the world as specified in the first paragraph above. The Society hereby grants back, without charge, to such company/employer, its subsidiaries and divisions, the right to make copies of and distribute the final published submission internally in print format or electronically on the Company's internal network. Copies so used may not be resold or distributed externally.

SEM grants to author and the owner or employer of a work for hire, the non-exclusive right to use all or part of the work referenced in this agreement in any book or article written by author; provided, that the copyright notice which appears on the journal or proceedings in which the work is first published, and a full citation of the publication is affixed to copies of such book or article so as to give reasonable notice of such copyright.

An author may self-archive an author-created version of his/her submission on his/her own website and his/her institution's repository provided acknowledgement is given to the original source of publication. An author may also transmit, print and share copies of the submission with colleagues.

In the case of a submission prepared under U.S. Government contract or grant, the U.S. Government may reproduce, without charge, all or portions of the submission and may authorize others to do so, for official U.S. Government purposes only, if the U.S. Government contract or grant so requires.

Corresponding Author	João M.P. Martins		
Affiliation	Universities of Bretagne-Sud (France) and Aveiro (Portugal)		
Author e-mail	joao.martins52@ua.pt		
Submission # / Title	Calibration of anisotropic plasticity models with an optimized heterogeneous test and the virtual fields method		
Signature	João Miguel Peixoto Martins	Date	25/02/2019
Owner signature (If applicable)		Date	
Check here if this is a U. S. Government work	○		

Upload the completed form with submission files.

* If you **do not want** your submission to be published by Springer, you must notify Shari Matthews, via email at shari@sem.org, with your submission # and submission title.

Calibration of Johnson-Cook Model Using Heterogeneous Thermo-Mechanical Tests

Author: João Peixoto Martins,António Andrade-Campos,Sandrine Thuillier

Publication: Procedia Manufacturing

Publisher: Elsevier

Date: 2020